

EUR 2762 e

EUROPEAN ATOMIC ENERGY COMMUNITY - EURATOM

THE INFLUENCE OF MASS TRANSFER ON
THE KINETIC OF GRAPHITE OXIDATION BY
LOW CONCENTRATION OF OXIDISING
IMPURITIES IN AN INERT CARRIER GAS

by

L.J. VALETTE

1967



Work performed at the
Dragon Project, Winfrith - England

LEGAL NOTICE

This document was prepared under the sponsorship of the Commission of the European Communities.

Neither the Commission of the European Communities, its contractors nor any person acting on their behalf :

Make any warranty or representation, express or implied, with respect to the accuracy, completeness, or usefulness of the information contained in this document, or that the use of any information, apparatus, method, or process disclosed in this document may not infringe privately owned rights; or

Assume any liability with respect to the use of, or for damages resulting from the use of any information, apparatus, method or process disclosed in this document.

This report and his annex are on sale at the addresses listed on cover page 4

at the price of FF 25.—	FB 250.—	DM 20.—	Lit. 3 120	Fl. 18.—
-------------------------	----------	---------	------------	----------

When ordering, please quote the EUR number and the title, which are indicated on the cover of each report.

Printed by Guyot, s.a.
Brussels, October 1967

This document was reproduced on the basis of the best available copy.

EUR 2762 e

THE INFLUENCE OF MASS TRANSFER ON THE KINETIC OF GRAPHITE OXIDATION BY LOW CONCENTRATION OF OXIDISING IMPURITIES IN AN INERT CARRIER GAS by L.J. VALETTE

European Atomic Energy Community - EURATOM

Work performed at the Dragon Project, Winfrith (England)

Brussels, October 1967 - 200 Pages - 51 Figures - 20 Tables - FB 250

Investigations have been carried out in the research and development programme of DRAGON in order to find out the reaction rates of chemical impurities present in helium with graphite at high temperature. In the temperature range to be expected in a H.T.G.C.R. the reaction rates can be mass transfer controlled. A pressurized loop has been built in order to investigate the mass transfer controlled reactions. The experimental investigations are correlated with theoretical predictions based on the boundary layer concept. In most cases a good prediction of the rates can be achieved by these theories and in the remaining cases a good insight in the mechanism of the mass transfer could be obtained by the analysis of the boundary layers surrounding the reacting body.

EUR 2762 e

THE INFLUENCE OF MASS TRANSFER ON THE KINETIC OF GRAPHITE OXIDATION BY LOW CONCENTRATION OF OXIDISING IMPURITIES IN AN INERT CARRIER GAS by L.J. VALETTE

European Atomic Energy Community - EURATOM

Work performed at the Dragon Project, Winfrith (England)

Brussels, October 1967 - 200 Pages - 51 Figures - 20 Tables - FB 250

Investigations have been carried out in the research and development programme of DRAGON in order to find out the reaction rates of chemical impurities present in helium with graphite at high temperature. In the temperature range to be expected in a H.T.G.C.R. the reaction rates can be mass transfer controlled. A pressurized loop has been built in order to investigate the mass transfer controlled reactions. The experimental investigations are correlated with theoretical predictions based on the boundary layer concept. In most cases a good prediction of the rates can be achieved by these theories and in the remaining cases a good insight in the mechanism of the mass transfer could be obtained by the analysis of the boundary layers surrounding the reacting body.

EUR 2762 e

EUROPEAN ATOMIC ENERGY COMMUNITY - EURATOM

THE INFLUENCE OF MASS TRANSFER ON THE KINETIC OF GRAPHITE OXIDATION BY LOW CONCENTRATION OF OXIDISING IMPURITIES IN AN INERT CARRIER GAS

by

L.J. VALETTE

Ingénieur civil mécanicien;
Ingénieur des constructions aéronautiques;
Ingénieur à l'Euratom, adjoint au chef de projet T.H.T.R.
(Thorium Hochtemperatur Reaktor Jülich)

Dissertation présentée pour l'obtention du diplôme de docteur
en sciences appliquées à l'Université de Bruxelles en 1966

1967



Work performed at the
Dragon Project, Winfrith - England

CONFIDENTIAL

CONFIDENTIAL

CONFIDENTIAL

CONFIDENTIAL

SUMMARY

Investigations have been carried out in the research and development programme of DRAGON in order to find out the reaction rates of chemical impurities present in helium with graphite at high temperature. In the temperature range to be expected in a H.T.G.C.R. the reaction rates can be mass transfer controlled. A pressurized loop has been built in order to investigate the mass transfer controlled reactions. The experimental investigations are correlated with theoretical predictions based on the boundary layer concept. In most cases a good prediction of the rates can be achieved by these theories and in the remaining cases a good insight in the mechanism of the mass transfer could be obtained by the analysis of the boundary layers surrounding the reacting body.

CONTENTS

	<u>Page -No.</u>
Acknowledgement	2
Detailed table of contents	3
List of illustrations	8
List of tables	10
List of symbols and abbreviations	12
List of references	21
 <u>Chapter</u>	
1. Introduction	25
2. Theoretical discussion and review of the relevant literature	30
3. Experimental techniques	78
4. Experimental equipment	85
5. Operating procedure	96
6. Experimental results and correlation with the theoretical predictions	101
7. Conclusion	110
 <u>Appendix</u>	
I Method for calculation of local mass transfer coefficient	114
II Development of C ¹⁴ labelling method for the P.C.T.E. graphite sample	116
ERRATA	185
Answer to the questions and remarks raised by the "commission of professors" of the Brussels university during the private defence of the thesis	189

ACKNOWLEDGEMENT

The author would like to take this opportunity to thank:

Prof. Dr. J. Guéron, general director, Dr. P. Caprioglio director of EURATOM and Mr. C. Rennie chief executive of the DRAGON Project who gave their permission to publish, as a doctor thesis, the work he had the opportunity to perform in the U.K.A.E.A. research establishment in Winfrith-Dorset/ENGLAND.

Dr. L. Shepherd and Dr. H. de Bruijn who charged him with the task of performing these tests.

Professor A. Jaumotte who accepted to sponsor this thesis and who supervised the work and assisted him with useful recommendations and suggestions.

Professor R. Jottrand who obligently and constructively commented on the work and results.

The whole scientific and supporting staff of the "DRAGON Mass Transport Group" in Winfrith and specially Mr. J. York for their assistance in performing the experiments.

The secretariat of "T.H.T.R.-Projektleitung" and the drawing section of the "Reaktor-entwicklung" department K.F.A. Jülich and the EURATOM "Service des publications" which helped to produce the printed version of this document.

DETAILED TABLE OF CONTENTS

	<u>Page-No.</u>
1. Introduction	25
1.1. General problem	25
1.2 Particular problem	26
1.2.1 Essential features of a H.T.G.C.R.	26
1.3 Object of the thesis	28
2. Theoretical discussion and review of the relevant literature	30
2.1 Graphite oxydation	30
2.1.1 Chemical regime	30
2.1.2 In pore diffusion regime	32
2.1.3 Mass transfer regime	33
2.2 Mass transfer and diffusion	35
2.2.1 Molecular diffusion	36
2.2.1.1 Definition of concentration, velocities and mass fluxes	36
2.2.1.2 Fick's law of diffusion	38
2.2.1.3 Diffusion of reacting gas A in the stationary gas He accompanied by a back-diffusion of the reaction product B	38
2.2.2 Diffusion coefficient	39
2.2.3 Molecular, momentum and heat transfer	41
2.3 Mass transfer in forced convection	42
2.3.1 Introduction	42
2.3.2 General theories and methods for the study of convective mass transfer	44
2.3.2.1 The general differential equation	44
2.3.2.1.1 The differential equations of the flow of a viscous fluid	44
2.3.2.1.2 The differential equations of heat and mass conduction	44
2.3.2.2 Concept of boundary layer and definition of the boundary layer equations	45

	<u>Page-No.</u>
2.3.2.3 The momentum and mass flow equations of the boundary layer	47
2.3.2.4 Concept of turbulence and eddy diffusivity	48
2.3.2.5 Mass transfer and fluid flow correlation—method of exchange of impulse	50
2.3.2.5.1 Impulse theory	51
2.3.2.5.2 Combined impulse and boundary layer theory	52
2.3.2.5.3 Improved impulse and boundary layer theory and universal velocity profile for turbulent flow in tube	52
2.3.2.6 Methods of similarity	54
2.3.3 The flow on flat plates and in tubes	56
2.3.3.1 The boundary layer on a plane plate in longitudinal flow	57
2.3.3.1.1 The laminar portion of the boundary layer	57
2.3.3.1.2 The turbulent boundary layer	58
2.3.3.2 Flow through a tube	60
2.3.3.2.1 Fully developed laminar flow	61
2.3.3.2.2 Fully developed turbulent flow	62
2.3.3.2.3 Friction factor in pipes	63
2.3.4 Theoretical and analytical expression of the mass transfer coefficient	63
2.3.4.1 Local and average mass transfer coefficient in a tube with $C_s = 0$, with non established velocity and concentration profile in laminar flow	64
2.3.4.2 Local and average mass transfer coefficient in a tube with $C_s \neq 0$, with non established velocity and concentration profile in turbulent flow	66
2.3.4.2.1 For distances smaller than x_e	67
2.3.4.2.2 For distances bigger than x_e	67
2.3.4.3 Average mass transfer coefficient in a tube with established velocity profile and non established concentration profile in laminar flow	68
2.3.4.4 Average mass transfer coefficient in a tube with established velocity profile and non established concentration profile in turbulent flow	70
2.3.4.5 Discussion on temperature and concentration to be used in the equations for determination of the gas constants	71
2.3.5 Experimental and semi-empirical values of the mass transfer coefficient	73
2.3.5.1 The constant multiplication factor A	73
2.3.5.2 The exponent of Re : a	74
2.3.5.3 The exponent of Sc : b	75
2.3.5.4 The exponent of $\left(\frac{\mu}{\mu_s}\right)$	75

2.3.5.5 The function of $\left(\frac{x}{d}\right)$	76
2.3.5.6 The function of Gr^d	77
3. Experimental techniques	78
3.1. Experimental variables	78
3.1.1 The graphite sample	79
3.1.2 The geometry of the sample and of the test section	79
3.1.3 The gas composition	79
3.1.4 The flow rate	80
3.1.5 The temperature	80
3.1.6 The pressure	81
3.2 Experimental techniques	81
3.2.1 Weight loss measurement	81
3.2.2 Gas analysis methods - The multi-pass depletion method	82
3.2.3 The Carbon ¹⁴ method	84
4. Experimental equipment	85
4.1. Experimental loop	85
4.1.1 The primary circuit	85
4.1.1.1 The experimental test section	85
4.1.1.1.1 The thimble heater MK III	86
4.1.1.1.2 The first pre-heater	86
4.1.1.1.3 The second pre-heater	86
4.1.1.1.4 The graphite sample furnace	87
4.1.1.2 The heat exchanger	88
4.1.1.3 The gas circulation	88
4.1.1.4 The surge tanks	88
4.1.1.5 The orifice plates	89
4.1.2 The helium processing circuit	89
4.1.2.1 The purifier	89
4.1.2.2 The impurity make-up system	90
4.1.2.3 The converter	
4.2 Measurement and control of the experimental variables	90
4.2.1 Temperature	90

4.2.1.1	Temperature measurement for safety purposes	91
4.2.1.2	Temperature measurement for operational purposes	91
4.2.1.3	Temperature measurement for experimental purposes	91
4.2.2	The flow rate	93
4.2.3	The pressure	93
4.2.4	The gas composition	93
4.2.4.1	The "Irgas" (Infra-Red gas analyser)	94
4.2.4.2	The Hersch cell	94
4.2.4.3	The gas chromatograph	94
4.2.5	The counting equipment	94
5.	Operating procedure	96
5.1	Introduction	96
5.1.1	The safety test	96
5.1.2	The calibration procedure	97
5.1.3	The routine checks	97
5.2	Adjustment of the flows	97
5.2.1	The flow in the main loop	98
5.2.2	The flow in the purifier converter	98
5.2.3	The flow in the instruments-line	98
5.2.4	The flow and pressure in the thimble	98
5.3.	Temperature adjustment	99
5.3.1	The gas temperature	99
5.3.2	The graphite temperature	99
5.4	The oxygen depletion test and CO, CO ₂ and C ¹⁴ build-up	99
6.	Experimental results and correlation with the theoretical predictions	101
6.1	Experimental results	101
6.2	Discussion of the Results	102
6.2.1	Tests performed with the flow as variable	102
6.2.1.1	Tests performed with an established velocity profile and non established concentration profile	102
6.2.1.1.1	Tests in laminar flow with long calming section in 0.6 cm diameter channel	102

6.2.1.1.2 Tests in turbulent flow with a long calming section	103
6.2.1.2 Tests performed with non established velocity profile and concentration profile	105
6.2.1.2.1 Tests in laminar helium flow in a 0.36 cm diameter channel with a sharp edge entrance	105
6.2.1.2.2 Tests in a helium flow in a 0.36 cm diameter channel with a short calming section	106
6.2.2 Tests performed with distance x from the entrance as variable in non established flow with non established concentration profile	107
6.2.2.1 Tests in laminar helium flow in 0.36 cm channel with a sharp edge entrance	107
6.2.2.2 Tests in turbulent helium flow in a 0.36 cm diameter channel with a sharp edge entrance	108
6.2.2.3 Tests in turbulent helium flow with a bellmouth inlet in 0.36 cm in diameter channel	109
6.2.2.4 Tests in turbulent nitrogen flow in 0.36 cm channel with a sharp edge entrance	109
7. Conclusion	110
7.1 Practical conclusion for H.T.G.C.R. design	110
7.2 Appreciation of methods used for estimation of the mass transfer tests	111
7.2.1 The dimensional analysis	111
7.2.2 The analogy with heat transfer	111
7.2.3 The use of hydrodynamic model	113

LIST OF ILLUSTRATIONS

- Fig. 1.1 Flow picture materialized by clouds of ammonium chloride "Lohrisch".
- Fig. 1.2 Schematic flow sheet of DRAGON Reactor primary circuit.
- Fig. 2.1 The three zones of the reaction rate in a porous graphite versus temperature.
- Fig. 2.2 Corrosion rate of grade 9 graphite with H_2O at 3.4 mm Hg as a function of burn-off.
- Fig. 2.3 Diffusion of a reacting gas and of its reaction products in stationary He.
- Fig. 2.4 Collision function for diffusion coefficient calculation.
- Fig. 2.5 Diffusivity of O_2 in He at 10, 15, 20 atmospheres versus temperature.
- Fig. 2.6 Diffusivity of O_2 in N_2 at 10, 15, 20 atmospheres versus temperature.
- Fig. 2.7 Element of a fluid near the wall for the calculation of the momentum equation.
- Fig. 2.8 Element of a fluid near the wall for the calculation of the mass flow equation.
- Fig. 2.9 Formation of the boundary layer along a flat plate.
- Fig. 2.10 Formation of the velocity and concentration boundary layers at the inlet of a tubular sample.
- Fig. 2.11 Universal velocity profile.
- Fig. 2.12 Streamline flow through a tube.
- Fig. 2.13 Pipe friction chart $\frac{\bar{z}}{P \cdot U^2}$ versus Re.
- Fig. 2.14 Concentration profile in laminar flow through the entrance region of a tube.
- Fig. 2.15 Theoretical mass transfer correlation for laminar flow in tubes.
- Fig. 3.1 Oxidation rate of grade 1 and grade 3 graphites with CO_2 .
- Fig. 3.2 Helium data at 20 atm.
- Fig. 3.3 Nitrogen data at 20 atm.
- Fig. 3.4 Relationship between Reynolds number (Re), mass flow (G), volumetric flow (Q) for different temperatures of He flow in a 6 mm diameter channel.
- Fig. 3.5 Relationship between Reynolds number (Re), mass flow (G), volumetric flow (Q), for different temperatures of N_2 flow in a 6 mm diameter channel.
- Fig. 3.6 Influence of the mass transfer regime on the reaction of graphite with CO_2 and O_2 for different mass transfer coefficient values.
- Fig. 3.7 Typical O_2 depletion test.
- Fig. 3.8 Graph for calculation of reaction rate with O_2 depletion method.
- Fig. 3.9 Arrhenius plot of the experimental rates measured in 20 atm. He with the gas analysis method.
- Fig. 3.10 Arrangement of C^{14} sample for local mass transfer measurement.

- Fig. 4.1 P.C.T.E. loop master flow sheet.
- Fig. 4.2 Pressurized Carbon Transport Experiment.
- Fig. 4.3 Thimble MK III.
- Fig. 4.4. Exploded view of Thimble MK III.
- Fig. 4.5 Entrance geometries used in the experimental programme.
- Fig. 4.6 Orifice plate calibration curves.
- Fig. 6.1 Mass transfer coefficient for different Re in laminar He flow with a long calming section 0.6 cm in diameter.
- Fig. 6.2 Mass transfer coefficient for different Re in turbulent He flow with a long calming section 0.6 cm in diameter.
- Fig. 6.3 Mass transfer coefficient for different Re in turbulent N₂ flow with a long calming section 0.6 cm in diameter.
- Fig. 6.4 Mass transfer coefficient as function of Re in non-established laminar He flow with a sharp edge entrance in 0.36 cm diameter channel.
a & b
- Fig. 6.5 Mass transfer coefficient as function of Re in He flow with a short calming section ($\frac{x_0}{d} = 36.2$) in a 0.36 cm diameter channel.
- Fig. 6.6 Mass transfer as a function of $(\frac{x}{d})$ in non-established laminar He flow (Re = 138) with a sharp edge entrance in 0.36 cm in diameter channel.
a & b
- Fig. 6.7 Average mass transfer as a function of $(\frac{x}{d})$ in non-established turbulent He flow with a sharp edge entrance 0.36 cm in diameter channel.
- Fig. 6.8 Average mass transfer coefficient as function of $(\frac{x}{d})$ in non-established turbulent He flow with a bellmouth entrance in 0.36 cm diameter channel.
- Fig. 6.9 Average mass transfer coefficient as a function of $(\frac{x}{d})$ in non-established N₂ turbulent flow with a sharp edge entrance 0.36 cm diameter channel.
- Fig. 6.10 Proportionality between k_c and $\frac{1}{P}$ or D
- Fig. 6.11 Values F_1 and F_2 to be used in Martinelli's equation for natural and forced mass convection in vertical tube with a uniform wall concentration.
- Fig. 6.12 Correlation between experimental values of heat and mass transfer with theoretical values.
- Fig. 6.13 Correlation between experimental values of mass transfer in He and N₂ flow in a 0.6 cm diameter channel with a long calming section.

LIST OF TABLES

Table:

- 2.1 Values used for calculation of the diffusion coefficient
- 2.2 Mass transfer values for parabolic velocity distribution and constant wall concentration
- 2.3 Summary of available formula in the literature for prediction of the mass transfer coefficient

- 3.1 Variables in the mass transfer study for the high temperature oxidation of graphite
- 3.2 Helium data at 20 atm
- 3.3 Nitrogen data at 20 atm

- 6.1 Mass transfer coefficient for different Re in laminar helium flow with a long calming section 0.6 cm in diameter
- 6.2 Mass transfer coefficient for different Re in turbulent He flow with a long calming section 0.6 cm in diameter
- 6.3 Mass transfer coefficient for different Re in turbulent N₂ flow with a long calming section 0.6 cm in diameter
- 6.4 Mass transfer coefficient as function of Re in non established laminar helium flow with a sharp edge entrance in a 0.36 cm channel
- 6.5 Mass transfer coefficient as function of Re in He flow with a short calming section $(\frac{x_0}{d})$ in 0.36 cm diameter channel

Table:

- 6.6 Mass transfer coefficient as function of $\frac{x}{d}$ in non established laminar helium flow (Re 1382) with a sharp edge entrance in 0.36 cm diameter channel
- 6.7 Average mass transfer coefficient as function of $\frac{x}{d}$ in non established turbulent helium flow with a sharp edge entrance in a 0.36 cm diameter channel
- 6.8 Average mass transfer coefficient as function $\frac{x}{d}$ in non established turbulent helium flow with a bellmouth entrance in a 0.36 cm diameter channel
- 6.9 Average mass transfer coefficient as function of $\frac{x}{d}$ in non established turbulent nitrogen flow with a sharp edge entrance 0.36 cm diameter channel
- 6.10 Cases under which mass transfer has been measured

LIST OF SYMBOLS AND ABBREVIATIONS

a	Ratio of the velocity at the edge of the boundary layer to the velocity in the free stream $= \frac{u}{u_{\infty}}$	
A	Avogadro number	
a_i	Symbol for $\frac{C \cdot P \cdot S_v}{C O_2 + C O}$ at the location i	
b	Ratio between the relative concentration at the edge of the boundary layer to the relative concentration of the free stream	
BET	measurement method of the total surface of a porous sample (external and internal surface)	cm^2
c	mean molecular velocity gas	cm/s
C	concentration of reacting or diffusing species	$mole/cm^3$
C_a	arithmetic mean concentration $C_s = \frac{C_{mo} + C_L}{2}$	$mole/cm^3$
C_A	concentration of substance A	$mole/cm$
C_b	concentration at the edge of the buffer layer	$mole/cm^3$
C_{He}	concentration of helium	$mole/cm^3$
C_i	concentration of species i	$mole/cm^3$
C_L	concentration at the outlet of the sample of length L	$mole/cm^3$
C_l	concentration at the edge of the laminar layer	$mole/cm^3$

C_{lm}	logarithmic mean of the concentration	$\frac{(C_s - C_o) - (C_s - C_L)}{\ln \frac{C_s - C_o}{C_s - C_L}}$	
C_m	bulk concentration or cup-mixing concentration	$C_m = \frac{1}{Q} \int_0^R u.C.2.\pi . r . dr$	mole/cm ³
C_{ma}	local mean concentration	$C_{ma} = \frac{1}{\pi . r^2} \int_0^R C . 2\pi . r . dr$	mole/cm ³
C_o	concentration at the sample inlet		mole/cm ³
c_p	specific heat at constant pressure		cal/g.°C
c.p.s.	count per second		
C_s	concentration at the sample surface		mole/cm ³
C_t	concentration in the turbulent region of the boundary layer		mole/cm ³
c_v	specific heat at constant volume		cal/g.°C
C_∞	concentration in the free stream		mole/cm ³
D	diffusion coefficient		cm ² /s
D_{eff}	effective diffusion coefficient in a porous medium		cm ² /s
D_{AB}	diffusion of substance A through substance B		cm ² /s
D_i	diffusion coefficient of species i		cm ² /s
d	diameter of a tube		cm
E	activation energy of chemical reaction		cal/mole

E_a	apparent activation energy		cal/mole
E	eddy diffusivity		cm^2/s
E_{m0}	eddy kinematic		cm^2/s
E_H	eddy thermal diffusivity		cm^2/s
e	thickness of the sample		cm
f_x	local friction coefficient	$\frac{\tau_w}{\rho_u u^2}$	
\bar{f}_x	average friction coefficient between $x = 0$ and x		
G	mass flow		g./s
Gz	Graetz number for mass transfer	$\frac{4}{\pi} \cdot \frac{G}{\rho \cdot D \cdot L} = \text{Re} \cdot \text{Sc} \cdot \frac{d}{L}$	
Gr	Grashof number	$\left(\frac{L^3 \cdot \rho^2 \cdot g \cdot \beta \cdot T_1}{\mu^2} \right)$	
g	acceleration due to gravity	981	cm^2/s
h^*	dimension factor h , which characterize the transition from zone I to zone II of the graphite oxydation		
h	heat transfer coefficient		$\text{cal}/\text{s} \cdot ^\circ\text{C} \cdot \text{cm}^2$
K	Boltzmann constant	1.38×10^{-16}	$\text{erg}/^\circ\text{K}$
k	heat conductivity		$\text{cal}/\text{cm} \cdot ^\circ\text{C} \cdot \text{s}$
k_c	mass transfer coefficient		cm/s
k_{ca}	mass transfer coefficient calculated on the arithmetic mean concentration basis		cm/s
$k_{c \ln}$	mass transfer coefficient calculated on the logarithmic mean concentration basis		cm/s

k_m	reaction rate constant per unit mass	$\frac{\text{mole}}{\text{g.s.}(\text{mole}/\text{cm}^3)}$	=	$\frac{\text{cm}^3}{\text{g.s.}}$
k_s	reaction rate per unit B.E.T. surface			cm/s
$k_{so} - k_{mo}$	frequency factor of the reaction rates			
k_{expo}	k_x, k_m, k_{exp}			cm/s
k_{ex}	local mass transfer coefficient at the location x			cm/s
k_{ex}	average mass transfer coefficient from $x = 0$ to x			cm/s
$k_{exp I}$	experimental reaction rate constant calculated per unit external area in zone I			cm/s
$k_{exp II}$	experimental reaction rate constant calculated per unit external area in zone II			cm/s
$k_{exp III}$	experimental reaction rate constant calculated per unit external area in zone III			cm/s
$k_{exp xi}$	experimental local reaction rate at the location xi			cm/s
$k_{c \infty}$	mass transfer coefficient in a fully established flow $x \infty$			cm/s
L	characteristic length of a body in a stream; or fully length of a sample			cm
L_p	mean length of pores in a sample			cm
l	mean free path			cm
M	Molecular weight			g/mole
m	mass of the sample			g
\dot{M}	rate of material transferred			mole/sec.
N_p	number of pores per sample			
n	order of a chemical reaction			
N	rate of transfer of moles per unit area			$\text{mole}/\text{cm}^2 \text{ s}$

N_i^*	molar diffusion flux of species i	mole/cm ²
Pr	Prandlt number $\frac{\mu \cdot c_p}{k}$	
Pr_t	turbulent Prandlt number E_{m_0}/EH	
P	pressure	g/cm ²
Q	volumetric flow in the loop	cm ³ /
q	rate of heat transfer	cal/cm ² .
Q_o	leak flow at N.T.P.	cm ³ /s
R	universal gas constant	cal/mole ^t
R	radius of a tube	cm
Re	Reynolds number calculated with the diameter as reference length	
Re_{cr}	critical Reynolds number	
Re_x	Reynolds number calculated with the distance x as reference length	
r	radial distance from the tube axis	cm
\bar{r}	mean radius of pores of one sample	cm
r_{AB}	molecular separation at collision	Å
S	total surface of a porous sample including the internal surface. Also called B.E.T. surface	cm ²
Sc	Schmidt number ν/D	
Sc_t	turbulent Schmidt number E_{m_0}/E_D	
Sr	Sherwood number $\frac{k_c \cdot L}{D}$ or $\frac{k_c \cdot d}{D}$	
s	external geometrical surface of the sample	cm ²
s'	surface of the C ¹⁴ labelled sample	cm ²

$T^{\circ}\text{C}$	temperature in centigrade	$^{\circ}\text{C}$
$T^{\circ}\text{K}$	absolute temperature	$^{\circ}\text{K}$
T_i	temperature at the outlet of the sample	$^{\circ}\text{C}$
T_m	bulk temperature or cu-mixing value	$^{\circ}\text{C}$
T_o	temperature at the inlet of the sample	$^{\circ}\text{C}$
T_s	wall temperature	$^{\circ}\text{C}$
t	time	s.
u	velocity component in the x direction	cm/s
u_l	velocity at the edge of the laminar boundary layer	cm/s
u_m	mean bulk velocity in a pipe $u_m = \frac{Q}{\pi \cdot r^2}$	cm/s
u	velocity component in the x direction in the unperturbed flow	cm/s
u'	fluctuating value of the velocity component in the x direction	cm/s
V_o	volume of gas in the loop reduced at N.T.P.	cm^3
v_{ext}	geometrical volume of a sample	cm^3
V_p	pore volume of a sample	cm^3
v	velocity component in the Y direction	cm/s
v_i	velocity of species i with respect to stationary axis	cm/s
v^*	local molar average velocity	cm/s
v'	fluctuating value of the velocity component in y direction	cm/s
v_{ppm}	volume per million (concentration)	
w	velocity component in the z direction	cm/s
w'	fluctuating value of the velocity component in the z direction	cm/s

x_e	distance from the entrance of a tube at which the boundary layers meet at tube axis	cm
x_{cr}	distance from the leading edge at which the flow becomes turbulent	cm
Y	molar function of reaction product B	
Z	molar function of oxydising impurity	

GREEK SYMBOLS

α	thermal diffusivity $\frac{k}{c_p \cdot \rho}$	cm^2/s
β	coefficient of thermal expansion	$\frac{1}{\text{C}}$
ν	kinematic viscosity	cm^2/s
δ	thickness of the boundary layer	cm
δ_l	thickness of the laminar boundary sublayer	cm
ϵ_{AB}	energy molecular interaction	cm
τ	shear stress in Newtonian flow	gf/cm^2
θ	porosity of sample	
θ	ratio between $\frac{T_m}{273}$ $^{\circ}\text{K}$	
μ	dynamic viscosity	$\text{g}/\text{cm} \cdot \text{s}$
ϕ	heat generated per unit volume unit time by internal friction in a fluid	$\text{cal}/\text{s cm}^3$
ρ	density of the fluid	g/cm^3

SUBSCRIPTS

a	arithmetic mean
A, B	values related to a gas A, B
b	value at the edge of the buffer layer
cr	value related to the critical Reynolds number
D	value related to mass transfer
H	value related to heat transfer
L	value related to the whole length of the sample
l_m	logarithmic mean
l	value at the edge of the laminar boundary layer
m	mean value or bulk value
m	value related to mass
m_0	value related to momentum transfer
o	inlet value or initial value or standard value
p	value related to the pores
S	value related to B.E.T. surface
s	values at the wall (surface)
T	value in the turbulent core
x	location x
\bar{x}	average value from inlet to location x

LIST OF REFERENCES

- 1.1 LOHRISCH, W.,
Forschungsarb. a.d. Geb. d. Ingenieurwes. No. 322, 46; (1929)
- 1.2 PERRY, R.L.,
Trans. Am. Soc. Mech. Engrs. 66, 447 (1944)
- 1.3 VALETTE, L. & VAN MASSENHOVE, G.,
Graphite oxidation under irradiation by tracers of CO₂ in a high pressure helium carrier gas. Dragon Project Report D.P.R.-No. 352 (1965)
- 1.4 BOELTER, L.M.K., et al,
Distribution of heat transfer rate in the entrance section of a circular tube. Nat. Advis. Comm. Aeronaut. Techn. Note 1451 (1948)
- 1.6 DALLE DONNE, M. & BOWDITCH, F.H.,
Experimental local heat transfer and friction coefficients for subsonic laminar transitional and turbulent flow of air or helium in a tube at high temperatures. Dragon Project Report D.P.R.-No. 184 (1963)
- 1.7 GILLILAND, E.R. & SHERWOOD, T.K.,
Ind. Eng. Chem., 26, 516 (1934)
- 1.8 HASLAM, et al,
Ind. and Eng. Chem., 16, 1224 (1929)
- 2.1 WALKER, P.L. et al,
Gas Reactions of Carbon. Advance in Catalysis, XI, 133-221, (1959), Academic Press Inc., New York
- 2.2 POINTUD, M.L. & VALETTE, L.,
Research and Development Division, sixth semi-annual report-Chapter 3, Dragon Project Report D.P.R.-No. 235
- 2.3 WHEELER, AHLBORN.,
Reaction rates and selectivity in catalyst pores. Advance in Catalysis III, 250-327 (1951), Academic Press Inc., New York
- 2.4 WICKE, E.,
Transportprozesse u. chem. Reaktion bei Umsetzungen gasförmig-fest. Accademia Nazionale dei Lincei, V^o Corso Estivo di Chimica - Varese (1960)
- 2.5 BIRD, R., et al,
Transport phenomena. John Wiley & Sons, Inc. New York - London
- 2.6 FICK, A.,
Ann. Phy. 94 (1855) 59 über Diffusion

- 2.7 GLASSTONE, S.,
Textbook of physikal Chemistry, Mac Millan and Co. Ltd., London (1960)
- 2.8 TREYBAL, R.E.,
Mass Transfer Operations. Mac Graw-Hill Book Comp., Inc. New York (1955) p. 17-23
- 2.9 HIRSCHFELD, J.O., et al,
Trans. Am. Soc. Mech. Engrs. 71, 921 (1949)
- 2.10 SHERWOOD, T.K.,
Properties of gases and liquids their estimation and correlation. Mac Graw-Hill
Book Comp., Inc. New York (1958)
- 2.11 DEFAY, R., & PRIGOGINE, I.,
Thermodynamique Chimique. Maison Desoer Editions, Liège (1950)
- 2.12 SCHLICHTING, H.,
Boundary Layer Theory. Mac Graw-Hill Book Comp., Inc. New York (1960)
- 2.13 PRANDTL, L.,
Guide à travers la mécanique des fluides . DUNOD Paris (1952)
- 2.14 POHLHAUSEN, E.,
Zeitschr. angew. Math. Mech. 1, 115 (1921)
- 2.15 ECKERT, E., & DRAKE, R.,
Heat and mass transfer. Mac Graw-Hill Book Comp., Inc. New York (1959) p. 133
- 2.16 PRANDTL, L.,
Zeitschr. angew. Math. und Mech. 5, 136 (1925)
- 2.17 LUDWIEG, G.H.,
Zeitschr. f. Flugwissenschaften 4, 73 (1954)
- 2.18 SHERWOOD, T.K. & WOERTZ, B.B.,
Ind. Eng. Chem. 31, 1034 (1939)
- 2.19 SHERWOOD, T.K. & PIGFORD, R.L.,
Absorption and extraction. Chem. Eng. Series-Mac Graw-Hill Book Comp. (1952)
- 2.20 REYNOLDS, O.,
Proc. Lit. Phil. Soc. of Manchester 14, 1875 (1874)
- 2.21 VON KARMAN, TH.,
Trans. Am. Soc. Mech. Engrs. 61, 705 (1939)
- 2.22 JAKOB, M.,
Heat transfer. 1, John Wiley & Sons Inc., New York (1958) p. 506 and 507
- 2.23 PRANDTL, L.,
Ergebnisse der aerodynam. Versuchsanstalt zu Göttingen Nr. 1, 136 (1921)

- 2.24 NIKURADSE, J.,
VDI-Forschungsheft No. 356 (1932)
- 2.25 REICHARDT, H.,
Zeitschr. angew. Math. und Mech. 20, 297 (1940)
- 2.26 ECKERT, E., & DRAKE, R.,
Heat and mass transfer. Mac Graw-Hill Book Comp., Inc. New York (1959) p. 224
- 2.27 ZAHM, A.F.,
Nat. Advis. Comm. Aeronaut. Rep. 287, p. 185 (1928)
- 2.28 MC ADAMS, W.H.,
Heat transmission. Mac Graw-Hill Book Comp., Inc. New York; Chem.Eng. Series
(1954) p. 126
- 2.29 ECKERT, E., & DRAKE, R.,
Heat and mass transfer. Mac Graw-Hill Book Comp., Inc. New York (1959)p.152;Fig.6.16
- 2.30 BLASIUS, H.,
Zeitschr. f. Math. und Physik 56, 1 (1908)
- 2.31 STANTON, T., & PANNELL, J.R.,
Phil. Trans. Roy. Soc. 214, 199 (1914)
- 2.32 MOODY, L.F.,
Trans. Am. Soc. Mech. Engrs. 66, 671 (1944)
- 2.33 LATZKO, H.,
Zeitschr. f. angew. Math. und Mech. 1, 268 (1921)
- 2.34 GRAETZ, L.,
Annalen d. Physik (N.F.) 25, 337 (1885)
- 2.35 NUSSELT, W.,
Zeitschr. d. Ver. deutsch. Ing. 54, 1154 (1910)
- 2.36 NORRIS, R.H., & STREID, D.D.,
Trans. Am. Soc. Mech. Engrs. 36, 525 (1940)
- 2.37 LEVEQUE, J.,
Annales des mines (12) 13, 201, 305, 381 (1928)
- 2.38 DESMON, L.G. & SAMS, E.W.,
Nat. Advis. Comm. Aeronaut. Mem. E 50 H 23 (1950)
- 2.39 CHOLETTE, A.,
Chem. Eng. Progress 44, 81 (1948)
- 2.40 DREW, T.B. et al,
Trans. Am. Inst. Chem. Engrs. 32, 271-305 (1936)
- 2.41 MARTINELLI, R.C., & BOELTER, L.M.K.,
Ohio Calif. (Berkeley) Publis. Eng. 5, (2) 23-58 (1942)

- 3.1 Metals Handbook. Trans. Am. Soc. Mech. Engrs. (1952) Lyman Taylor (editor)
- 3.2. KEYES, F.G.,
The heat conductivity, viscosity, specific heat and Prandtl numbers for thirteen gases.
(U.S.A.E.C.) PROJECT SQUID TN 37 (1952), New PROJECT REPORT N.P.-No. 4621
- 3.3 MARIEN, P.,
Correlations for calculating the local heat transfer for helium in the turbulent regime.
DRAGON PROJECT Internal Document D.P.R.D.D.-No. 1187 (1964)
- 3.4 TZEDERBER, N., & POPOV, V.,
An experimental Study of thermal conductivity of Helium. Moscow Power Inst. TA58/10-4
(1961)
- 3.5 ZAITSEVA, L.S.,
An Experimental investigation of the heat conductivity of mono-atomic gases over wide
temperature intervals. Physics Faculty of the Moscow Aviation Institute (1958)
- 3.6 STROOM, P.D. et al.,
Helium Prandtl number measurements and calculated viscosity and thermal conductivity.
International Heat Transfer Conference University of Colorado (1961)
- 3.7 LANDOLT - BÖRNSTEIN
Zahlenwerte und Funktionen aus Physik, Chemie, Stronomie, Geophysik und Technik
Band IV Technik 1. Teile: Stoffwerte und mechanisches Verhalten von Nichtmetallen
Berlin -Göttingen-Heidelberg, Springer-Verlag (1955)
- 3.8 NATIONAL BUREAU STANDARDS
Tables of thermal properties of gases circular 564
- 3.9 VALETTE, L., & VAN MASSENHOVE, G.,
Graphite oxidation under irradiation by traces of CO₂ in a high pressure helium carrier
gas. Proceedings of the sec.Industr. Carbon and Graphite Conf.London (7-9 April 1965)
- 3.10 VALETTE, L.,
The gas depletion method. Research and Development Div. 5.semi-annual report
D.P.R.-No. 165, p. 94
- 4.1 VAN MASSENHOVE, G.,
Design of I.P.C.T.L. . C.E.N.-Mol, internal document
- 4.2 CHRISTENSEN, T.B., et al.,
Analysis of trace impurities in helium. DRAGON PROJECT REPORT D.P.R.-No. 241
- 6.1 HALL, G.W.,
The Journal of Mechanical Engineering science (1963) p. 91
- 6.2 COCHO, G.,
These Annexe. Institut mecanique appliqué Université libre de Bruxelles
- 7.1 COULSON, J.M., & RICHARDSON, J.F.,
Chemical Engineering. Vol. 1, 235, Pergamonpress (1959) Oxford
- 7.2 JOTTRAND, R.,
Industrie chimique Belge no. 3 - 1964

THE INFLUENCE OF MASS TRANSFER ON THE KINETIC OF GRAPHITE
OXIDATION BY LOW CONCENTRATION OF OXIDISING
IMPURITIES IN AN INERT CARRIER GAS

by
Léon Jean Valette

I. INTRODUCTION

1.1 General Problem

In an element (solid, liquid or gas) where a concentration gradient of one substance exists a mass transfer is set up, the transport takes place in a direction such as to convey the substance from the higher concentration to the lower concentration.

An interphase mass transfer occur between a gas or a liquid and a solid or liquid. Steady interphase mass transfer exists when one of the phases acts as a source of the transport element, while the other phase acts as a sink of the same element. In this thesis we deal only with a steady interphase transport between gas and solid.

The mass transfer depends on the rate of diffusion of the transported element and on the convective movements established by the flowing gas. In the bulk of the flowing gas the magnitude of the molecular diffusion is very small compared to the "eddy diffusion" process which takes place in a turbulent fluid. The turbulence contributes to a rapid transfer of impurities in the bulk of the fluid whilst the molecular diffusion is responsible for the transport in the interphase laminar boundary sublayer.

Knowledge of the properties of the boundary layer proves, as in the heat transfer studies, to be of paramount importance for the theoretical formulation of the mass transfer rate. The similarity which exists between the heat, momentum and mass transfer is used for theoretical prediction of the rate of mass transfer. On the other hand the analogy which exists between heat and mass transfer has been used experimentally by several workers to find a solution to

difficult cases of heat transfer or to visualize some cases of gas flow [1.1] [1.2]. Fig. 1.1 gives a typical flow picture presented by clouds of ammonia chloride obtained in mass transfer tests by Lohrisch.

Knowledge of the laws governing mass transfer are essential for scientists and engineers working in physical chemistry and chemical engineering. The optimisation of the design of evaporation, dehumidification, distillation, absorption and extraction plants etc... depends on how accurately the rate of transfer of material from one phase to another can be predicted. Similarly, the study of the kinetic of heterogeneous reactions and catalytic processes indicates that the reaction rate can be limited by the rate of transport of the reacting elements. In most cases, when the chemical reaction is part of a production process, the optimum yield can be obtained by designs which eliminate the mass transfer limitations. In some other cases, when the reactions are parasitic, such as corrosion, the mass transfer limitation of the reactions can be beneficial. In any case, a better understanding of the underlying phenomena is required.

1.2 Particular Problem

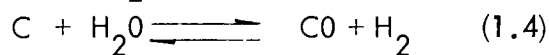
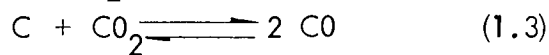
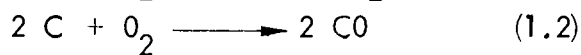
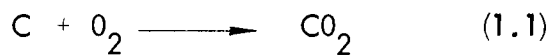
In a high temperature gas cooled nuclear reactor (H.T.G.C.R.) the hot graphite fuel element surface reacts with trace amounts of oxidising impurities contained in the helium coolant. The graphite reaction rate, at the highest temperature in the core, may be mass transfer controlled. The accurate knowledge of the maximum oxidation rate is useful in order to specify the admissible level of corrosive impurities in the primary circuit.

1.2.1 Essential Features of a H.T.G.C.R.

The high temperature gas cooled reactors are being developed in order to take among other, the thermodynamic advantages that a high temperature gas cycle can provide, e.g. high efficiency steam cycle, or the use of gas turbine, direct conversion, etc. The coolant in such reactors reaches temperatures in excess of 750°C . With this high coolant temperature the fuel operates at $1,300^{\circ}\text{C}$ and above. Ceramic fuels and materials, such as uranium carbide and graphite, are used at these high temperatures.

A brief description of the O.E.C.D. DRAGON Reactor experiment will give an idea of the conditions under which the gaseous impurity corrosion problem may occur in a H.T.G.C.R. Fig. 1.2 gives a schematic view of the reactor primary circuit. The uranium (fissile material) carbide fuel consists of ≈ 250 micron diameter particles coated

with alternated layers of impermeable pyrolytic carbon and silicon carbide. These particles are agglomerated together with a carbonised binder to form the fuel cartridges. The cartridges, which are hollow cylinders, are centrally mounted on a fuel spine and are contained in graphite sleeves. The helium coolant flows at 20 atm pressure at high velocity and Re number (15,000) in a trefoil shaped channel between the graphite sleeves. A small amount of the helium is diverted from the main stream and is used as a flushing flow ($Re \approx 80$), for the fission products, in the annular gap between the fuel spine and the fuel cartridges. The maximum temperature of the fuel and the sleeves are respectively as high as $1,600^{\circ}\text{C}$ and $1,200^{\circ}\text{C}$. Although helium is used as coolant and drastic leak tightness specifications are imposed for the primary circuit components, it is expected that impurities like water may leak in from the heat exchangers or may be degassed from the primary circuit components. This water, in contact with the hot graphite under irradiation, will produce gaseous impurities such as O_2 , CO_2 , CO and H_2 . The O_2 is created by radiolysis of CO_2 and H_2O [1.3]. Under the operating temperature of the reactor, following reactions can occur:



Some of these reactions are reversible in the temperature range existing in the reactor primary circuit. Carbon transport will result from the combined effect of corrosion of the high temperature graphite in the core and deposition of carbon on metallic surfaces at lower temperatures. A small concentration of impurities (few volume per million vpm) in the coolant might then be sufficient to cause severe localised attack of the fuel elements and consequently limit the useful life of a fuel charge. In the high temperature range, the oxidation reaction will be limited by the mass transfer of the oxidising impurities in the carrier gas. The investigations carried out, in connection with this study are intended to provide information on the mass transfer limitation of the reaction and are useful for further design work on H.T.G.C.R. power reactors or any other advanced type of high temperature reactor.

1.3 Object of the Thesis

In this thesis we review the literature on graphite oxidation which shows broadly that the graphite oxidation reaction can be divided into three temperature zones. The third of the zones is completely mass transfer controlled.

The theories applicable to mass transfer are derived from boundary layer theories similarly to those applicable to heat transfer. From these theories we derive analytical equations applicable to the flow conditions used in our experiments. The experimental results are correlated to these equations and moreover they are correlated to heat transfer measurements performed by other workers in flow condition similar to those used in our experiment [14], [1.5] [1.6]. The correlation is performed on average mass transfer coefficients measured in laminar and turbulent flow in circular channels with different geometries. The following cases are examined:

- a) Average mass transfer coefficient k_{cx} measured at different distances x from the inlet
 - 1.) in laminar flow with non established velocity and concentration profiles.
 - 2.) in turbulent flow with non established velocity profile and concentration profiles.

- b) Average mass transfer coefficient k_c over the whole length L of the sample.
 - 1.) in laminar flow with established velocity and non established concentration profile.
 - 2.) in laminar flow with non established velocity profile and non established concentration profile.
 - 3.) in turbulent flow with established velocity profile and non established concentration profile.
 - 4.) in turbulent flow with non established velocity and concentration profiles.

In all the experiments heat transfer takes place at the same time as mass transfer. It can be seen from the theory, that at the low concentration of oxidising impurities ($\sim 50 \text{ vpm } O_2$) used in our experiments the mass transfer does not affect the heat transfer. The only correction to be taken into account in the calculation of the mass transfer coefficients relates to the temperature profile created by the heat transfer. This correction is generally achieved by the selection of a suitable reference temperature for calculation of the properties of the gas.

Due to the complexity of the experimental techniques required to measure the mass transfer coefficients by keeping track of the oxidation rate of graphite at high temperature, the ex-

perimental equipment had certain limitations so that it was not possible to measure the very simple cases such as isothermal fully established velocity and concentration profiles. However a good correlation of the experimental and theoretically predicted values obtained in the more complex flow conditions provides a much more convincing argument as to the applicability of the theories on the prediction of mass transfer rates. The main contribution on the experimental side will be made in the laminar flow region because the theoretical expressions are more precisely established and moreover very few experiments for mass transfer in the laminar flow are reported on in the literature [1.7], [1.8].

The experimental data available in the literature for the mass transfer in laminar and in turbulent flow are very scanty compared to those available for heat transfer and in general are not so extensively analyzed.

For the sake of comparison with our results we transpose the experimentally established semi-empirical equations and experimental results for heat transfer to equivalent expressions of mass transfer. This substitution is theoretically justified within some limits. We hope that the good agreement obtained between our measured data and those calculated will strengthen confidence in the extrapolation of the available expression for heat transfer coefficient to any similar case of mass transfer.

2. THEORETICAL DISCUSSION AND REVIEW OF THE RELEVANT LITERATURE

2.1 Graphite Oxidation

Extensive work on graphite oxidation has been reported on in the literature. We restrict our discussion of graphite oxidation to those points which are strictly relevant to the subject of the thesis. Although most of the reported results are not directly applicable to H.T.G.C.R. systems, it is clearly established that the heterogeneous reaction with porous graphite is governed by three main processes:

The chemical rate purely dependent on the mechanism of the chemical reaction.

The diffusion of the oxidising impurities in the pores towards the internal reacting graphite surfaces.

The diffusion of the oxidising impurities through the gaseous boundary layer surrounding the graphite.

Fig. 2.1 represents the three zones of reaction rate of a porous carbon versus temperature [2.1].

2.1.1 Chemical Regime

At lower temperatures when the whole internal surface of the graphite is accessible to the concentration C_m the combustion rate is governed solely by the chemical reaction rate. The rate of combustion per unit external surface can be expressed by:

$$\text{Rate} = k_{\text{exp}_1} \cdot C_m^n \cdot s = k_s \cdot C_m^n \cdot S \quad \text{or} \quad k_{\text{exp}_1} = k_s \cdot \frac{S}{s} \quad (2.1)$$

$$= k_m \cdot C_m^n \cdot m \quad \text{or} \quad k_{\text{exp}_1} = \frac{k_m \cdot m}{s} \quad (2.2)$$

The chemical rate constant is related to the temperature by the Arrhenius equation:

$$k_{\text{exp}_1} = k_{\text{expo}} \cdot e^{-E/RT}$$

$$k_s = k_{s0} \cdot e^{-E/RT} \quad \text{or} \quad k_m = k_{m0} \cdot e^{-E/RT} \quad (2.3)$$

In the above equations :

k_{exp_I}	- Experimental reaction rate constant expressed per unit external area in Zone I	cm/s (for first order reaction)
C_m	- Concentration of impurity in the bulk gas	mole/cm ³
s	- External geometrical surface of the sample	cm ²
k_s	- Reaction rate constant per unit B E T surface	cm/s
R	- Universal gas constant	cal/mole °K
E	- Activation energy	cal/mole
n	- Order of the chemical reaction	
S	- Internal surface of the porous sample or B E T surface	cm ²
k_m	- Reaction rate constant per unit mass	$\frac{\text{mole}}{\text{g.s. (mole/cm}^3\text{)}}$ for first order reaction
m	- Mass of the sample	g

The k_{exp_I} expressed by the equations (2.1) and (2.2) is dependent on the geometrical characteristics of the sample, the surface to volume ratio in particular.

The kinetic measurements are intended to determine the order of the reaction (exponent n), the frequency factor k_{so} and the activation energy E . These values depend on the gaseous reactant and the quality of the graphite (purity and structure). The value of k_s and k_m and consequently k_{exp} varies with burn-off (see Fig. 2.2) and this variation depends on the type of graphite used [2.2]. From this figure it can be seen that by an appropriate pre-oxidation of the sample a region of stable k_{exp} can be reached where useful and accurate measurements can be performed to investigate the influence of the other variables on the reaction rate. The activation energies given in the literature are respectively 80 kcal/mole, 75 kcal/mole, 45 kcal/mole, for the reaction of graphite with CO_2 , H_2O and O_2 [2.1]. In the temperature and concentration range (above 900°C with 500 μ atm O_2) of interest to this study the reaction rates are first order.

2.1.2 In Pore Diffusion Regime

At higher temperature a concentration gradient of the oxidising impurity is established in the porous material because the rate of depletion of the oxidising impurity must be counter balance by the diffusion of this impurity into the pores. In this zone the reaction rate per unit external surface area has an apparent activation energy half of the true chemical activation energy.

The theory of in-pore diffusion is developed from the calculation of the rate of reaction in a single pore which is then extrapolated to a porous pellet [2.3] [2.4]. The concentration profile (required as a driving force for the reactant) along a single pore is calculated and from this profile the effective reaction rate is obtained. The ratio between the effective reaction rate and the reaction which would occur if a uniform concentration C_m existed in the pore gives the "utilisation factor". The transition between zone I and zone II is considered to occur in the temperature range where this utilisation factor becomes smaller than 0.9.

The rigorous treatment for a single pore is extended to the practical case of graphite pellets which is assumed to be a bundle of N_p pores of mean radius \bar{r} and the mean length L_p . In the model of the porous material, the number of N_p of pores, their length L_p and the radius \bar{r} , are related to the porosity (θ), the geometrical volume (v_{ext}) the geometrical surface (s), the pore volume (V_p) and the B E T (S) of the pellet. The expression of the rate per pellet is obtained by substituting N_p , L_p and \bar{r} by their expression as function of (θ , \bar{r} , v_{ext} , V_p , S) in the rate equation for a single pore multiplied by N_p , the expression of $k_{exp II}$ (Experimental reaction rate constant expressed per unit external area in zone II) obtained is:

$$k_{exp II} = \sqrt{\frac{2 \cdot k_s \cdot Deff \cdot \theta}{\bar{r}}} \cdot \tanh(h^*) \quad (2.4)$$

$$\text{with } h^* = L_p \cdot \sqrt{\frac{2 \cdot k_s \cdot \theta}{Deff \cdot \bar{r}}} \quad (2.5) \quad h^* \text{ is a dimensionless factor whose}$$

value is used to characterize the transition from zone I to zone II.

In the equation (2.4) and (2.5) D_{eff} is the effective diffusion coefficient in the porous material which is a fraction of the bulk gaseous diffusion coefficient D . The Tortuosity factor of a porous material can be defined as the ratio of the bulk gaseous diffusion and the D_{eff} in the porous material. In the material with very fine pores (of the same order of magnitude as the mean free path of the gas) the D_{eff} includes also the diffusion resulting from the Knudsen or molecular flow.

For $h^* < 1$, ($\tanh^* = h^*$), the equation (2.4) reduces to $k_{exp} = -k_s \frac{S}{r}$ (2.1)

While for $h^* > 2$ the equation reduces to

$$k_{exp_{II}} = \sqrt{\frac{2 \cdot k_s \cdot D_{eff} \cdot \theta}{r}} \quad (2.6)$$

which is the expression of a reaction

occurring in the in pore diffusion controlled zone.

It may then be seen that for $h^* < 1$ the reaction proceeds in zone I and for $h^* > 2$ the reaction proceeds in zone II. It can also be seen that in that zone II the $k_{exp_{II}}$ is proportional to $e^{-E/2RT}$ which gives an apparent activation energy half of that one of the chemical rate.

From these equation it can be seen that the $k_{exp_{II}}$ is increasing with the square root of the chemical reaction rate k_s , the effective diffusion coefficient D_{eff} and the porosity θ while it is inversely proportional to the square root of the mean pore radius. The values of h^* increases with decreasing D_{eff} and r which means that the transition from zone I to zone II will occur earlier in impermeable graphite (low D_{eff} , and low r)

2.1.3 Mass Transfer Regime

At higher temperature the reaction rate of the graphite becomes very high and the rate determining step becomes the diffusion of the oxidising impurities through the gaseous boundary layer surrounding the sample.

The oxidation rate is then equal to the mass transfer rate and which can be expressed as follows:

$$k_{exp_{III}} \cdot s \cdot C_m = k_{exp_{II}} \cdot s \cdot C_s = k_c \cdot s \cdot (C_m - C_s) \quad (2.7)$$

with

$k_{\text{exp III}}$	- Experimental reaction rate constant per unit external surface area in zone III	cm/s
k_c	- Mass transfer coefficient	cm/s
C_s	- Concentration of oxidising impurity at the surface of the graphite	mole/cm ³

This equation means that the experimental rate measured by taking into account the concentration C_m in the bulk gas is equal to the rate calculated by using the extrapolated rate $k_{\text{exp II}}$ at higher temperature Fig. 2.1 and the actual concentration C_s at the wall

of the reacting graphite. These two rates are equal to the rate of transfer of oxidising impurities to the graphite surface under the concentration gradient $(C_m - C_s)$. The coefficient k_c is nothing else but the mass transfer coefficient of the oxidising impurities through the carrier gas. Introducing in equation (2.7) the expression of $k_{\text{exp II}}$ as defined in

equation (2.4) one obtains the following general equation.

$$k_{\text{exp III}} \cdot s \cdot C_m = s \cdot C_s \cdot \sqrt{\frac{2 \cdot k_s \cdot \text{Deff} \cdot \theta}{\bar{r}}} \cdot \tanh(h^*) \quad (2.8)$$

$$= k_c \cdot s \cdot (C_m - C_s)$$

From equation (2.8) the value of C_s can be calculated

$$C_s = \frac{k_c \cdot C_m}{\sqrt{\frac{2 \cdot k_s \cdot \text{Deff} \cdot \theta}{\bar{r}}} \cdot \tanh(h^*) + k_c} \quad (2.9)$$

Introducing this value of C_s in the first equality of equation (2.7) one obtains:

$$k_{\text{exp III}} = \frac{1}{\frac{1}{\sqrt{\frac{2 \cdot k_s \cdot \text{Deff} \cdot \theta}{\bar{r}}} \cdot \tanh(h^*)} + \frac{1}{k_c}} \quad (2.10)$$

It can be seen that equation (2.10) is the general equation covering the three regimes.

1. If the rate of impurities to the surface is very much higher than the combustion rate

$$k_c \gg \sqrt{\frac{2 \cdot k_s \cdot \text{Deff} \cdot \theta}{\bar{r}}} \cdot \tanh(h^*)$$

which is generally the case at low temperatures and small values of h^* ; equation (2.10) reduces to

$$k_{\text{expIII}} = \sqrt{\frac{2 \cdot k_s \cdot \text{Deff} \cdot \theta}{\bar{r}}} \cdot \tanh(h^*)$$

similar to equation (2.4) which has been shown to be equal to

$$k_{\text{expI}} \text{ for } h^* < 1 \quad \text{and} \quad k_{\text{expII}} \text{ for } h^* > 2.$$

2. On the other hand if the combustion rate is much faster than the rate of transfer of impurities to the reacting surface then

$$k_c \ll \sqrt{\frac{2 \cdot k_s \cdot \text{Deff} \cdot \theta}{\bar{r}}} \cdot \tanh(h^*),$$

which is the case at very high temperatures and high values of h^* ; then equation (2.10) reduces to; $k_{\text{expIII}} = k_c$ which means that at very high temperatures when $C_s \approx 0$ the experimental reaction rate is equivalent to the rate of mass transfer of impurities through the gaseous boundary layer.

In the transition between zone II and zone III the C_s is not zero and the following equation is applicable;

$$k_c = \frac{k_{\text{expIII}}}{1 - \frac{k_{\text{expIII}}}{k_{\text{expII}}}} \quad (2.11)$$

The determination of k_{expII} is required in order to find the mass transfer coefficient.

2.2 Mass Transfer and Diffusion

In the previous chapter we have seen that at high temperatures the reaction rate of oxidation becomes equal to the mass transfer rate of the oxidising impurities to the surface of the reacting graphite.

The process of mass transfer of the oxidising impurity from the bulk of the gas to the graphite surface is the result of molecular diffusion and convective transfer (eddy diffusion).

2.2.1 Molecular Diffusion

The diffusion of a gas is the property by which the gas moves under a concentration gradient in order to annihilate this gradient. If a continuously renewed gas mixture is in contact with a solid wall acting as a sink for one of the components of the mixture, a steady-state diffusion is established between the bulk of the gas and the wall. This steady-state diffusion can be contrasted with the unsteady-state diffusion which results, for instance, when a partition separating two gases is suddenly removed and the gases mix, on which their local concentration changes continuously until the concentration of both components of the gas mixture is even throughout the container. In this study we deal with steady-state diffusion, assuming that the temporary or localized concentration fluctuations are negligible compared to the concentration gradient established between the bulk gas and the graphite walls.

2.2.1.1 Definition of Concentration, Velocities and Mass Fluxes

In this investigation we are interested in finding out the mass flux of one of the species (e.g. oxygen) diffusing through other species towards the reacting graphite surface. In order to define this mass flux we must give the units in which the concentrations are expressed and the reference frame in which the flux is considered [2.5].

In a multi-component system the concentration of the various species may be expressed in different ways. We limit our discussion to the molar concentration C_i which is the number of moles of species i per unit volume of solution.

In a diffusing mixture the various chemical species are moving at different velocities and the purely molecular diffusion process is accompanied by a bulk flow. This can easily be explained by consideration of the simple case of the species A diffusing through stagnant He. Species A is moving in direction y by molecular diffusion under the impulse of the concentration gradient $\frac{d C_A}{dy}$. As the total pressure in the gas mixture is constant, a similar gradient $\frac{d C_{He}}{dy}$ exists in the stagnant He, which will

then force the helium to diffuse in the opposite direction to the diffusing species A. Helium should be stationary and thus a bulk flow must be established in order to counterbalance the tendency of He to diffuse. This bulk flow induces also a net flow of species A which is to be added to the molecular diffusion process, in order to find the total mass flux or mass transfer. We use in the discussion the scalar representation of vectors like $v \cdot N$; this is strictly valid only for an unidirectional transfer.

Let v_i denote the velocity of the i^{th} species, with respect to the stationary coordinate axis. Then for a mixture of n species the local mass average velocity v is defined as:

$$v = \frac{\sum_{i=1}^n \rho_i \cdot v_i}{\sum_{i=1}^n \rho_i} \quad (2.12)$$

Similarly a local molar average velocity v^* may be defined as:

$$v^* = \frac{\sum_{i=1}^n C_i \cdot v_i}{\sum_{i=1}^n C_i} \quad (2.13)$$

Note that $C_i \cdot v^*$ is the local rate at which moles pass through a unit cross section placed perpendicular to the velocity v^* .

One can also define the diffusion velocity of the species i with respect to v^* as

$$v_i - v^*$$

The molar flux of species i is a vector quantity denoting the moles of species i passing through a unit area per unit time. The motion may be referred to stationary coordinates or to the local molar average velocity v^* .

The molar flux relative to stationary coordinates is

$$N_i = C_i \cdot v_i \quad (2.14)$$

The molar flux relative to the molar average velocity v^* is

$$N_i^* = C_i \cdot (v_i - v^*) \quad (2.15)$$

2.2.1.2 Fick's law of Diffusion

The molar rate of transfer in the direction y per unit area due to molecular motion is given by Fick's first law of diffusion [2.6]

$$N_i^* = -D_i \cdot \frac{dC_i}{dy} \quad (2.16)$$

This equation states that the species i diffuses in the direction of decreasing concentration of i , and it is similar to Fourier's equation for heat conduction. In the system of units selected D_i is expressed in cm^2/s .

This Fick's law gives the molar flux relative to the molar average velocity v^* . In this case we are interested in discovering the molar flux relative to the stationary coordinate fixed to the reacting graphite surface.

From equation (2.15) and (2.13) it can be seen that

$$N_i^* = C_i \cdot v_i - \frac{C_i}{C} \cdot \sum_{j=1}^n C_j \cdot v_j \quad (2.17)$$

$$N_i^* = N_i - x_i \cdot \sum_{j=1}^n N_j \quad (2.18)$$

Equation (2.18) means that the molar flux N_i is simply the combination of the molar diffusion flux N_i^* and of the bodily transport of species i due to the local molar flux of the mixture.

2.2.1.3 Diffusion of the Reacting Gas A in the stationary Gas He Accompanied by a Back-Diffusion of the Reaction Product B

In the case at issue in this thesis, the oxidising impurity diffuses towards the graphite, where the reaction products diffuse back to the bulk flow, Fig. 2.3. If the following reactions with the graphite we assumed





One can note from equation (2.18) that the diffusion rate of A towards the graphite is given by

$$N_A = -D_A \frac{d C_A}{dy} + x_A (N_A + N_B + N_{He}) \quad (2.20)$$

On the other hand the stoichiometry of the reaction (2.19) gives

$$n N_A = -N_B$$

This latest equality introduced in equation (2.20) gives

$$N_A [1 - x_A (1 - n)] = -D_A \cdot \frac{d C_A}{dy} + x_A \cdot N_{He} \quad (2.21)$$

For very small values of x_A this equation reduces to

$$N_A = -D_A \cdot \frac{d C_A}{dy} = N_A^* \quad (2.16)$$

In our experiment we have always used small molar fractions of O_2 in He ($5 \cdot 10^{-5}$) and consequently we shall assume throughout the discussion that N_{O_2} is given by equation (2.16).

2.2.2 Diffusion Coefficient

In the previous chapter we have introduced the concept of diffusion coefficient whose unit are $L^2 \cdot T^{-1}$. This coefficient is an expression of a property of the gases of moving under a concentration gradient in order to absorb this gradient.

The diffusion of a gas is related to the molecular velocities in the gas. However, the rate at which the gases are able to diffuse is much smaller than the speed of molecules which is given by [2.7]

$$\bar{c} = \sqrt{\frac{8 RT}{\pi \cdot M}} \quad (2.22) \text{ where } M \text{ is the molecular weight of the gas.}$$

The slow diffusion rate results from the fact that a gas molecule cannot travel a great distance in one direction before colliding with other molecules. The average distance between successive collisions is called to mean free path

$$\ell = \frac{1}{\sqrt{2} \cdot \pi \cdot n \cdot \sigma^2} \quad (2.23)$$

Where n is the number of molecule per unit volume

σ ist the collision diameter

Equation (2.23) can also be written

$$\ell = \frac{R \cdot T \cdot A}{P \cdot \sqrt{2} \cdot \pi \cdot \sigma^2} \quad (2.24)$$

where A is the Avogadro number.

The diffusion is then the resulting displacement in one direction of the gas molecule travelling randomly at high velocity between successive collision. The kinetic theory of the gas lead to the following expression

$$D = \frac{1}{3} \cdot \bar{c} \cdot \ell \quad (2.25)$$

From this equation it can be seen that D increases with 3/2 power of temperature, decreases with 1/2 power of M and is inversely proportional to P and a function of the collision diameter. For the interdiffusion of two gases the properties of both gases must be taken into account for the calculation of D_{AB} .

Hirshfeld, Bird, Spatz, have summarized a method which appears in the following equation for calculating D in the absence of experimental data [2.8] [2.9]

$$D_{AB} = \frac{9.292 \cdot 10^{-3} \left[\frac{1}{M_A} + \frac{1}{M_B} \right]^{1/2}}{P \cdot (r_{AB})^2 \left[f(Kt/E_{AB}) \right]} \quad (2.26)$$

r_{AB} molecular separation at collision
 $(r_A + r_B) / 2$

E_{AB} energy mol. interaction ; erg
 $\sqrt{E_A \cdot E_B}$

$K =$ Boltzmann constant $= 1.38 \times 10^{-16}$ erg/ $^{\circ}$ K

$f(Kt/\epsilon_{AB}) =$ a collision function given by Fig. 2.4

In Figures 2.5 and 2.6 the diffusion coefficient for O_2 in He and N_2 are presented for different temperatures and pressures.

The values used for the calculation are in Table 2.1

In equation (2.26) the term of energy of molecular interaction has been introduced to take care of the intermolecular forces in real gases. According to equation (2.26) the D_{AB} is not dependent on the relative concentration of the two gases present: this coincides with experimental results. The use of values calculated by (2.26) introduces an error of 3% at the most [2.10] [2.11]

2.2.3 Molecular, Momentum and Heat Transfer

A similarity of process exists between heat, momentum and mass transfer. Advantage will be taken later of this similarity of process to develop the theory of mass transfer. We briefly show below the similarity of the expressions defining the three processes. In all three processes, any local concentration of heat, momentum or mass is destroyed by a diffusion of heat, momentum or mass, moreover these processes are very often interconnected and occur simultaneously. For purely molecular transfer the following equations can be used

$$\text{Momentum transfer} - \tau = -\mu \frac{du}{dy} = -\frac{\mu}{\rho} \cdot \frac{d(\rho \cdot u)}{dy} = -\nu \frac{d(\rho \cdot u)}{dy} \quad (2.27)$$

$$\text{Heat transfer} - q = -k \cdot \frac{dT}{dy} = -\frac{k}{C_p \rho} \cdot \frac{d(C_p \cdot \rho \cdot T)}{dy} \quad (2.28)$$

$$\text{Mass transfer} - N = -D \cdot \frac{dC}{dy} \quad (2.16)$$

$\tau =$ shear stress in Newtonian fluid which can be considered the rate of momentum diffusion g_f/cm^2

$\frac{\mu}{\rho} = \nu$ kinetic viscosity can be considered as the momentum diffusion coefficient. From the kinetic theory of gases it can be seen that cm^2/s

$$\mu = 1/3 \cdot \bar{c} \cdot \rho \cdot l$$

consequently $D = \nu$ for a perfect gas. See equation (2.25)

q is the rate of heat transfer $\text{cal/cm}^2 \cdot \text{s}$
 k is the heat conductivity coefficient which from the kinetic theory is calculated as $\text{cal/cm} \cdot ^\circ\text{C} \cdot \text{s}$
 $k = 1/3 \cdot \rho \cdot \bar{c} \cdot \ell \cdot c_v$

$\frac{k}{c_p \cdot \rho}$: is the thermal diffusivity and is comparable to D cm^2/s

$c_p \cdot \rho \cdot T$: is the heat concentration per unit volume in the gas cal/cm^3

The comparison of equation (2.16) (2.27) (2.28) shows that heat transfer, mass transfer and momentum transfer are very similar indeed. By the grouping of the dimensional diffusivity defined above one arrives at the dimensionless number

$$Sc = \frac{\mu}{\rho \cdot D} = \frac{\nu}{D} \quad \text{and} \quad Pr = \frac{\mu \cdot c_p \cdot \rho}{k} = \frac{\mu \cdot c_p}{k}$$

These numbers are very useful in the development of the theory of heat and mass transfer and we will meet them often in the next chapters dealing with the convective mass transfer. For an ideal gas these numbers should be equal to 1 and in practice for gases far from the liquefaction point the values of Sc and Pr do not depart too much from 1.

2.3 Mass Transfer in forced Convection

2.3.1 Introduction

We have seen that in practice to be able to predict the reaction rates in the mass transfer controlled conditions for graphite oxidation it is necessary to find a mass transfer coefficient k_c which can be defined as $\dot{M} = \text{rate} = k_c \cdot s \cdot \Delta C$ or (2.29)

$$N = k_c \cdot \Delta C$$

where: N is the rate of transfer of moles per unit area ($\text{mole/cm}^2 \cdot \text{s}$)

This term k_c is similar to the heat transfer coefficient h defined by the "Newton cooling law"

$$q = h \cdot s \cdot \Delta T \quad (2.30)$$

These equations seem magically simple, but this apparent simplicity is destroyed by the fact that in a flowing gas so many variables which are specific to the flow and diffusion process influence k_c . So that the experimental determination and the theoretical prediction

of the influence of each variable on k_c become very difficult.

It must be theoretically possible to solve the problem of mass transfer without using the mass transfer coefficient k_c . This could be done by using an equation similar to equation (2.16).

$$N = -D \cdot \frac{\Delta C}{\Delta Y}$$

where D is the diffusion coefficient of the reacting agent in the bulk fluid and ΔY the thickness of a layer of fluid in contact with the wall, through which the concentration would change linearly with the distance from the surface. This procedure fails again because the concentration does not change linearly close to the wall but the gradient is concentrated mainly in a thin layer close to the wall and consequently $\frac{\Delta C}{\Delta Y}$ is not known.

The only way of solving the problem of mass flow is to recognize the interconnection of mass transport by molecular diffusion and by convective transport (or mechanical transport in the bulk flow). This brings us to the introduction of two essential concepts "the turbulence and the boundary layer", which will be discussed more extensively later on. In the case of a fast flowing gas the velocities, temperatures and concentrations are equilised by turbulent motions in the bulk of the flow while near the walls a thin boundary layer exists in which the transport of momentum, heat and mass is proceeding by molecular process. The difficulties of all problems of heat and mass transfer by convection are due to this combination of both mechanisms each of them being governed by rather complicated laws. The complete analysis of the problem lead to a system of several differential equations which in practice are difficult to solve. By the introduction of the boundary layer concept, the general differential equations can be simplified and in some cases solution are available. The use of the boundary layer concept and of the methods of similarity introduce other approximate expressions for the mass transfer coefficient which are more accessible to the calculation and serve as a good guide for the experimental investigation and correlation of the results.

In this chapter after reviewing the general methods used in heat transfer (transposed to mass transfer) we shall present the theoretically available formula to be applied in the case of combined mass transfer and flow used in our experimental equipment. Finally we also gather from the literature the semi-empirical expressions applicable to our case.

2.3.2 General Theories and Methods for the Study of Convective Mass Transfer

2.3.2.1 The general differential Equation

2.3.2.1.1 The Differential Equations of the Flow of a Viscous Fluid

The fundamental hydrodynamic equations are based on two of the most general laws of physics i.e. the law of conservation of mass and Newton's law which states that

$$\text{force} = \text{mass} \times \text{acceleration.}$$

By consideration of the balance of forces (inertia, pressure and viscous forces) on an element of incompressible fluid, with constant properties, moving with regard to a stationary coordinate system x, y, z with velocity u, v, w , Navier and Stokes derived the following equations [2.12]

$$\rho \left(\frac{\partial u}{\partial t} + u \frac{\partial u}{\partial x} + v \frac{\partial u}{\partial y} + w \frac{\partial u}{\partial z} \right) = - \frac{\partial p}{\partial x} + \mu \left(\frac{\partial^2 u}{\partial x^2} + \frac{\partial^2 u}{\partial y^2} + \frac{\partial^2 u}{\partial z^2} \right) \quad (2.31)$$

$$\rho \left(\frac{\partial v}{\partial t} + u \frac{\partial v}{\partial x} + v \frac{\partial v}{\partial y} + w \frac{\partial v}{\partial z} \right) = - \frac{\partial p}{\partial y} + \mu \left(\frac{\partial^2 v}{\partial x^2} + \frac{\partial^2 v}{\partial y^2} + \frac{\partial^2 v}{\partial z^2} \right) \quad (2.32)$$

$$\rho \left(\frac{\partial w}{\partial t} + u \frac{\partial w}{\partial x} + v \frac{\partial w}{\partial y} + w \frac{\partial w}{\partial z} \right) = - \frac{\partial p}{\partial z} + \mu \left(\frac{\partial^2 w}{\partial x^2} + \frac{\partial^2 w}{\partial y^2} + \frac{\partial^2 w}{\partial z^2} \right) \quad (2.33)$$

The condition of continuity and conservation of mass must be satisfied

$$\frac{\partial \rho}{\partial t} + \frac{\partial u}{\partial x} + \frac{\partial v}{\partial y} + \frac{\partial w}{\partial z} = 0 \quad (2.34)$$

2.3.2.1.2 The Differential Equations of Heat and Mass Conduction

These equations are derived from energy and mass balance consideration on a stationary volume element located within the flow field.

The energy balance results in

$$\left(\frac{\partial T}{\partial t} + u \frac{\partial T}{\partial x} + v \frac{\partial T}{\partial y} + w \frac{\partial T}{\partial z} \right) = \frac{k}{\rho C_p} \left(\frac{\partial^2 T}{\partial x^2} + \frac{\partial^2 T}{\partial y^2} + \frac{\partial^2 T}{\partial z^2} \right) + \phi \quad (2.35)$$

ϕ being the heat generated per unit time and unit volume by internal friction. For small velocities the temperature changes caused by this internal friction are small and are usually disregarded.

The mass conduction equation is derived in a similar manner and is

$$\frac{\partial C}{\partial t} + u \frac{\partial C}{\partial x} + v \frac{\partial C}{\partial y} + w \frac{\partial C}{\partial z} = D \left(\frac{\partial^2 C}{\partial x^2} + \frac{\partial^2 C}{\partial y^2} + \frac{\partial^2 C}{\partial z^2} \right) \quad (2.36)$$

These general differential equations should provide the solution to any problem of heat and mass transfer in a forced flow.

The exact solutions of these equations is practical only for very few cases (e.g. laminar flow in a tube). But the introduction of the boundary layer concept will in some cases simplify the equations and yield a solution (e.g. flow and heat transfer on flat plate in laminar flow). Moreover these equations will give a guidance for the development of similarity methods which have been successfully used in heat and mass transfer.

2.3.2.2 Concept of Boundary Layer and Definition of the Boundary Layer Equations

If the velocity field is measured in the immediate vicinity of a wall on which a fluid is flowing a steep velocity profile is observed. The velocity begins with a zero value at the wall and increases within a thin layer of thickness δ to the value of the undisturbed stream which occurs at some distance from the body. Outside the boundary layer, the velocity gradient normal to the direction of flow is usually so low that the viscosity effects can be ignored. Hence it can be assumed that each flow can be divided into two regions, namely the boundary layer to which the viscosity effect is confined and the main flow outside the boundary layer which can be considered as frictionless. This concept is essential for the flow, heat and mass transfer calculation and was utilized by L. Prandtl to develop this boundary layer theory (1904) [2.13]

Similarly when mass transfer occurs between a flowing gas and a solid wall a concentration gradient is set up near the wall. Within a small distance from the wall the concentration varies from the value C_s at the wall to nearly the value C_m of the main stream. This small distance δ_c is called "mass transfer boundary layer" by analogy with

the velocity boundary layer. The thickness of both layers is not necessarily the same. For the fluid with $Sc > 1$ the "Velocity boundary layer" is thicker than the "mass transfer layer". In this "layer" the mass transfer occurs only by molecular diffusion.

Boundary layer equations

Prandtl concluded in his paper that in fluids of low viscosity the action of viscosity can be neglected except in a thin layer along the solid surfaces, on this basis he then proceeded to simplify the Navier-Stokes equations applicable in the boundary layer by estimating the order of magnitude of the different term in these equations.

Similarly E. Pohlhausen 1921 simplified the boundary layer energy equation for the flow on a flat plate (two dimensional flow) [2.14]. He assumed that the flow velocities are sufficiently small for the viscous dissipation term to be ignored in the boundary layer energy equation.

With this concept and assuming constant properties of the fluid, constant velocity outside the boundary layer, the complete set of boundary layer equations which describe the combined momentum mass, and energy transport in a two-dimensional steady laminar boundary layer of a two component mixture are simplified to [2.15]

$$\text{Momentum} \quad \rho u \frac{\partial u}{\partial x} + \rho v \frac{\partial u}{\partial y} = \mu \frac{\partial^2 u}{\partial y^2} - \frac{\partial p}{\partial x} \quad (2.37)$$

$$\text{Energy} \quad u \frac{\partial T}{\partial x} + v \frac{\partial T}{\partial y} = \alpha \frac{\partial^2 T}{\partial y^2} \quad (2.38)$$

$$\text{Mass} \quad u \frac{\partial C}{\partial x} + v \frac{\partial C}{\partial y} = D \frac{\partial^2 C}{\partial y^2} \quad (2.39)$$

$$\text{Continuity} \quad \frac{\partial u}{\partial x} + \frac{\partial v}{\partial y} = 0 \quad (2.40)$$

with the following boundary condition

$$\text{at } y = 0 \quad u = 0 \quad v = 0 \quad C = C_s \quad T = T_s$$

$$\text{at } y \rightarrow \infty \quad u = u_\infty \quad C = C_\infty \quad T = T_\infty$$

These equations are known as boundary layer equations and are more easy to handle than equations (2.31) to (2.36).

2.3.2.3 The Momentum and Mass Flow Equations of the Boundary Layer

The laminar boundary layer equations discussed above can be solved for the determination of the characteristics of the boundary layer and the heat and mass transfer coefficients in laminar boundary layers of different shapes.

In some cases however it is much easier to use an approximate method introduced by T_h. von Karman. This method is much simpler and has the advantage of being applicable to situations for which the exact solution is impossible.

The momentum equation is the expression of the equilibrium between the forces of inertia resulting from the change of momentum in an element of fluid near the surface and the external forces which are acting on the surface and within the element of fluid. [2.15]

In a fluid of density ρ and viscosity μ flowing along a surface, a boundary layer of thickness δ is established. The velocity of the fluid in the layer is u at the distance y from the surface and u_∞ outside the boundary layer.

Let us consider the equilibrium of forces on an element Fig. 2.7 of fluid limited by two planes parallel to the surface of the paper, and unit distance apart, the planes 1.2 and 3.4 distance dx apart from each other and the plane 2.4 parallel to the surface at a distance $l > \delta$. The forces acting on the element are the forces due to change of momentum

$$-\rho \cdot dx \cdot \frac{d}{dx} \int_0^l (u_\infty - u) \cdot u \cdot dy + \rho \cdot dx \cdot \frac{du_\infty}{dx} \int_0^l u \cdot dy \quad (2.41)$$

The shear stress at the surface $-\tau_s \cdot dx$

The pressure forces $-\frac{dp}{dx} \cdot dx$

For a flow where the main stream velocity u_∞ remains constant the term $\frac{dp}{dx}$ is negligible and the momentum equation can be written

$$-\rho \frac{d}{dx} \int_0^l (u_\infty - u) \cdot u \cdot dy = \tau_s \quad (2.42)$$

As no assumption has been made as to the nature of the flow during the derivation of the equation, it is applicable to laminar as well as turbulent flow.

The momentum equation can be integrated when the relation between u and y is known.

von Karman has integrated this equation by using an expression for a $u = f(y)$ profile which fulfils the boundary conditions that the experimentally measured profiles are known to fulfil.

The Mass Flow Equation of the Boundary Layer

The consideration of the mass balance in the fluid element contained between the faces (1.2), (2.4), (4.3) and (1.3) of an element fluid as defined above, see Fig. 2.8, leads to "the mass flow equation of the boundary layer"

$$\frac{d}{dx} \int_0^{\delta} u \cdot (C_{\infty} - C) \cdot dy = D \cdot \left(\frac{dC}{dy} \right)_{y=0} \quad (2.43)$$

For the integration, a relation between C and y must be available.

2.3.2.4 Concept of Turbulence and Eddy Diffusivity

Outside the boundary layer the flow may proceed in a turbulent manner, in this region the fluid is flowing in a disorderly manner. On the time average components of the velocity u, v, w are superimposed fluctuating values u', v', w' contributing to the transfer of momentum and mass. The resulting rates of transfer are orders of magnitude larger than the corresponding rates in laminar flow.

O. Reynolds has demonstrated that the transition from laminar to turbulent flow occurs at what is called the critical Reynolds number, Re_{cr}

If one considers the flow along a flat plate a boundary layer is established at the leading edge. The thickness of the boundary layer increases along the plate. At a certain distance x_{cr} corresponding to $Re_{x_{cr}} = \frac{u_{\infty} \cdot x_{cr} \cdot \rho}{\mu}$ the boundary layer becomes turbulent while a laminar sublayer is formed Fig. 2.9. The value of the $Re_{x_{cr}}$ depends on the disturbances existing in the upstream flow and the disturbances created by the leading edge. A closer examination of the flow pattern indicates that an intermediate zone called the "buffer zone" exists between the turbulent boundary layer and laminar sub-layer.

Similar consideration of the flow pattern in tubes indicates that at the entrance of the tube a boundary layer is established in a similar manner to the flat plate Fig. 2.10. The boundary layer presents a zero thickness at the inlet and then increases along the tube. At a certain distance x_e from the entrance, the boundary layers become so

thick that they join on to the axis of the channel. If the boundary layers are laminar at the moment of contact a laminar flow is set up in the tube which presents a parabolic distribution of the velocity. On the other hand, if the boundary layers are turbulent at the moment of contact a turbulent flow is set up in the tube and presents a velocity distribution which is flatter than the profile in laminar flow. In a tube the Re are expressed as function of the mean velocity u_m and the diameter d of the tube. It is found that the flow is turbulent in the channel when

$$Re_{cr} = \frac{u_m \cdot d}{\nu} = 2,300 \text{ to } 3,000$$

Eddy Diffusion

By analogy with the molecular diffusion which is applicable in laminar flow and in stagnant gas, a theory of "eddy diffusion" has been developed in order to interpret the mass transfer which occurs in a turbulent flow. In the turbulent flow, discrete particles of the gas, called eddies, are randomly agitated in all directions, the velocities (u' , v' , w') being superimposed on the average velocity in the flow direction. In the mass transfer process we are merely interested in the eddies travelling perpendicularly to the main flow. Following Prandtl and Taylor [2.16] these eddies travel a distance λ called "mixing length" before losing their identity. These "eddy" can also participate in the processes of transfer, of momentum, heat and mass, if the local velocity, temperature and concentration are not uniform throughout the fluid.

A similar reasoning to that developed for molecular diffusion in the kinetic theory of gases leads to the definition of the turbulence "eddy kinematic viscosity", "eddy diffusion coefficient" and "eddy heat conduction".

The turbulent diffusivity for momentum (E_m), heat (E_H) and mass transfer (E_D) are found to be proportional to $u' \cdot \lambda$. From these diffusivity coefficients the shear stress, the heat and mass transfer in a purely turbulent flow where no viscosity forces exists can be obtained by the following equations similar to (2.16) (2.27) (2.28)

$$\tau = - E_m \cdot \frac{\partial \rho \cdot u}{\partial y} \quad (2.44)$$

$$q = - E_H \cdot \frac{\partial (c_p \cdot \rho \cdot \theta)}{\partial y} \quad (2.45)$$

$$N_A = - E_D \cdot \frac{\partial C_A}{\partial y} \quad (2.46)$$

The ratio of the eddy kinematic viscosity to the eddy thermal diffusivity E_m/E_H is called turbulent Prandtl number, while E_m/E_D is called turbulent Schmidt number. Generally the turbulent Pr_t and Sc_t are considered to be equal to one for the calculation of heat and mass transfer coefficient. The results obtained with this simplified assumption agree with the observed phenomena although Sage and Ludwig [2.17] have shown that Pr_t and Sc_t are not constant and are different from 1. Other values are quoted by Sherwood and Woertz, $Pr_t = 0.7$ to 0.9 and $Sc_t = 0.63$ [2.18] [2.19].

The molecular diffusivity for each fluid depends on temperature alone while the turbulent diffusivity varies with Re and will thus be negligible near the walls and paramount in the bulk of the fluid. The total momentum, heat and mass transfer in all the regions of fluid is given by:

$$\tau = -\left(\frac{\mu}{\rho} + E_M\right) \frac{\partial(\rho u)}{\partial y} \quad (2.47)$$

$$q = -\left(\frac{k}{c_p \cdot \rho} + E_H\right) \frac{\partial(c_p \cdot \rho \cdot T)}{\partial y} \quad (2.48)$$

$$N_A = -(D + E_D) \frac{\partial C_A}{\partial y} \quad (2.49)$$

which is another set of equation which could be used to calculate the heat and mass transfer coefficients.

Woertz has experimentally measured the E_D values of water in CO_2 and He, the values found being 2 orders of magnitude higher than the molecular diffusion coefficients [2.18]

2.3.2.5 Mass Transfer and Fluid Flow Correlation - Method of Exchange of Impulse

In this section similarity relation between different components of the convection process are developed in line with Reynolds [2.20] original idea of proportionality between the velocity and temperature field near a heat exchanging surface. The theories resulting from the use of these similarities is known under the name of impulse theory. As it will be seen later the combination of impulse and boundary layer theories is the most powerful tool available for the study of mass transfer in turbulent flow.

2.3.2.5.1 Impulse Theory

The first attempt due to Reynolds considers the simple situation which occurs in a turbulent flow when an element m of the fluid is transferred from a region of concentration C_∞ and velocity u_∞ to a solid wall of area s with lower concentration C_s and where $u = 0$. [2.20]

If the element m is transferred during the time t the resulting mass transfer rate is:

$$\frac{m}{\rho} \cdot \frac{(C_\infty - C_s)}{t} = - N \cdot s \quad (2.50)$$

and a momentum transfer

$$\frac{m}{t} \cdot u_\infty = \tau_s \cdot s \quad (2.51)$$

where τ_s is the shear stress over the surface s . By eliminating m , s and t from both equations

$$\begin{aligned} \frac{C_\infty - C_s}{\rho \cdot u_\infty} &= - \frac{N}{\tau_s} \\ \frac{N}{C_\infty - C_s} &= k_c = \frac{\tau_s}{\rho \cdot u_\infty} \\ \frac{k_c}{u_\infty} &= \frac{\tau_s}{\rho \cdot u_\infty^2} \end{aligned} \quad (2.52)$$

As it will be seen, the Blasius equation for turbulent flow is:

$$\frac{\tau_s}{\rho \cdot u_\infty^2} = 0,023 \cdot Re^{-0,25} \quad (2.53)$$

Thus

$$\frac{k_c}{u_\infty} = 0,023 \cdot Re^{-0,25} \quad (2.54)$$

which is an expression of the k_c but in this expression the Sc is missing due to the simplifying assumptions used to develop the expression, e.g. the turbulence of the fluid extends to the wall and no physical variation of the fluid exists from the main stream to a position near the wall.

2.3.2.5.2 Combined Impulse and Boundary Layer Theory

In fact a laminar boundary layer (concept introduced by Prandtl) exists between the main flow and the wall. In this boundary layer of thickness δ and where a large velocity gradient exists the transfer process proceeds in line with the molecular process. If we accept the assumption of Taylor and Prandtl that the concentration and the velocity gradient in the gas are such that at the edge of the boundary layer the concentration and the velocity are respectively

$$b \cdot (C_\infty - C_s) = (C_l - C_s) \text{ and } a \cdot u_\infty = u_l$$

where a and b are coefficients smaller than 1 and whose value depends on the velocity and concentration profile in the flowing gas. Now applying the Reynolds analogy for the turbulent portion of the fluid while the molecular diffusion equation is applied in the laminar boundary layer, a better expression of the mass transfer coefficient is arrived at

$$\frac{Sr}{Re \cdot Sc} = \frac{k}{u_\infty} = \frac{\tau}{\rho u^2} \frac{s}{(1 + a(Sc-1))} \quad (2.55)$$

in which the Schmidt number is introduced. The appropriate value of $a = \frac{u_l}{u_\infty}$ will be derived from the knowledge of the velocity distribution in the flowing gas. The same equation was obtained by another method due to von Karman (1939) [2.21] which is developed starting from equation (2.47) (2.48) and (2.49) [2.22]

Although the Prandtl-Taylor expression is already better than the simple Re analogy (good agreement is obtained with Sc up to 2) it is still approximate because it has disregarded the "buffer zone" between the laminar layer and the turbulent zone. A complete knowledge of the concentration profile and velocity profile is required for complete analytical expression of $\frac{k}{u_\infty}$

2.3.2.5.3 Improved Impulse and Boundary Layer Theory - and Universal Velocity Profile for Turbulent Flow in Tube

The above expressions have been derived by assuming the existence of a sharp transition between the turbulent boundary layer and the laminar sub-layer. In practice a gradual decrease of turbulence is observed when the wall is approached.

Semi-empirical expression taking the real velocity profile in a tube have been introduced by Prandtl [2.23], Nikuradse [2.24], Reichardt [2.25] and von Karman. The velocities are made dimensionless by dividing them by the shear stress velocity

$$u^+ = u \cdot \sqrt{\frac{\rho}{\tau_s}} \quad (2.56)$$

The distance from the walls are made dimensionless by

$$y^+ = y \cdot \frac{\sqrt{\tau_s/\rho}}{v} \quad (2.57)$$

The turbulent velocity profile plotted in a $u^+ = f(y^+)$ plot are independent of the Re and is given by Fig. 2.11

in the sublaminar layer

$$u^+ = y^+ \quad (2.58)$$

in the transition zone $5 < y^+ < 30$

$$u^+ = -3.05 + 5 \cdot \ln y^+ \quad (2.59)$$

in the turbulent core $30 < y^+$

$$u^+ = 5.5 + 2.5 \cdot \ln y^+ \quad (2.60)$$

For a rough tube an equation taking into account the relative roughness is available.

Using this velocity profile Th. von Karman derived an expression for k_c taking into account the concentration and velocity gradient in the buffer layer.

We have seen that equations (2.44) and (2.45)

$$\tau = - (v + E_{mb}) \cdot \frac{\partial (\rho \cdot u)}{\partial y} \quad (2.44)$$

$$N_A = - \left(\frac{v}{Sc} + \frac{E}{Sc_t} m_b \right) \cdot \frac{\partial C_A}{\partial y} \quad (2.45)$$

where Sc_t is the turbulent Schmidt number $= \frac{E}{E_{mb}}$ are applicable in the entire zone of the flow. Moreover, as Sc_t is considered equal to 1

$$N_A = - \left(\frac{v}{Sc} + E_{mb} \right) \cdot \frac{\partial C_A}{\partial y} \quad (2.61)$$

The eddy diffusivity E_m can be determined from equation (2.44) when τ and the velocity profile are known.

Introducing this value in (2.61) one can find the concentration field. By using the values given by the universal velocity profile in equation (2.44) the E_m can be determined and the concentration gradient across the various flow zones can be calculated. The concentration gradient across the laminar sub-layer is [2.26]

$$\Delta C_l = N_A \cdot \sqrt{\frac{\rho}{\tau_s}} \cdot 5 Sc \quad (2.62)$$

the buffer layer is

$$\Delta C_b = N_A \cdot \sqrt{\frac{\rho}{\tau_s}} \cdot 5 \ln (5 Sc + 1) \quad (2.63)$$

Across the turbulent core

$$\Delta C_t = N_A \cdot \sqrt{\frac{\rho}{\tau_s}} \cdot \left[\frac{u_\infty}{\sqrt{\tau_s/\rho}} - 5 (1 + \ln 6) \right] \quad (2.64)$$

The whole concentration gradient is obtained by summing up all the three gradients across the three layers

$$C_s - C_\infty = N_A \cdot \sqrt{\frac{\rho}{\tau_s}} \left[\frac{u_\infty}{\sqrt{\tau_s/\rho}} + 5 (Sc-1) + 5 \ln 5 \frac{Sc+1}{6} \right] \quad (2.65)$$

The dimensionless mass transfer coefficient

$$\begin{aligned} \frac{k_c}{u_\infty} &= \frac{N_A}{(C_\infty - C_s) \cdot u_\infty} \\ &= \frac{\tau_s / u_\infty^2}{1 + \sqrt{\tau_s/\rho} \frac{u_\infty^2}{u_\infty^2} \left\{ 5 (Sc - 1) + 5 \ln \left[(5 Sc + 1) / 6 \right] \right\}} \end{aligned} \quad (2.66)$$

When applied to fully developed flow in channel using u_m and Re it yields

$$\frac{k_c}{u_m} = \frac{0.032 \text{ Re}^{-0,25}}{1 + 0.82 \text{ Re}^{-1/8} \left[(Sc - 1) + \ln (5/6 Sc + 1/6) \right]} \quad (2.67)$$

2.3.2.6 Methods of Similarity

Solution for the differential equation (2.31) to (2.36) and even for the simplified equation (2.37) to (2.40) have been found for only few cases. Application of the prin-

principle of similarity to these equations has made it possible to gain a large number of results as well as a clear insight into the complex mechanisms of convective processes. So many variables influence the convective mass transfer coefficient k_c that it is very difficult to determine experimentally the effect of each variable. With dimensional analysis it is possible to find the general form of expressions which depends on few dimensionless groups of the variables only and so simplify the planning of experimental programmes and the correlation of the results.

Different methods have been used to form the dimensional grouping, for a survey of the methods reference can be made to Zahn [2.27] and Mc Adams [2.28]

We only briefly mention the different methods

1. the Rayleigh method, also known as the algebraic method
2. the differential method - which consists in a rearrangement of the differential equations
3. the method based on a consideration of the requirements for geometrical, kinetic and dynamic similarity.

Dimensional analysis is particularly valuable where the mathematical relations are unknown or complex. It should however be kept in mind that the prerequisite for the successful use of the method is to know what quantities are involved in the phenomena studied. The quantities may be determined intuitively but it is safer to start from well known differential equations.

Using the methods of similarity it has been shown that the local mass transfer coefficient at the point $x.y.z$ is described by an equation of the type

$$S_r = f(x, y, z, Re, Sc)$$

where S_r is the Sherwood number $= \frac{k_c x}{D}$

and the average k_c is given by

$$\begin{aligned} S_r &= f(Re, Sc) \text{ this last function being of the type} \\ S_r &= A \cdot (Re)^a \cdot (Sc)^b \end{aligned} \quad (2.68)$$

a and b being exponents to be found experimentally.

The dimensionless numbers which will be used all over the thesis and which are partly used in equation (2.68) are

$\frac{k \cdot x}{D}$	Sherwood number analogous to the Nusselt number in heat transfer	Sr
$\frac{xu \cdot \rho}{\mu}$	Reynolds number	Re
$\frac{\mu}{\rho \cdot D}$	Schmidt number	Sc
$\frac{k}{u} = \frac{Sr}{Re \cdot Sc}$	Equivalent to the Stanton number in heat transfer	St
$\frac{4}{\pi} \cdot \frac{G}{\rho \cdot D \cdot L} = Re \cdot Sc \cdot \frac{d}{x}$	Equivalent to the Graetz number	Gz
$(L^3 \cdot \rho^2 g / \mu^2) \beta \Delta T$	Grashof number	Gr

2.3.3 The Flow on Flat Plates and in Tubes

We have seen that before it is possible efficiently to perform the calculation of convective mass transfer it is essential to know the characteristics of the boundary layer through which the transfer takes place when a fluid is flowing along a surface. These characteristics (mainly the thickness) of the layer can be obtained by solving either the differential equations of the boundary layer equation (2.37) or by solving the momentum equation for the boundary layer (2.42). For the laminar flow on flat plate and in the tube both solutions have been done and are in good agreement. [2.29]

Although in our equipment we are only concerned with flow in tubes, we need the flat plate solution for two reasons

1. in laminar flow with a short inlet section the solution applicable to the flow on a flat plate is also applicable to the flow in a tube as long as the boundary layer thickness is smaller than $\frac{d}{2}$.
- 2- in turbulent flow the solution for fully established flow in a tube can be easily extrapolated from the calculations performed for the flat plate.

2.3.3.1 The Boundary Layer on a Plane Plate in Longitudinal Flow

2.3.3.1.1 The Laminar Portion of the Boundary Layer

The laminar boundary layer equation for a flat plate, at constant pressure and in steady state has been solved by Blasius [2.30]

We give below the development of the momentum equation for the boundary layer (2.42) which gives a solution in good agreement with the exact solution of the laminar boundary layer. For the streamline boundary layer the relation of u as function of y is in line with experimental measurements of the type

$$u = a + by + cy^2 + dy^3 \quad (2.69)$$

with the following boundary conditions

$$u = 0 \quad \text{non-slip condition} \quad \text{at} \quad y = 0$$

$$\frac{\partial^2 u}{\partial y^2} = 0 \quad \text{derived from the boundary layer equation for } y = 0 \quad (2.37)$$

This condition physically means that $(\frac{\partial u}{\partial y})_{y=0} = \text{c s t}$ or that the viscous drag of the fluid must be constant in y direction near the surface.

$$\text{at } y = \delta$$

$$u = u_\infty$$

$$\frac{\partial u}{\partial y} = 0 \quad \text{because the velocity profile should join smoothly the region of } u_\infty = \text{constant at distance } \delta$$

With these conditions the coefficient of the velocity profile equation are found and equation (2.69) becomes

$$\frac{u}{u_\infty} = \frac{3}{2} \cdot \frac{y}{\delta} - \frac{1}{2} \left(\frac{y}{\delta} \right)^2 \quad (2.70)$$

The velocity gradient at the wall is

$$\left(\frac{\partial u}{\partial y} \right)_{y=0} = \frac{3}{2} \cdot \frac{u_\infty}{\delta} \quad (2.71)$$

The shear stress at the wall is

$$\tau_s = \mu \cdot \left(\frac{\partial u}{\partial y} \right)_{y=0} = \frac{3}{2} \cdot \frac{u_\infty}{\delta} \cdot \mu \quad (2.72)$$

with equation (2.70) and (2.72) the momentum equation resolves to

$$\frac{39}{280} \rho \cdot u_{\infty}^2 \cdot \frac{d\delta}{dx} = \frac{3}{2} \cdot \frac{\rho \cdot u_{\infty}^3}{\delta} \quad (2.73)$$

or

$$\delta \cdot d\delta = \frac{140}{13} \cdot \frac{\nu}{u_{\infty}} \cdot dx \quad (2.73)$$

The integration gives

$$\delta = 4.64 \sqrt{\frac{\nu \cdot x}{u_{\infty}}} + \text{const.} \quad (2.74)$$

The integration const = 0 if x is measured from the leading edge.

In dimensionless form

$$\frac{\delta}{x} = \frac{4.64}{\sqrt{Re_x}} \quad (2.75)$$

The local shearing stress at the surface at point x is

$$\tau_s = -\frac{3}{2} \cdot \mu \cdot \frac{u_{\infty}}{\delta} = \frac{0.323 \cdot \rho \cdot u_{\infty}^2}{\sqrt{Re_x}} \quad (2.76)$$

the local friction coefficient defined as $\frac{\tau_s}{\rho \cdot u_{\infty}^2} = f$

$$f = \frac{\tau_s}{\rho \cdot u_{\infty}^2} = \frac{0.343}{\sqrt{Re_x}} \quad (2.77)$$

The average friction factor along a plate is the integrated average

$$f_x = \frac{1}{x} \int_0^x f \cdot dx$$

$$f_x = \frac{0.646}{Re_x} \quad (2.78)$$

N.B. Other friction factors are used in the literature such as Fanning or Darcy friction factor =

$$f' = 2 \cdot \frac{\tau_s}{\rho \cdot u_{\infty}^2} \quad f'' = \frac{8 \cdot \tau_s}{\rho \cdot u_{\infty}^2}$$

2.3.3.1.2 The Turbulent Boundary Layer

In the turbulent boundary layer the velocity profile is much more curved than in the laminar boundary layer and is described fairly well by the equation "Blasius

equation"

$$u = \left(\frac{y}{\delta} \right)^{1/7} \cdot u_{\infty} \quad (2.79)$$

The shear stress is also given by the Blasius expression valid for Re_x not exceeding 10^7

$$\tau_s = 0.0228 \cdot \rho \cdot u_{\infty}^2 \left(\frac{v}{u_{\infty} \cdot \delta} \right)^{1/4} \quad (2.80)$$

By introducing these values of u and τ_s in the momentum equation and solving for δ one obtains

$$\delta = 0.376 \cdot x^{0.8} \cdot \left(\frac{v}{u_{\infty}} \right)^{0.25} + \text{Const.} \quad (2.81)$$

In accordance with Prandtl the expression (2.81) agrees fairly well with the boundary layer thickness measurement if the const. is taken equal to 0, which means that the thickness of the turbulent boundary layer behaves as it begins at the leading edge with a zero thickness. This is only an approximation because the turbulent boundary layer is preceded by a laminar layer which is thinner as well as by a transition zone.

In the dimensionless form (2.81) becomes

$$\frac{\delta}{x} = \frac{0.376}{(Re_x)^{0.2}} \quad (2.82)$$

The laminar sub-layer; for the mass transfer calculation it is necessary to know the thickness of the boundary sub-layer as mentioned in paragraph 2.3.2.5. We calculate first the velocity u_1 at the edge between the sub-layer and the turbulent layer. In the thin sub-layer the shear stress is constant and the velocity profile can be considered as linear. The shear stress is given

$$\tau_s = \mu \cdot \frac{\partial u}{\partial y} = \mu \cdot \frac{u}{y}$$

Introducing the value τ_s from equation (2.80)

$$u = 0.0228 \cdot \rho \cdot \frac{u_{\infty}^2}{\mu} \cdot \left(\frac{v}{u_{\infty} \cdot \delta} \right)^{1/4} \cdot y$$

solving for y and taking into account that

$$\text{for } y = \delta_1 \quad u = u_1$$

$$\frac{\delta_1}{\delta} = \frac{u_1}{u_{\infty}} \cdot \frac{1}{0.0228} \cdot \left(\frac{v}{u_{\infty} \cdot \delta} \right)^{0.75}$$

on the other hand by equation (2.79)

$$\frac{\delta_l}{\delta} = \left(\frac{u_l}{u_\infty}\right)^7$$

Equating both expressions we get

$$\frac{u_l}{u_\infty} = 1.878 \cdot \left(\frac{V}{u_\infty \cdot \delta}\right)^{1/8}$$

By equation (2.81) the value of x can be introduced in the equation

$$\frac{u_l}{u_\infty} = 2.12 \cdot \left(\frac{V}{u_\infty \cdot x}\right)^{0.1} = \frac{2 \cdot 12}{(Re_x)^{0.1}} \quad (2.83)$$

The sub-layer thickness is then

$$\delta_l = \delta \cdot \frac{190}{(Re_x)^{0.7}} = \frac{71.5}{(Re_x)^{0.9}} \cdot x \quad (2.84)$$

It can be seen that δ_l is proportional to $x^{0.1}$ and to $u_\infty^{-0.9}$ thus δ_l increases slowly with x but decreases sharply with u_∞ . Consequently mass transfer will increase rapidly with velocity in the main stream. The local shear stress at the wall is given by

$$\tau_s = \frac{\mu \cdot u_l}{\delta_l} = \frac{0.0296}{(Re_x)^{0.2}} \cdot \rho \cdot u_\infty^2 \quad (2.85)$$

The total friction factor on the plate is obtained by adding the average $f_{\bar{x}}$ in the laminar boundary layer up to x_{cr} and the $f_{\bar{x}}$ of the turbulent layer from x_{cr} to x

$$f_{\bar{x}} = \frac{1}{x_{cr}} \int_0^{x_{cr}} \frac{0.323}{\sqrt{Re_x}} + \frac{1}{x-x_{cr}} \int_{x_{cr}}^x \frac{0.0296}{(Re_x)^{0.2}} \quad (2.86)$$

2.3.3.2 Flow through a Tube

As already pointed out in the inlet section of the tube the boundary layer gradually increases in thickness from the entry point up to the distance x_e where the boundary layers formed at the wall are so thick that they join in the middle of the tube.

Fully developed flow then is obtained.

Along the entrance region the velocity profile is gradually formed. The velocity u_{∞} at the axis gradually increases to reach the value of the established flow.

The properties of the boundary layer in the inlet region in laminar flow can be calculated using the expressions established for the flat plate. For the fully established laminar flow an exact solution of the Navier Stokes equations is possible, and gives the characteristics of the so called Poiseuille flow. For the fully developed turbulent flow the expressions applicable to the flat plate can be used, but the thickness of the boundary layer should be replaced by $\frac{d}{2}$. It is also normal practice to use the average velocity $u_m = \frac{Q \times 4}{\pi \cdot d^2}$ instead of the velocity u_{∞} .

The quasi-stabilization length can be calculated for a laminar boundary layer equation (2.75)

$$\frac{x_e}{d} = 0.0288 \cdot Re \quad (2.87)$$

For a $Re = 3,000$ the whole entrance region is laminar, the entrance length being $\approx 100 d$.

Above the critical Re_{cr} the boundary layer becomes turbulent in the entrance region and thickens more rapidly, so that the entrance length is at first decreased down to $40 d$ in the turbulent flow but then starts to increase again.

2.3.3.2.1 Fully Developed Laminar Flow

By considering the equilibrium between the viscous and pressure forces on a cylindrical element of fluid in a fully developed laminar flow one finds an expression for the $\frac{du}{dr}$ which by integration gives the velocity profile Fig. 2.12

The non-slip condition giving the boundary condition at the wall

$$u = - \frac{d P}{4 \cdot \mu \cdot dx} (R^2 - r^2) \quad (2.88)$$

The velocity thus varies parabolically across the section with the maximum u_m at the axis.

$$u_{\infty} = - \frac{d^2}{16 \mu} \cdot \frac{dP}{dx} \quad (2.89)$$

With this parabolic profile the average velocity is 1/2 the u_{∞}

$$u_m = \frac{Q \cdot 4}{\pi \cdot d^2} = 1/2 u_{\infty} \quad (2.90)$$

The shear stress is

$$\tau_s = 8 \text{ Re}^{-1} \cdot \rho \cdot u_m^2 \quad (2.91)$$

2.3.3.2.2 Fully Developed Turbulent Flow

All the equations expressing the boundary layer characteristics on the flat plate hold true for the flow in a tube if the boundary layer thickness δ and the velocity u_{∞} are replaced by the radius $\frac{d}{2}$ and the velocity at the axis respectively.

The Prandtl seventh power becomes in this case

$$u = u_{\infty} \left(\frac{y}{R} \right)^{1/7} \quad (2.92)$$

The average velocity u_m calculated with such a velocity profile is

$$u_m = 0.82 u_{\infty} \quad (2.93)$$

In practice the mean value is smaller than $0.82 u_{\infty}$ because the seventh power law is not applicable in the laminar sub-layer. If, in the expression of the shear, the velocity profile and the thickness of the sub-layer the values d and u_m are used one obtains from equations (2.82) and (2.85) 2.

$$\tau_s = \frac{0.0384 \cdot \rho \cdot u_m^2}{(\text{Re})^{1/4}} \quad (2.94)$$

$$\frac{u}{u_m} \Big|_{-} = \frac{2.44}{\text{Re}^{1/8}} \quad (2.95)$$

$$\frac{\delta}{d} \Big|_{-} = \frac{63.5}{\text{Re}^{1/8}} \quad (2.96)$$

2.3.3.2.3 Friction Factor in Pipes

For stabilized flow it is experimentally shown that the friction factor is a function not only of Re as discussed in the previous paragraph, but of

$$\frac{\epsilon}{d} \text{ relative roughness of the pipe}$$

$$f = \frac{\tau_s}{\rho \cdot u_m^2} = f \left(\frac{\epsilon}{d} \cdot \frac{u_m \cdot d}{\nu} \right)$$

Stanton and Pannell, and later on Moody [2.31] [2.32] plotted the function $\frac{\tau_s}{\rho \cdot u_m^2}$ as function of Re and the curves obtained for different ϵ/d cover all flow conditions irrespective of the type of the pipe diameter and the velocity. See Fig. 2.13 This graph covers;

- the laminar region $Re < 2000$ and $\tau_s / \rho u_m^2 = 8 Re^{-1}$ as shown by equation (2.91)
- the transition or critical region $2000 < Re < 3000$ is characterized by an instability of the measured $\tau_s / \rho u_m^2$
- the turbulent region $3000 < Re$: the friction factor is a function of Re and ϵ/d ; the curve for a smooth pipe should compare with equation (2.94).
- the quadratic region when the friction factor is independent of Re and is only a function of ϵ/d

2.3.4 Theoretical and Analytical Expression of the Mass Transfer Coefficient

We are interested in finding the analytical expression giving the mass transfer coefficient in the following cases corresponding to tests performed

- a) Local and average mass transfer coefficient in a tube at constant concentration $C_s = 0$
 1. in laminar flow with non established velocity and concentration profile.
 2. in turbulent flow with non established velocity and concentration profile.
- b) Average mass transfer coefficient in a tube at constant concentration $C_s = 0$
 1. in laminar flow with established velocity profile and non established concentration profile.

2. in turbulent flow with established velocity profile and non established concentration profile.

2.3.4.1 Local and Average Mass Transfer Coefficient in a Tube with $C_s = 0$, with non established Velocity and Concentration Profile in Laminar Flow

In the inlet region of a tube, as long as the thickness of the laminar boundary layer is small compared to the radius of the tube the equations of the flow on a flat plate can be used.

We give below the solution of the flow on a flat plate obtained by the integration of the "Mass flow equation of the boundary layer" (2.43). The exact solution of the laminar boundary layer energy equation (2.38) was obtained by E. Pohlhausen in 1921 and is in good agreement with the result of the approach method based on the heat flow equation of the boundary layer. Consequently a similar exact solution of the boundary layer mass equation (2.39) could also be found and the result would be in good agreement with the solution of the "Mass flow equation of the boundary layer".

If one considers a plate in a flow on which mass transfer starts at a distance x_0 from the leading edge, the velocity and mass transfer boundary layer are established as shown in Fig. 2.3 . The following conditions at limit are used

$$\begin{aligned} y = \infty \quad C &= C_{\infty} \quad \text{and} \quad \frac{\partial C}{\partial y} = 0 \\ y = 0 \quad C &= C_s \\ \text{and} \quad D \cdot \left(\frac{\partial C}{\partial y} \right)_{y=0} &= \text{const.} \quad \text{or} \quad \left(\frac{\partial^2 C}{\partial y^2} \right)_{y=0} = 0 \end{aligned}$$

and should fit to a concentration profile of the type

$$C = a + by + cy^2 + dy^3$$

By introducing the relative concentration term

$$\epsilon = C - C_s \quad \text{and} \quad \epsilon_{\infty} = C_{\infty} - C_s$$

one finds the concentration distribution

$$C = \left(\frac{3y}{2\delta_c} - \frac{1}{2} \left(\frac{y}{\delta_c} \right)^3 \right) C_\infty \quad (2.98)$$

with

$$\left(\frac{\partial C}{\partial y} \right)_{y=0} = \frac{3 C_\infty}{2 \delta_c} \quad (2.99)$$

This value of C and u as defined in (2.98) and (2.70) may be introduced in the mass flow equation. It is assumed that the ratio $\sigma = \frac{\delta_c}{\delta} < 1$ and consequently that the integral of equation (2.43) is zero outside the mass transfer boundary layer.

One finds the differential equation

$$\sigma^3 + \frac{4}{3} \cdot x \cdot \frac{d\sigma^3}{dx} = \frac{13}{14} \cdot \frac{1}{Sc} \quad (2.100)$$

The solution of which gives for the boundary conditions

$$\sigma = \frac{1}{\sqrt[3]{Sc}} \cdot \sqrt[3]{1 - \left(\frac{x_0}{x} \right)^{3/4}} \quad (2.101)$$

If the mass transfer starts from the beginning of the plate then

$$x_0 = 0 \quad \text{and} \quad \sigma = \frac{1}{\sqrt[3]{Sc}} \quad (2.102)$$

These calculations have been performed assuming $\sigma < 1$ which is the case for $Sc > 1$

The mass transfer coefficient k_{cx} at the location x can be defined as

$$N_A = k_{cx} (C_s - C_\infty) = -k_{cx} C_\infty \quad (2.103)$$

on the other hand the mass transfer rate per unit area

$$N_A = -D \left(\frac{\partial C}{\partial y} \right)_{y=0} = -\frac{3}{2} \cdot \frac{D}{\delta_c} \cdot C_\infty = -\frac{3}{2} \frac{D}{\sigma \cdot \delta} \cdot C_\infty \quad (2.104)$$

equating (2.103) and (2.104) one finds

$$k_{cx} = \frac{3}{2} \frac{D}{\delta \cdot \sigma} \quad (2.105)$$

Substituting δ and σ by their values in (2.101)

$$k_{cx} = \frac{3}{2} \cdot D \cdot \frac{1}{4.64} \sqrt{\frac{\rho \cdot u_{\infty}}{\mu \cdot x}} \cdot \frac{Sc^{1/3}}{\left(1 - \left(\frac{x_0}{x}\right)^{3/4}\right)^{1/3}} \quad (2.106)$$

or in the dimensionless form

$$Sr_x = \frac{k_{cx} \cdot x}{D} = 0.332 \cdot Sc^{1/3} \cdot Re_x^{1/2} \cdot \frac{1}{\left(1 - \left(\frac{x_0}{x}\right)^{3/4}\right)^{1/3}} \quad (2.107)$$

For $x_0 = 0$

$$Sr_x = 0.332 \cdot Sc^{1/3} \cdot Re_x^{1/2} \quad (2.108)$$

The mass transfer coefficient has an infinite value at the leading edge $x = 0$ where the thickness of the boundary layer is zero, afterwards the k_c value decreases with increasing boundary layer thickness.

The average k_{cx} over the distance x is given by

$$k_{cx} = \frac{1}{x} \int_0^x k_c \cdot dx = 2 k_{cx} \quad (2.109)$$

which means that average mass transfer coefficient from $x = 0$ to x equals twice the value of the local mass transfer coefficient at the distance x

2.3.4.2 Local and Average Mass Transfer Coefficient in a Tube with $C_s = 0$, with non established Velocity and Concentration Profile in Turbulent Flow

Owing to the complicated flow condition the theoretical determination of the mass transfer from a fluid in turbulent flow through a tube is much more difficult than in laminar flow. Latzko [2.33] devoted to the heat transfer problem a thorough theoretical investigation. He started from equations and concepts similar to those of equation (2.47) to (2.49) defined in paragraph 2.3.2.4.

He derived expressions for the heat transfer coefficient in the inlet section of a tube. We will merely transpose the equations to the mass transfer problem.

Two regions have to be distinguished, first: the region where the boundary layer is smaller than $\frac{d}{2}$ and second: the region when $\delta > \frac{d}{2}$.

2.3.4.2.1 For Distances smaller than x_e

(2.110) $\frac{x}{d} < \frac{x_e}{d} = 0.625 \text{ Re}^{0.25}$ where x_e is the establishment length, that is the distance from the inlet to the point where the concentration distribution has attained its fully developed form. The following equation is proposed

$$k_{cx} = 0.0384 \frac{G \cdot 4}{\pi \cdot d^2 \cdot \rho \text{Re}^{0.25}} \times B' = k_{c\infty} \cdot B' \quad (2.111)$$

$$= 0.0384 \frac{u_m}{\text{Re}^{0.25}} \times B'$$

where

$$B' = \frac{1.143 - 0.032\xi + 0.00148\xi^{1.865}}{1.340 (4\xi^2 - 22\xi + 165)^{3/4} \cdot \xi^{1/4} [1 - 0.133 + 0.024\xi^2 + (0.00148\xi^{1.865} - 0.032\xi) \times (0.52\xi - 0.14\xi^2)]}$$

and

$$\xi = \frac{\delta}{R} = 1.41 \cdot \text{Re}^{-1/5} \cdot \left(\frac{x}{d}\right)^{4/5} - 0.048 \cdot \text{Re}^{-2/5} \left(\frac{x}{d}\right)^{8/5} + 0.168 \cdot \text{Re}^{-3/5} \left(\frac{x}{d}\right)^{12/5}$$

ξ as the relative thickness of the boundary layer.

The average mass transfer coefficient between inlet and x is given as $k_{c\bar{x}}$

$$k_{c\bar{x}} = 1.11 \cdot k_{c\infty} \left[\text{Re}^{-1/5} \cdot \left(\frac{x}{d}\right)^{4/5} \right]^{-0.275} \quad (2.112)$$

2.3.4.2.2 For Distances bigger than x_e

$$\frac{x}{d} > \frac{x_e}{d} = 0.625 \text{ Re}^{0.25}$$

$$k_{cx} = 0.0384 \frac{u}{Re^{0.25}}$$

$$x \left[\frac{0.874 \ell - \frac{0.1510}{Re^{0.25}} \cdot \frac{x}{d} + 0.0298 \ell}{0.873 \ell - \frac{0.1510}{Re^{0.25}} \cdot \frac{x}{d} + 0.0068 \ell + \frac{2.844}{Re^{0.25}} \cdot \frac{x}{d}} \right]$$

The corresponding average mass transfer coefficient between inlet and x is given by

$$k_{cx} = k_{c\infty} \left(1 + 0.144 Re^{0.25} \cdot \frac{d}{x} \right) \quad (2.113)$$

2.3.4.3 Average Mass Transfer Coefficient in a Tube with established Velocity Profile and non established Concentration Profile in Laminar Flow

This problem is similar to the one treated by Graetz [2.34] and then by Nusselt [2.35] for the heat transfer. In this case the sample at uniform temperature was assumed to be preceded by a tranquilization length and the parabolic velocity profile was fully established while the gas temperature profile was uniform at the inlet of the sample and different from the tube temperature. A similar reasoning can be performed by replacing the temperature profile by the concentration profile. In our case however both temperature and concentration profiles are established simultaneously but as mentioned earlier the heat transfer profile influence only the mass transfer process by its effect on the gas properties. This is taken care of by selection of the right reference temperature for the calculation.

In this case the differential boundary layer for mass conduction transformed into polar coordinate is

$$u \frac{\partial C}{\partial x} = D \left(\frac{\partial^2 C}{\partial r^2} + \frac{1}{r} \cdot \frac{\partial C}{\partial r} + \frac{\partial^2 C}{\partial x^2} \right) \quad (2.114)$$

This equation can be further simplified owing to the fact that the concentration gradient in the axial direction is negligible, and consequently $\frac{\partial^2 C}{\partial x^2} = 0$.

The u profile is known, see equation (2.88). The solution of this differential equation has been performed by separation of variables, assuming that the concentrations can be

expressed as a product of a function depending only on the radius and another one depending on the axial location. It is found that the concentration-difference C decreases in the axial direction in the same way as an e function. The concentration variation in the radial direction is described by Bessel functions. Fig. 2.14 illustrates the type of concentration profile existing in the entrance region of the tube.

For a constant wall concentration the profile changes in the x direction continuously. In the fully developed region, however, this change occurs in such a way that the profiles at all x stations along the tube are similar to one another and that only the scale changes. Fig. 2.14 shows this condition beyond a value of $(1/Re \cdot Sc) \cdot \frac{x}{d} = 0.05$ or $Gz = 200$.

The analytical expression calculated for the integrated mass transfer up to a distance x of the entrance is given as

$$\dot{M} = \pi r^2 \cdot u_m \cdot C_{\infty} (1 - 0.820 e^{-\beta_0 x} - 0.0972 e^{-\beta_1 x} - 0.0135 e^{-\beta_2 x})$$

$$\text{with } m_n = \frac{\beta_n^2}{2} \cdot \frac{D}{r^2 \cdot u_m} \quad \text{and} \quad \begin{aligned} \beta_0 &= 2.705 \\ \beta_1 &= 6.66 \\ \beta_2 &= 10.3 \end{aligned}$$

\dot{M} - total amount of material mole/s transferred

C_{∞} - concentration at the entrance mole/cm³

The cup-mixing or bulk concentration at any position x is given by

$$\frac{C}{C_o} = 0.820 e^{-\beta_0 x} + 0.0972 e^{-\beta_1 x} + 0.0135 e^{-\beta_2 x}$$

With these elements in hand it is possible to calculate the mass transfer coefficient at any position.

The numerical computation has been performed by R.H. Norris and Al [2.36]

The transposed results for mass transfer are presented in Table 2.2 and Fig. 2.15 in the form of $Sr = \frac{k \cdot d}{D}$ versus the dimensionless factor $\frac{4}{\pi} \times \frac{G}{\rho D \cdot L} = Re \cdot Sc \cdot \frac{d}{L}$, which

is nothing other than the Graetz number.

The numerical values were calculated for $\frac{k_c \cdot d}{D}$ using Graetz's equation up to $Gz = 150$ and for $Gz > 2000$ using Leveque approximation [2.37] (extrapolated from the Leveque solution for a flat plate). For the intermediate values of Gz (150 to 2000) a linear interpolation on the log-log plot was used. This combination corresponding to the following equation

$$Sr = 1.615 Gz^{1/3} = 1.615 Re^{1/3} \cdot Sc^{1/3} \cdot \left(\frac{d}{x}\right)^{1/3} \quad (2.115)$$

is the one which yield the best prediction. The concentration difference used for the calculation is the arithmetic mean concentration difference

$$C_0 - \frac{C_0 + C_L}{2} = C_s$$

The temperature to be used in the calculation should also be

$$T_s = T_0 - \frac{T_0 + T_L}{2}$$

The results of calculation based on the log mean concentration are also presented in table 2.2 and in Fig. 2.15.

$$\text{log mean concentration} = \frac{(C_s - C_0) - (C_s - C_L)}{\ln \frac{C_s - C_0}{C_s - C_L}}$$

In the range of Gz used in the experiment 50 the calculation performed using the log mean temperature should give the same results as the calculation based on the arithmetic mean concentration.

2.3.4.4 Average Mass Transfer Coefficient in a Tube with established Velocity Profile and non established Concentration Profile in Turbulent Flow

In the same paper as already discussed in the paragraphs 2.3.42 Latzko [2.33] derived an equation for the local heat transfer coefficient based on the local mean temperature instead of the cup mixing temperature. The average mass transfer coefficient between inlet and distance x is given by

$$k_{c\bar{x}} = 0.0384 \cdot u_m \cdot Re^{-1/4} \left[1 + 0.067 Re^{0.25} \frac{d}{x} + \frac{d}{x} \left(\frac{0.1}{2.7} \cdot Re^{0.25} \cdot e^{-\frac{2.7}{0.25} \cdot \frac{x}{d}} + \frac{0.9}{29.27} Re^{0.25} \cdot e^{-\frac{29.27}{Re^{0.25}} \cdot \frac{x}{d}} + \frac{0.023}{31.96} Re^{0.25} \cdot e^{-\frac{31.96}{Re^{0.25}} \cdot \frac{x}{d}} \right) \right]$$

which for $\frac{x}{d} > 5$ reduces to

$$\begin{aligned} k_{c\bar{x}} &= 0.0384 \cdot u_m \cdot Re^{-1/4} \left(1 + 0.067 Re^{0.25} \cdot \frac{d}{x} \right) \quad (2.116) \\ &= k_{c\infty} \left(1 + 0.067 Re^{0.25} \cdot \frac{d}{x} \right) \end{aligned}$$

For the case where the calming section preceding the test section is too short to have reached fully established hydrodynamic flow Latzko offers an approximate graphical method which combines, the values calculated with no calming section and with very long calming section.

2.3.4.5 Discussion on the Temperature and Concentration to be used in the Equations for Determination of the Gas Constants

As it can be observed the various formulae proposed for the mass transfer coefficients are calculated either on the basis of local mean concentration in a section

$$C_{ma} = \frac{1}{\pi d^2} \int_{r=0}^r C \cdot 2\pi r \cdot dr \quad (2.117)$$

or cup-mixing concentration

$$C_m = \frac{\dot{M}}{Q} = \frac{1}{Q} \int_{r=0}^r u \cdot C \cdot 2\pi r \cdot dr \quad (2.118)$$

or arithmetic mean concentration

$$C_a = C_s - \frac{C_{mo} + C_{mL}}{2} \quad (2.119)$$

or Log mean concentration

$$C_{lm} = \frac{(C_s - C_{mo}) - (C_s - C_{mL})}{\ln \frac{C_s - C_{mo}}{C_s - C_{mL}}} \quad (2.120)$$

In our experiment, as will be seen, the depletion of impurities is negligible along the channel and consequently $C_{mo} \approx C_{mL}$, which result gives no difference between C_a and C_{lm} . The difference between C_{ma} and C_m might be more significant. But in the non established concentration profile dealt with, it is impossible to calculate this difference and for the purpose of the calculation we only use C_m which is in fact the measured value by the gas analysis equipment.

On the other hand during the mass transfer process heat transfer occurs as well and there the difficulty is to find the right temperature at which the gas properties should be calculated.

We find it logical either to use the bulk temperature which is the average between the cup-mixing temperature at the inlet and outlet of the sample

$$T_m = \frac{T_{mo} + T_{mL}}{2}$$

or the film temperature which we define as the arithmetic mean between the wall temperature and the T_m

$$T_f = \frac{T_s + T_m}{2} = T_s \frac{1 + \frac{T_{mL} + T_{mo}}{2}}{2}$$

The use of this temperature will be discussed in the chapter dealing with the results.

2.3.5 Experimental and Semi-Empirical Values of the Mass Transfer Coefficient

Although some experimental work has been performed by some workers on mass transfer tests aimed at correlation with the theoretical predictions, very few of these experiments reported in the literature can be specifically compared to the flow and temperature condition dealt with in our experiments. We have therefore found suitable experimental results in the heat transfer field and transposed them as if they were obtained in mass transfer tests. In the theoretical approach to the problem we have seen that both processes are similar; we are also trying to correlate our mass transfer results with semi-empirical equation applicable to heat transfer.

Most of the results presented in the literature can be compared to the general formula

$$S_r = A \cdot Re^a \cdot Sc^b \left(\frac{\mu}{\mu_s} \right)^c \cdot f\left(\frac{x}{d}\right) \cdot f(Gr) \quad (2.121)$$

with A, a, b, c constants to be determined experimentally, all the gas properties are introduced at bulk gas temperatures. The three first terms on the right hand side are generally sufficient to take account of the cases of fully established flow with small temperature differences.

This equation is also valid for the flow in the laminar region. For tubes with long calming section, the theoretical equation is of the type

$$S_r = A \cdot (Gz)^n = A' \cdot Re^n \cdot Sc^n \cdot \left(\frac{d}{x}\right)^n \quad (2.121)$$

for the tubes with short calming section

$$S_r = 0.664 \cdot Re_x^{1/2} \cdot Sc^{1/3} \quad (2.109)$$

which could be rewritten

$$S_r = 0.0664 \cdot Re^{1/2} \cdot Sc^{1/3} \cdot d^{1/2} \cdot \left(\frac{d}{x}\right)^{1/2} \quad (2.122)$$

but the use of equation (2.109) in the form (2.122) should be used with caution because it could be misleading.

The corrective terms

$\left(\frac{\mu}{\mu_s}\right)^c$ is introduced to take into account the large temperature gradient which exists between the wall and the gas. Some time this corrective factor is replaced by a factor $\left(\frac{T_s - T_m}{T_s}\right)^c$

For the gases owing to the insensitivity of their properties this correction factor is not too large. It could well be eliminated if the properties introduced in the dimensionless groups were the correct one. Some authors even recommend the use of two temperatures for the calculation, e.g. use of the film temperature for all the properties and to use the bulk temperature for evaluation of the gas velocity [2.38]. The best temperature should be the one which brings the smallest exponent to $(\frac{\mu}{\mu_s})$ corrective factor.

$f(\frac{x}{d})$ takes into account the disturbing effect of the entrance effect.

$f(Gr)$ takes into account the effect of natural convection

This corrective factor is important mainly in the very small laminar flow region.

We present the summary of the information gathered in the literature in table 2.3.

2.3.5.1 The Constant Multiplication Factor A:

For the laminar flow:

short calming section: the only experimental value measured by Jakob and Dow on axial flow along the external surface of a cylinder gives a value 0.663, near enough to the theoretical one 0.664.

long calming section: the value A proposed in the literature varies between 1.42 to 1.8 at the exception of the value proposed by Cholette 0.5 [2.39].

In the turbulent flow:

for the turbulent flow of gases through circular tubes the most commonly proposed value of A is 0.023. More recent values for A have been given which vary from 0.021 to 0.03 [1.5].

The Latzko theoretical value is 0.0384.

2.3.5.2 The Exponent of Re : a

In the laminar region:

short calming section: the coefficient $1/2$ corresponds to the theoretically predicted one

but it must be pointed out that this value has never been measured for flow in tubes but for flow on flat plates only

long calming section: the value of $1/3$ proposed by most of the authors is in good agreement with the curves which fit the theoretical predictions by Graetz [2.34] and Leveque [2.37], only Cholette [2.39] and Drew and Al [2.40] propose a different exponent.

For turbulent flow:

most of the authors agree on a value of $0.75 < n < 0.85$. The value given by Latzko is 0.75

2.3.5.3 The Exponent of Sc : b

Most of the proposed exponents for Sc are between 0.3 and 0.4. The value of $1/3$ being the most proposed. The Schmidt number being small, the resulting error in the wrong choice of b between 0.3 and 0.4 only yield marginal error on the mass transfer coefficient. Latzko proposes an exponent equal to one in his equations and this will yield too high results for $Sc > 1$.

2.3.5.4 The Exponent of $(\frac{\mu_m}{\mu_s})^c$

The term $(\frac{\mu_m}{\mu_s})^c$ is introduced to take into account the large temperature gradient which exists between the gas near the bulk gas. Some time this corrective factor is given under the form $(\frac{T_s}{T_m})^{c'}$. In the literature it is often recommended to neglect this corrective factor for the gases due to the relative unsensitivity of the properties to the temperature. But in the operating conditions where the temperature gradient is great one ought to use this corrective factor. It could be eliminated if the properties of the gas are introduced in the dimensionless groups at the correct reference temperature, some authors even recommend to use two temperatures for the calculations, for example use the film temperature for all the properties and the bulk temperature for evaluation of the gas velocity [2.39]

The recommended exponent by most of the authors for

$$\frac{\mu}{\mu_s} \text{ is } \approx 0.14$$

The recommended exponent for

$$\left(\frac{T}{T_m}\right)$$

in turbulent flow with air, varies, from - 0.25 to - 0.575 while for He it varies from - 0.185 to - 0.73.

Dalle Donne [1.5] who performed heat transfer tests with He and air recommend the use of the corrective factors

$$\left(\frac{T}{T_o}\right)^{-0.255} \text{ for air and } \left(\frac{T}{T_o}\right)^{-0.180} \text{ for He}$$

based on the ratio between the wall temperature and the inlet gas temperature in laminar flow the exponent of $\frac{T}{T_m}$ varies from - 0.30 to 0.13. One can summarize by stating that the discrepancies of the c' coefficient is very large.

2.3.5.5 The function $\frac{x}{d}$

This function is introduced in order to take into account the flow conditions existing at the entrance of a tube.

In the laminar flow

for the short inlet tube: this function for flat plate is included in the $(Re_x)^{1/2}$ term as predicted by the theory, see equation (2.109)

for the long inlet tube: this function is $\left(\frac{d}{x}\right)^{1/3}$ for the region $Gz > 10$.

In the turbulent flow

the corrective factor is introduced under two forms $1 + f_1 \left(\frac{d}{x}\right)$ or $\left(\frac{d}{x}\right)^n$. These two types of function correlate the results well for the small x values but for $x \rightarrow \infty$ the second type of function would yield the absurd result $Nu_\infty = 0$.

2.3.5.6 The Function f (Gr)

This function is introduced mainly in the laminar flow to take into account the effect of natural convection which becomes important at the small flow rate in vertical tubes. Most of formulæ proposed are valid for liquid. The expression developed by Martinelli et al [2.41] is analytically derived and is

$$\frac{k_c \cdot d}{\rho_c \cdot D} = 1.75 F_1 \sqrt[3]{\frac{G}{\rho_c \cdot D \cdot L} + 0.0722 \left(\frac{d}{L} \cdot Gr \cdot Sc\right) F_2}$$

The dimensionless factor F_1 and F_2 are dependent on the ratio $\frac{T_L - T_o}{T_a}$

3. EXPERIMENTAL TECHNIQUES

The objects of the tests is to provide experimental values of the mass transfer coefficient which could be compared with the values predicted by the theoretical and semi-empirical expressions of the previous section.

It is convenient first to consider the experimental variables and available technique for measurement of the mass transfer coefficient before going into a detailed description of the experimental equipment used for the tests. This way of proceeding enables the reader to appreciate the complexity of the problem and the suitability of the equipment to perform the tests.

3.1 Experimental Variables

We have seen from paragraph (2.3.5) that all the formulae for calculation of k_c can be conveniently presented in the following form

$$k_c = A \cdot Re^a \cdot Sc^b \cdot \left(\frac{\mu}{\mu_s}\right)^c \cdot f\left(\frac{x}{d}\right) \cdot f(G_r) \cdot \frac{D}{d}$$

$$k_c = A \cdot \left(\frac{4G\rho}{\pi d\mu}\right)^a \cdot \left(\frac{\mu}{\rho D}\right)^b \cdot \left(\frac{\mu}{\mu_s}\right)^c \cdot f\left(\frac{x}{d}\right) \cdot f(G_r) \cdot \frac{D}{d}$$

which depends on a certain number of "secondary variables" which are the dimensionless grouping Re , Sc , Gr , $\frac{x}{d}$, $\frac{\mu}{\mu_s}$ and on the diffusion coefficient D . On the other hand the variables which are directly available to the experimentalist are the nature of the sample, the geometry (x and d) of the sample, the mass flow rate (G), the temperature (T , T_s), the gas composition (ρ , μ , D) and the pressure (P).

The change of one of these experimental variables may influence more than one of the "secondary variables". Table 3.1 summarises the field of influence of each of the experimental variables. In this table the influence of one of the "experimental variables" (the others remaining unchanged) on each of the secondary variables is indicated in the appropriate column by the property through which the effect occurs. For instance, the gas composition affects the Re by the change of the viscosity μ if the mass flow and the geometry are unchanged.

3.1.1 The Graphite Sample

The type of graphite used does not affect the measured rate of mass transfer, but the chemical reactivity and the pore structure may affect the transition point between the various oxidation regimes as defined in Fig. 2.1. The influence of the presence of catalyst such as Fe, Va and Ni on the frequency factor of one given type of graphite can be seen in Fig. 3.1. For our tests we should use graphite gas reaction rate presenting a transition point to the mass transfer controlled region at a temperature as low as possible to avoid operating at very high temperature. For instance the use of $\text{CO}_2 - \text{C}$ reaction would require a sample temperature 200 to 300° C higher than the ($\text{O}_2 - \text{C}$) reaction to be mass transfer controlled. Another important factor which should be carefully checked is the change in the reactivity of the graphite with burn-off (as seen in Fig. 2.2); this may affect the calculated k_c if the reaction does not proceed far enough in zone III or in the fully mass transferred controlled reaction region.

$$k_c = \frac{k_{\text{exp III}}}{1 - \frac{k_{\text{exp III}}}{k_{\text{exp II}}}}$$

3.1.2 The Geometry of the Sample and of the Test Section

The geometry of the sample influences the Re , Sr , the $f(\frac{x}{d})$ and Gr number by the intermediary of d . We perform tests with 8 mm bore channel housing a sample 6 mm or 3.6 mm in internal diameter. The geometry and the length of the upstream channel influences the local mass transfer coefficient in the non stabilised velocity and concentration profiles.

3.1.3 The Gas Composition

We have selected one reacting impurity O_2 for the tests, but the carrier gas has been changed.

Owing to the small concentration of O_2 used, at the most 1000 μ atm, we use the carrier gas properties in order to calculate the Re , the Sc , the Gz and Gr numbers and the diffusion coefficient. The properties of He used for the calculation are given in table 3.2 and Fig. 3.2. The density values were taken from the "Metals Handbook A.S.M.E." [3.1], the viscosity was

taken from Keyes [3.2], the thermal conductivity and Prandlt number were derived from a private communication by Dr. Marien [3.3] based on several documents [3.4], [3.5], [3.6]. The viscosity values used in the calculation are in good agreement with those obtainable in Landolt-Börstein [3.7] and in ref. [3.3].

The diffusion coefficient has been calculated using equation (2.26) from Hirschfeld et al [2.9].

The Nitrogen properties presented in Table 3.3 and Fig. 3.3 have been taken from the DRAGON Data sheet based on the "Tables of thermal properties of Gases" by The National Bureau of Standards. [3.8]

A comparison of Fig. 2.5 with Fig. 2.6 shows the influence of the gas composition on the Diffusion coefficient of O_2 in the He and N_2 . In Figs. 3.4 and 3.5 one can compare the Re resulting from similar mass flow of He and N_2 in a 6mm diameter channel. The Schmidt number used for the calculation for He and N_2 is 1.704 and 0.528 respectively.

3.1.4 The Flow Rate

The flow rate influences the Re. In Figs. 3.4 and 3.5 the relationship between mass flow rate and Re is given for He and N_2 in a 6 mm diameter channel.

3.1.5 The Temperature

The gas temperature is a very important variable, since it affects the term $\frac{\mu}{\mu_s}$ the Re, the Gr and the diffusion coefficient. In non isothermal tests (gas temperature different from sample temperature) we have seen from paragraph 2.3.4.5, that several choices can be made for the gas temperature, either the film temperature T_f or the bulk temperature T_m . The choice should be made with a view to minimizing the $(\frac{\mu}{\mu_s})^c$ correction factor in equation (2.121). The influence of gas temperature on the diffusion coefficient D and Re for He and N_2 are shown in Figs. 2.5, 2.6, 3.4 and 3.5 respectively.

The sample temperature is less important variable, in our investigation. The main requirement should be that the sample temperature be well above the temperature of transition between zone II and zone III of the graphite oxidation $\sim 700^\circ \text{C}$, for O_2 carbon reaction in 20 atm He. The sample temperature of course affects the T_f the correction factor $(\frac{\mu}{\mu_s})^c$ and the Gr.

3.1.6 The Pressure

The pressure influences the D and the Gr. The effect of pressure on the D is shown in Fig. 2.5 and 2.6. It may be observed that the Sc is not affected by the pressure nor by the temperature change because the influence on ρ and μ is offset by the influence on D .

3.2 Experimental Techniques

Several techniques are available for measuring the graphite oxidation rate. These techniques give experimental rates expressed per unit geometrical surface of the graphite in contact with the gas. The plotting of these rates in an Arrhenius diagram clearly shows the transition between $k_{\text{exp III}}$ and $k_{\text{exp II}}$. Knowledge of these experimental rates leads to the determination of the mass transfer rate by

$$k_c = \frac{k_{\text{exp III}}}{1 - k_{\text{exp III}} / k_{\text{exp II}}}$$

3.2.1 Weight Loss Measurement

The weight loss measurement, in which the weight of sample is determined before and after the test is an obvious technique to be used in the experiments. The reaction rate can be calculated from the weight loss by taking into account the duration of the test, the concentration of the impurity maintained and the surface of the sample. However, this technique suffers from the following drawbacks:

1. The degassing and regassing of the sample can affect the weighing accuracy.
2. The weight loss measurement is affected by the removal of dust by erosion.
3. To reach measurable weight loss the equipment must run for a long period rendering

the experiments time-consuming and also requiring a perfect control of all the variables over long periods.

4. The removal of the sample from a pressurized loop for weighing is a very difficult operation.

Owing to these drawbacks the method is only used occasionally to confirm the accuracy of the gas analysis methods described below. In Fig. 3.6 we give typical a Arrhenius plotting of results obtained in C.E.N. Mol [3.9] for thermal reaction between CO₂, O₂ and graphite. The rates are based on the weight loss measurement. It can be seen that the O₂ carbon reaction enters in zone III at ~ 750° C in 10 atm He.

3.2.2 Gas Analysis Methods

These methods constitute an attractive way of measuring the experimental rates by determining the change in gas composition resulting from the reactions with the graphite. Gas analysis methods can measure instantaneous rates of reaction. From the various gas analysis methods available we have selected the "Multi-pass-depletion method".

The Multi-pass-depletion method

At the high flow rate required for the tests, the gas composition change along the specimen is negligible but one can use the multi-pass-depletion method which consists in the measurement of the rate of disappearance of the oxidising impurity and the build up of the reaction products when the gas is recirculated in a closed loop on the sample. The rate of decrease in the concentration of the oxidising impurities depends on the experimental reaction rate, on the loop volume and on the leak rate out of the loop.

For a reaction of the type



the instantaneous decrease in concentration of the oxidising impurities is given by [3.10]

$$\frac{dZ}{dt} = - \left(\frac{k_{\text{exp}} \cdot s}{V_o} \cdot \frac{P}{\theta_m} + \frac{q_o}{V_o} \cdot dt \right) \cdot Z \quad (3.1)$$

the Instantaneous build-up of the reaction products is given

$$\frac{dY}{dt} = 2 \cdot \frac{k_{\text{exp}} \cdot s \cdot Z}{V_o} \cdot \frac{P_m}{\theta_m} - \frac{q_o}{V_o} \cdot Y \quad (3.2)$$

Z is the molar fraction of the oxidising impurity A

Y is the molar fraction of the reaction product B

V_o is the volume of He in the loop in cm^3 at N.T.P.

q_o is the leak flow in cm^3/s at N.T.P.

s is the reacting surface of the sample in cm^2

k_{exp} is the reaction rate constant cm/s

P_m pressure in atm, and temperature in $^{\circ}\text{K}$ in the reaction chamber

$$\theta_m = \frac{T_m}{T_o}$$

If we define $\alpha = \frac{k_{\text{exp}} \cdot s}{V_o} \cdot \frac{P_m}{\theta_m}$ and $\beta = \frac{q_o}{V_o}$

These differential equations can be solved for the following boundary condition

$$t = t_o \quad Z = Z_o \quad \text{and} \quad Y = 0$$

The solutions are

$$Z = Z_o \cdot e^{-(\alpha + \beta) t} \quad (3.3)$$

and

$$Y = 2 \cdot Z_o \cdot e^{-\beta t} (1 - e^{-\alpha t}) \quad (3.4)$$

The leak flow can be eliminated from the equation by dividing (3.4) by (3.3) and the combined equation is

$$\ln \left(1 + \frac{Y}{2Z} \right) = \alpha t$$

or

$$k_{\text{exp}} = \frac{1}{t} \cdot \ln \left(1 + \frac{Y}{2Z} \right) \cdot \frac{V_o \cdot \theta_m}{s \cdot P_m} \quad (3.6)$$

Parasitic oxidation can occur with the hot structural components of the furnace and the stoichiometric balance of the reaction can be upset. A convenient way of checking the stoichiometry of the reaction is obtained by plotting $\ln \left(1 + \frac{Y}{2Z} \right)$ against t which should give a straight line in the absence of parasitic reactions. Fig. 3.7 gives a typical plot of the concentration of O_2 , CO_2 , CO and count per second (c.p.s.) evolution as function of time in the closed circuit during the reaction rate measurement.

Fig. 3.8 shows a plot of $\ln \left(1 + \frac{Y}{2Z} \right) f(t)$

Y being the concentration of $\text{CO} + 2 \times$ concentration of CO_2 and Z being the concentration of O_2 taken from Fig. 3.7. The points in Fig. 3.8 are on a straight line and indicate that the stoichiometry is correct and the slope of the line gives the value α from which k_{exp} can be calculated. Fig. 3.9 shows a typical Arrhenius plot of the experimental rate obtained in 20 atm He with the gas analysis for the graphite O_2 reaction. It can be seen that the transition between zone II and zone III of the reaction is well marked and occurs at 650° C in a flow regime with $\text{Re} \approx 2.000$.

3.2.3 The Carbon¹⁴ Method

With the C^{14} method the reaction rate is measured by the activity build-up in the circuit as a result of gasification in form of CO^{14} and CO_2^{14} of a C^{14} labelled sample. By suitable calibration a relationship between 'count per sec. (c p s) and the vpm C (Carbon atom) appearing in the gas phase could be established. With this relationship the equations developed for the gas analysis method could be used for the calculation of k_{exp} . The relationship depends on the specific activity of the sample and the efficiency of the counting equipment. The Carbon¹⁴ method allows the continuous measurement of the reaction rate of one specimen (labelled) in the presence of other graphite specimens. However, we have not used the C^{14} method for the calculation of the average mass transfer coefficient for a whole sample. We have only used the method for the determination of local mass transfer coefficient, by measuring the activity build-up created in the loop by a short C^{14} labelled sample which is moved in position along the bigger graphite sample as indicated in Fig. 3.10

The method for calculation of the local mass transfer coefficient is given in Appendix I. The labelling method adopted consists in the equilibration of the graphite sample with C^{14} at high temperature (2000° C) followed by a heat treatment at 2500° C to make the C^{14} distribution more uniform. Details of the technique are given in appendix II. The counting equipment uses a standard scintillation counter with a plastic phosphor in the gas stream.

EXPERIMENTAL EQUIPMENT

In this section we shall deal with the experimental equipment used to measure the mass transfer rate of oxidising impurities in a carrier gas by determining oxidation rate of a graphite sample with or without C^{14} . Firstly, we describe the loop and its various components and then we analyse the performance of the analytical equipment by considering the accuracy of control and measurement of the experimental variables. From this analysis we may determine the expected scatter in the results.

4.1 Experimental Loop

The pressurized carbon transport loop, P.C.T.E., built in Winfrith was designed for tests on graphite oxidation under conditions in which the reaction would be mass transfer controlled. The loop consists of a primary circuit, a purification and gas processing circuit, a gas analytical device and a counting device, and finally, of a water cooling circuit and ancillaries. Fig. 4.1 gives a general flow sheet of the loop which with the legend is self explanatory. Fig. 4.2 gives a general view of the control panel and some major components.

4.1.1 The Primary Circuit

The primary circuit includes the circulating pump (2), the ballast tanks (3), the main flow meter (F.13), the heat exchanger (4), the throttle valve (V.2) which is used to regulate the flow in the purification system. The furnace (1) is mounted on a by-pass of the main primary circuit. With this arrangement it is possible to regulate the flow through the furnace down to very small values while a large flow is maintained in the primary circuit in order to keep a good mixing of the gas needed for the short response time of the gas analysis equipment. The control of the flow passing through the furnace is achieved by the automatic valve AV 6 actuated by the flow controller (F.14). Several gas sample lines and pressure taps are provided in the main circuit and in the furnace as indicated by Fig. 4.1.

4.1.1.1 The Experimental Test Section

Several types of furnaces have been considered and tried out. Finally the thimble heater furnace based on the design produced for the in-pile carbon transport loop in C.E.N., Mol, was selected. [3.°]

4.1.1.1.1 The Thimble Heater MK III

The thimble heater MK III consists of a pressure vessel (20 atm nominal) containing three furnaces in series, Fig. 4.3 and Fig. 4.4. The gas flows upwards in the furnaces and comes down along the pressure vessel which is water cooled. The first furnace is used to pre-heat the gas up to a temperature of 800°C. The second furnace is also a pre-heater where the gas is isothermally stabilised before entering the sample. The third furnace houses the graphite sample. The gas flowing downward along the pressure vessel is cooled down to room temperature before leaving the thimble.

4.1.1.1.2 The First Pre - Heater

The gas flows inside the stainless steel strip, wound into a helical spiral, and is heated by "Joule" effect. The metal strip is notched in such a way as to produce variable resistance along the length of the heater. The resistance decreases towards the outlet end of the pre-heater and so more power is dissipated at the inlet side of the heater where the gas is cold. This arrangement gives the maximum gas temperature for a maximum admissible temperature of the stainless steel. At the maximum power of the furnace, 14 kW 3 g/s of helium can be heated up to 800°C. The stainless steel cannot be run much above 850°C for structural reasons and also for compatibility with the oxidising impurity contained in the gas. By pre-oxidising the heater in air a protective oxide film is formed which reduces the further parasitic uptake of oxygen by the heater during the tests. Unfortunately the protection is never perfect and the pre-heater cannot be used during the depletion tests above 350°C of the inlet gas in the sample. For this reason the isothermal tests were excluded from our programme. The pre-heater and the up going flow are insulated from the downflowing gas by three concentric tubes and two steel thermal shield tubes. One of the thermal shields acts as a return for the current.

4.1.1.1.3 The Second Pre-Heater

The gas coming from the first pre-heater is isothermally stabilised in a silica tube 100 cm long and 6 cm in diameter. The tube is surrounded by a molybdenum wire

wound heater insulated by alumina tubes. The power of the furnace is 8 kW. The gas temperature is measured after the graphite sample. Pressure points are provided at both ends of the stabilisation length and after the sample.

4.1.1.1.4 The Graphite Sample Furnace

The graphite sample is housed in a graphite support tube which distribute evenly along the sample the heat generated by a 2 kW molybdenum wire furnace. The molybdenum wire is electrically insulated by alumina beads and is housed between two concentric ceramic tubes. Several sample arrangements are possible within the space available in the graphite support tube (0.8 cm i.d) depending on the flow condition required for the tests. For the tests with fully established flow a sample 0.8 cm in outer and 0.6 cm in internal diameter is used and the i.d of the sample and of the upstream and downstream tranquilization length are smoothly matched Fig. 4.5 a .

For tests in non stabilized flow two cases have been used:

1. insert a 0.8 cm o.d. and 0.36 cm i.d. sample in the graphite support tube this causes a change in the velocity profile at the point where the mass transfer starts Fig. 4.5 b corresponding to the case $x_o = 0$ and $x = 11$ cm at the end of the sample.
2. insert a 0.36 cm i.d. sample preceded by a 0.36 cm i.d. and 13 cm long stainless steel tube corresponding to the case $x_o = 13$ cm and $x_L = 24$ cm Fig. 4.5 c .

For the investigation relating to the local mass transfer coefficient in non stabilized flow, use is made of a sample which is only partly C^{14} labelled as shown in Fig. 4.5 d . In an attempt to eliminate the effect of the sharp edge or right angle effect created by arrangement Fig. 4.5 d , a bellmouth entrance was used in some cases as shown in Fig. 4.5 e . From the heat transfer point of view the test section can be considered as a section with constant heat input, consequently the gas temperature increases linearly along the furnace. The graphite sample temperature is not directly measured but the graphite holder temperature is measured by three thermocouples embedded in it.

If the graphite sample is 1 cm longer

than the graphite support tube for handling purpose. It may be assumed that the samples' temperature drops rapidly down to approximately the gas temperature in the last centimeter and consequently 10 cm should be considered as the useful length for the calculation of mass transfer rates. We have seen from paragraph 3.1.5 that the acceptable tolerance on the graphite temperature is large as long as one makes sure that the graphite surface is well above the transition temperature between zone II and zone III . ($\sim 650^{\circ}\text{C}$ to 700°C). For this reason the tests have always been performed at a graphite temperature of 950°C .

4.1.1.2 The Heat Exchanger

A heat exchanger is located between the furnace exit and the pump. This heat exchanger is used to drop the gas temperature below 100°C for the protection of the pump.

4.1.1.3 The Gas Circulation

A diaphragm compressor "Corblin" 2 A 30 driven by a fixed speed 3 H.P. motor is used to circulate the gas in the loop. Two oil actuated diaphragm are used, a mild steel one in contact with the oil and a stainless steel one in contact with the gas. This type of circulator represents the advantage of being leak tight but unfortunately it gives a pulsating flow. The pulsation period is 5 cycles / s which is much greater than the minimum period required for the flow to be considered as quasi steady. The oscillations are damped further by the use of surge tanks. The pump will deliver a maximum volumetric flow of $\sim 1\text{ l/s}$ or 3 g/s of He or 21 g/s of N_2 at 20 atm at room temperature.

4.1.1.4 The Surge Tanks

Two of these tanks are fitted in the circuit, one at the inlet and one at the outlet to the pump. Their function is to dampen any oscillation produced in the gas flow due to the pulsating action of the diaphragm. Their volume is large (12 litres each) compared with the total volume of the primary circuit fitted with the thimble MK III (37 litres including the two dump tanks).

4.1.1.5 The Orifice Plates

The primary circuit flow is measured with an orifice plate (F. 13) and a differential pressure cell P 10. The flow through the thimble is also measured with the orifice plate (F. 14) and the d.p. cell P 17 which controls the flow by acting on the automatic valve AV 6. Several size orifice plates are used in (F. 14), giving a wide range of flow. See Fig. 4.6 .

4.1.2 The Helium Processing Circuit

Part of the gas flow is diverted when required to the He processing circuit by opening the valves V 3 and V 4 and throttling the main valve V 2. The He processing circuit eliminates unwanted impurities from the gas and maintains the required level of the impurity to be studied. As the loop was developed to perform oxidation tests with H_2O and CO_2 as well as O_2 in He, the equipment contains some He processing components such as the converter which are not relevant to the work performed with O_2 as impurity. This equipment will only be described briefly. The unwanted impurities are removed by purification plant. The level of required reactant is maintained either by a converter or an injection system.

4.1.2.1 The Purifier

The gas is purified by the "oxidation absorption" method. The purification unit remove the products degassed at the beginning of a run, by the various components of the loop (metals, graphites, ceramics, etc.). The main gases released, CO_2 , CO , H_2O , H_2 , CH_4 , N_2 , O_2 . During the tests the purifier has to cope with the reaction products and the air which leaks in.

The purifier consists of three beds in series:

1. The first bed contains copper oxide in a water-cooled pressure vessel. The bed is heated by a 4 kW "Thermocoax" wire-wound heater. The walls of the pressure vessel are protected by ceramic tube surrounded by a number of concentric steel radiation shields. The CuO , as pellets or wire, at $400^\circ C$ oxidizes H_2 and CO to H_2O and CO_2 . In order to remove O_2 part of the bed is reduced to Cu which at the operating temperature acts as a getter for

the O_2 .

2. The oxidized gases are removed (H_2O and CO_2) in a bed containing "Molecular Sieve" type 5 A at ambient temperature.
3. When He is used as carrier gas the remaining traces of O_2 , N_2 and any residual gases are finally removed by a silicagel trap operating at liquid N_2 temperature. With N_2 as carrier gas this final bed is not used but practice has shown that the gas purity achieved is more than adequate for the tests.

The purification line is fitted with two rupture discs, two flowmeters, one orifice plate for the measurement and control of large flows up to 1 g / s of He at 20 atm and a variable area flowmeter for the small flows (<0.1 g / s). Sampling points are provided after each bed in order to measure their efficiency. A tapping for the vacuum is provided for the regeneration of the beds, and is also used to vacuum down the whole circuit before introducing the carrier gas.

4.1.2.2 The Impurity Make-up System

This circuit is essentially a vessel of known volume which can be evacuated and filled to a known pressure with the desired impurity; when the isolation valves are opened this impurity is swept into the main circuit. The circuit is equipped with the usual instruments for measuring flow and pressure.

4.1.2.3 The Converter

As mentioned earlier, the converter was intended for use in tests with CO_2 and H_2O as oxidizing impurities. The level of oxidizing impurities was then maintained by re-converting the reaction products into the reacting gas.

4.2 Measurement and Control of the Experimental Variables

4.2.1 Temperature:

The temperature measurements in the system can be divided into three groups;

- temperature measurements for safety
- temperature measurement for operational purpose
- temperature measurement for the experiment

In all cases chromel-alumel 1/16" stainless steel sheathed thermocouples are used. These thermocouples with Ti stabilized austenitic stainless steel sheaths are reliable below 1000°C.

4.2.1.1 Temperature Measurement for Safety Purposes

Thermocouples are installed on the pressure vessel to ensure that during operation the vessels and tube walls do not exceed the design temperature. The pressure vessels are designed for the maximum specification of 20 atm at 350°C. During normal operation all the walls are water-cooled and operate at ~50°C. All the safety thermocouples are fitted with shut-off trips, set for a maximum temperature of 200°C, except the one protecting the pump, which is set at 100°C.

4.2.1.2 Temperature Measurement for Operational Purposes

The temperatures of the beds are measured during normal operation and during regeneration. The thermocouples measuring these temperatures are also fitted with shut-off trips. We have, for example:

	<u>Normal Temperature</u>	<u>Shut-off Temperature</u>
CuO	400°C	500°C
Mol Sieve (Regeneration)	350°C	360°C

4.2.1.3 Temperature Measurement for Experimental Purposes

For the purpose of the experiments the temperature of the graphite and of the gas in the reaction furnace must be known. The thermocouples used for this purpose are calibrated and the temperature could be measured within 1°C accuracy. However, the location of the thermocouples in the small space of the reaction chamber and also the very high power

density of the heater and cooling rate of the gas makes it very difficult to have an accurate temperature measurement.

In the thimble MK III, the graphite thermocouples are imbedded in the graphite support tube in order to eliminate the influence of heat conduction along the thermocouple sheath from the furnace. With this arrangement it is expected to have a true reading of the graphite temperature within $\pm 5^{\circ}\text{C}$ at the point of measurement but of course the axial temperature distribution would certainly have a much greater scatter $\pm 30^{\circ}\text{C}$.

The gas thermocouples are protected from the interference of the furnace by radiation shields. It is also anticipated that an accuracy of $\pm 5^{\circ}\text{C}$ can be obtained. One of this thermocouples is installed at the inlet of the stabilization preheater and another gas thermocouple is installed at the outlet of the sample.

We have calculate the possible interference of the stagnation temperature on the gas temperature readings and it can be seen to be negligible.

In the theoretical discussion we have seen that the graphite temperature is important in the chemical and in-pore diffusion regimes, but not in the mass transfer regime. For example, a variation of $\pm 10^{\circ}\text{C}$ results in a change of reaction reate of $\pm 15\%$ for a reaction with 25 kcal/mole activation energy, while in the mass transfer regime the activation energy is zero and the influence of sample temperature variation is negligible.

The gas temperature and the sample temperature influences the $k_{\text{exp III}}$ through their effect on the properties of the gas and on the diffusion coefficient. From Fig. 2.5 it can be seen that at around 800°C an error of $\pm 5^{\circ}\text{C}$ will induce an error in the D of $\pm 0.8\%$ in the estimation of D which can be considered as negligible.

During the tests the graphite temperature is automatically controlled through $\bar{T} \cdot C 10$ and an automatic controller.

4.2.2 The Flow Rate

The flow rate through the various parts of the circuit are measured. For large flow at high pressure we use orifice plates of standard or near-standard designs. The accuracy of these flow measurements can be considered to be $\pm 2\%$. A typical calibration curve for the flow meter F14 with different size orifices is given in Fig. 4.3.

For small flows: where the pressure differences developed in orifice plates are inconveniently small, use is made at 20 atm "Fischer and Porter Ltd." "Variable area flowmeters" of 1/16" and 1/8" sizes. The calibration of these flowmeters is easily done by the soap bubble technique at atmospheric pressure. This calibration corresponds with the calculated values obtained from the data given by the manufacturer.

The influence of the flow measurement on the flow is reflected through its effect on the Re . We have seen that in the mass transfer controlled region the $k_{exp,III}$ was proportional to $Re^{0.83}$ in turbulent flow so an error of $\pm 2\%$ on the flow will yield an error of $\pm 1.76\%$ on the measured mass transfer rate.

4.2.3 The Pressure

The pressure is measured at several points for safety reasons, but it is also measured for experimental purposes in the furnace, near the flowmeters and in the instrument lines.

The commercial instruments available are precise within 1% of their range.

This error of measurement results in an error of 1% on the reaction products measured by the infra-red gas analysers and 1% inaccuracy in the calculation of the diffusion coefficient.

The pressure is controlled in the furnace by an automatic valve AV5 actuated by P3 which admits fresh carrier gas to the system through the purifier.

4.2.4 The Gas Composition

The impurity content of the gas is measured by several instruments. The Hersch cell for O_2 and the gas chromatograph for general purposes are working at atmospheric pressure while

The "Irgas" are operating under 20 atm pressure. Since comprehensive surveys of gas analysis methods are available elsewhere we will not give detailed description of the instruments

4.2.4.1 The "Irgas" (Infra-Red Gas Analyser)

The "Irgas" are used to measure CO and CO₂. They indicate directly the partial pressure of CO and CO₂, the flow rate having no effect and the total pressure very little effect. Sample cells are available for use up to 20 atm pressure and about 80°C.

Sensitivity. The ranges at a total pressure of 20 atm are:

for CO₂ full scale deflection (f.s.d) 50 v.p.m. limit
of detection approximately 0.2 v.p.m.

for CO f.s.d. 60 v.p.m. limit of detection approximately
0.5 v.p.m.

These instruments should be calibrated regularly because they present a zero drift and calibration change. A cross sensitivity between CO and CO₂ can also introduce an error of 1% in the readings.

4.2.4.2 The Hersch Cell

The Hersch cells are used for O₂ detection.

The sensitivity of the instrument is very good and gives a limit of detection of 0.1 v.p.m.

4.2.4.3 The Gas Chromatograph

The gas chromatograph is used to measure the other impurities such as N₂, CH₄, as well as to ensure that the circuit is free of any other gases before the start of the tests.

4.2.5 The Counting Equipment

The counting equipment consists of a standard scintillation counter with a plastic phosphor inserted in an instrument by pass line.

The counting can be performed by measuring directly the activity of CO_2^{14} and C^{14} in the primary circuit gas.

If greater sensitivity is required the gaseous C^{14} can be converted into CO_2^{14} in a small CuO bed and concentrated in a liquid N_2 -cooled trap, the concentrated gas is counted after a certain time interval.

5. OPERATING PROCEDURE

5.1 Introduction

In this section we discuss the way the experimental equipment described in section four is operated taking into account the requirement of the experimental techniques described in section three and based on the experience gained during the commissioning period and calibration runs.

We describe in detail the operation to be done in order to perform O_2 depletion and C^{14} build-up test starting with a fully pressurized and calibrated rig.

Before reaching this stage the loop went through a lengthy and tedious commissioning and calibration period. We only mention for reference the steps of this preoperational period which can be divided into three parts:

- the safety tests
- the calibration tests
- routine checks of equipment

5.1.1 The Safety Tests

Are imposed by the safety committee to ensure that during normal operation as well as under faulty conditions non of the components of the loop runs with pressure and temperature in excess to the design value. The main steps of the safety acceptance are:

Acceptance of loop components, including hydraulic tests, leak tests and radiography of welds and components

Pressure test of the fully assembled loop

Temperature measurement and recording of transient under normal operating condition and under faulty operation of the heater and failure of the cooling gas flow.

5.1.2 The Calibration Procedure

The calibration procedure was established to find out the response of the system to the variation of any of the experimental variables. The main steps were:

- calibration of flowmeter
- calibration of furnaces
- calibration and determination of sensitivity of instruments and counting equipment
- response time of the injection system
- operating performance of the purification system and establishment of the regeneration procedure
- volume measurement of the circuit
- determination of the leak-rate by outleakage and through the instrument
- determination of the compatibility problems between the reagent and the loop's material

5.1.3 The Routine Checks

The routine checks are the checks to be performed before starting a serie of experiments.

They are dictated by experience and one can mention

the leak tightness check

the zero adjustment of instruments

Once the loop is ready to run the three main operations for the performance of a test are

adjustment of the flow

adjustment of the temperature

injections of the impurity.

2 Adjustment of the Flows

During the tests there is flow in various parts of the system, the main loop, the purifier converter, the instruments and the thimble.

5.2.1 The Flow in the Main Loop

The flow in the main loop is maintained as high as possible to ensure a good mixing of the impurities and of the reaction products in the carrier gas. The flow is controlled by the Automatic AVIO and the manual valve V1, they are generally adjusted in order to create a pressure drop of 1.3 atm across the pump.

5.2.2 The Flow in the Purifier Converter

The converter is isolated by the valves VP 25 and VP 27. The pressure drop required to bypass some flow in the purifier is obtained by adjusting the position of the valve V2 in the main circuit. The flow is maintained in the purifier as long as required by acting on VP 24 and VP 20. At all time the valve VP 31 in the bypass line of the impurity make-up tank is open, in order to continuously purge the return line from the purification and injection system; because an interference from impurities trapped in this line has been observed.

5.2.3 The Flow in the Instruments-Line

During the performance of a test the flow from the thimble is continuously monitored by a sample taken to the instruments through VIN 242. The pressure of 19.75 kg/cm^2 is maintained in the "Irgas" by adjusting the valve VIN 53 in the return line. The required flow through the C^{14} counting equipment is obtained by adjustment of the valves VIN 83 and VIN 88.

5.2.4 The Flow and Pressure in the Thimble

The flow in the thimble is adjusted following the requirements of the experimental programme. The required flow is automatically controlled by the combined action of the automatic valve AV 6, the flowmeter F 14 and the pressure transducer P 17. In order to counteract the influence in the thimble of the pressure distribution change along the circuit which results of a change of flow, the inlet valve V 201 to the thimble is kept fully open while the outlet valve V 202 is adjusted in order to maintain a correct pressure. The absolute pressure of 20 atm at the sample location is maintained by the action of the pressure controller P(3) actuated by a signal coming from the reaction chamber through VIN 45 and commanding the injection of clean He in the circuit from the bottle through the automatic valve AV 5 and through the purifier.

5.3 Temperature Adjustment

In practice the gas temperature is raised first to its desired level and then the graphite temperature is increased to reach the $\sim 950^{\circ}\text{C}$.

5.3.1 The Gas Temperature

The first preheater is normally used to preheat the gas up to 200°C and the reading of T 9 is controlled by feedback to the main heater through an autocontrol.

The second preheater is raised to the required power and the reading at T 11 is allowed to stabilize. The flow is then varied over the operating range and the readings of T 11 as function of flow is taken. These readings are considered as the inlet gas temperature to the sample during the tests.

5.3.2 The Graphite Temperature

The graphite heater is then switched on and the power raised in order to reach a temperature such as $\frac{T 8 + T 10}{2} = 950^{\circ}\text{C}$. The power of the heater is controlled by T 10 acting on the automatic control of the graphite furnace.

During the temperature increase and during a certain time the degassed impurities are removed by the purifier.

5.4 The Oxygen Depletion Test and CO , CO_2 and C^{14} Build-up

When the flow, pressure, temperatures are set and the circuit is completely degassed and the instrument calibrated the loop is ready for injection of O_2 and measurement of the reaction rate by O_2 depletion and CO , CO_2 and C^{14} build-up.

The following operations are performed:

Isolate the impurity make-up tank by closing VP 28 and VP 30,

Evacuate the impurity make-up tank by opening VAC 18,

Admit $\sim 1,5$ atm oxygen in the impurity make-up tank by closing VAC 18 and opening VP 29,

Pressurize to 20 atm the impurity make-up tank by closing VP 29 and opening VP 28,

Inject oxygen in the circuit by opening VP 30 after having controlled that the purifier is isolated,

Allow the impurity make-up tank to be purged during 1 minute then close VP 30 and VP 28.

After five minutes take the reading on CO, CO₂, O₂ "Irgas" on the C¹⁴ counting equipment. These readings are repeated at 5 minutes intervals up to 50 minutes elapsed time of test. Twenty minutes after the start of the experiment take a complete set of readings of temperature, pressure, flow etc.

Fig. 3.7 gives a typical set of readings obtained during a test.

6. EXPERIMENTAL RESULTS AND CORRELATION WITH THE THEORETICAL PREDICTIONS

6.1 Experimental Results

We have seen in the theoretical discussion that in all cases the mass transfer coefficient can be predicted by an equation of the type

$$Sr = A \cdot Re^a \cdot Sc^b \cdot \left(\frac{\mu}{\mu_s}\right)^c \cdot f\left(\frac{x}{d}\right) \cdot f(Gr) \quad (2.121)$$

The constants A , a , b , c and the function of the Grashof number $f(Gr)$ depend on the flow conditions and the temperature distribution, while the function $f\left(\frac{x}{d}\right)$ depends on the geometry of the entrance region of the test section. The values of D , Sc , Re and $\frac{\mu}{\mu_s}$ are linked with the nature of the carrier gas. In our experimental programme we have performed tests with different entrance geometries, different carrier gases, namely He and N_2 and different flow conditions. In these different experimental cases, all other conditions being kept constant, we have varied either the flow G (in other words the Re) or the value x or $\left(\frac{x}{d}\right)$.

The entrance geometries used are shown in Fig. 4.5

1. Fig. 4.5 a shows the test section 0.6 cm in diameter preceded by a long calming section of ~ 100 cm giving a $\frac{x}{d} \approx 167$
2. Fig. 4.5 b shows the test section 0.36 cm in diameter preceded by a long section 0.6 cm in diameter and ~ 100 cm long; this geometry creates a "sharp edge entrance"
3. Fig. 4.5 c shows the test section 0.36 cm in diameter preceded by a short calming section 0.36 cm in diameter and 13 cm long ($\frac{x}{d} = 36.2$). The calming section is itself preceded by a long section 0.6 cm in diameter and ~ 87 cm long
4. Fig. 4.5 d consists of an entrance geometry identical to the one shown in Fig. 4.5 b "sharp edge entrance", but it includes a C^{14} sample shown in its first position. With this geometry the C^{14} sample can be moved along the test section, thus making it possible to investigate $k_c = f\left(\frac{x}{d}\right)$
5. Fig. 4.5e shows the 0.36 cm diameter test section preceded by a 0.6 cm diameter tube, the tube and the sample being connected by a conical graphite section.

With these different entrance geometries we have varied as mentioned above the flow conditions, the carrier gas and the x/d ratio. The different cases investigated are summarized in table 6.10. This table indicates the variable which has been used (either G or $\frac{x}{d}$) for a specific test made within a flow regime (laminar or turbulent) with one entrance geometry and with one carrier gas. The table also indicates the table and figure to which the reader should refer to find the detailed experimental values. The theoretical formulae which should fit the experimental data are indicated on each table giving the detailed experimental values. Corresponding figures compare the theoretical lines to the actual experimental plot.

One difficulty arises in preparing table 6.10, it is the definition of the flow regime under which the tests with the short "calming tubes" and with the "sharp edge entrance" were performed. If we refer to the Re calculated from the diameter, the flow becomes turbulent above $Re = 3,000$, but for short calming sections $Re = 3,000$ can be reached well before the Re_x critical of $4 \cdot 10^5$ is reached.

For the purpose of classification we will base our flow regime on the Re as it is generally done in the literature, an exception being made for case IV, where the Re_x is the leading parameter in the literature. We will see later in the discussion that this practice of basing the flow regime on Re for relatively short tubes may be misleading and give rise to the use of the wrong formulae for the prediction of the k_c .

For all cases the mass transfer coefficients are presented in the dimensionless form $\frac{k_c \cdot d}{D}$, which has the advantage of eliminating the influence of the test section diameter and the effect produced by the diffusion coefficient. The proportionality of k_c to the diffusion coefficient, demonstrated in earlier qualitative tests, is shown in Fig. 6.10.

5.2 Discussion of the Results

6.2.1 Tests Performed with the Flow as Variable

6.2.1.1 Tests Performed with an Established Velocity Profile and non Established Concentration Profile

6.2.1.1.1 Tests in Laminar Flow with Long Calming Section in 0.6 cm Diameter Channel

Theoretically, this case is covered by the Graetz-Leveque equations.

$$Sr = 1.615 Gz^{1/3} = 1.615 Re^{1/3} \cdot Sc^{1/3} \cdot \left(\frac{d}{x}\right)^{1/3} \quad (2.115)$$

Fig. 6.1 shows the experimental points and the theoretical line which is valid within the following limits:

lower limit (under which the concentration profile is fully established and $Sr = 3.65$)

$$Gz = 10 \text{ equivalent in our case to } Re = 92$$

upper limit

$$Re = 3,000 \text{ where the flow is no longer laminar}$$

From Fig. 6.1 it can be seen that the experimental points above $Re = 1,000$ are $\sim 20\%$ higher than the theoretically predicted values. Below $Re = 1,000$ the values depart from the theoretical line.

This discrepancy at the lower Reynolds number is probably due to interference mass transfer created by natural convection occurring in the vertically heated test section. Martinelli et al [2.41] have treated an analytically similar case for heat transfer and the corresponding equation for mass transfer can be proposed

$$\frac{k_c \cdot d}{D} = 1.75 \cdot F_1 \cdot \sqrt[3]{\frac{G}{\rho \cdot D \cdot L} + 0.0722 \left(\frac{d}{L} \cdot Gr \cdot Sc\right)^n} \cdot F_2$$

The dimensionless factors F_1 and F_2 are given in Fig. 6.11. The Gr used is based on the initial ΔT in the section 0. The calculated values are compared to the experimental values and the theoretical Graetz-Leveque predictions in Fig. 6.12 (line b). On the same graph the lines a and a' show the limit of dispersion of experimental values measured in heat transfer tests by Dalle Donne and Baldwin [1.5] with helium and large temperature gradient between wall and gas. The correlation between the Martinelli values and the experimental values is better (10 to 15% lower) than the one obtained by the Graetz-Leveque theory. The measurement accuracy of the mass transfer coefficient is well within the precision of the heat transfer measurements under similar conditions.

6.2.1.1.2 Tests in Turbulent Flow with a Long Calming Section

The case II presented in Fig. 6.2 and table 6.2 relates to measurements performed in He.

The case III presented in Fig. 6.3 and table 6.3 relates to measurements performed in N_2 .

The equation which, according to Lutzko, should cover this case is

$$Sr = \frac{k_c \cdot d}{D} = 0.0384 \cdot Re^{0.75} \cdot Sc \cdot (1 + 0.067 Re^{0.25} \frac{d}{x}) \quad (2.116)$$

The lower limit of applicability of this equation is $Re = 3,000$ below which the flow becomes laminar. As can be seen from Fig. 6.2, the correlation between the theoretical values and the measured values in He is not good at all while the correlation for the nitrogen tests Fig. 6.3 up to $Re = 50,000$ is very good.

The weakness of the Lutzko equation comes from the fact that the $k_{c\infty}$ for fully established flow is given by equation

$$k_c = 0.0384 \cdot Re^{0.75} \cdot Sc$$

where the exponent of Sc is one. This equation correlates well the results of fluid with the Sc number between 0.7 and 1, but gives the wrong value as soon as the Sc valid departs from these limits.

In Fig. 6.13 we correlate the experimental results with the well-known equation for fully established turbulent flow

$$\frac{k_c \cdot d}{D} \cdot \frac{1}{Sc^{1/3}} = 0.023 Re^{0.8}$$

This correlation is good for the tests performed in He and N_2 .

It is not surprising with a long calming section that the equations giving the mass transfer coefficient for a fully established flow correlates well with the experiments, because Boelter et al [1.4] have shown in heat transfer tests how rapidly the fully established value of transfer is reached and have proposed the following equation (transposed for mass transfer)

$$k_c = k_{c\infty} \left(1 + K \frac{d}{L}\right) \text{ for } \frac{L}{d} > 5$$

with $K = 1.4$. In our case with $\frac{d}{L} = \frac{1}{16.65}$ we should expect an entrance effect of 8.5 % of the $k_{c\infty}$

The deviation from the theoretical prediction, of the values obtained at a higher Re than 50,000 for N₂, results from a particularity of the experimental furnace, which for the good heat transfer occurring at this high Re changes its temperature distribution and the results obtained above, Re = 50,000, relate only to the reaction rate occurring on a smaller section of the sample, so that these results should be disregarded in the present analysis.

6.2.1.2 Tests Performed with non Established Velocity Profile and Concentration Profile

6.2.1.2.1 Tests in Laminar Helium Flow in a 0.36 cm Diameter Channel with a Sharp Edge Entrance

The type of mass transfer presented in table 6.4 and in Fig. 6.4 should, according to the relevant literature, be predicted by the equation applicable for laminar mass transfer over a flat plate; as long as the boundary layer remains smaller than half the diameter of the channel and the flow does not become turbulent.

$$Re_x < 4 \cdot 10^5$$

The equation applicable in this case is

$$Sr_x = \frac{k_c \cdot x}{D} = 0.664 \cdot Sc^{1/3} \cdot Re_x^{1/2} \quad (\text{see Fig. 6.4b}) \quad (2.109)$$

For the comparison of the order of magnitude of these results with those obtained in the other flow regimes we also present these results in $\frac{k_c \cdot d}{D} = f(Re)$ graph

Fig. 6.4a is based on the following modified equation.

$$Sr = \frac{k_c \cdot d}{D} = 0.664 \cdot Sc^{1/3} \cdot Re^{1/2} \cdot \left(\frac{d}{x}\right)^{1/2} \quad (2.122)$$

In Fig. 6.4a $\delta < \frac{d}{2}$ giving the lower limit of validity of the equation corresponds to $Re > 1,195$, as can be calculated from equation (2.74). The upper limit of validity of the equation is given by the condition of non-turbulence $Re_x < 4 \cdot 10^5$ corresponding in our case to $Re < \sim 12,500$.

The correlation between the experimental points and the theoretical prediction is good. At the lower Re_x a bigger dispersion of points is observed; this can be ex-

plained either by the influence of natural convection or by the fact that in this region of Re the thickness of the boundary layer approaches the value of $\frac{d}{2}$.

It should also be observed that in this case, although the flow is laminar, the value of Re can be as high as 10,000. In such a case one might be tempted to use the Latzko equation (2.113) for

$$\frac{L}{d} > 0.625 \cdot Re^{0.25}$$

$$\frac{k_c \cdot d}{D} = 0.0384 Re^{0.75} \cdot Sc \left(1 + 0.144 Re^{0.25} \cdot \frac{d}{x} \right)$$

which should be applicable to the non-established velocity and concentration profile in turbulent flow, but would in our case yield values 4 times too big.

6.2.1.2.2 Tests in a Helium Flow in a 0.36 cm Diameter Channel with a Short Calming Section

The experimental test section is represented in Fig. 4.5c. The table 6.5 and Fig. 6.5 present the experimental values obtained in the Re range between 1,142 and 11,580 corresponding to $69,000 < Re_x < 701,000$.

Four different zones can be distinguished in this case:

The zone A: below $Re = 1,500$

in this zone the flow is laminar and the thickness of the velocity boundary layer $\delta > \frac{d}{2}$ at the sample inlet. In this region the mass transfer coefficient should be predicted by equation (2.115)

$$St_r = \frac{k_c \cdot d}{D} = 1,615 \cdot Gz^{1/3}$$

The zone B: where $1,500 < Re < 2,730$

in this zone the flow is still laminar but the point where $\delta = \frac{d}{2}$ lies somewhere between the inlet and the outlet of the sample. No analytical expression is available for this undefined flow condition.

The zone C: included above $Re = 2,730$ and below $Re \sim 7,500$ to $9,200$ (corresponding to $Re_x \sim 450,000$ to $550,000$.)

In this zone where $\delta < \frac{d}{2}$ and the film is laminar, the following equation should be applicable

$$Sr = 0.664 \cdot Re^{1/2} \cdot Sc^{1/3} \cdot \left(\frac{d}{L+x_0}\right)^{1/2} \cdot \frac{1}{\sqrt[3]{1 - \left(\frac{x_0-x}{L+x_0}\right)^{3/4}}} \quad (2.107)$$

The zone D: where $Re_x > 550,000$

The flow should be turbulent.

In Fig. 6.5 we have drawn the theoretical lines. The experimental points do not fit these lines very well but it should be observed that the four zones predicted theoretically can be seen and that in any case the theoretical prediction is better than that obtainable from the Latzko semi-empirical equation derived from a graphical combination of equations (2.113) and (2.116)

Here again it should be pointed out that the laminar flow equation should be applied in some case although $Re > 3,000$.

6.2.2 Tests Performed with Distance x from the Entrance as Variable in non Established Flow with non Established Concentration Profile

6.2.2.1 Tests in Laminar Helium Flow in 0.36 cm Channel with a Sharp Edge Entrance

The geometry of the experimental set up used for these tests is shown in Fig. 4.5d. The experimental results relevant to this case are presented in table 6.6 and Fig. 6.6.

The theoretical equation applicable to this case is the one for the mass transfer over a flat plate in laminar flow

$$\frac{k_c \cdot x}{D} = 0.664 \cdot Sc^{1/3} \cdot Re_x^{1/2} \quad (2.109)$$

$\frac{k_c \cdot x}{D}$ is plotted in Fig. 6.6b as function of x it can be seen that the $k_c \cdot x$ varies

proportionally $x^{-1/2}$.

For the comparison of the order of magnitude of these results with those obtained in the other flow regimes we also present the results in $\frac{k_{cx} \cdot d}{D}$ form following equation

$$Sr_x = \frac{k_{cx} \cdot d}{D} = 0.664 \cdot Sc^{1/3} \cdot Re^{1/2} \cdot \left(\frac{d}{x}\right)^{1/2} \quad (2.112)$$

illustrated in Fig. 6.6 a

The equation is valid for $\delta < \frac{d}{2}$ which sets up an upper limit to $\frac{x}{d} = 32$.

The Reynolds number used in this case is Re 1,382. It can be seen from Fig. 6.6 that the experimental values are in rather good agreement with the theoretical prediction.

6.2.2.2 Tests in Turbulent Helium Flow in a 0.36 cm Diameter Channel with a Sharp Edge Entrance

The experimental set up used in the test is the same as in the previous case. The tests have been done for several Re

$$\begin{aligned} Re &= 7,920 \\ &9,900 \\ &11,900 \\ &14,850 \end{aligned}$$

The experimental results obtained in this case are different from those shown in Fig. 6.6. In the logarithm plot they describe in the down stream region a slope corresponding to $\left(\frac{d}{x}\right)^{1/2}$ power while in the up-stream region the slope is smaller. The same results plotted on normal paper do show a similar shape to the results obtained by L.M.K. Boelter et al in heat transfer in the inlet region of a tube preceded by a square edge orifice entrance. Similarly the k_{cx} can be expressed by an equation of the type

$$k_{cx} = k_{c\infty} \left(1 + K \frac{d}{x}\right) \text{ for } \frac{x}{d} > 5 \text{ with the value of } 7 < K < 12.$$

Boelter et al, who were able to investigate the region of $\frac{x}{d}$ ranging between 0 and 5 suggested that the shape of the k_{cx} as a function of $\frac{x}{d}$ for this type of inlet was due to an air pocket created by the orifice, which should reduce the heat transfer in the inlet region. We believe that in our particular case the flow and boundary layer are still

laminar non-established and consequently the $(\frac{d}{x})^{1/2}$ slope would be justified, but at the inlet of the sample the air pocket created by the sharp edge entrance would disturb the mass transfer in that region and cause the reduced transfer rate observed.

This "air-pocket" or "Separation bulb" has also been described by Hall and Chocho Gil [6.1] [6.2]

6.2.2.3 Tests in Turbulent Helium Flow with a Bellmouth Inlet in 0.36 cm in Diameter Channel

In an attempt to eliminate the influence of the sharp edge entrance a conical junction was created between the 0.6 cm up-stream channel and 0.36 cm test section. The curve obtained for $\frac{k_{cx} \cdot d}{D}$ is of similar type as the one described in § 6.2.2.2. But here again the flow and mass transfer are so complex that it is very hard to give a theoretical explication fo the phenomena, and unfortunately no similar case has been treated in heat transfer for purposes of comparison.

6.2.2.4 Tests in Turbulent Nitrogen Flow in 0.36 cm Channel with a Sharp Edge Entrance

The Fig. 6.9 gives the experimental points of $\frac{k_{cx} \cdot d}{D}$ as f $(\frac{x}{d})$. The experimental points in the region $\frac{x}{d} < 5$ are lacking and a detailed analysis of the results is impossible in this region. We can only compare the coefficient $K \approx 3$ obtained from

$$k_{cx} = k_{c\infty} (1 + K \frac{d}{x})$$

in this case and the experimental value measured by Boelter et al with a short calming section or with a sharp edge entrance. A good agreement is obtained from this comparison.

7. CONCLUSION

7.1 Practical Conclusion for H.T.G.C.R. Design

The rate of oxidation of the graphite by chemical impurities present in the helium coolant flow of H.T.G.C.R. reactors will be mass transfer controlled once the rate of transfer of reagents to the graphite surface becomes smaller than the rate of the chemical reaction. The "lowest mass transfer coefficient" for a gas flowing in a channel is achieved for the fully established (concentration and velocity) laminar flow and is given by the following expression 7.1

$$\frac{k_c \cdot d}{D} = 3.65$$

The lower temperature at which the graphite oxidation would then be mass transfer controlled under these conditions is such that

$$k_{\text{exp}} > k_c = \frac{3.65 \times D}{d}$$

In our graphite oxidation experiments with various flow regime and different carrier gas (He and N_2) we have measured $\frac{k_c \cdot d}{D}$ values ranging from 4 to ~ 100 .

In helium at 20 atm the oxygen graphite reaction (commercially available nuclear graphites) started to be mass transfer controlled at $\sim 700^\circ\text{C}$ in the laminar flow range under our experimental conditions. The H_2O and CO_2 graphite reaction would only be mass transfer controlled at temperature in excess of 1000°C for similar experimental conditions.

The transition point depends on the diffusion coefficient, on the chemical reactivity of the graphite and on the hydraulic diameter of the reacting channel. In a reactor the temperature at which the oxidation rate would be mass transfer controlled, for a given flow regime and geometry, will decrease

1. with decreasing diffusion coefficient, achieved either by using higher pressure or a lower coolant temperature or also using a different carrier gas
2. with increasing hydraulic diameter of the reacting channel
3. with increasing reactivity of the graphite, induced for example by the influence of catalytic fission products like Sr, Ba.

7.2 Appreciation of Methods used for Estimation of the Mass Transfer Tests

Once the graphite oxidation is mass transfer controlled it follows laws which can be predicted by three main methods based on

- dimensionless analysis
- analogy with heat transfer
- analysis of hydrodynamic models

7.2.1 The Dimensional Analysis

The dimensionless analysis is nothing else than a method to organize the empirism. To be effective it should be applied with caution and following scientific criteria. The selection of the dimensionless numbers used should lead to easy expressions and their combination should be based on the tradition and guided by a good physical sense. By the non respect of these rules many workers produced semi-empirical expressions which are so complex that they fail to fulfill the following objectives which could be met by the semi-empirical expressions obtained by the dimensional analysis

- a) predict the behaviour of one plant under new operating conditions
- b) predict the behaviour of a new plant based on the experience gained with a plant of different size.

The dimension analysis method do not investigate the mechanism of the transport phenomena and the semi-empirical expression obtained by the correlation of experimental investigation by this method do not allow the prediction or the interpretation of transfer rates obtained under quite new conditions.

For example the interpretation of the inlet geometry effect on short reacting samples as measured could not be covered and interpreted by semi-empirical expression available in the literature.

7.2.2 The Analogy with Heat Transfer

The heat and mass transfer proceed from the similar physical processes e.g. heat and mass

diffusion and convective current . It should then be possible to predict the rate of mass transfer from the information obtained in heat transfer. Our experiments have confirmed that this procedure is very fruitful because most of our results have been correlated with experimental expressions transposed from heat transfer tests to mass transfer.

The substitution of the following terms should be done for this transposition

q	heat flux	—————	N	mass flux
$\frac{k}{c_p \cdot \rho}$	thermal diffusivity	—————	D	mass diffusion coefficient
$(c_p \cdot \rho \cdot T)$	thermal concentration	—————	C	mass concentration
$\frac{\mu \cdot c_p}{k}$	Prandtl no.	—————	$\frac{\nu}{D}$	Schmidt no.
$\frac{h \cdot x}{k}$	Nusselt no.	—————	$\frac{k \cdot x}{c \cdot D}$	Sherwood no.

This method of substitution is advantageous because it allows the use of a large background of heat transfer investigations. Generally heat transfer measurement being easier to perform than mass transfer tests the substitution method could be used in order to obtain mass transfer values.

The substitution method has the following limitation [7.2]

- a) No equivalent of heat radiation exists in mass transfer and the substitution is only valid for heat transfer tests obtained under conditions where radiation contribution is negligible.
- b) For the application of the analogy the geometries used should be similar. Unfortunately the geometries of heat transfer are generally not interesting for mass transfer. But for our specific case of the oxidation rate of graphite in coolant channels of nuclear reactor a vast amount of information is available in the heat transfer literature.

We could mention that the Lewis analogy

$$k_c = \frac{h}{c_p \cdot \rho}$$

is a particular case of transposition of the heat transfer results to mass transfer cases. This analogy is based on the simplifying assumptions that $Nu = Sr$ and $(Sc) = (Pr)$ which is often the case for the gases.

2.3 The Use of Hydrodynamic Model

The third method used to predict the mass transfer uses hydrodynamic models which try to interpret the phenomena underlying the mass transfer. From these models, mathematical expressions are derived and compared to experimental results.

Several models like

- the laminar film theory
- the Reynolds analogy
- the impulse method
- the penetration model

have been used with more or less success but these models only yield qualitative information.

The conjunction of these models with the "boundary layer" model proves to be the most powerful tool available to interpret the results. An understanding of the physical phenomena occurring in the "boundary layer" attached to the reacting sample helped us during this study to select the expression appropriate to the flow condition and geometries used in our experiments. In the simple cases the agreement between the prediction and the measurements has been very good. In more complex cases which are still defying a rigorous mathematical analysis the agreement between theory and the results is not so good but the observed phenomena can be qualitatively interpreted by the "boundary layer" model.

We feel that this method although sometimes leading to complicated mathematical development is the best approach to the problem in order to achieve the final goal of predicting performance of a plant in any operating conditions from a mathematical model.

APPENDIX I

Method for Calculation of Local Mass Transfer Coefficient

During the experiment the k_{exp} for the whole sample is measured as well as $\frac{cps}{CO_2 + CO}$. Only a small portion of the sample is labelled.

The cps is \approx to the local reaction

The $(CO_2 + CO)$ is \approx to the total reaction

Thus

$$a_i = \frac{cps_i}{CO_2 + CO} \approx K \frac{k_{exp i} \cdot s'}{k_{exp} \cdot s} \quad (A.II.1)$$

K is constant

a_i symbol for $\frac{cps_i}{CO_2 + CO}$ at the location i

$k_{exp i}$ local mass transfer coefficient at the location i

s' surface of the C^{14} labelled sample

s total surface of the sample

In order to find the value of the constant let us add all the a_i

$$\sum_{i=1}^n a_i = \sum_{i=1}^n \frac{k_{exp i} \cdot s'}{k_{exp} \cdot s} \cdot K = K \quad (A.II.2)$$

Consequently from (A.II.1) and Introducing the value of K from (A.II.2)

$$k_{exp i} = \frac{a_i \cdot k_{exp} \cdot s}{C \cdot K \cdot s'}$$

As the length of the C^{14} s' is constant

$$k_{exp x_1} = \frac{a_i \cdot k_{exp} \cdot s}{K \cdot s'}$$

$$k_{\exp x_2} = \frac{1}{2} \sum_{i=1}^2 \frac{a_i \cdot k}{K \cdot s^i} \exp \frac{\cdot s}{\cdot}$$

$$k_{\exp x_n} = \frac{1}{n} \sum_{i=1}^n \frac{a_i \cdot k}{K \cdot s^i} \exp \frac{\cdot s}{\cdot}$$

APPENDIX II

Development of C^{14} Labelling Method for the P.C.T.E.

M. Everett

Following the work of Kanter⁽¹⁾ and of Feldman⁽²⁾ on the self-diffusion of C atoms in graphite, it was decided to attempt to use the high temperature exchange of $C^{14}O$ with graphite as a means of labelling.

A technique has been developed which uses inexpensive $C^{14}O_2$ as the starting material. One can thus obtain specimens with a relatively high specific activity (about 1 mc/g) which greatly increases the utility of the specimens for graphite corrosion experiments. The labelling procedure which consists of the two main stages is described below;

a) Degassing and C^{14} Exchange Process

The specimen is directly heated without radiation shields in a low voltage resistance furnace and degassed at $2000^{\circ}C$ in purified helium for 3 hours. The helium is purified by circulation through a molecular sieve bed at $-196^{\circ}C$ (see Fig. A. II.1). After pumping away the helium, 5 ml NTP of carbon dioxide containing 10mc of $C^{14}O_2$, is expanded into the furnace. The temperature is raised to $2000^{\circ}C$ again and the furnace operated as a closed system. Carbon dioxide is converted to carbon monoxide by reaction with the sample and exchange of carbon atoms slowly takes place between the carbon monoxide and the graphite at $2000^{\circ}C$. During this operation the count rate shown by a gas-cell scintillation counter attached to the system, (see Fig. A. II.1), falls from 55,000 c.p.s. to about 5,000 c.p.s over a period of 4-5 hours, indicating that approximately 90% of the C^{14} has been transferred to the specimen. The specimen is allowed to cool and the residual active carbon monoxide trapped in a molecular sieve bed at $196^{\circ}C$.

This "exchange" process provides a high concentration of C^{14} at the surface of the specimen and it is necessary to heat to temperatures of $2400^{\circ}C$ for several hours in a second process to diffuse the C^{14} into the specimen.

b) C¹⁴ Diffusion Process

The resistance furnace is reassembled with the specimen surrounded by one pyrographite and two normal graphite radiation shields. The specimen is degassed in vacuo at 1000°C for 10 minutes and the furnace then filled with dry helium. Helium is purified, as before, by circulation through a -196°C molecular sieve bed. The temperature of the specimen is raised to 2400°C and maintained there for 4 hours. The temperature is raised to 2500°C or 2600°C for as long (usually 30-60 min.) as the specimen can be run without risk of physical damage, which usually occurs if the electrical resistivity of the sample rises by more than 20%. Under these conditions sufficient diffusion of carbon atoms takes place to give a reasonably uniform distribution of C¹⁴ throughout the sample. The specimen is removed to a glove box and trimmed to length. Off-cut portions are cast in epoxy-resin, polished and used for the preparation of autoradiographs enabling the distribution of C¹⁴ to be examined.

- References: (1) M.A. Kanter - The Mechanism for Atom Motion in Graphite Crystals. Conference on the Kinetics of High Temperature Processes pp 61-66. Technology Press. Massachusetts Institute of Technology, 1958.
- (2) M.H. Feldman - et al. Studies of Self-Diffusion in Graphite using C¹⁴ Tracer. J. Appl. Phys. 23 1200-1206 (1952).

Apparatus for C^{14} labelling of graphite

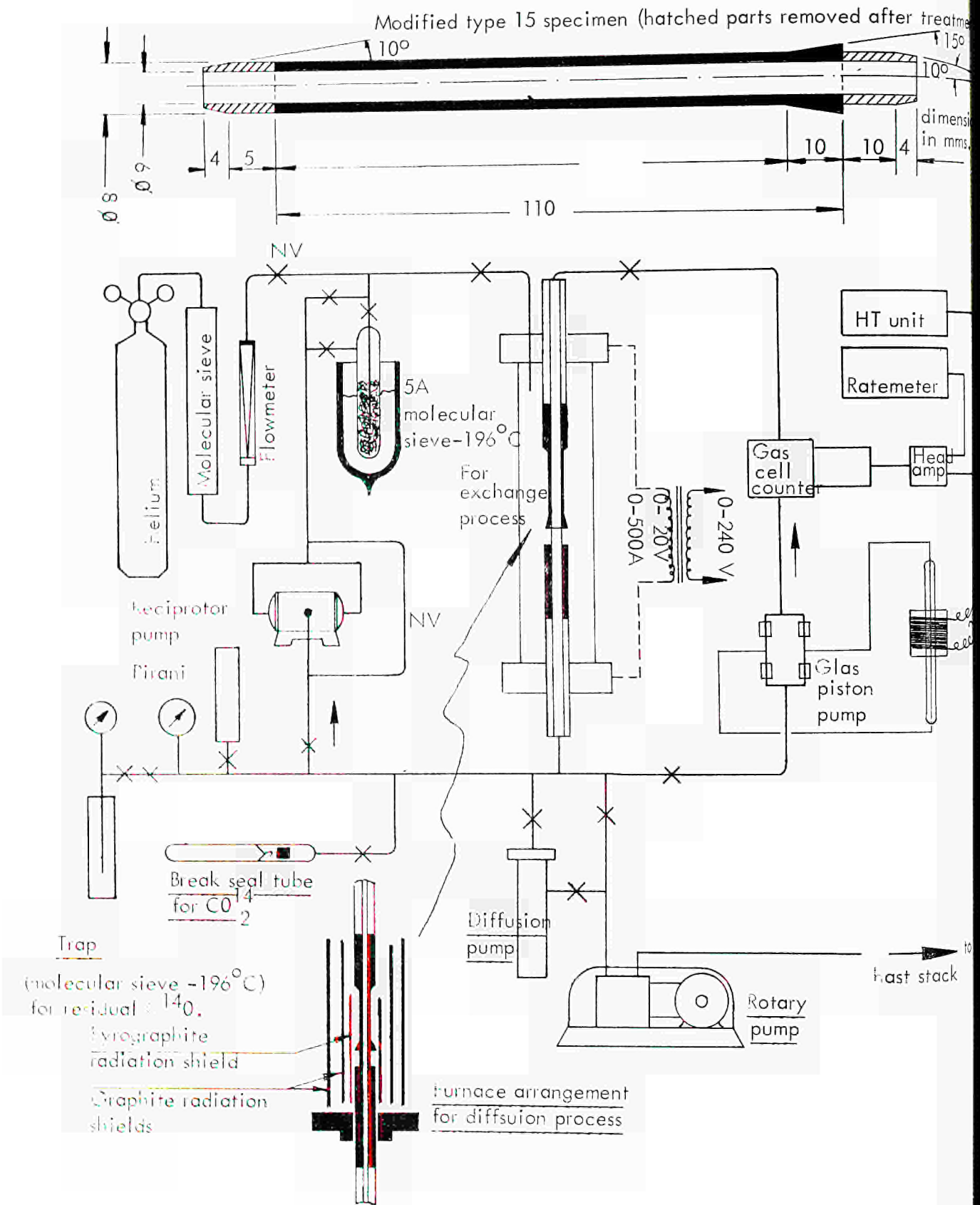


Fig. A. 11.1

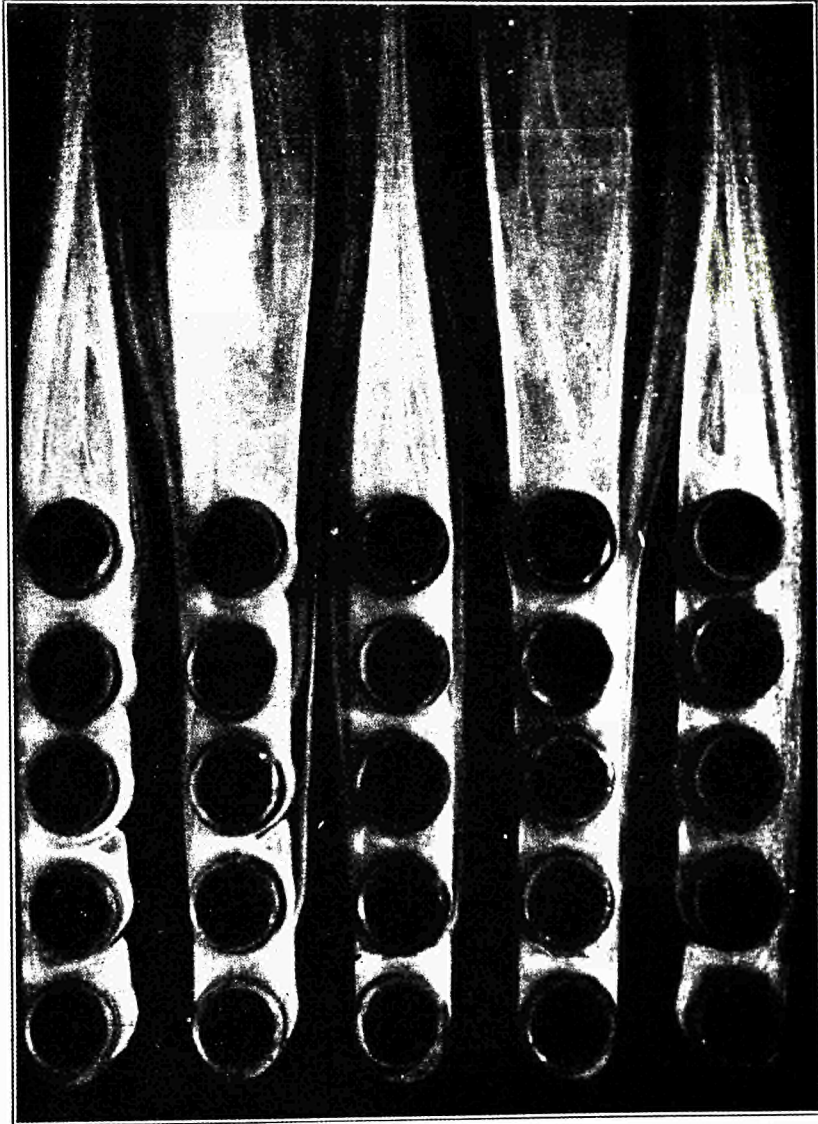


Fig. 1.1

Flow picture materialized by clouds of ammonium chloride "Lohrisch".

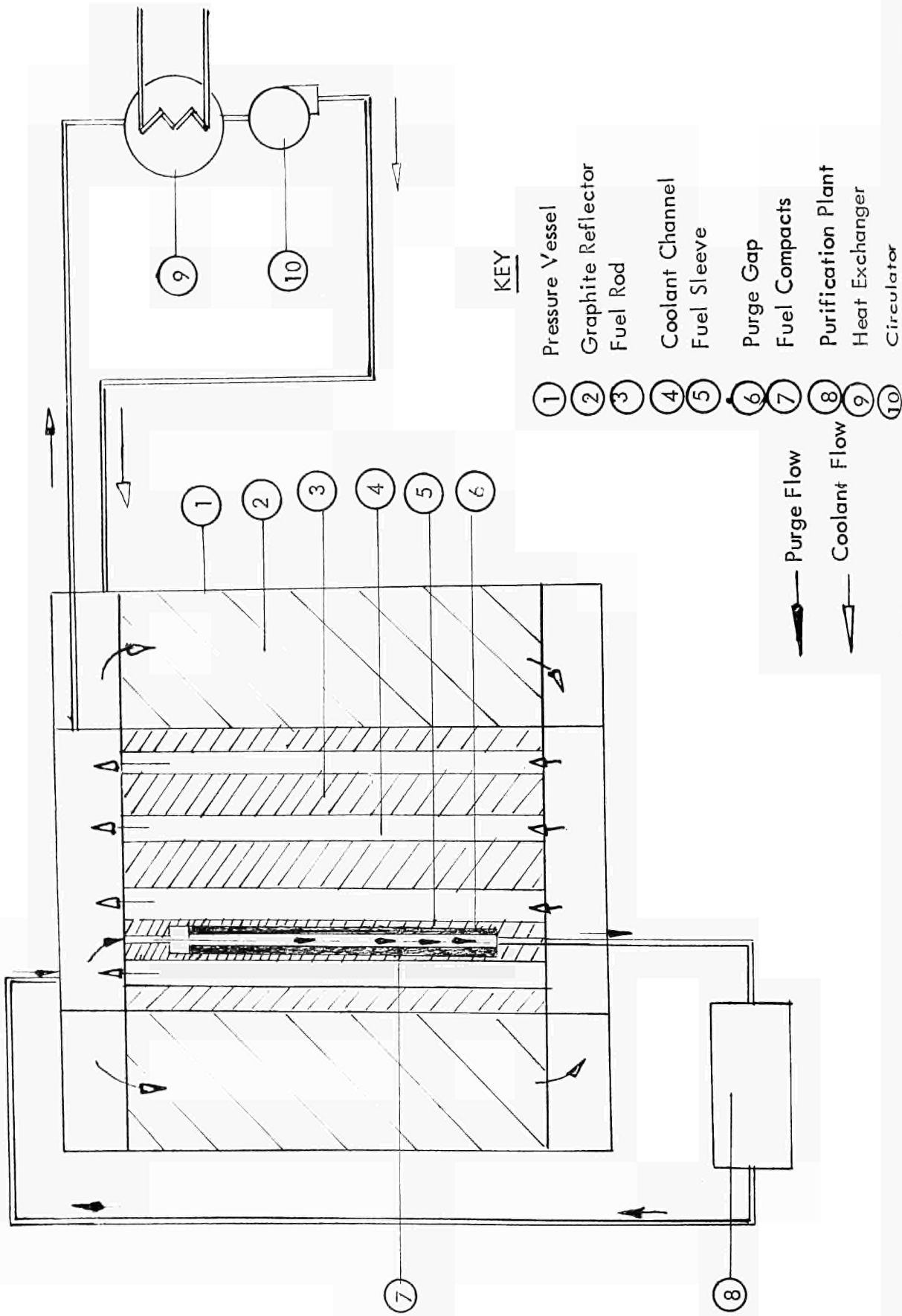


Fig. 1.2

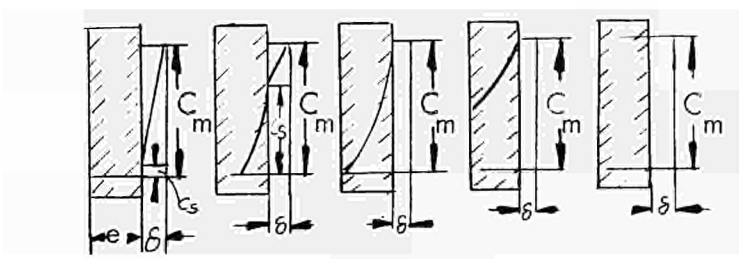
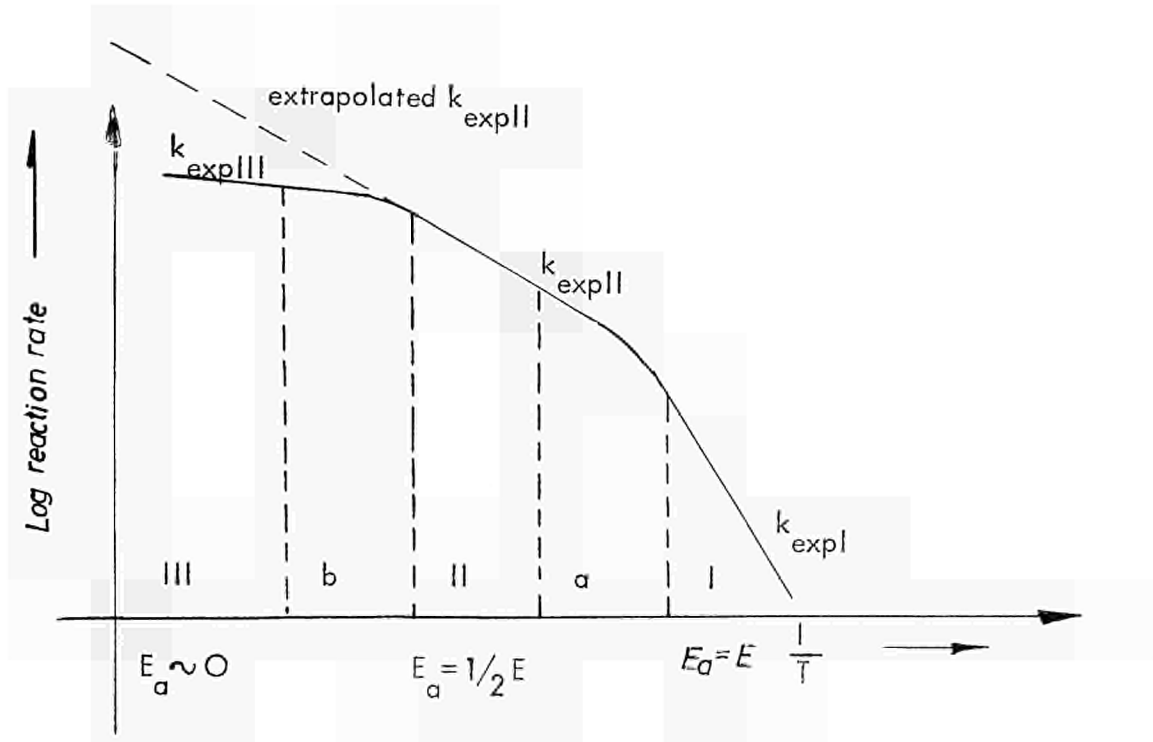
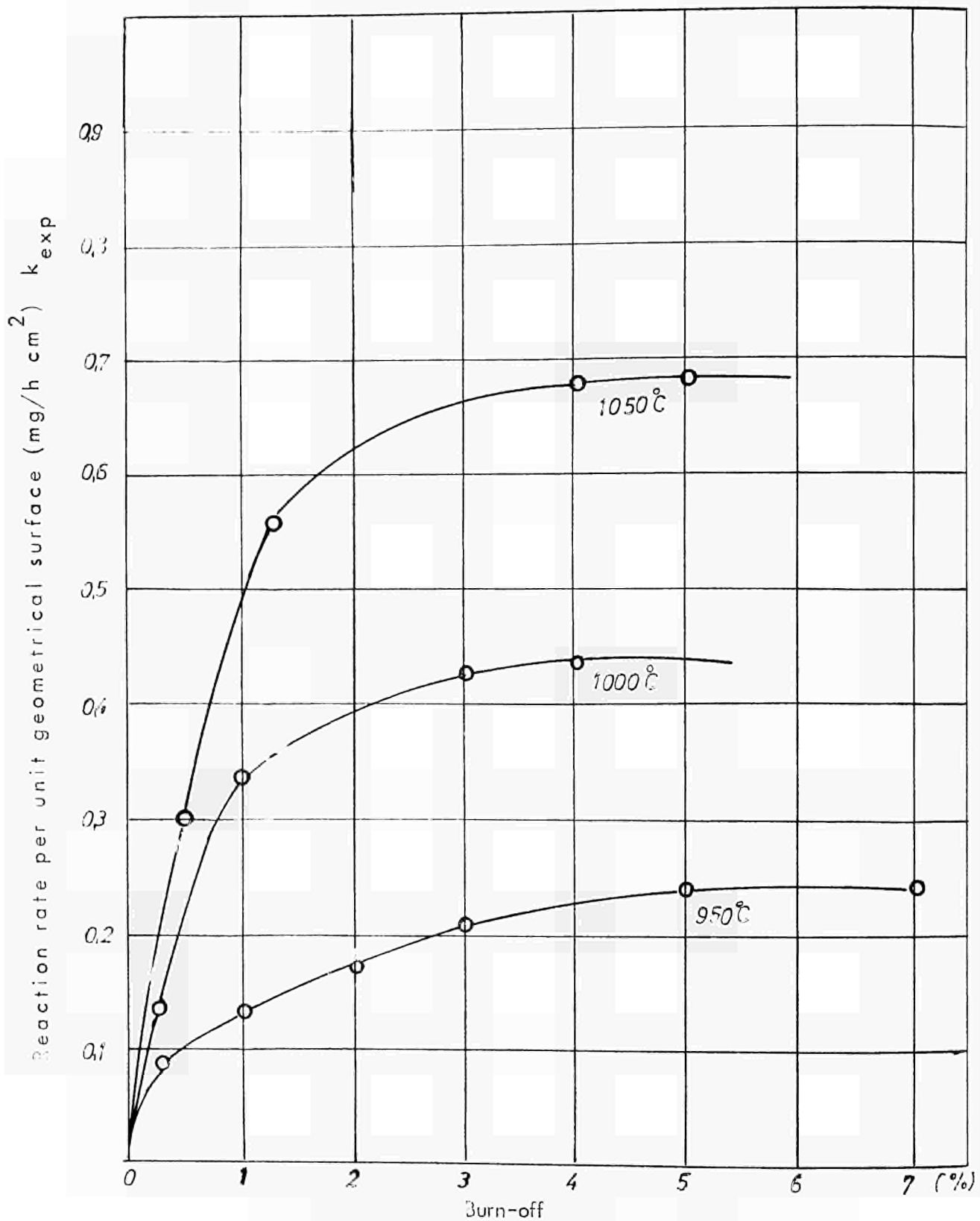


Fig. 2.1

The three zones of the reaction rate in a porous graphite v.s. temperature " Advance in Catalysis" Volume XI

Gas Reactions of Carbon - P.L.Walker et Al.



Corrosion rate of grade - 9 graphite with H_2O at 3.4 mm Hg as a function of burn-off

Fig. 2.2

Diffusion of a reacting gas and its reaction products
in stationary He

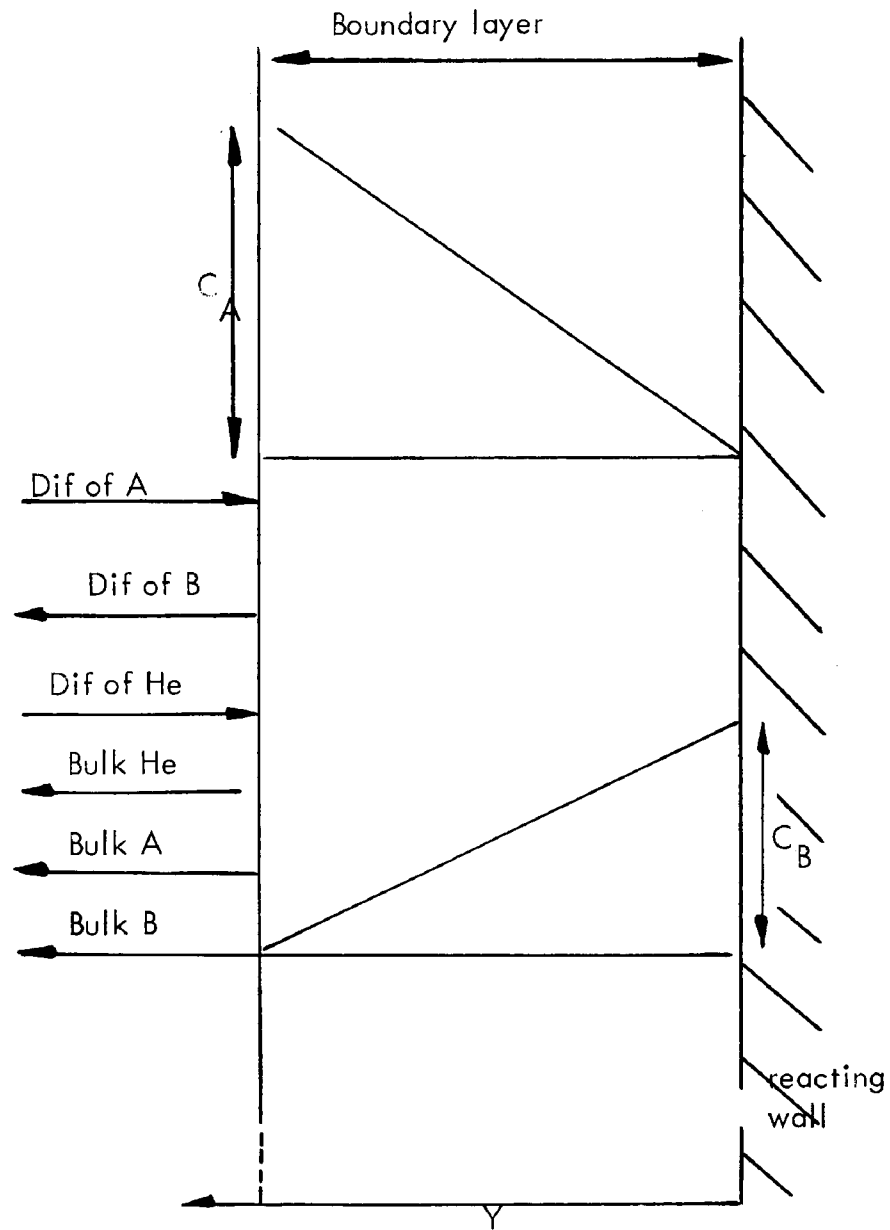
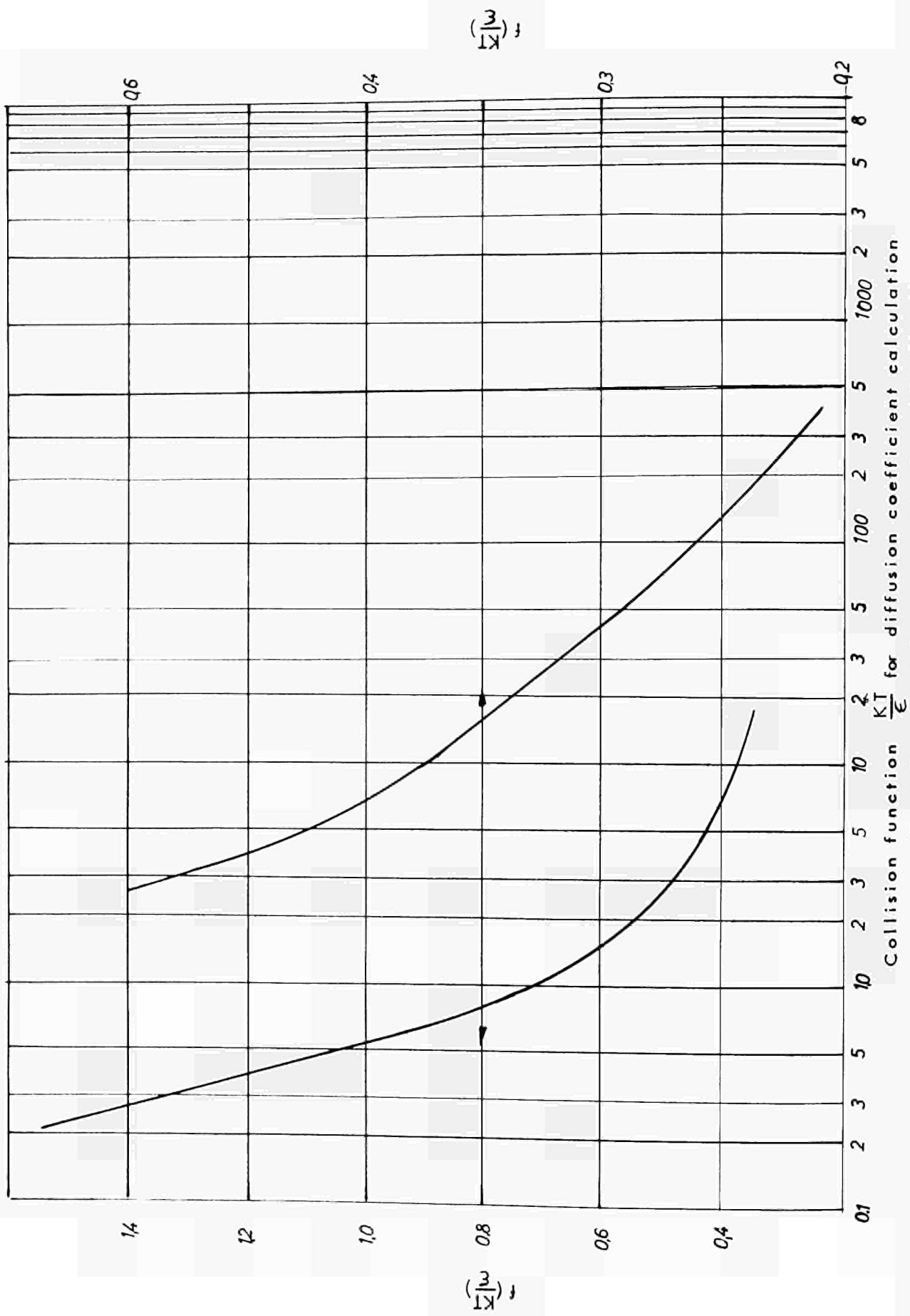


Fig 23



(Tray ball - mass transfer operations - Mc Graw Hill 1955-p.20)
Fig. 2.4

Diffusivity of O_2 in He at 10, 15, 20 atmospheres v. s. temperature

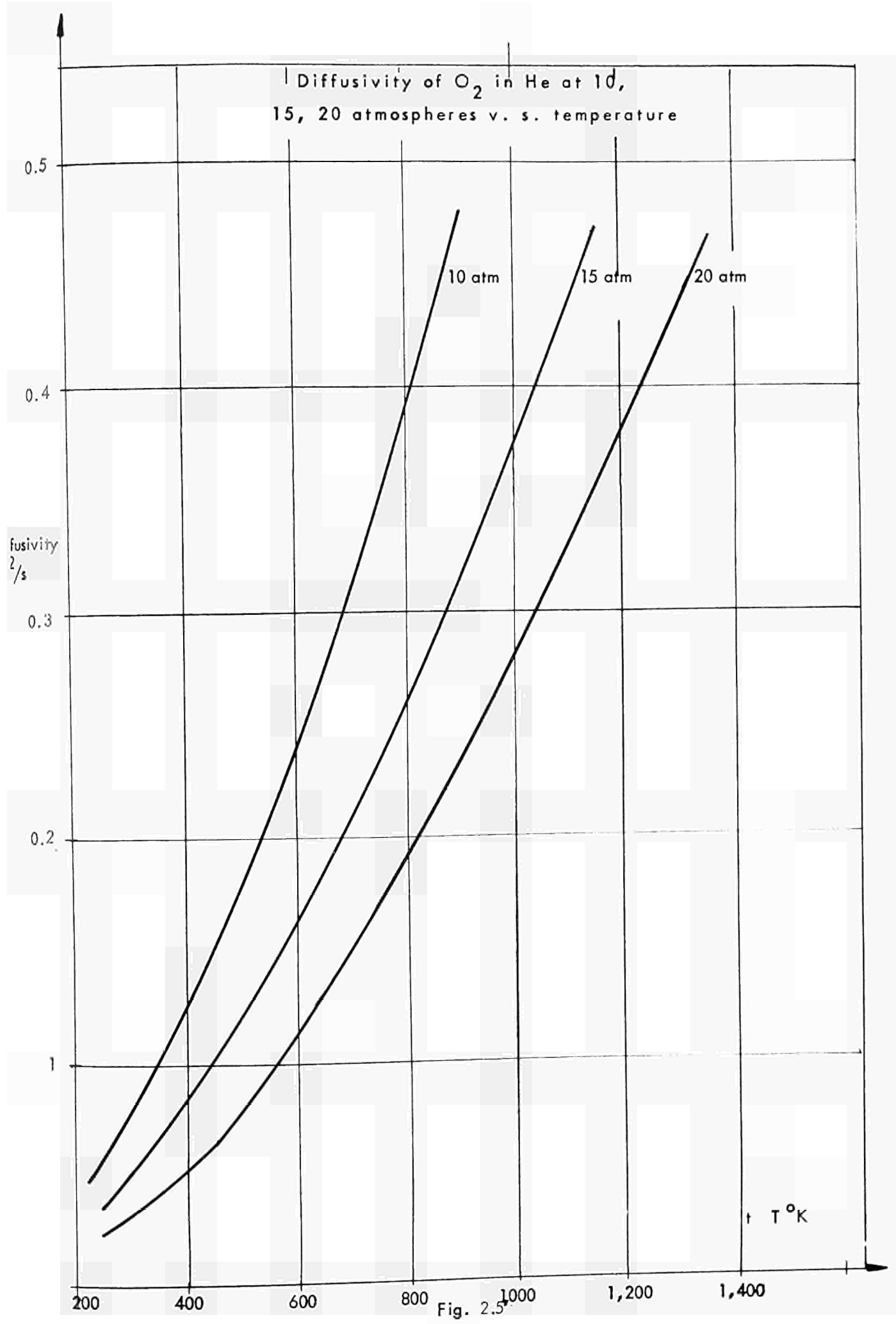
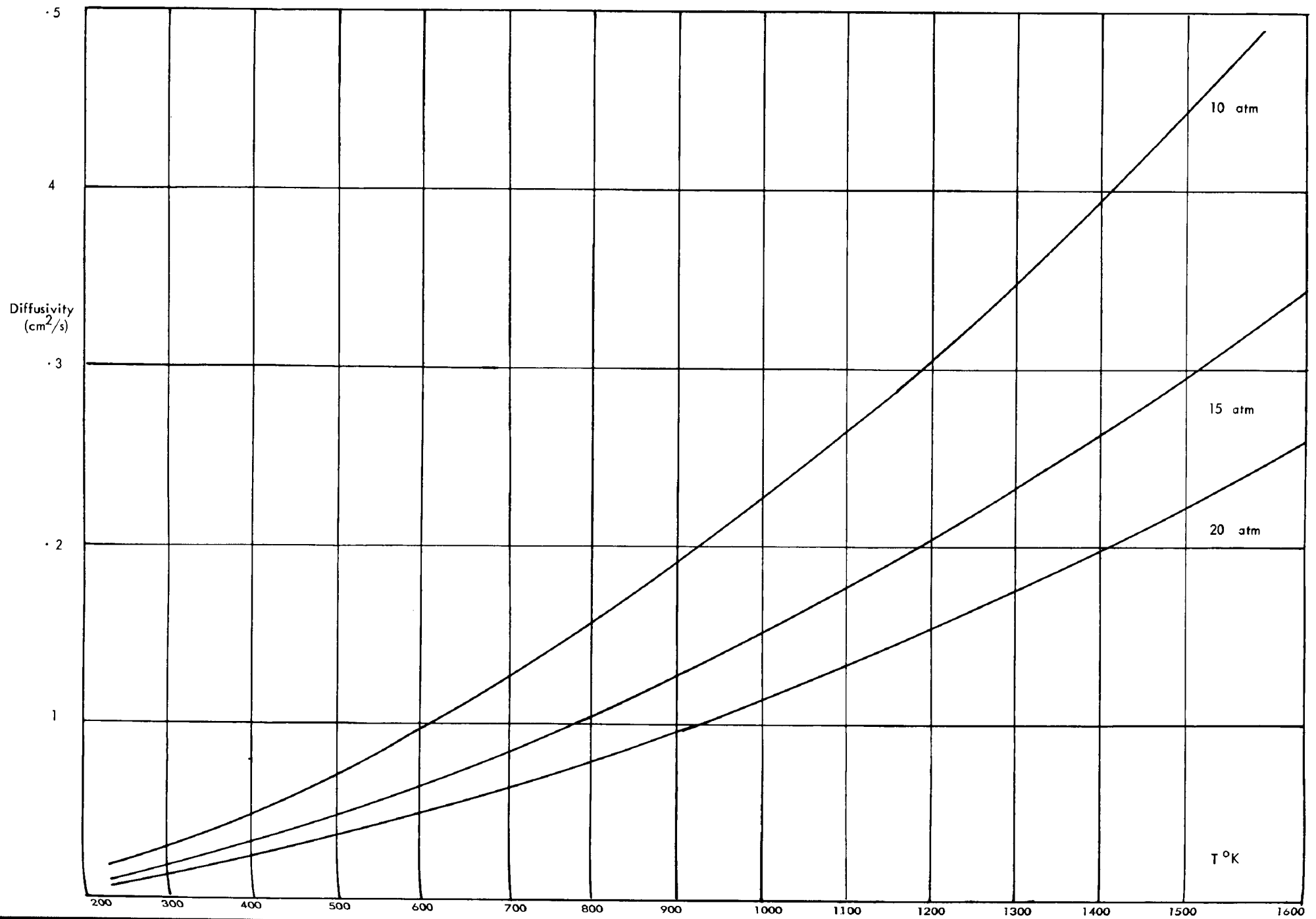
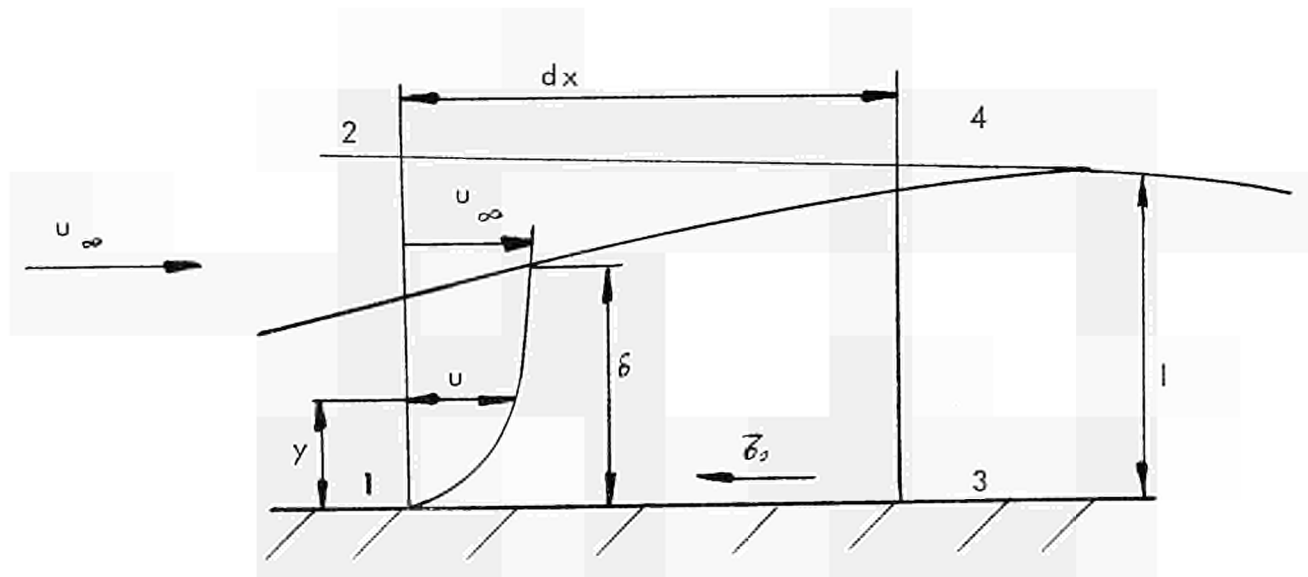


Fig. 2.5

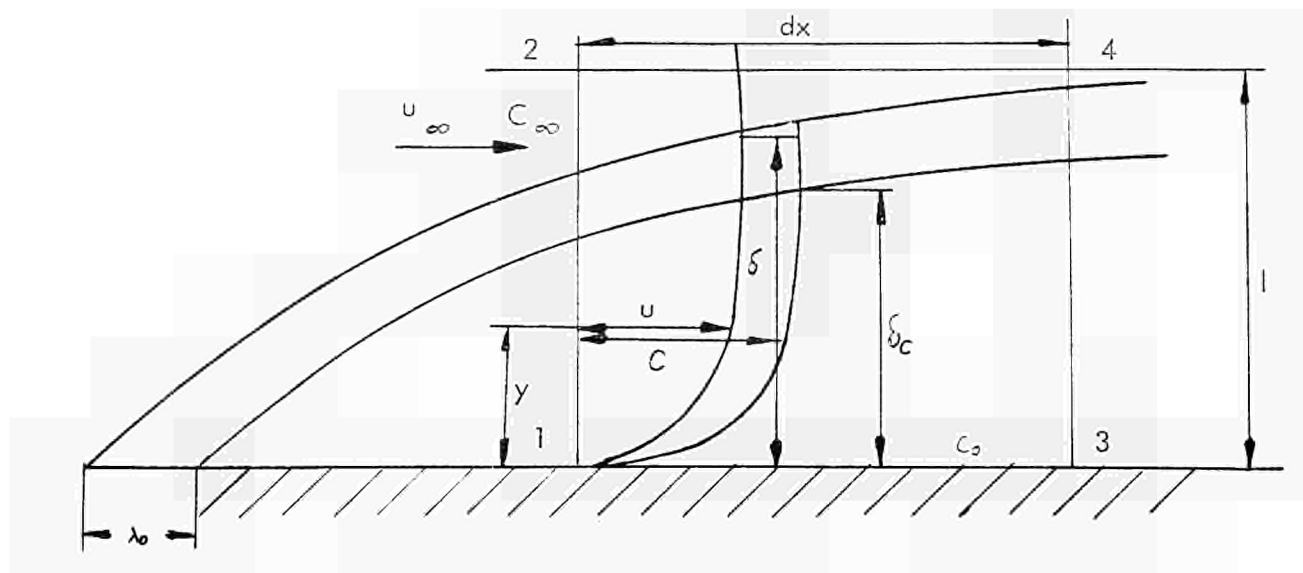
Fig. 26 Diffusivity of Oxygen in Nitrogen at 10,15,20 atmospheres versus temperature





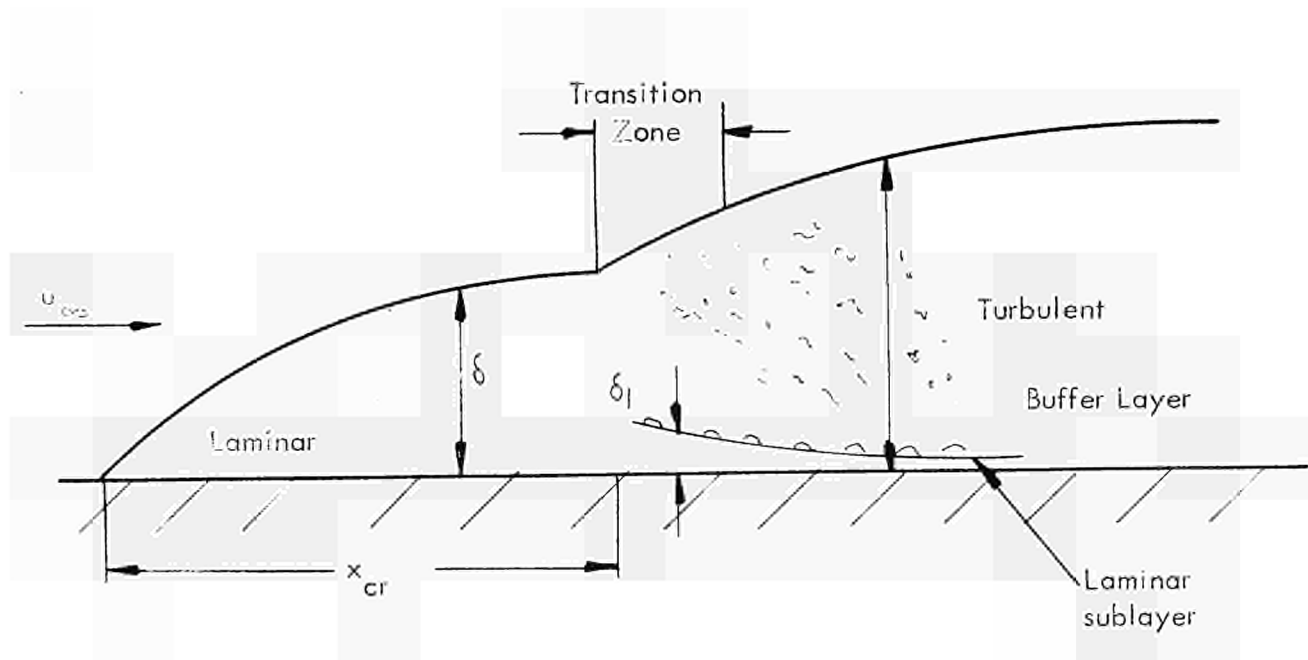
Element of a fluid near the wall for the calculation of the momentum equation

Fig. 2.7



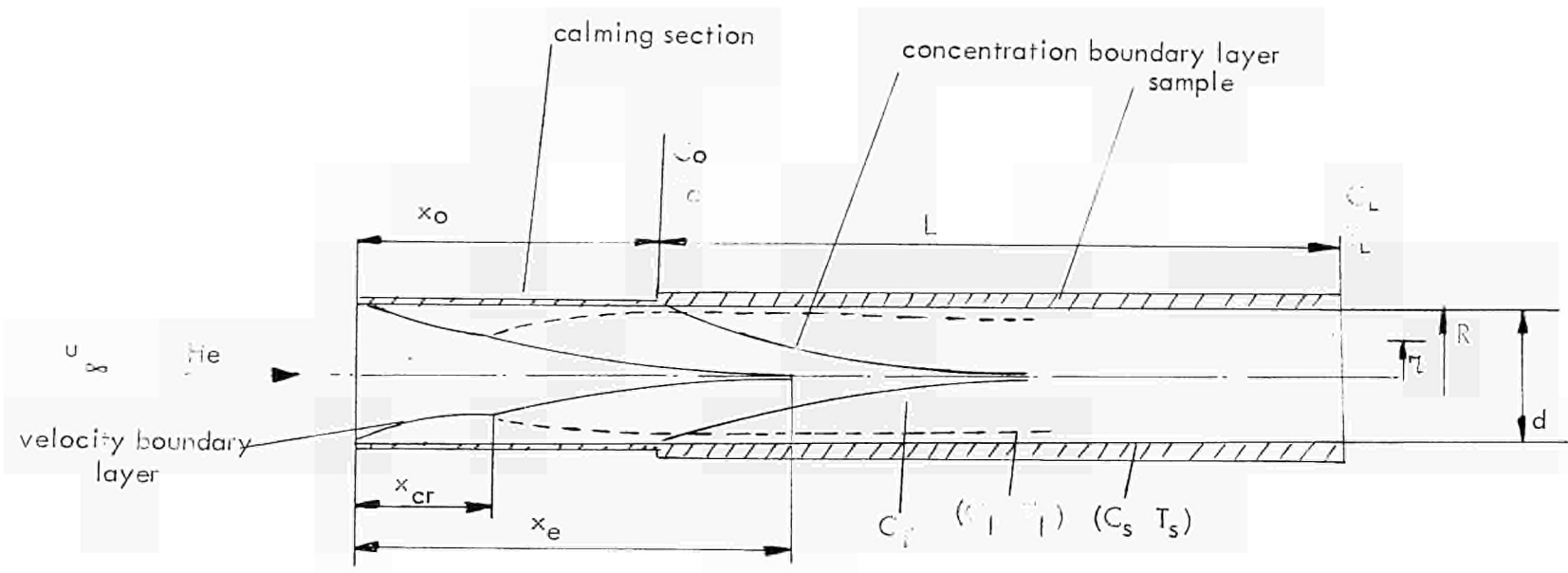
Element of fluid near the wall for the calculation of the mass flow equation

Fig. 2.8



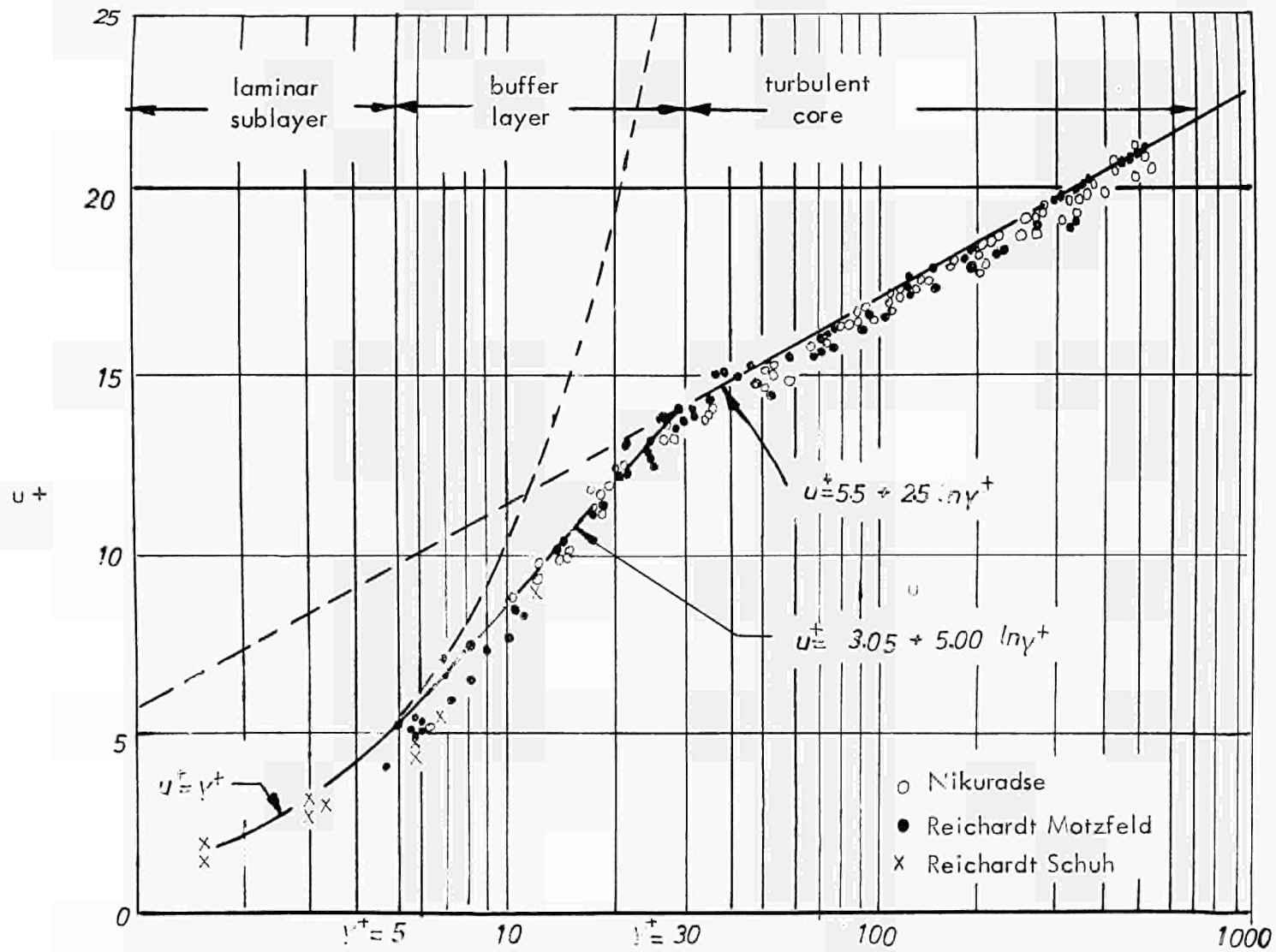
Formation of the boundary layer along a flat plate

Fig. 2.9



Formation of the velocity and concentration boundary layers at the inlet of a turbular sample

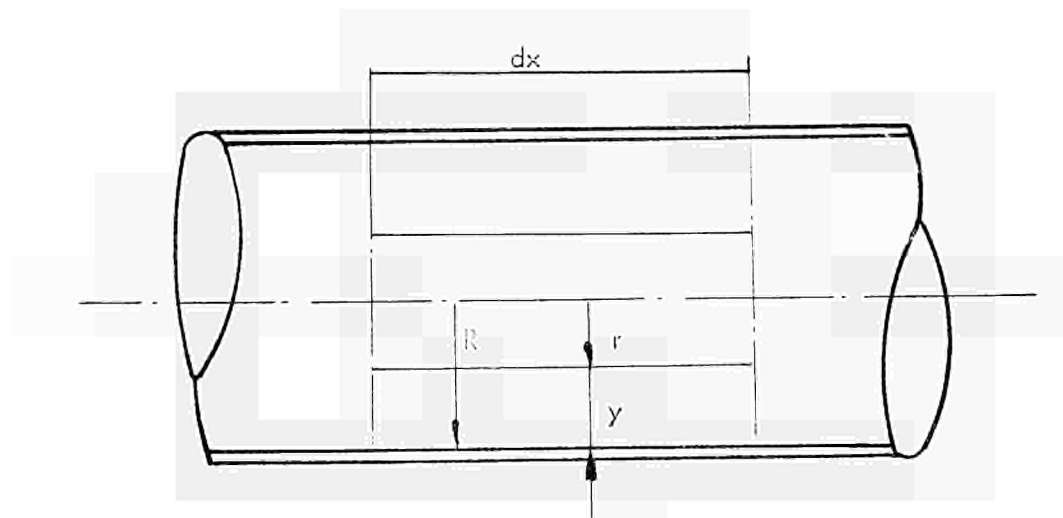
Fig. 2.10



Universal velocity profile

(from R.C. Martinelli, Trans. ASME, 69 : 947 - 959 (1947).)

Fig. 2.11



Streamline flow through a tube

Fig. 2.12

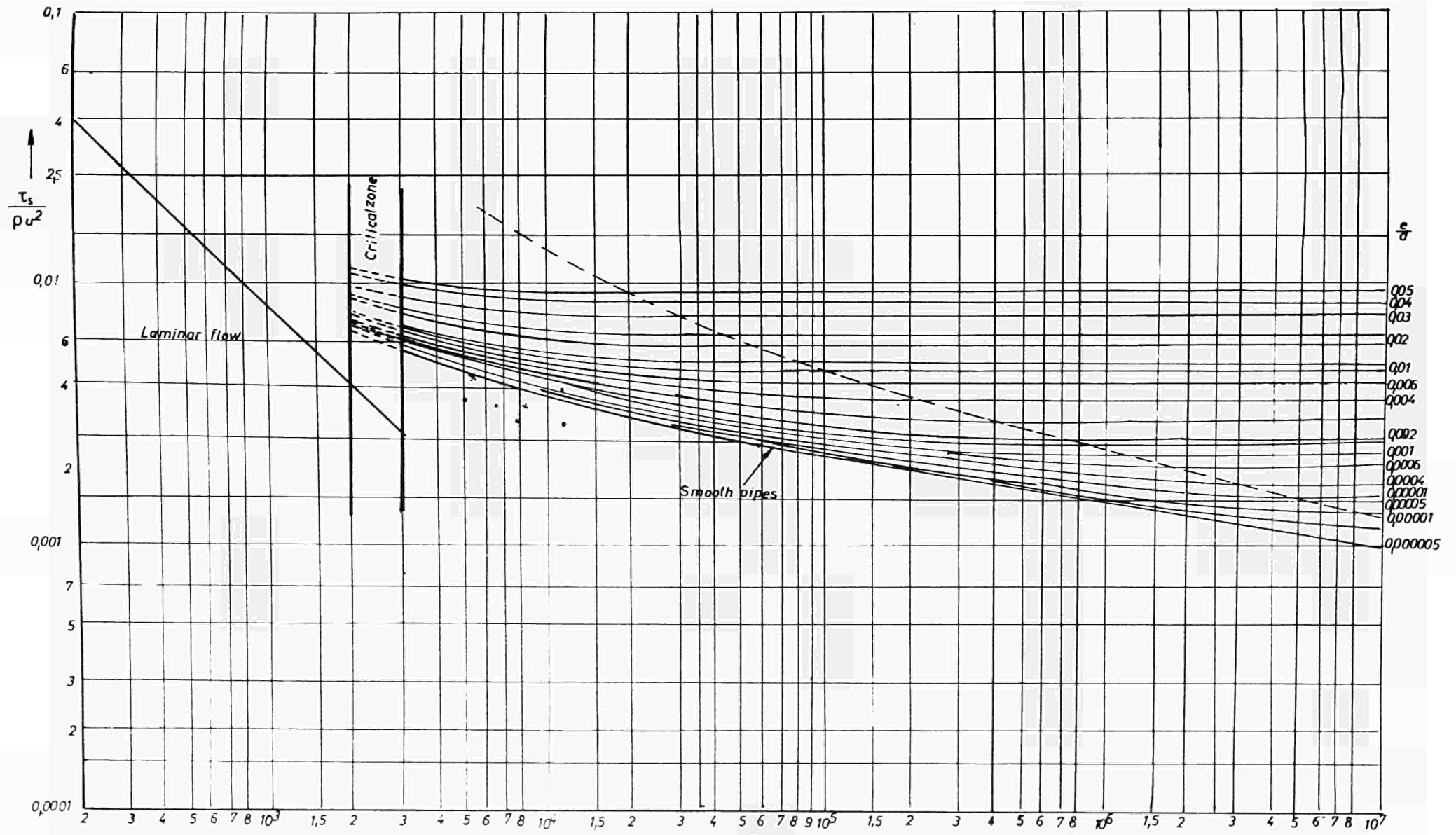
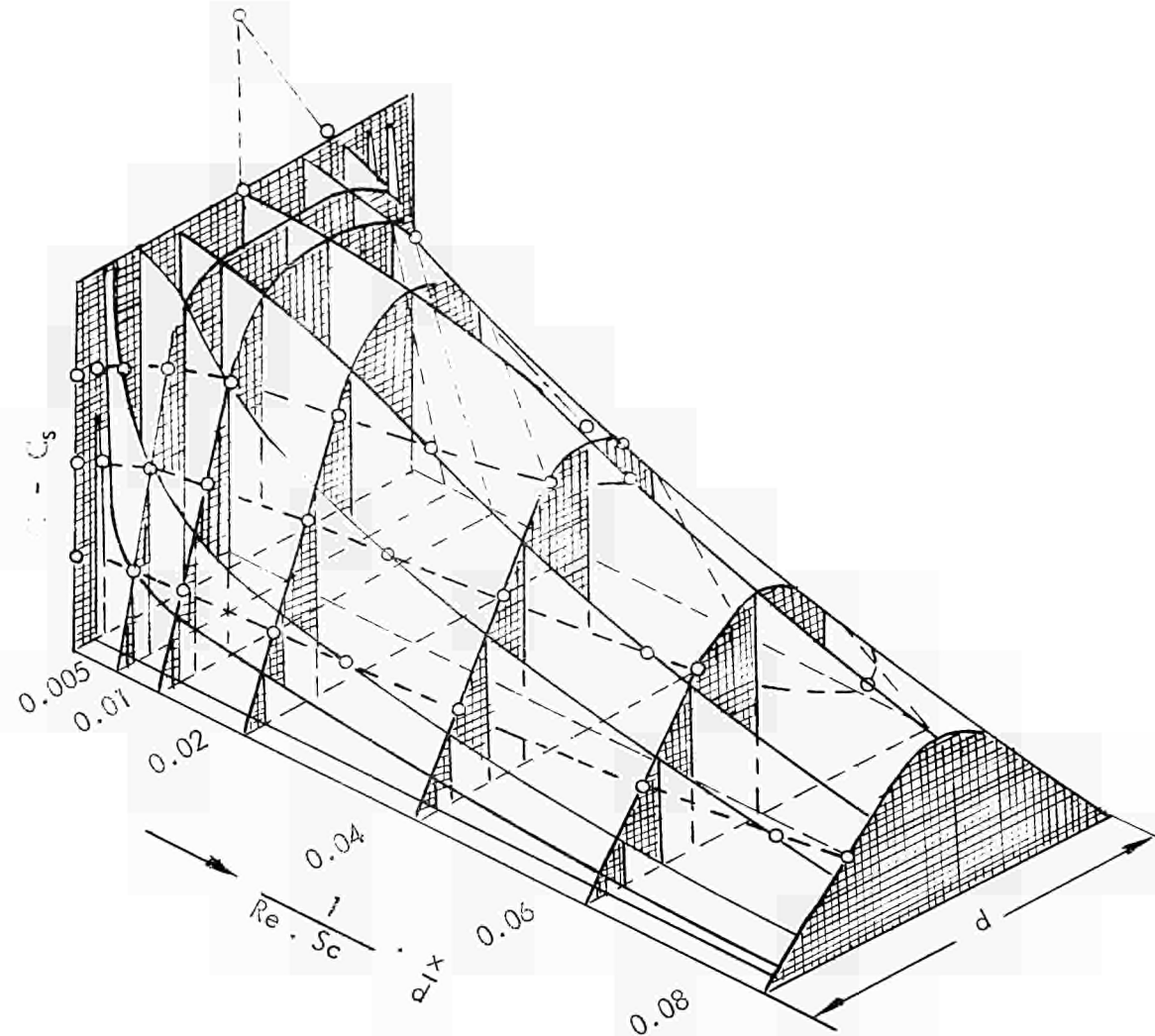


Fig. 2B Pipe friction chart $\frac{\tau_s}{\rho u^2}$ versus Re

$$Re = \frac{u d \rho}{\mu}$$



Concentration profile in laminar flow through
the entrance region of a tube

(From L. Prandtl, "Strömungslehre", 3d ed.,
p. 377, Fig. 305, VIEWEG-Verlag Brunswick,
GERMANY 1949)

Fig. 214

Theoretical mass transfer correlation for laminar flow in tubes
 - Results shown for logarithmic mean and arithmetic mean values

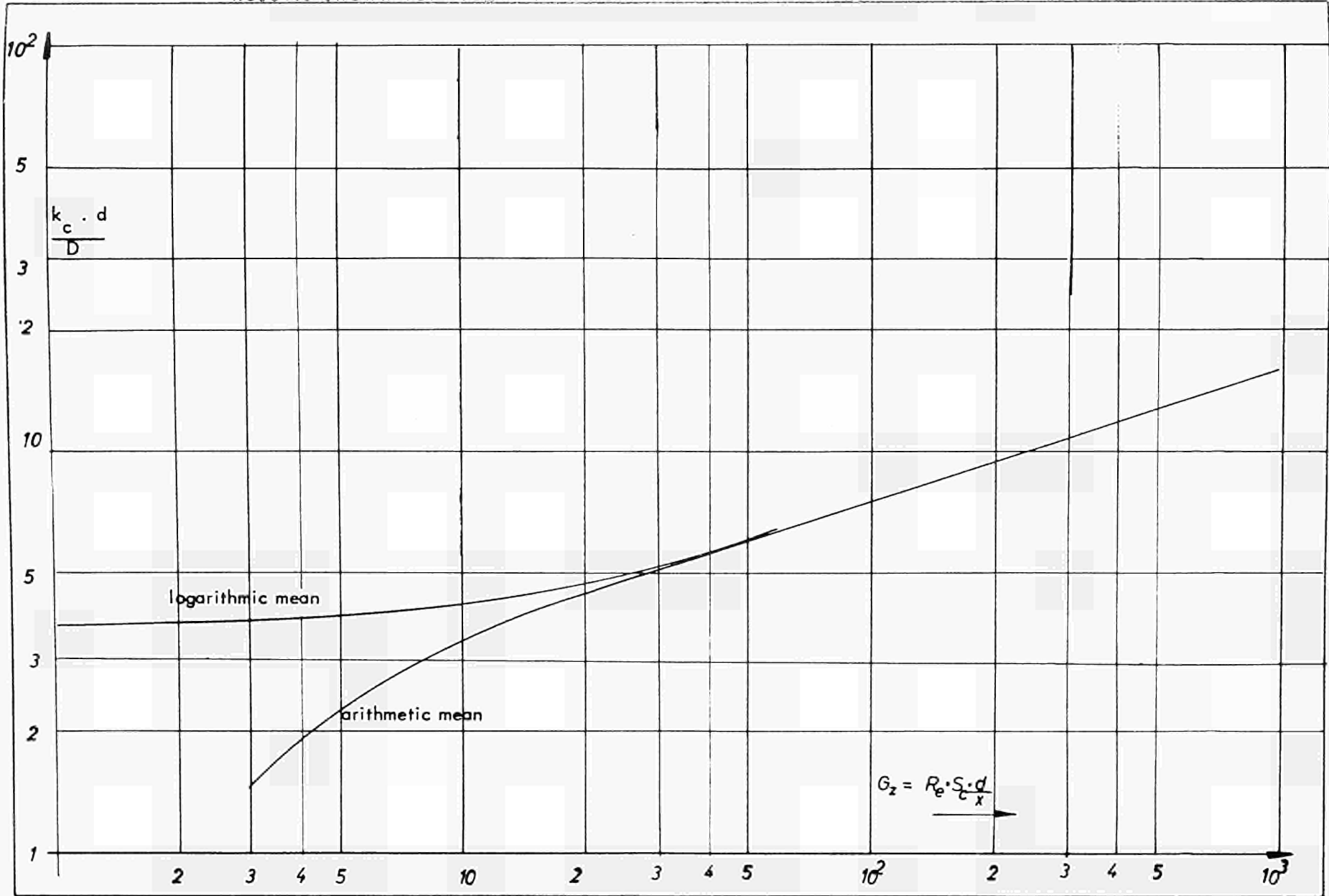
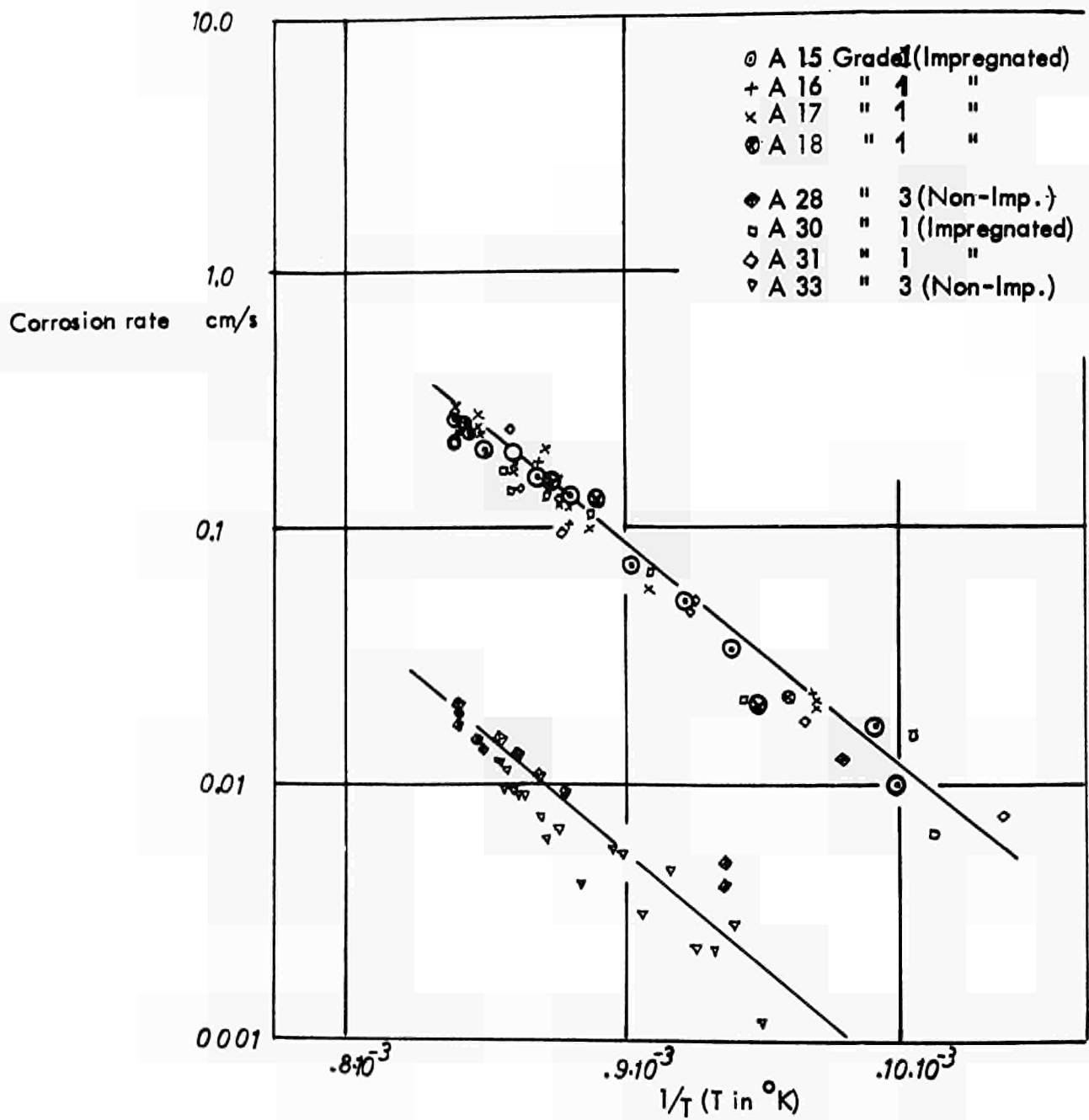


Fig. 215

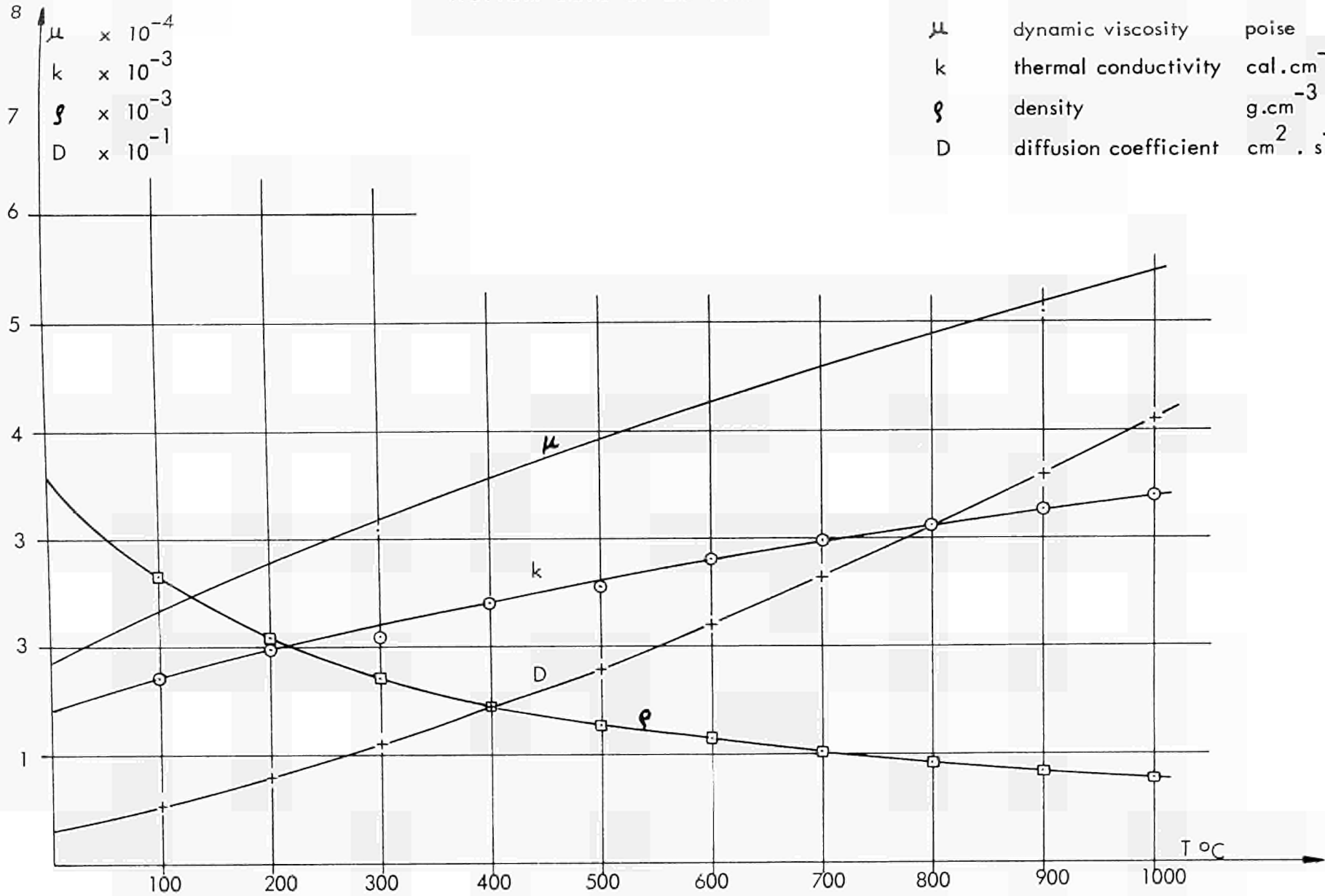


Oxidation rates of Grade 1 and Grade 3 Graphites
with CO_2

Grade 3 = purified Grade 1

Fig. 3.1

Helium data at 20 atm



μ dynamic viscosity poise
 k thermal conductivity cal.cm⁻¹.s⁻¹.°C⁻¹
 ρ density g.cm⁻³
 D diffusion coefficient cm².s⁻¹

Fig. 3.2

Nitrogen data at 20 atm.

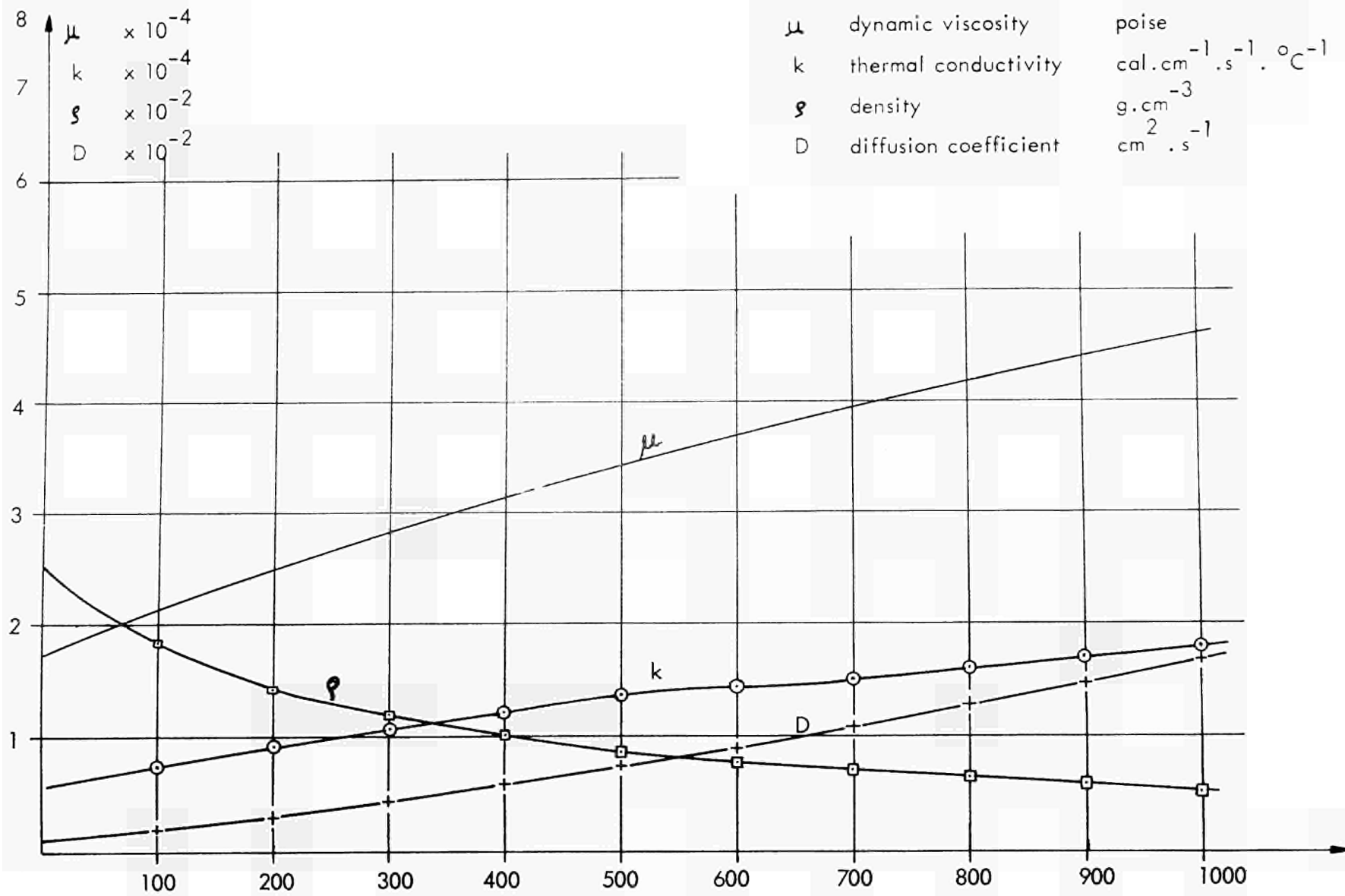


Fig. 3.3

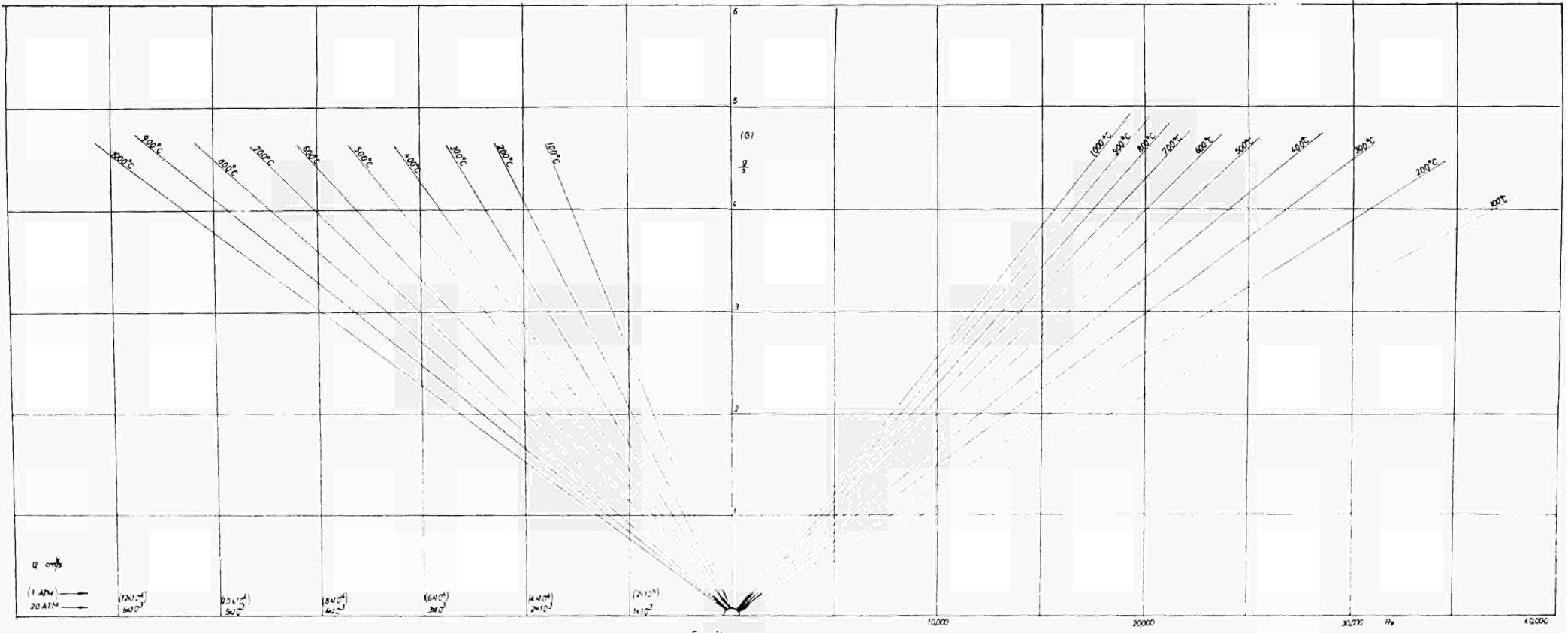


Fig. 3A
 Relationship between Re , mass flow, volume flow
 for different temperatures of the flow in a 5 mm. low density channel

Fig. 3.5

Relationship between Reynold's number (Re), mass flow (G), volumetric flow (Q) for different temperatures of N_2 flow in a 6mm diameter channel

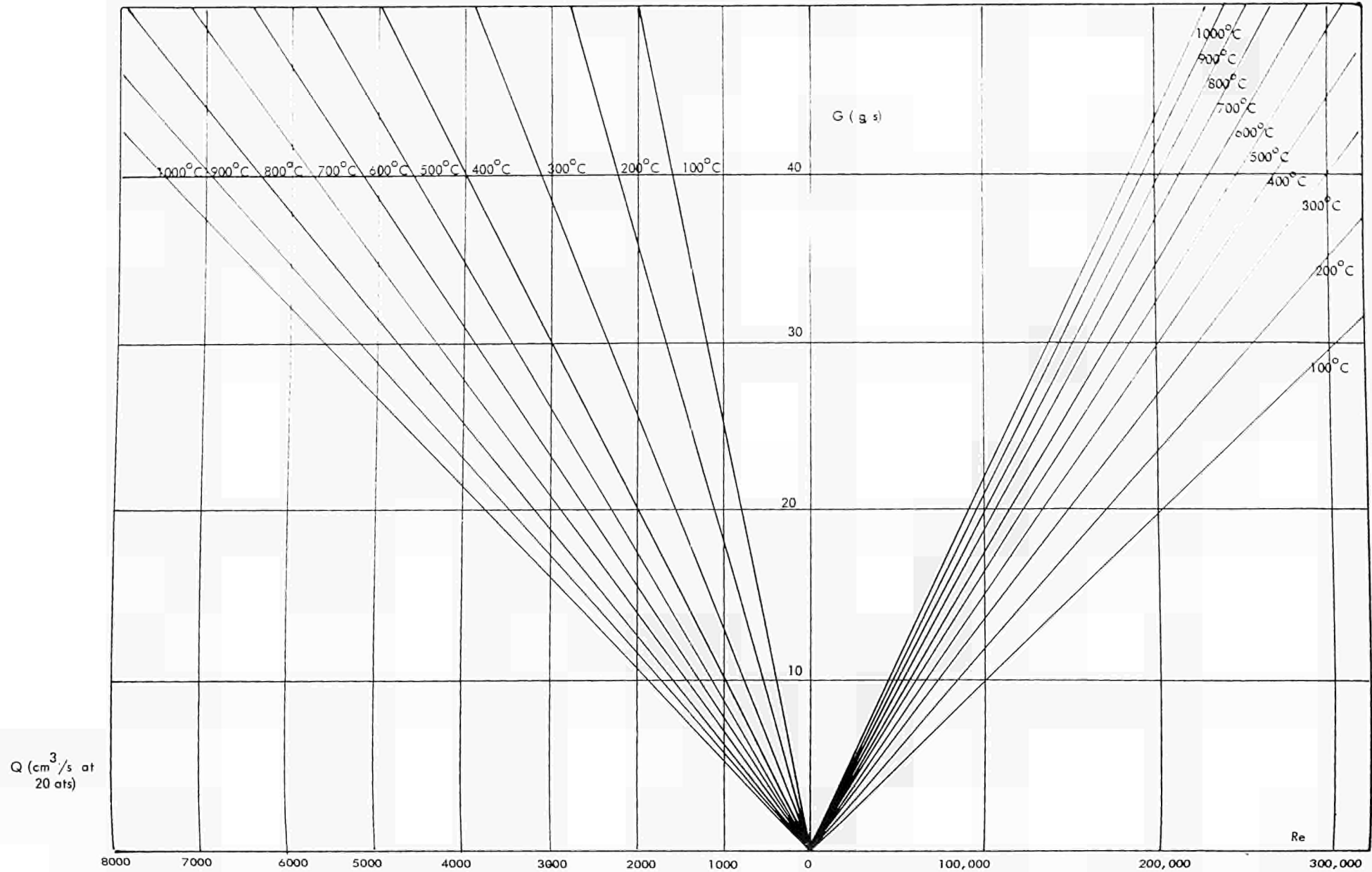
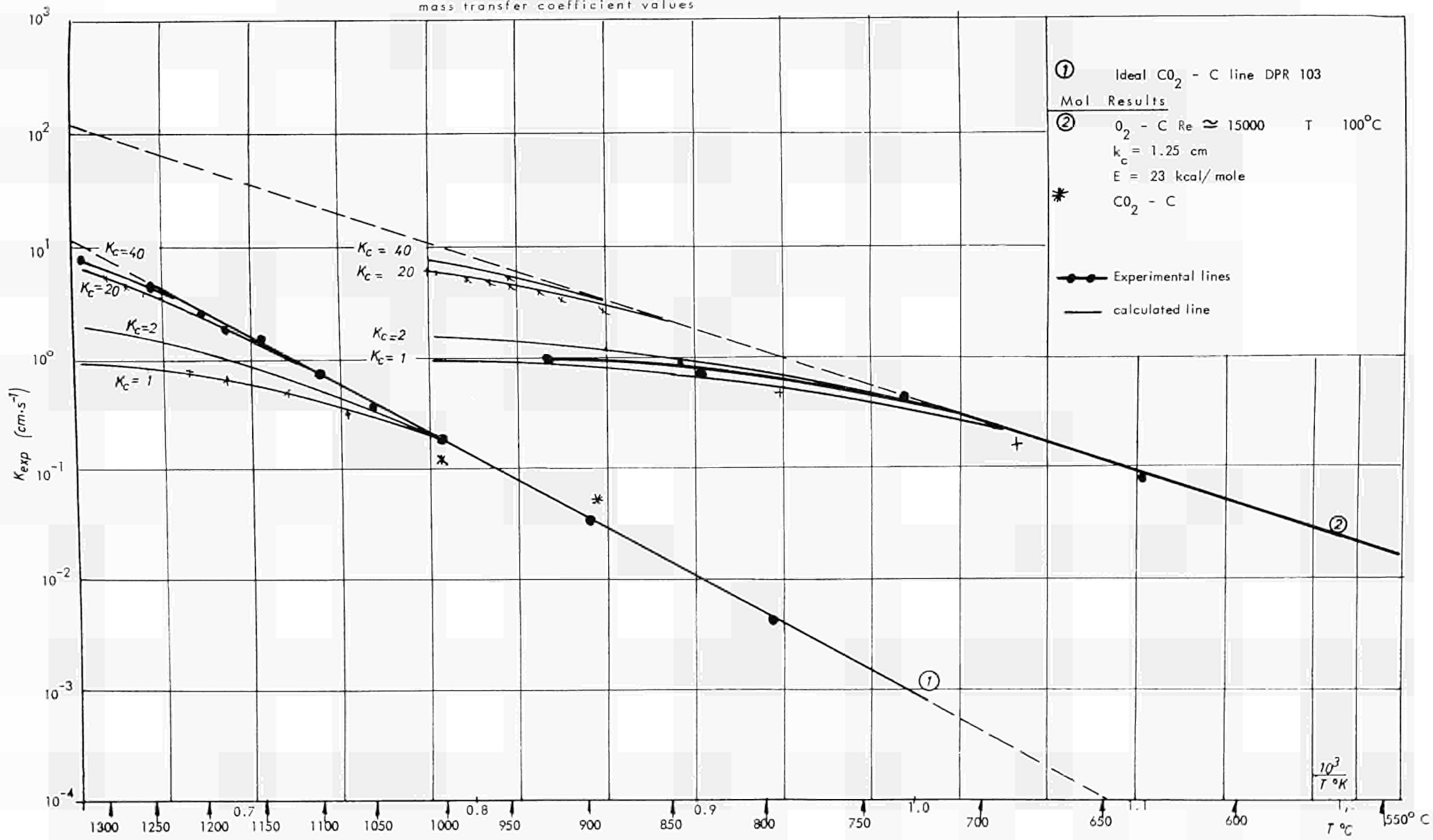
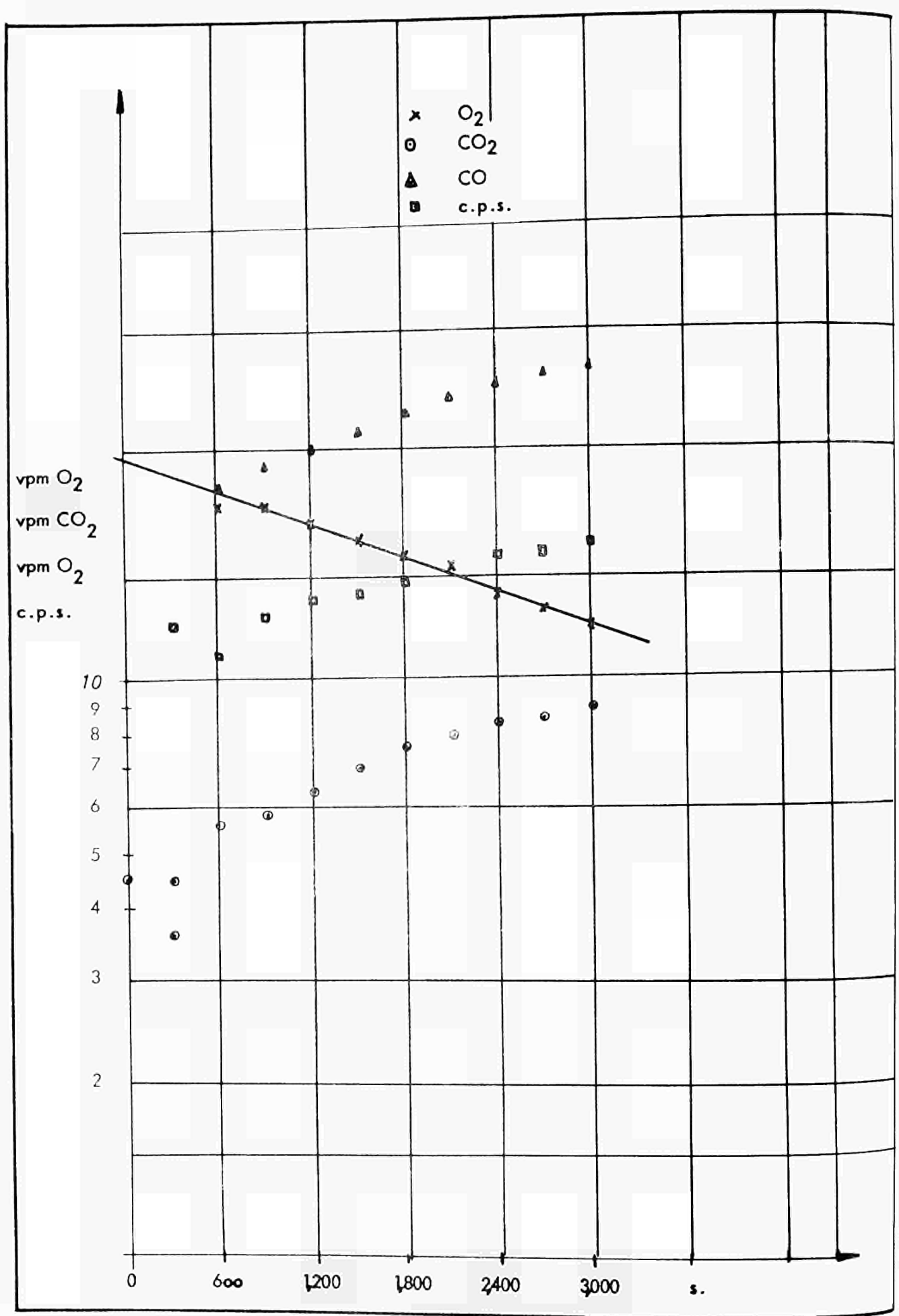


Fig. 3.6 Influence of the mass transfer regime on the reaction of graphite with CO_2 and O_2 for different mass transfer coefficient values





Typical O₂ Depletion Test
 Fig. 3.7

Graph for calculation of the reaction rate
with O_2 depletion method

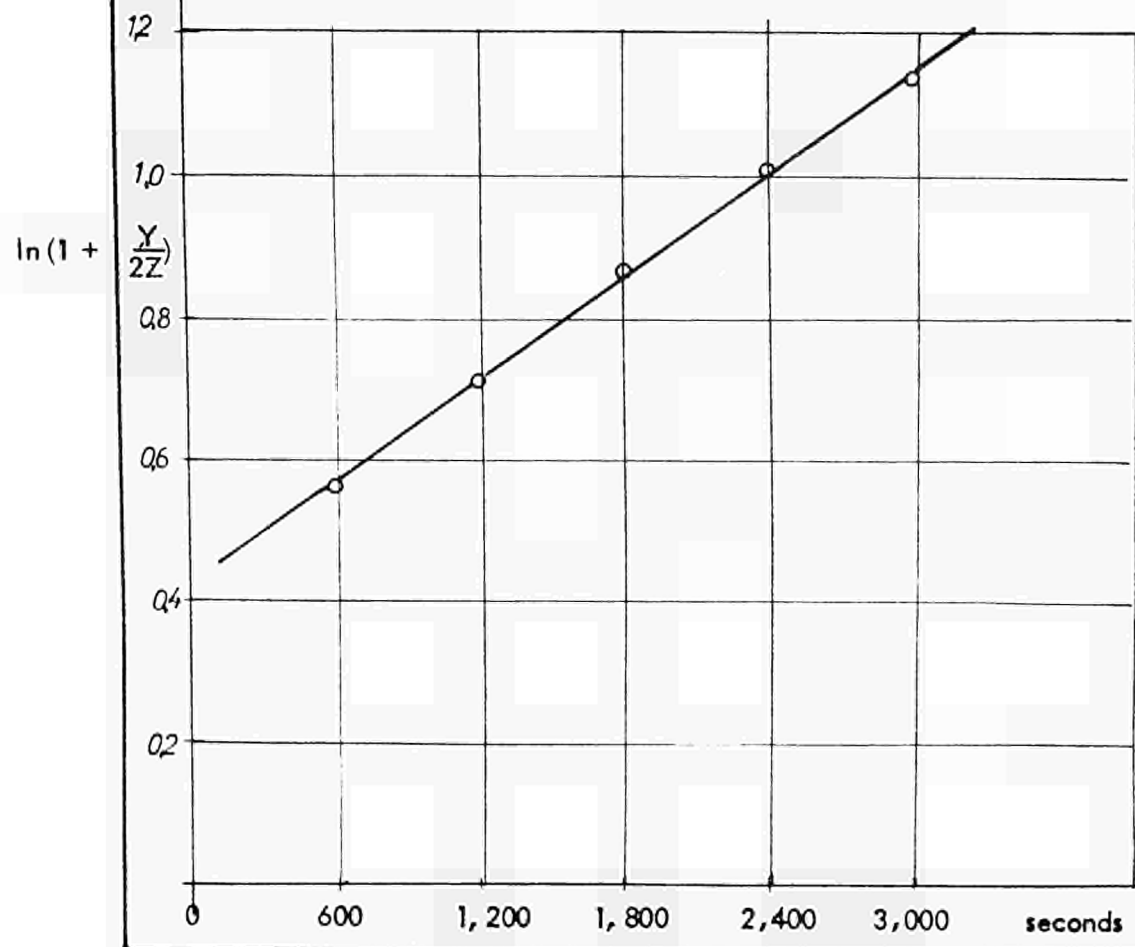


Fig. 3.8

Arrhenius plot of the experimental rates
 measured in 20 atm. He with the gas analysis method
 $Re \approx 2.000$

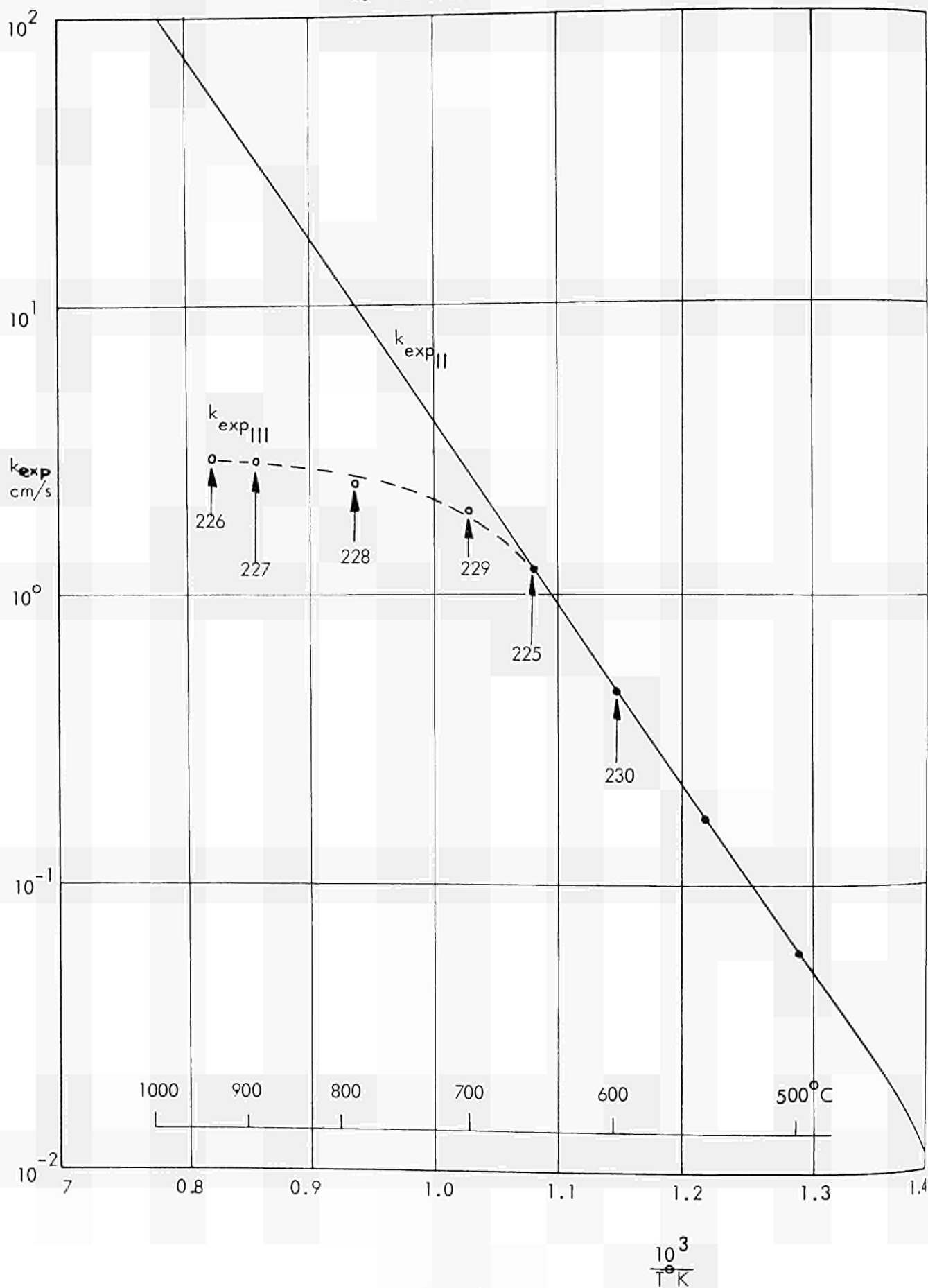


Fig. 3.9

Arrangement of C^{14} sample for local mass transfer measurement

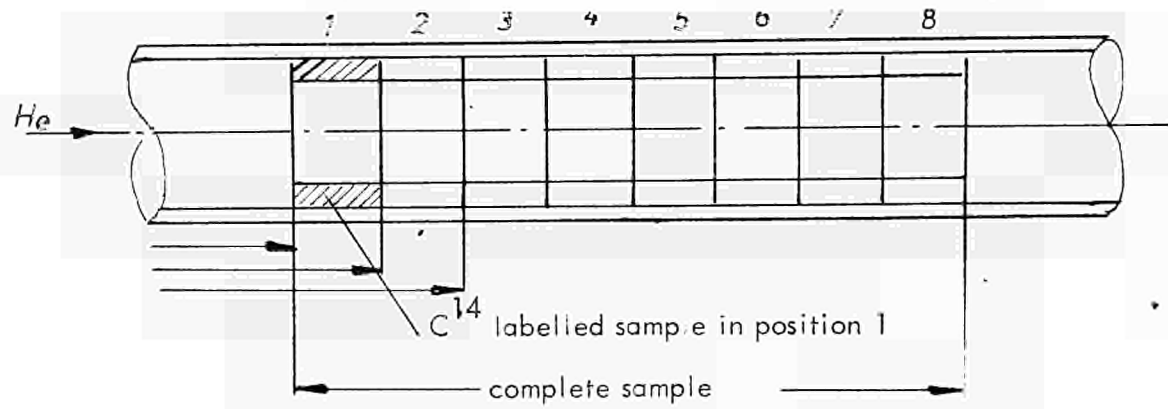


Fig. 3.10



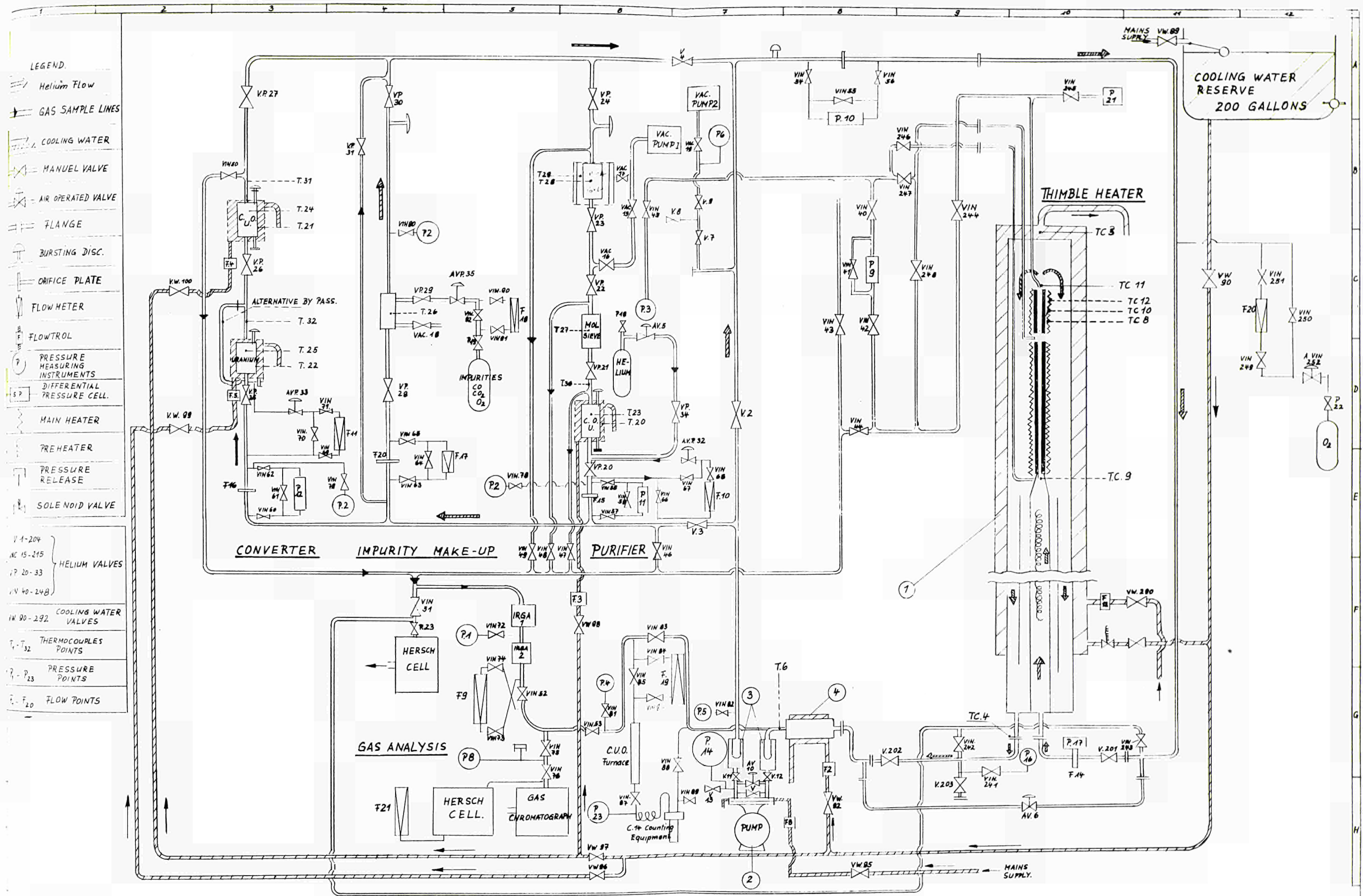
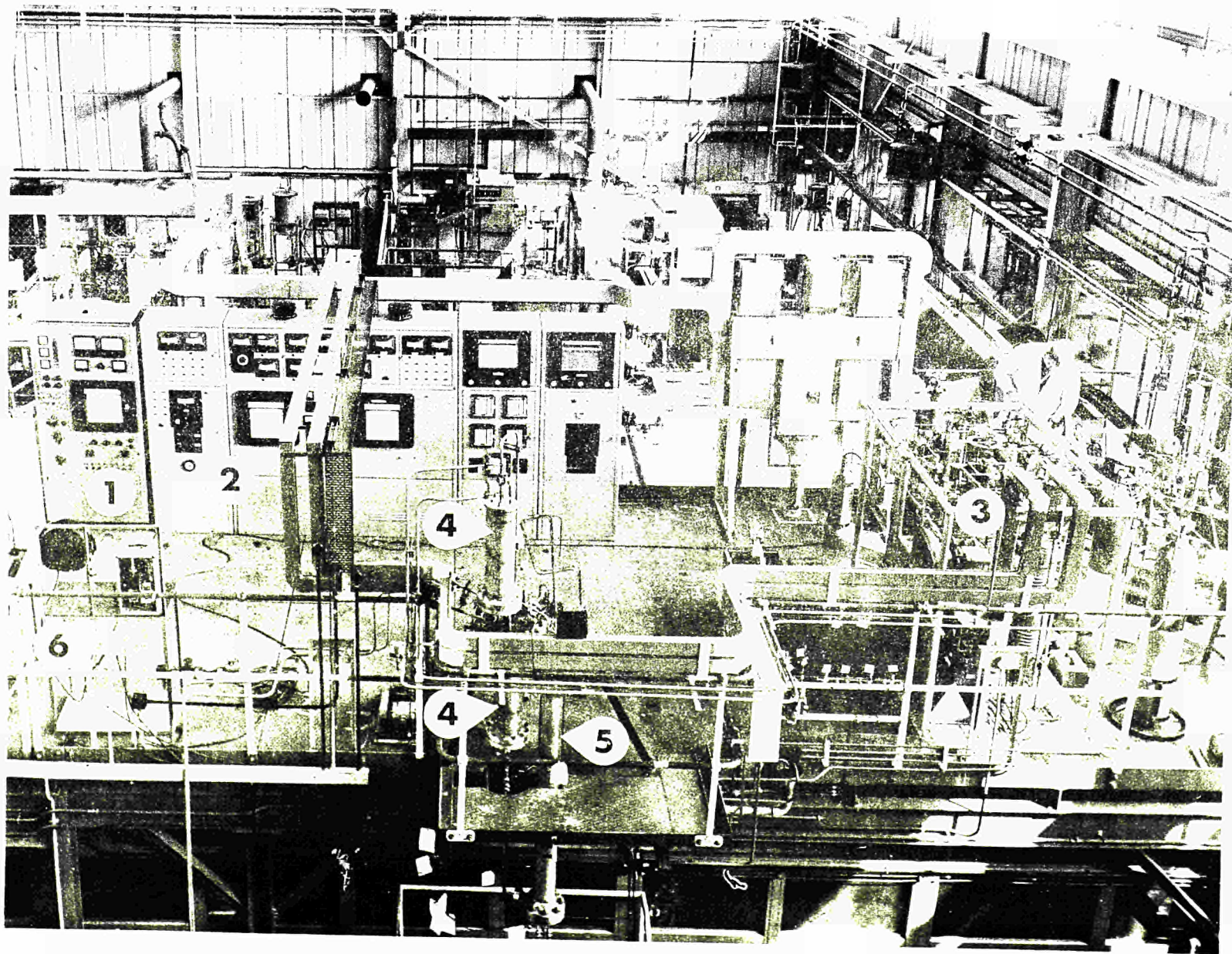


Fig. 4.1
P.C.T.E. LOOP MASTER
FLOW SHEET





1 GAS
CHROMATOGRAPH

2 CONTROL
PANEL

3 PURIFIER

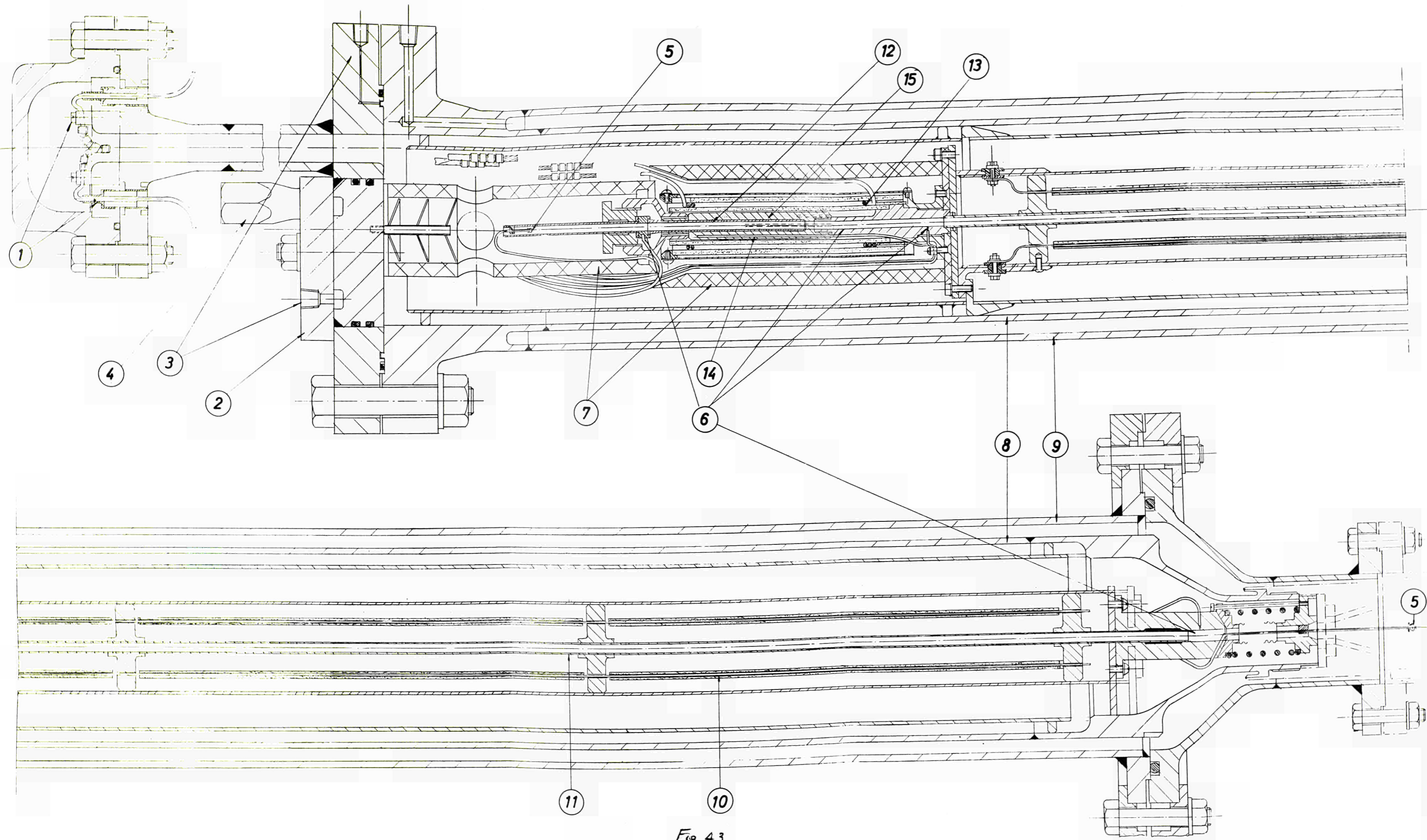
4 SURGE
TANKS

5 FURNACE

6 ANALYTICAL
INSTRUMENTS

FIG. 4.2. PRESSURIZED CARBON TRANSPORT EXPERIMENT





- | | |
|----|---|
| 1 | Electrical connection |
| 2 | Access cover for removal of sample |
| 3 | Cooling water outlets |
| 4 | Thermocouples and gas sample lines outlet |
| 5 | Gas thermocouples |
| 6 | Gas sample point |
| 7 | Radiation shield |
| 8 | Pressure tube |
| 9 | Cooling water jacket |
| 10 | Molybdenum preheater |
| 11 | Flow stabilisation tube |
| 12 | Graphite sample |
| 13 | Graphite sample heater |
| 14 | Graphite's thermocouples |
| 15 | Graphite support tube |

Fig 4.3
THIMBLE MK III



CONDITIONS

HELIUM PRESSURE
20 ATMS
HELIUM INLET
TEMP. 20°C
OVERALL
HEIGHT 25 feet
MAX. GAS TEMP. 800°C.
MAX. SAMPLE
TEMP. 1100°C.
HELIUM FLOW
0-3 GMS./SEC.
REYNOLDS NUMBER
500-20,000
WITH HELIUM

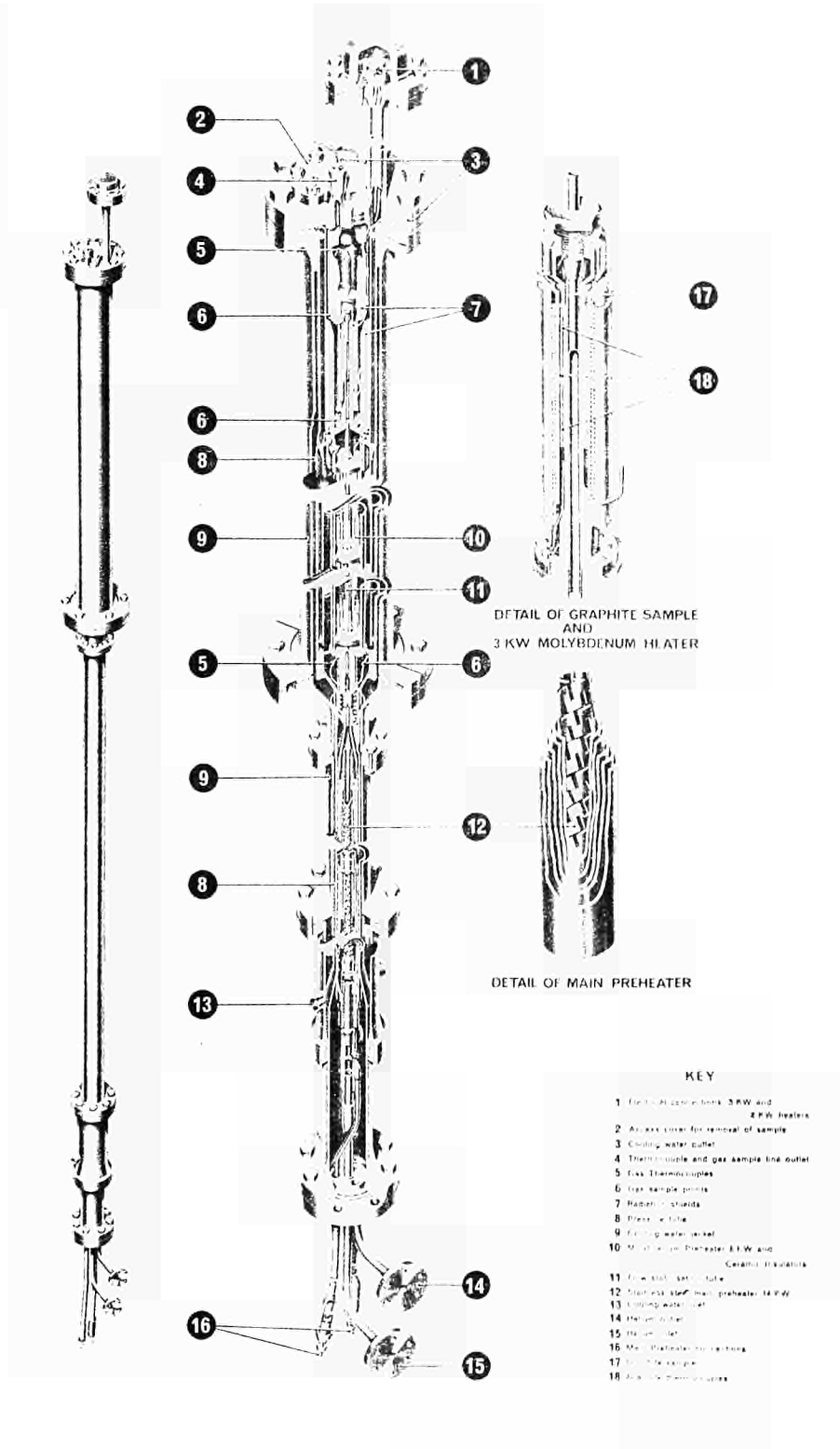


Fig. 4.4. Exploded view of Thimble MK III.

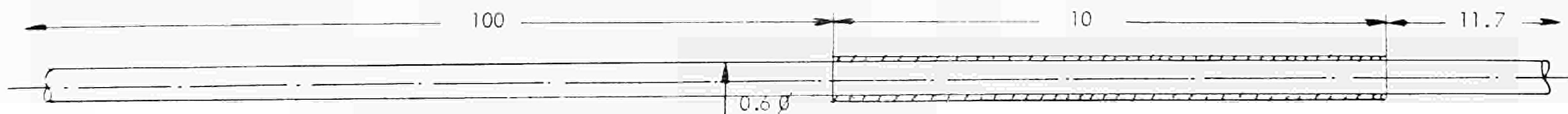


Fig. 4.5a 0.6 cm Ø channel with a long calming section

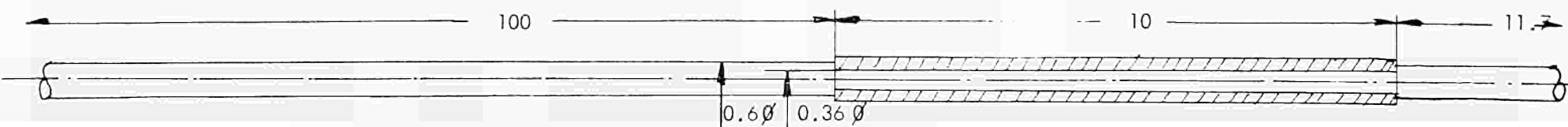


Fig. 4.5b 0.36 cm Ø channel with a sharp edge entrance

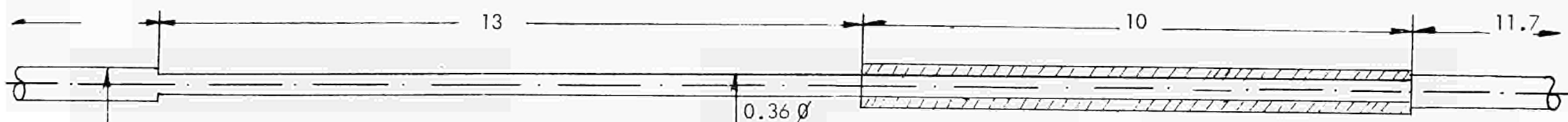


Fig. 4.5c 0.36 cm Ø channel with short calming section (13cm)



Fig. 4.5d 0.36 cm Ø channel with right angle entrance and with C^{14} sample at location x_1

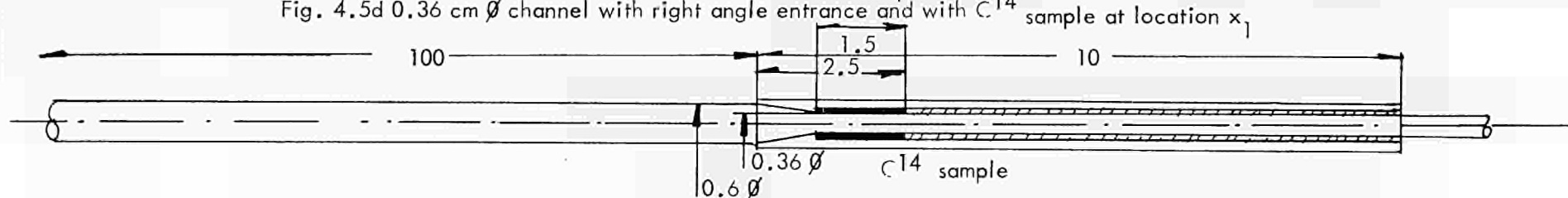
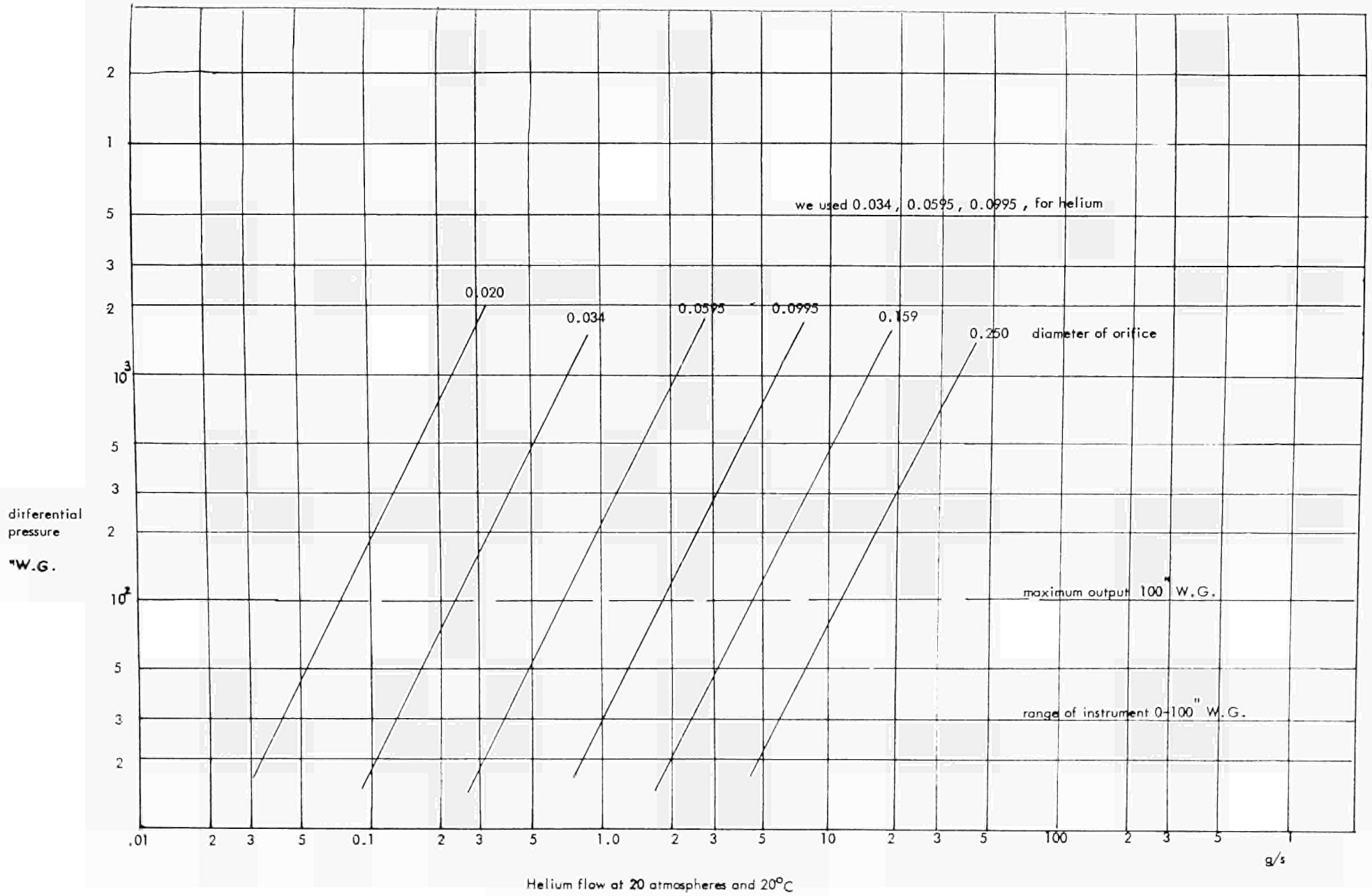


Fig. 4.5e 0.36 cm Ø channel with a bellmouth entrance and with a C^{14} sample at location x_1

Fig. 46 Orifice plate calibration curves



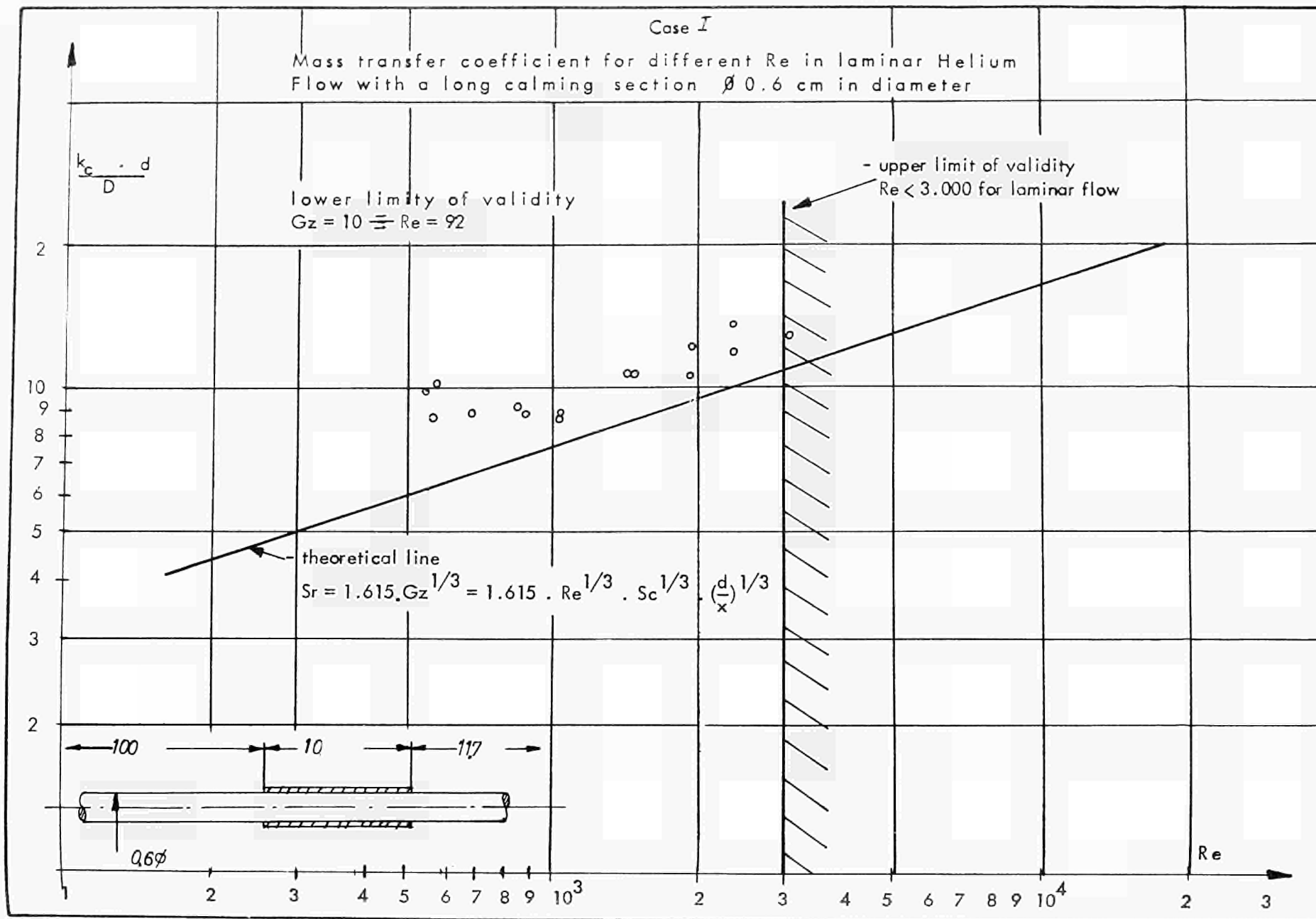


Fig. 6.7

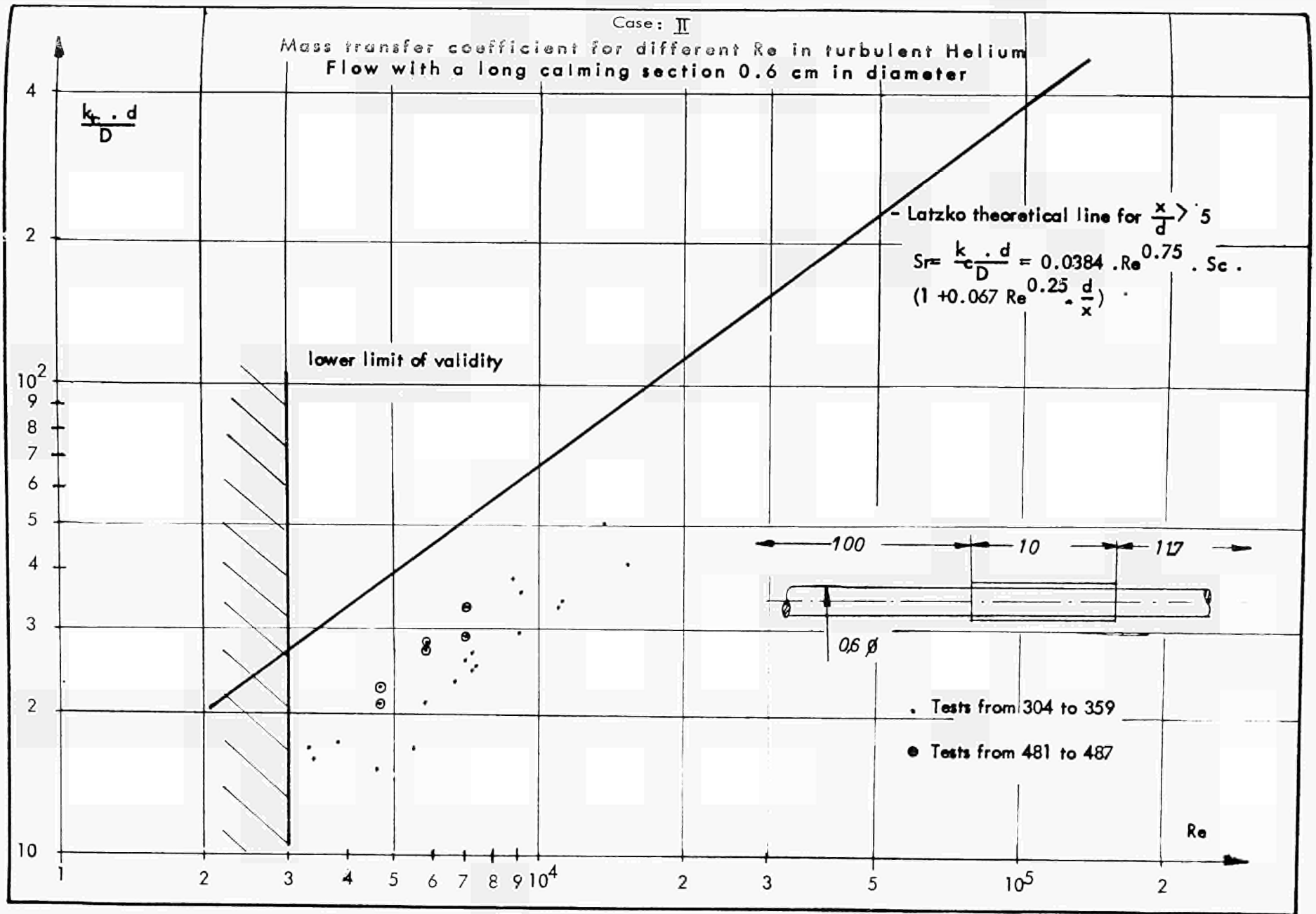


Fig. 62

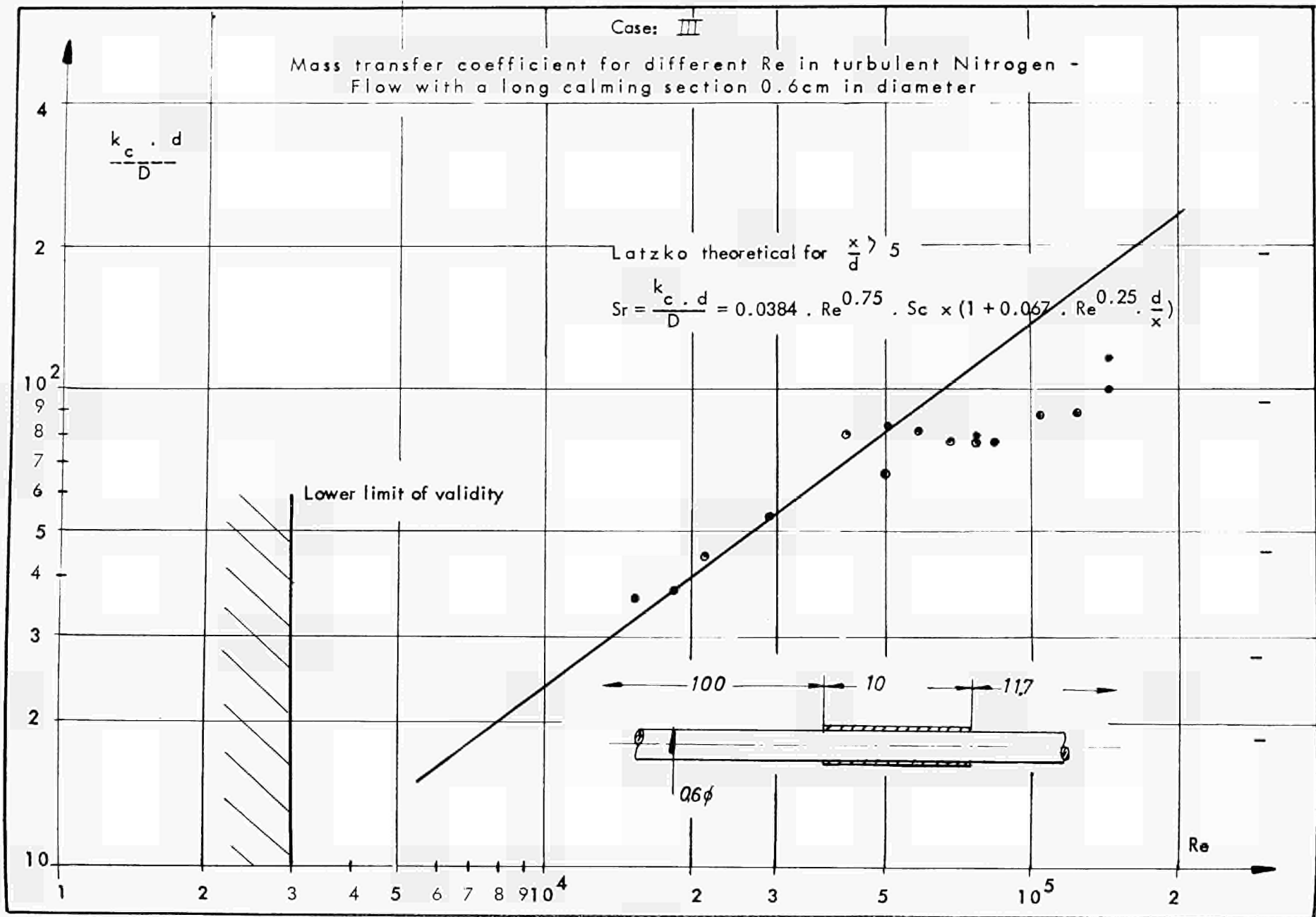


Fig. 6.3

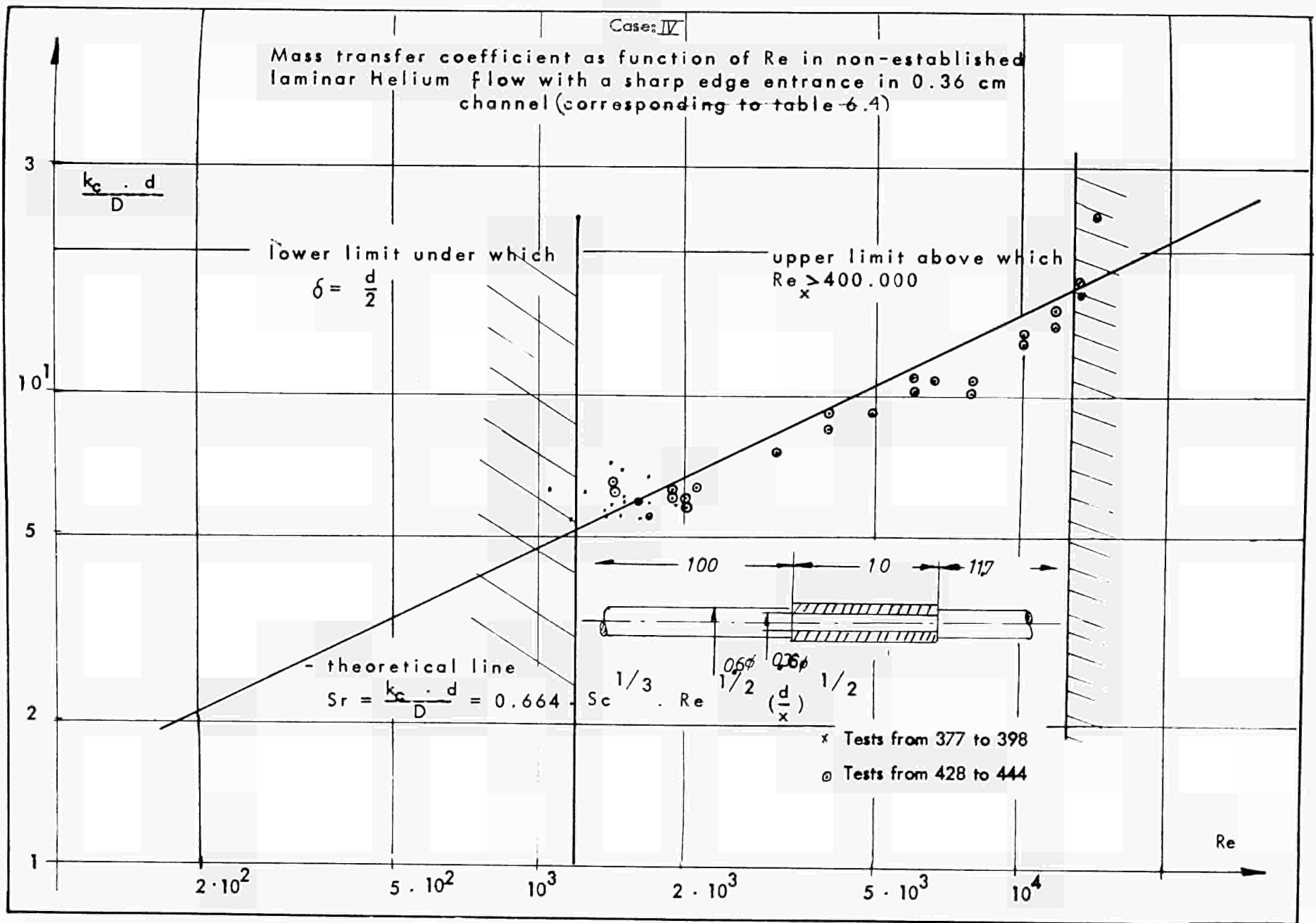


Fig. 64_a

Mass transfer coefficient as function of Re_x in non-established laminar helium flow with a sharp edge entrance in 0.36 cm channel

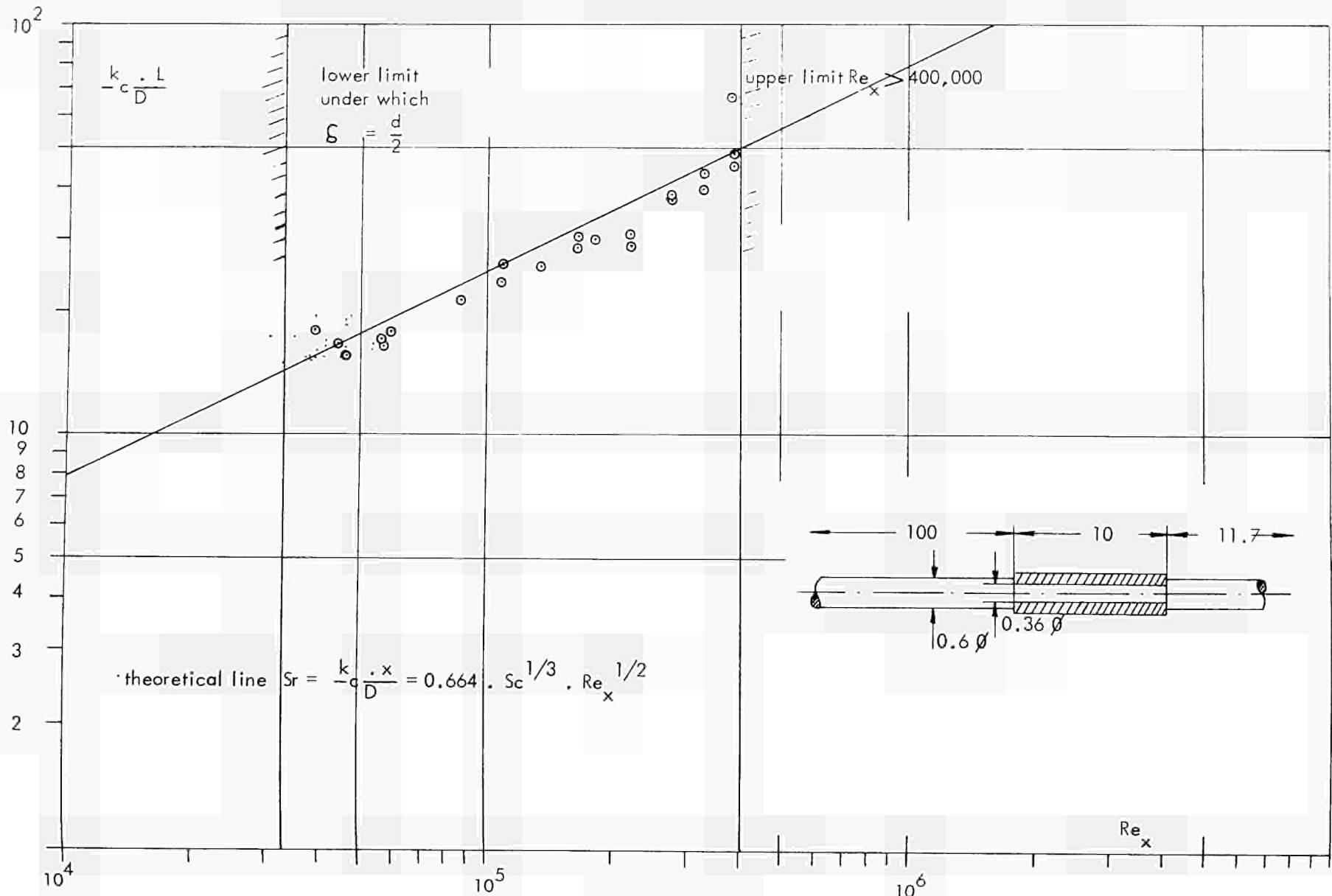


Fig. 6.4 b

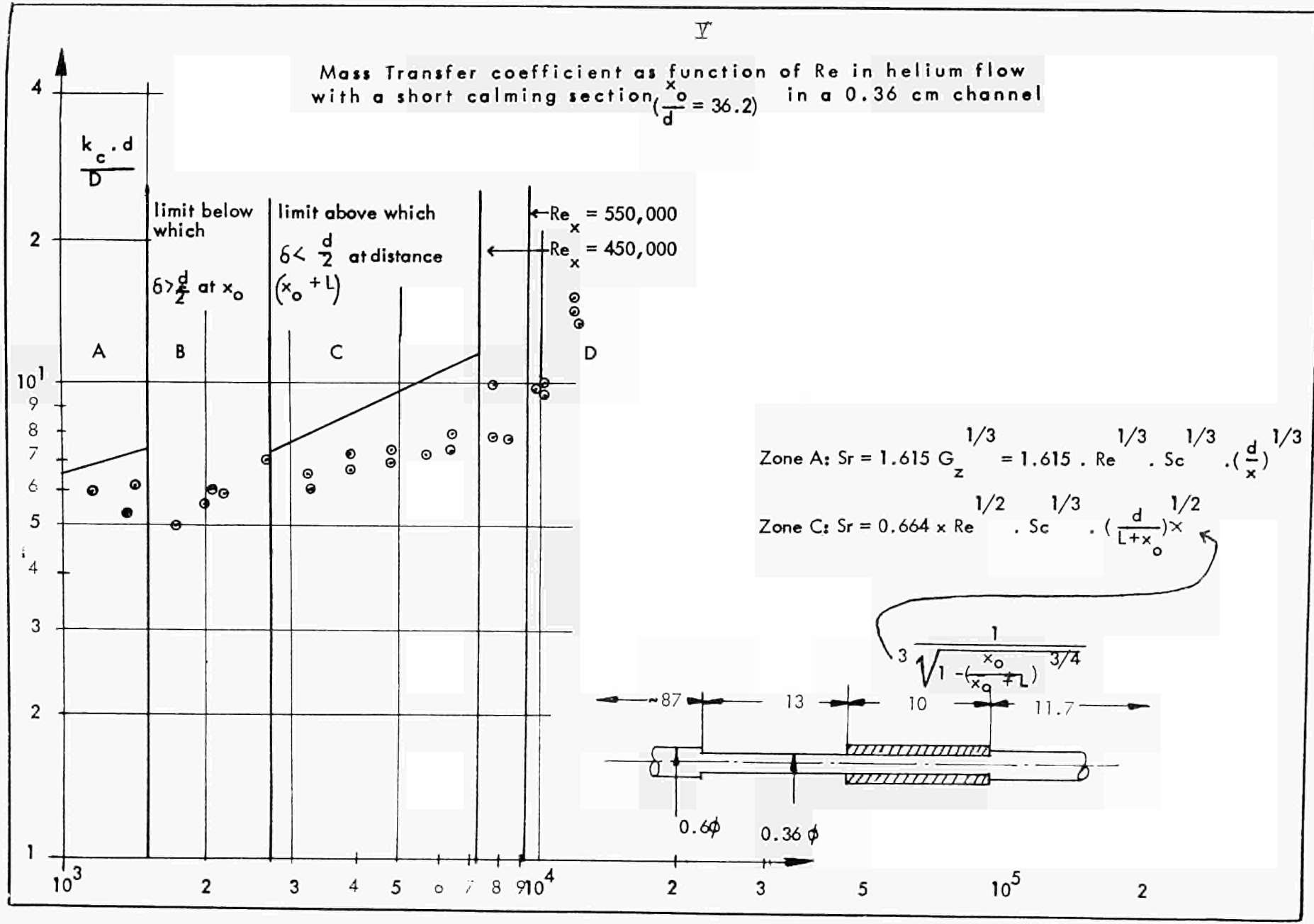


Fig. 6.5

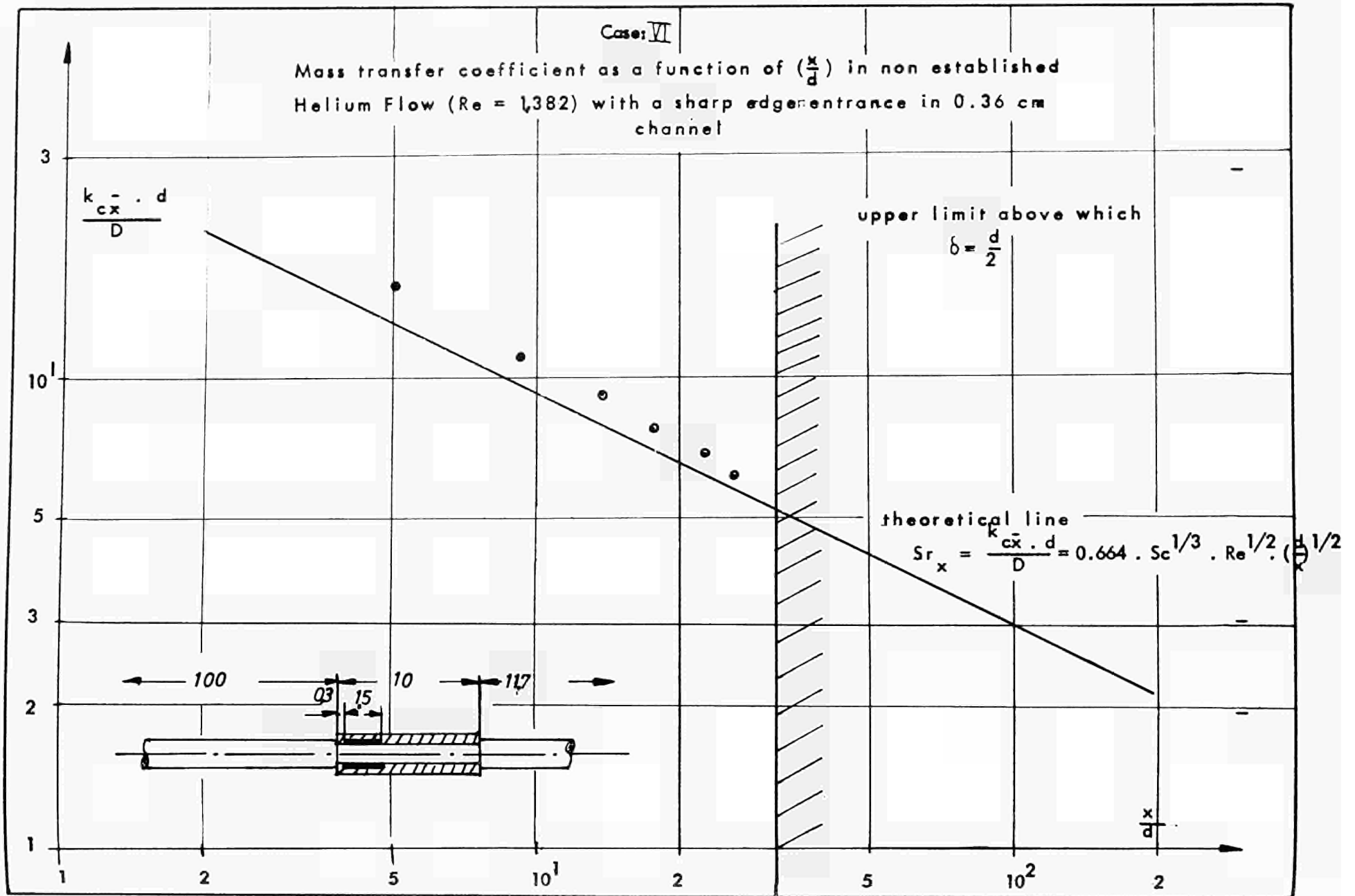
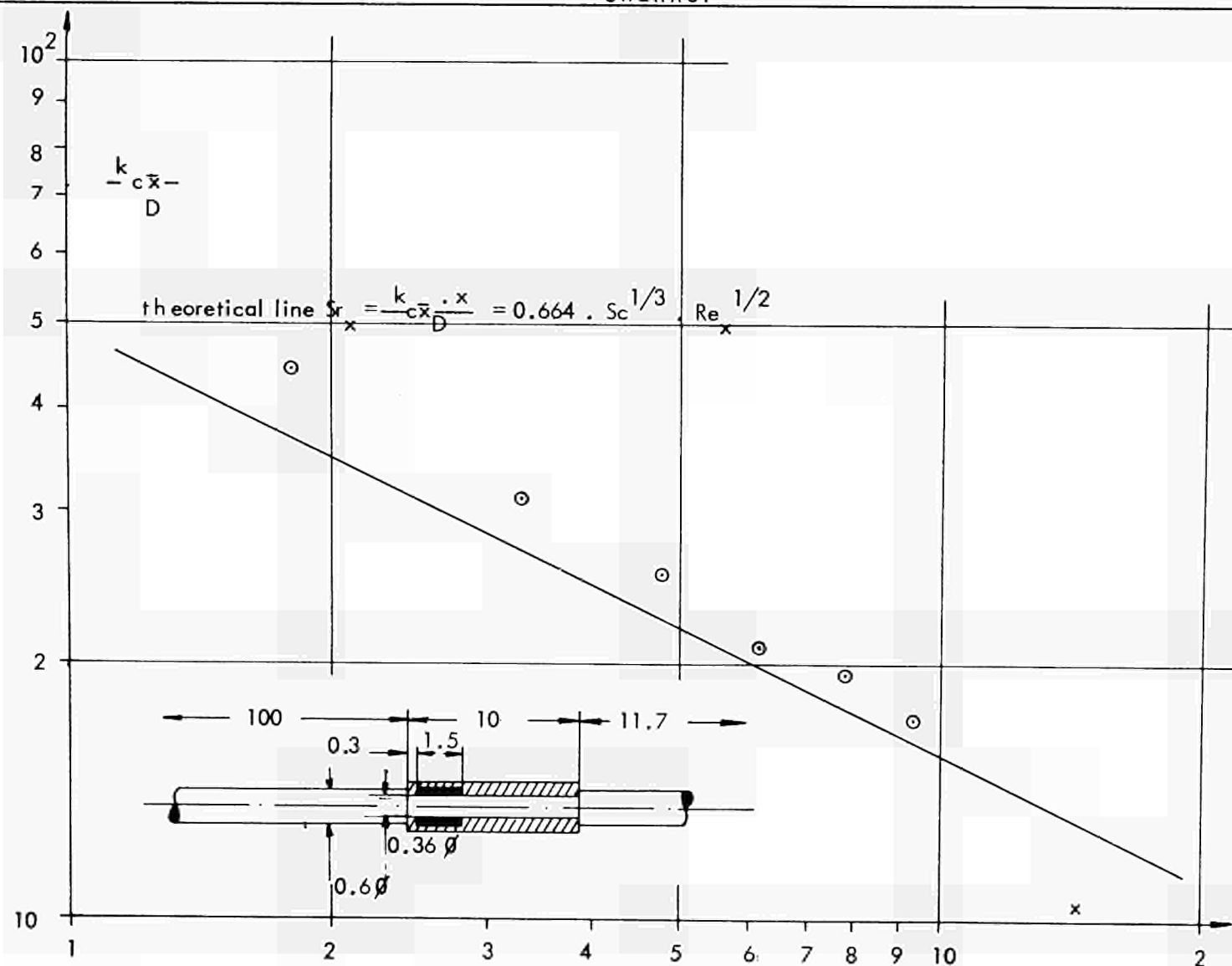


Fig. 66 a

Mass transfer coefficient as function of x in non established helium flow ($Re = 1.382$) with a sharp edge entrance in 0.36cm channel



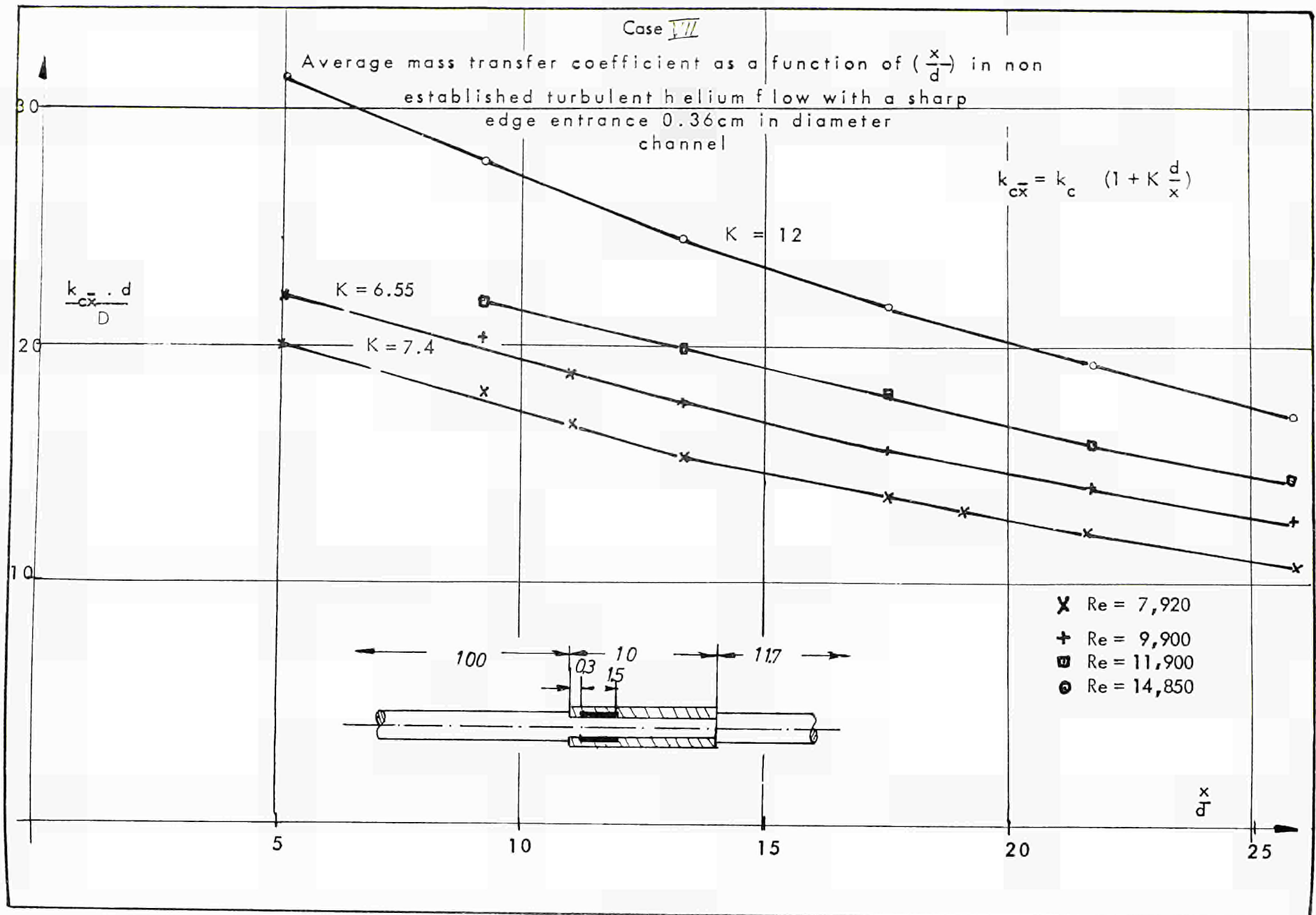


Fig. 67

Average mass transfer coefficient as function of $(\frac{x}{D})$ in non established turbulent helium flow with a bellmouth inlet in a 0.36cm diameter channel

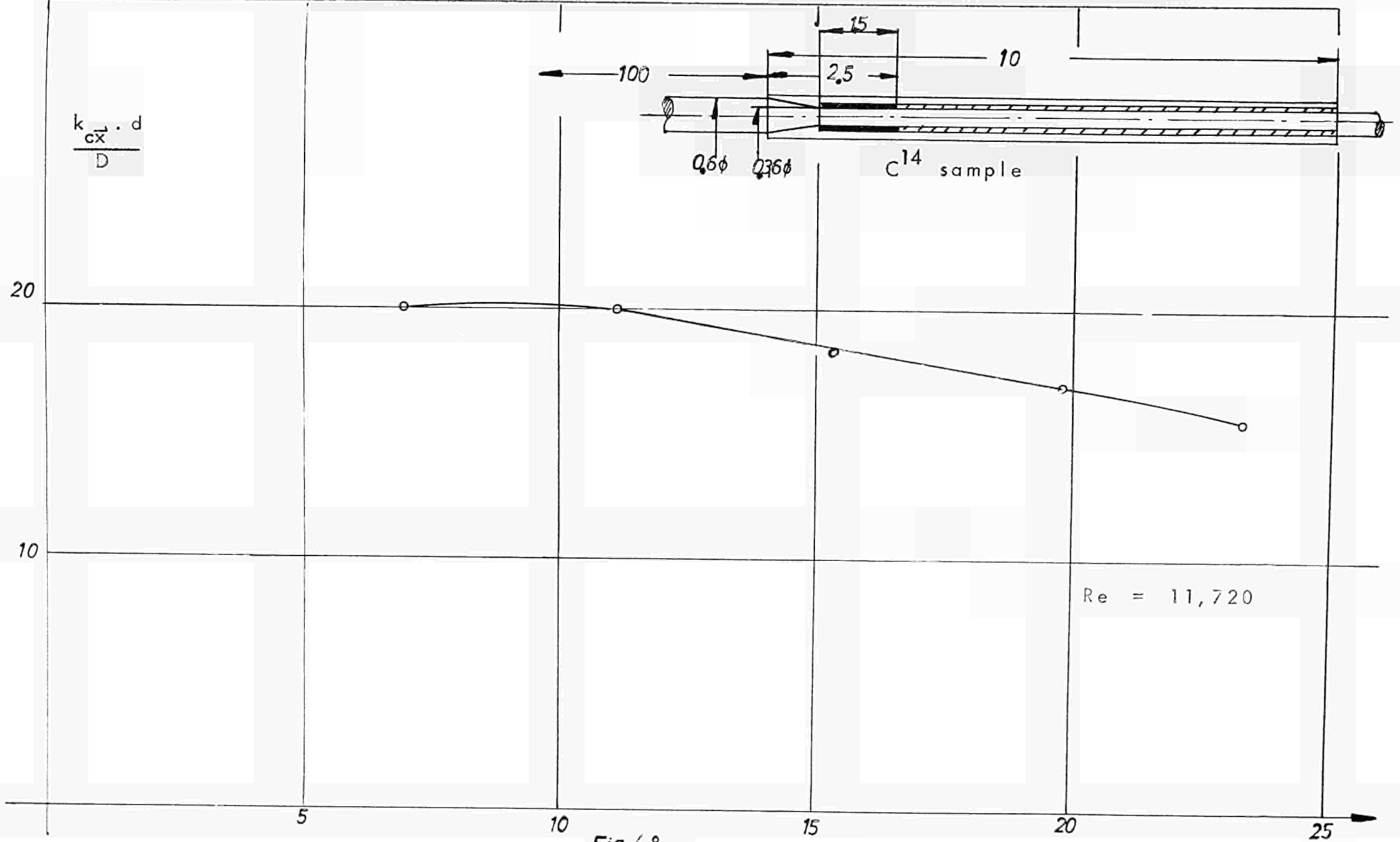


Fig 6.8

CASE I

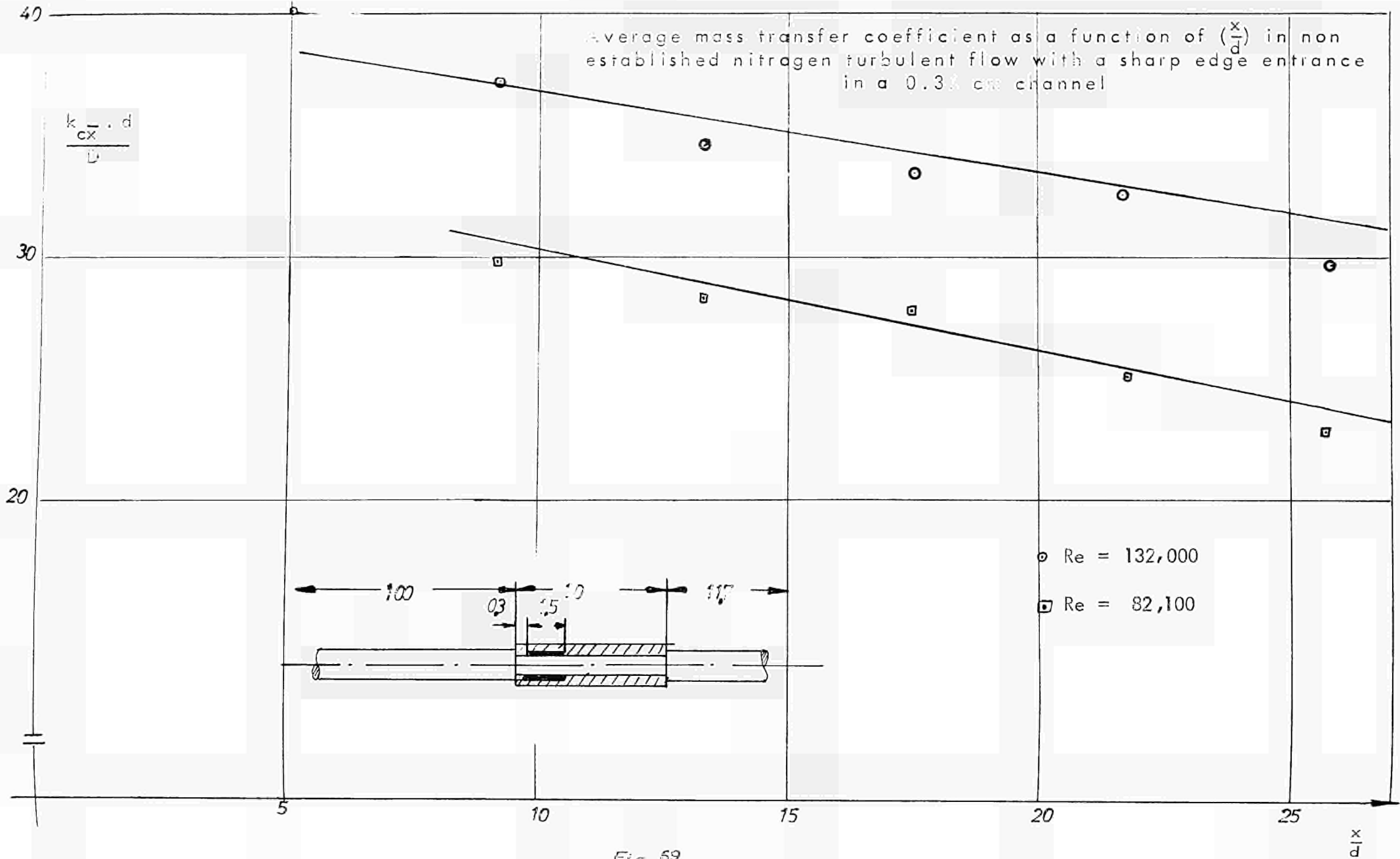


Fig 69

Proportionality between k_c and $\frac{1}{P}$ or D

960 °C $Re \approx 2700 - 3000$

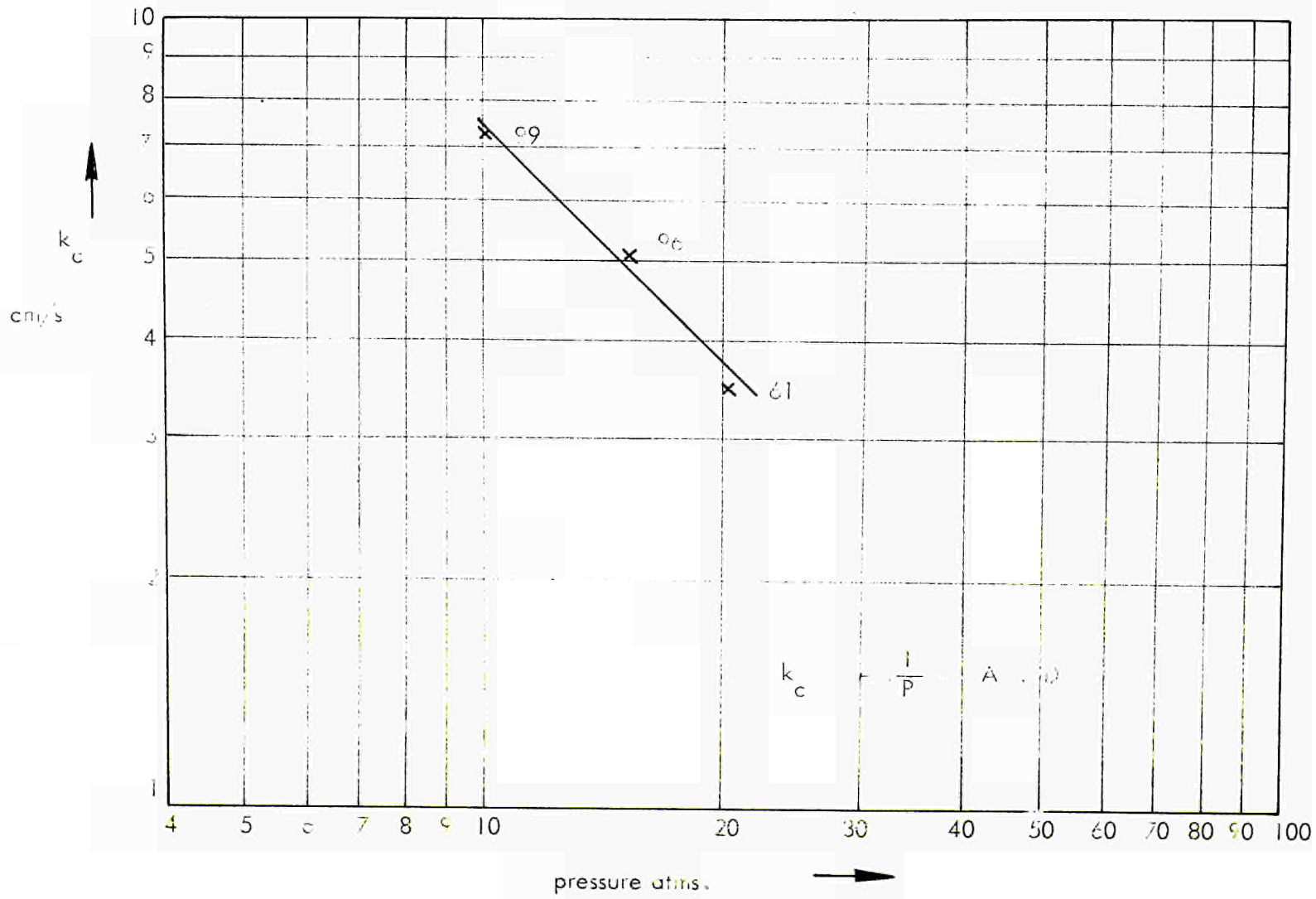


Fig. 6.10

Values F_1 and F_2 to be used in Martinelli's equation for natural and forced mass convection in vertical tube with uniform wall concentration

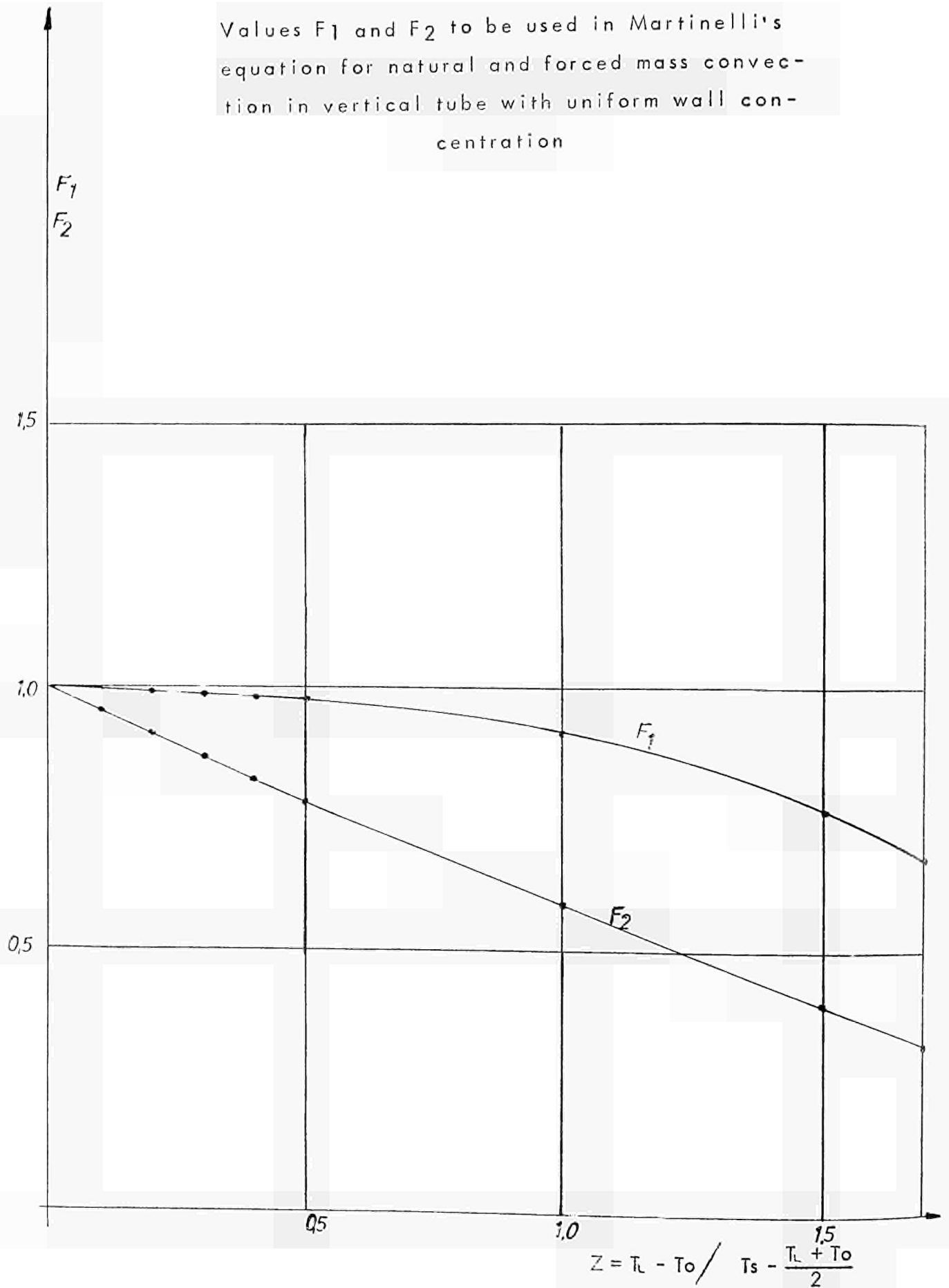


Fig. 6.11

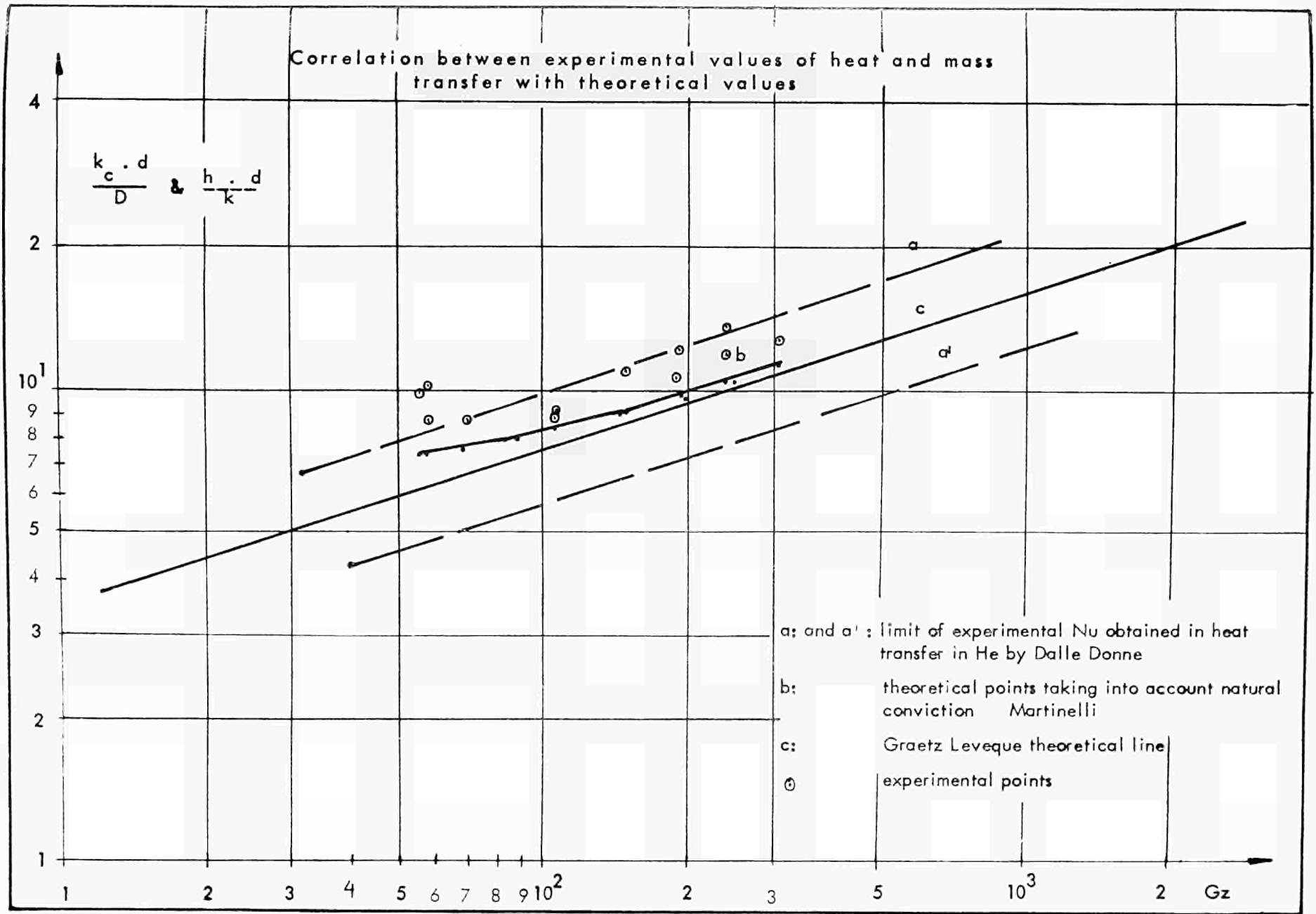


Fig. 6.12

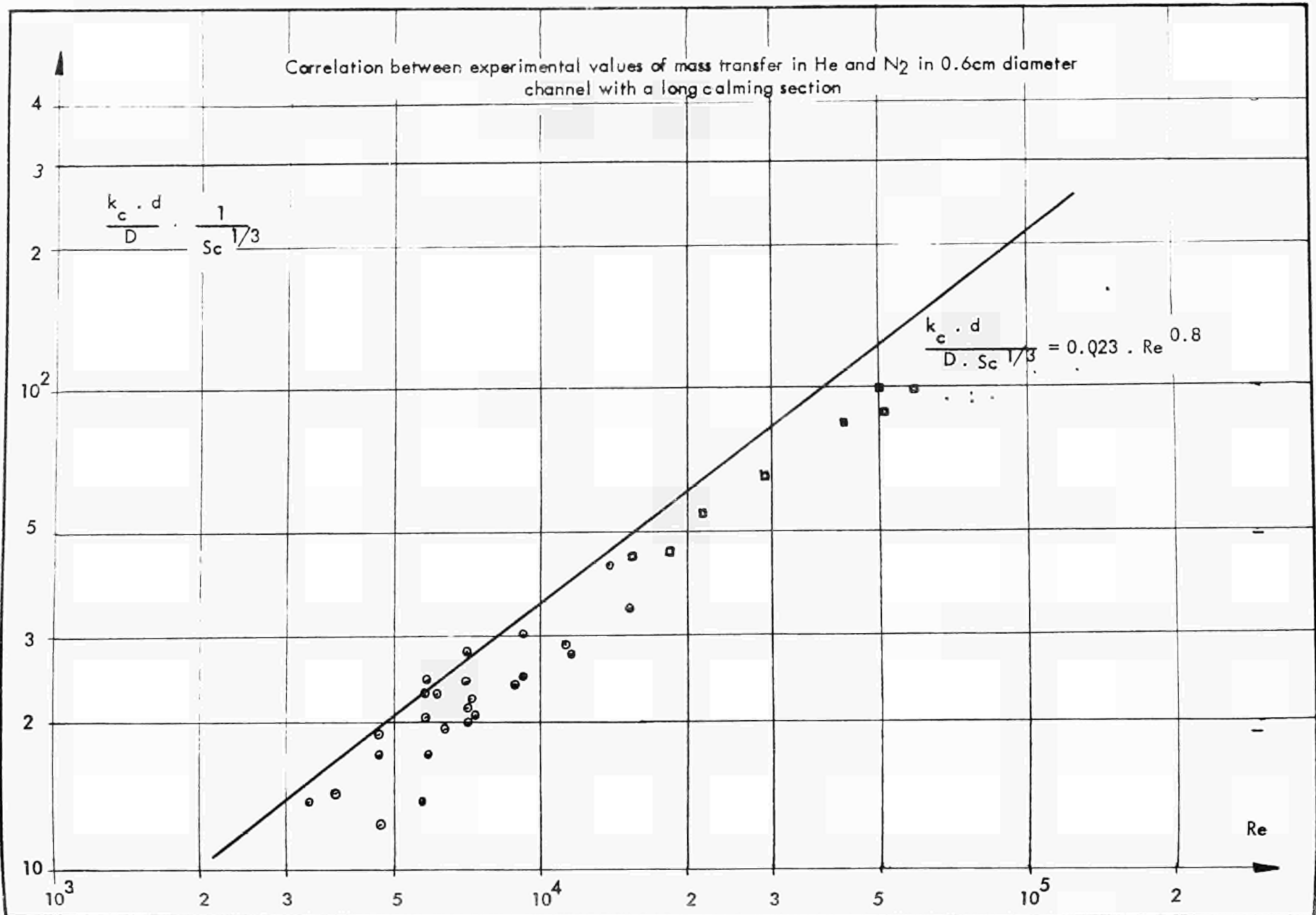


Fig. 613

Table 2.1

Values used for calculation of the diffusion coefficient

From Hirschfeld, Bird and Spotz

Gas	ϵ/K °K	r, A
O ₂	110.3	3, 433
A	124.0	3, 418
He	6.03	2.7
N ₂	91.46	3, 691

Table 2.2

Mass transfer values for parabolic velocity distribution and constant wall concentration

From R.H. Norris & D.D. Streid - Trans. A.S.M.E. - 8 - 1940

$Gz = Re \cdot Sc \cdot \frac{d}{x}$	$\frac{k_{ca} \cdot d}{D}$	$\frac{k_{clm} \cdot d}{D}$
1	0.50	3.68
2	0.99	8.76
3	1.48	3.81
4	1.92	3.86
5	2.29	3.91
6	2.60	3.96
7	2.86	4.01
8	3.07	4.06
9	3.25	4.11
10	3.41	4.16
12	3.66	4.26
15	3.96	4.41
20	4.38	4.70
25	4.72	4.97
30	5.02	5.22
40	5.52	5.67
60	6.32	6.48
90	7.24	7.30
130	8.18	8.23
200	9.45	9.45
300	10.8	10.8
400	11.9	11.9
600	13.6	13.6
1.000	16.1	16.1
2.000	20.3	20.3
3.000	23.3	23.3
4.000	25.6	25.6
6.000	29.3	29.3
10.000	34.8	34.8
20.000	43.8	43.8
30.000	50.2	50.2
40.000	55.2	55.2

Table 2.3

Summary of available formula in the literature for prediction of the mass transfer coefficient: $Sr = A \cdot Re^a \cdot Sc^b \cdot \left(\frac{x}{d}\right)^c \cdot f \cdot \left(\frac{x}{d}\right) \cdot f \cdot (Gr)$

Type of work	Reference	Authors	Year	Re	$\frac{x}{d}$	Entrance Geometry	A	a	b	c	$f\left(\frac{x}{d}\right)$	$f \cdot (Gr)$
Non established concentration and velocity profile (short calming section)												
Laminar												
Exp H.T	T.A.S.M.E. 68,123	M. Jakob and W. Dow	1946	Re_x		flow outside cylinder	0.592	$\frac{1}{2}$	$\frac{1}{3}$			
Turbulent												
Exp H.T	Heat Transfer p 547	M. Jakob					0.036	0.8	$\frac{1}{3}$	0.14	$\frac{1}{\left(\frac{d}{x}\right)^{1/8}}$	
Exp H.T	N.A.C.A. T.N 1451	Boelter, Young, Iverson	1948		$x/d \geq 5$	short calming					$(1 + 0.7 \frac{d}{x})$	
					$x/d > 5$	sharp edge					$(1 + 3 \frac{d}{x})$	
					$x/d \geq 5$	square-edge orifice					$(1 + A \frac{d}{a}) \quad 7 < A < 17$	
Theor H.T	N.A.C.q T.M 1068	Latzko	1944		$x/d < 0.693 \cdot Re^{1/4}$		0.0384	0.75	1		$1.11 \cdot Re^{-1/5} \cdot \left(\frac{d}{x}\right)^{4/5}$	-0.275
					$x/d > 0.693 \cdot Re^{1/4}$		0.0384	0.75	1		$1 + 0.144 \cdot Re^{0.25} \cdot \frac{d}{x}$	
Exp. H.T	Heat Transmission p 226	Mc. Adams	1954	$Re > 10,000$			0.023	0.8	$\frac{1}{3}$	0.14		
Theor H.T	Thesis Univ. Calif.	Iverson	1943		$x/d < Re^{1/4}$						$1.13 / Re^{0.2214} \times \left(\frac{d}{x}\right)^{0.1144}$	
					$x/d > Re^{1/4}$						$1 + 0.128 \cdot Re^{0.25} \cdot \frac{d}{x}$	
Established flow and non established concentration profile												
Laminar												
Exp H.T	Ind. Eng. chem. 28 - 1429	Sieder & Tate	1936				1.86	1/3	1/3	0.14	$\left(\frac{d}{x}\right)^{1/3}$	$0.8 \cdot 1 + 0.05(Gr)^{-1/3}$ for $Gr > 25,000$
Exp H.T	Chem. Eng. Prog. 44, 81	Cholette	1948		10 to 63	$Gz < 5$	0.5	1	1		d/x	
						$5 < Gz < 150$	1.42	0.4	0.4		$(d/x)^{0.4}$	
Exp H.T	T.A.I ch. Eng. (32, 271 (305))	Drew, Hodell, Mc. Adams	1936				1.62	1/3	1/3		$(d/x)^{1/3}$	
Theor H.T	I. Techn. Phys. (U.S.S.R.)	E.A. Sidow	1957			for $Gz > 10$	1.65	1/3	1/3		$(d/x)^{1/3}$	
Theor H.T	Univ. Calif. Publ. Eng. 5 (2) 23-58	Martinelli & Boelter				complicated equation given in the text (equation 6.1)						
	Trans A.S.M.L 525	Norris & Straid	1940			$Gz \geq 10$	1.65	1/3	1/3		$(d/x)^{1/3}$	
Turbulent												
Theor H.T	N.A.C.A.T.M. 1068	Latzko	1944		$x_0/d \geq 5$		0.0384	0.75	1		$1 + 0.067 \cdot Re^{0.25} \cdot d/x$	
Exp. H.T	N.A.C.A.T.N. 1451	Boelter, Young, Iverson	1948		$x_0/d \geq 5$						$(1 + 1.4 \frac{d}{x})$	
Exp. H.T	Z. Ver. Deut. Ingr. Verfahr - 4	H. Hausen	1943				0.116	$Re^{2/3} - 1.5$	1/3	0.14	$1 + (d/x)^{2/3}$	
Exp. M.T	Ing. & Eng. Chim.	E.R. Gilliland & T.K. Sherwood	1934		$\frac{x_0}{d} = 56 \frac{L}{d} = 44$		0.023	0.83	0.44			

Table 3.1

Variables in the mass transfer study for the high temperature oxidation of graphite

Experimental Variables	Secondary Variables					
	Re	Sc		$f(\frac{x}{d})$	Gr	D
Nature of sample						
Geometry	d			$x \cdot d$	d L	
Temperature Gas Sample	μ	μ and ρ	μ μ_s		$\rho, \mu, \Delta T$ ΔT ρ, μ	$T^{3/2}$
Gas Composition	μ	" μ, ρ, D "	μ		ρ	M
Pressure		ρ, D				$\frac{1}{P}$
Gas Flow	G					

Table 3.2

Helium data at 20 atm

T °C	$\mu \cdot 10^{-4}$	$k \cdot 10^{-3}$	Pr	$\rho \times 10^{-3}$	D	Sc
0	1.86	1.42	0.681	3.572	0.031	1.68
100	2.33	1.71	0.708	2.622	0.052	1.71
200	2.77	1.97	0.733	2.062	0.078	1.72
300	3.18	2.19	0.755	1.704	0.11	1.69
400	3.56	2.40	0.771	1.448	0.146	1.685
500	3.92	2.59	0.786	1.262	0.178	1.745
600	4.26	2.77	0.799	1.116	0.218	1.75
700	4.58	2.94	0.810	1.003	0.263	1.74
800	4.89	3.10	0.820	0.908	0.309	1.74
900	5.18	3.26	0.829	0.832	0.358	1.735
1000	5.46	3.40	0.836	0.766	0.41	1.735

- μ = Viscosity poise
- k = Thermal conductivity $\text{cal} \cdot \text{cm}^{-1} \cdot \text{s}^{-1} \cdot \text{°C}^{-1}$
- Pr = Prandtl Number
- ρ = Density $\text{g} \cdot \text{cm}^{-3}$
- D = Diffusion coefficient $\text{cm}^2 \cdot \text{s}^{-1}$
- Sc = Schmidt Number
- cp = Specific heat $\text{cal} \cdot \text{g}^{-1} \cdot \text{°C}^{-1}$

Table 3.3

Nitrogen data at 20 atm

T °C	$\mu \times 10^{-4}$	$k \cdot 10^5 \cdot 10^{-5}$	Pr	$\rho \times 10^{-3}$ 20 atm	D 20 atm	Sc	c_p
0	1.7	5.75	0.76	25.2	0.012	0.563	· 258
100	2.11	7.5	0.71	18.3	0.022	0.526	· 2536
200	2.49	9.1	0.695	14.25	0.032	0.545	· 254
300	2.84	10.55	0.691	11.8	0.045	0.533	· 2572
400	3.16	11.90	0.692	10.01	0.059	0.537	· 262
500	3.42	13.1	0.697	8.7	0.074	0.531	· 2674
600	3.69	14.15	0.71	7.75	0.091	0.522	· 273
700	3.95	15.15	0.725	6.94	0.108	0.577	· 278
800	4.18	16.07	0.735	6.31	0.127	0.520	· 2828
900	4.4	16.9	0.75	5.78	0.147	0.517	· 287
1000	4.6	17.7	0.76	5.31	0.168	0.515	· 2908

- μ = Viscosity poise
- k = Thermal conductivity $\text{cal} \cdot \text{cm}^{-1} \cdot \text{s}^{-1} \cdot \text{°C}^{-1}$
- Pr = Prandtl Number
- C_p = Specific heat $\text{cal} \cdot \text{g}^{-1} \cdot \text{°C}^{-1}$
- ρ = Density $\text{g} \cdot \text{cm}^{-3}$
- D = Diffusion coefficient $\text{cm}^2 \cdot \text{s}^{-1}$
- Sc = Schmidt Number

Table 6.1

Mass transfer coefficient for different Re in laminar helium flow with a long calming section 0.6 cm in diameter

Test No	Initial Impurity vpm	Graphite T_s °C	Inlet Gas T_o °C	Outlet Gas T_L °C	Gas T_m °C	Film T_F °C	$\mu_f \times 10^{-5}$ g · s ⁻¹ · cm ⁻¹	$\mu_m \times 10^{-5}$ g · s ⁻¹ · cm ⁻¹	Flow g · s ⁻¹	Re _m	D _m	k_c cm · s ⁻¹	D _F cm ² · s ⁻¹	Re _F	$\frac{k_c \cdot d}{D_F}$
488	68	949	320	504	412	680	45.2	36.1	0.65	3,820	0.148	5.13	0.254	3,050	12.8
489	64.5	950	320	509	414.5	680	45.2	36.1	0.505	2,970	0.148	5.75	0.254	2,340	13.7
490	55.5	949	320	514	417	684	45.4	36.3	0.41	2,400	0.149	5.15	0.255	1,920	12.15
491	57.2	952	310	556	438	695	45.7	37.1	0.305	1,745	0.157	4.70	0.26	1,420	10.82
492	58	949	320	536	428	688	45.5	36.7	0.41	2,370	0.153	4.55	0.257	1,910	10.6
493	63	951	390	508	419	685	45.4	36.4	0.505	2,940	0.150	5.06	0.255	2,360	11.95
494	70	952	320	506	413	682	45.3	36.1	0.65	3,820	0.148	5.45	0.253	3,050	12.93
495	64	945	310	546	433	689	45.5	36.9	0.31	1,785	0.155	4.64	0.257	1,445	10.82
496	59	949	300	540	420	684	45.4	36.4	0.222	1,295	0.150	3.69	0.255	1,038	8.71
497	57.5	950	300	535	417	683	45.4	36.3	0.223	1,295	0.149	3.80	0.254	1,042	8.98
498	52	950	282	531	406	678	45.2	35.9	0.184	1,088	0.146	3.78	0.252	865	9.04
499	62	949	282	531	406	678	45.2	35.9	0.187	1,106	0.146	3.715	0.252	878	8.88
500	60	950	262	510	386	668	44.8	35.2	0.144	869	0.139	3.63	0.248	682	8.78
501	65	950	262	504	386	668	44.8	35.2	0.144	865	0.139	3.63	0.248	682	8.73
502	56.5	954	250	486	368	661	44.6	34.5	0.115	680	0.133	4.00	0.244	547	9.83
503	50	949	252	491	371	660	44.6	34.6	0.12	240	0.133	4.125	0.244	471	10.15
504	63	951	200	458	329	640	43.9	33	0.117	750	0.120	3.38	0.235	565	8.65

$$Sr = \frac{k_c \cdot d}{D} = 1.615 \cdot Gz^{1/3} = 1.615 \cdot Re^{1/3} \cdot Sc^{1/3} \cdot \left(\frac{d}{x}\right)^{1/3} \quad \text{valid } Gz > 10$$

k_c = Average mass transfer coefficient over the whole length of the Sample cm/s

D = Diffusion coefficient of oxygen in Helium cm²/s

L = x = Sample length 10 cm

Re = Reynolds Number relativ to d

Sc = Schmidt Number $Sc = 1.794$ $Sc^{1/3} = 1.202$

d = Internal diameter 0.6 cm

T_s Graphite surface temperature

T_o Gas inlet temperature

T_L Gas outlet temperature

$$T_m = \frac{T_o + T_L}{2}$$

$$T_F = \frac{T_s + T_m}{2}$$

Table 6.2

Mass Transfer coefficient for different Re in turbulent He flow with a long calming section 0.6 cm in diameter

k_c = Average mass transfer coefficient over the whole length of the sample cm/s

D = Diffusion coefficient of oxygen in helium cm²/s

$L=x$ = Sample length 10 cm

d = Internal diameter of sample 0.6 cm

Re = Reynolds Number relative to d

Sc = Schmidt Number $Sc = 1.704$

$$\frac{1}{Sc^J} = 1.202$$

$$Sr = \frac{k_c \cdot d}{D} = 0.0384 \cdot Re^{0.75} \cdot Sc \cdot (1 + 0.067 \cdot Re^{0.25} \cdot \frac{d}{x})$$

valid for $\frac{x}{d} > 5$

Properties evaluated at $T_m = \frac{T_o + T_L}{2}$

Test No.	Initial Impurity vpm	Graphite T °C ^s	Gas Inlet T _o °C	Gas Outlet T _L °C	Gas T _m °C	T _F °C	$\mu_m \times 10^{-5}$ g cm ⁻¹ s ⁻¹	Flow g · s ⁻¹	Re _m	D _m cm ² · s ⁻¹	k _c cm · s ⁻¹	$\frac{k_c \cdot d}{D_m}$	$\frac{k_c \cdot d}{D_m} \cdot \frac{1}{Sc^{1/3}}$
304	46.2	950	15	170	92.5	521	22.9	1.0	9,220	0.051	3.10	36.5	30.4
305	52.8	950	15	170	92.5	521	22.9	1.5	13,900	0.051	4.33	51	42.5
311	58.5	953	315	511	413	683	36.1	1.5	8,820	0.148	7.27	39	24.2
312	59.0	950	338	502	415	683	36.2	1.0	5,860	0.148	5.17	21	17.45
316	48.0	946	15	196	105.5	526	23.5	0.65	5,860	0.054	3.17	35.2	29.3
317	44.5	958	333	495	414	686	36.1	0.65	3,805	0.148	4.25	17.25	14.35
324	54.2	948	15	270	142	545	25.1	0.4	3,365	0.063	3.45	32.8	27.3
343	65	950	296	434	315	632	32.4	1.0	6,350	0.116	4.55	23.5	19.55
344	64	950	346	570	458	704	37.7	1.25	7,020	0.164	7.05	25.75	21.41
345	62.5	951	15	201	108	529	23.6	1.25	11,260	0.054	3.14	34.9	29.05
346	52.5	948	15	203	109	529	23.6	0.8	7,160	0.054	2.43	27	22.45
347	58.1	949	15	233	124	537	24.3	1.75	15,200	0.058	4.04	41.4	34.5
348	70	952	268	552	410	681	36	1.25	7,360	0.157	6.57	25.16	20.95
349	57	951	303	517	410	681	36	0.8	4,700	0.157	3.96	15.18	12.6
350	63	949	160	340	250	600	29.8	0.8	5,700	0.095	2.64	16.7	13.91
351	59.5	950	127	373	250	600	29.8	1.0	7,120	0.095	3.88	24.5	20.4
352	61.5	951	112	400	256	603	30	1.25	9,200	0.096	4.78	29.8	24.9
353	75	951	96	404	250	600	29.8	1.5	11,060	0.095	5.34	33.7	28.1
355	70	948	15	212	114	531	23.9	0.65	5,780	0.056	2.77	29.7	24.78
356	37.8	949	15	276	145	547	25.3	0.4	3,350	0.064	1.77	16.7	13.91
357	26.0	951	150	350	250	600	29.8	0.4	2,850	0.095	1.77	11.2	9.35
358	58.0	952	141	359	250	600	29.8	0.4	2,850	0.095	2.53	15.95	13.3
359	58.0	951	260	560	410	681	36	0.04	2,350	0.157	3.17	12.1	10.1
481	67.5	955	320	521	421	688	36.5	0.8	4,650	0.151	5.3	21	17.47
482	71	952	320	524	422	687	36.5	0.8	4,650	0.151	5.78	22.95	19.1
483	62	951	320	524	422	686	36.5	1.0	5,810	0.151	6.29	24.9	20.7
484	62	951	320	526	423	687	36.5	1.0	5,810	0.151	7.05	28.05	23.3
485	69	952	320	526	423	687	36.5	1.0	5,870	0.151	7.08	28.1	23.35
486	65	950	320	222	421	685	36.5	1.2	6,970	0.151	8.5	33.7	28
487	82	953	320	528	424	688	36.5	1.2	6,970	0.151	7.39	29.3	24.4

Table 6.3

Mass transfer coefficient for different Re in turbulent N₂ flow with a long calming section 0.6 cm in diameter

- k_c Average mass transfer coefficient over the whole length of the sample cm/s
- D Diffusion coefficient of oxygen in nitrogen cm/s
- L=x Length of sample 10 cm
- d Internal diameter of sample 0.6 cm
- Re Reynolds Number relative to d
- Sc Schmidt Number 0.528 Sc^{1/3} = 0.81
- G Mass flow g/s
- T_s Mean graphite wall temperature °C
- T_m Bulk gas temperature °C
- T_F Film temperature °C

$$Sr = \frac{k_c \cdot d}{D} = 0.0384 \cdot Re^{0.75} \cdot Sc \times (1 + 0.067 Re^{0.25} \cdot \frac{d}{x})$$

Properties evaluated at $T_m = \frac{T_o + T_L}{2}$

Test No.	Initial Impurity vpm	Graphite T _s °C	Gas T _o °C	Gas T _L °C	T _m °C	T _F °C	μ _m × 10 ⁻⁵ g · cm ⁻¹ · s ⁻¹	Flow G g · s ⁻¹	Re _m × 10 ³	D _m	k _c cm s ⁻¹	$\frac{k_c \cdot d}{D_m}$	$\frac{k_c \cdot d}{D_m} \cdot \frac{1}{Sc^{1/3}}$
591	42	950	360	541	450	700	32.8	11.9	77	0.068	8.95	79	97.5
592	45	952	364	543	453	702	32.9	10.55	68.1	0.068	7.75	77.4	95.5
593	48	953	368	552	460	706	33.1	9.25	59.3	0.0685	9.28	81.2	100.2
594	40	952	374	552	463	708	33.2	7.9	50.5	0.069	9.46	82.2	101.5
595	34	951	380	547	463	707	33.2	6.6	42.2	0.069	8.1	69.5	85.7
596	39.5	949	360	537	448	699	32.8	11.9	77	0.068	8.6	75.9	93.7
597	40	951	374	557	465	708	33.2	7.9	50.5	0.070	7.58	64.5	79.5
598	48	949	357	538	447	698	32.7	13.0	84.4	0.067	8.58	76.7	94.7
599	41.5	948	342	517	429	688	32.2	19.2	126.5	0.064	9.46	88.5	109.3
600	43	952	350	528	439	695	32.5	16.0	100.5	0.066	9.65	86.7	107
601	46	951	336	502	419	685	31.9	21.7	144.4	0.065	10.70	99	122.3
602	49	951	336	505	420	685	31.9	21.7	144.4	0.065	12.5	115.5	142.5
603	38	952	379	552	465	708	33.2	4.52	28.9	0.070	6.20	53.1	65.7
604	37	957	378	527	452	704	32.9	3.32	21.4	0.068	5.05	44.2	54.7
605	35.5	951	376	528	452	701	32.9	2.84	18.35	0.068	4.2	37.1	45.7
606	35.5	952	375	528	451	701	32.9	2.37	15.3	0.068	4.13	36.5	45

Table 6.4

Mass transfer coefficient as function of Re in non established laminar helium flow with a sharp edge entrance in a 0.36 cm channel

$$Sr_x = \frac{k_c \cdot x}{D} = 0.664 \cdot Sc^{\frac{1}{3}} \cdot Re_x^{\frac{1}{2}}$$
 or

$$Sr_x = \frac{k_c \cdot d}{D} = 0.664 \cdot Sc^{\frac{1}{3}} \cdot Re_x^{\frac{1}{2}} \cdot \left(\frac{d}{x}\right)^{\frac{1}{2}}$$
 as long as $Gr < \frac{d}{2}$ or $Re_x \geq 43 \times \left(\frac{x}{d}\right)^2 = 33,100$ or $Re \geq 1.195$

Properties evaluated at $T_m = \frac{T_o + T_L}{2}$

k_c = Average mass transfer coefficient over the length of the sample cm/s
 D = Diffusion coefficient of oxygen in helium cm²/s
 $L = x$ = Sample length 10 cm
 Re_x = Reynolds Number relative to the distance $x = L$
 Sc = Schmidt Number $Sc = 1.704 Sc^{\frac{1}{3}} = 1.202$
 d = Internal diameter of sample 0.36 cm

$Re_x = \frac{4 G \cdot x}{\pi \cdot d^2 \cdot \mu}$
 at $Re_x = 10,000$ $k_c / D = 7.96$ theor. or at $Re = 1,000$; $\frac{k_c \cdot d}{D} = 4.79$
 at $Re_x = 40,000$ $k_c / D = 15.92$ theor. or at $Re = 10,000$; $\frac{k_c \cdot d}{D} = 15.17$

Test No.	Initial Impurity vpm	Graphite $\frac{T}{\text{°C}}$	Gas inlet T_o °C	Gas outlet T_L °C	T_m °C	$\mu_m \times 10^{-5}$ $\frac{\text{g}}{\text{cm s}}$	Flow $\frac{\text{g}}{\text{s}}$	Re_m	$Re_{mm} \times 10^3$	D_m $\frac{\text{cm}^2}{\text{s}}$	k_c cm s^{-1}	$\frac{k_c \cdot d}{D_m}$	$\frac{k_c \cdot L}{D}$
377	36.7	952	16	474	245	29.7	0.14	1,668	46.3	0.093	1.52	5.875	16.3
378	38.5	955	16	476	246	29.7	0.14	1,688	46.3	0.093	1.73	6.7	18.6
379	33.0	955	16	476	246	29.7	0.14	1,668	46.3	0.093	1.75	6.78	18.8
381	43.8	951	236	588	412	36.1	0.14	1,370	38	0.148	2.27	5.51	15.3
382	44.0	951	236	588	412	36.1	0.14	1,370	38	0.148	2.25	5.51	15.3
363	40.2	954	171	523	347	33.7	0.14	1,469	40.7	0.126	1.94	5.54	15.4
384	43.0	955	286	584	435	36.95	0.17	1,627	45.2	0.156	2.37	5.46	15.2
385	45.0	950	300	608	454	37.6	0.22	2,070	57.5	0.163	2.70	5.95	16.5
387	38.0	949	251	443	347	33.7	0.105	1,100	30.6	0.126	2.20	6.29	17.4
388	40.0	949	14	390	202	27.8	0.11	1,400	38.9	0.079	1.54	7.01	19.5
389	41.8	949	230	456	343	33.5	0.11	1,162	32.4	0.125	1.88	5.42	15
390	42.0	948	146	432	289	31.4	0.11	1,238	34.4	0.107	1.86	6.25	17.4
391	49.3	949	243	545	394	35.45	0.15	1,495	41.5	0.142	2.32	5.88	16.3
392	49.0	949	243	545	394	35.45	0.15	1,495	41.5	0.142	2.40	6.08	16.8
393	53.0	950	270	594	432	36.85	0.20	1,920	53.3	0.154	2.49	5.82	16.1
394	50.6	950	270	594	432	36.85	0.20	1,920	53.3	0.154	2.55	5.98	16.6
396	41.2	948	16	434	225	28.8	0.137	1,682	46.8	0.086	1.66	6.97	19.4
397	46.8	950	266	504	385	35.1	0.137	1,382	37.2	0.138	2.11	5.5	15.3
398	44.5	947	170	490	330	33.0	0.131	1,402	39	0.120	1.925	5.78	16
428		948	284	532	409	36.0	0.6	5,900	164.2	0.146	10.8	30	
429		948	284	536	411	36.0	0.6	5,900	164.2	0.146	10.2	28.3	
430		950	284	536	411	36.0	0.4	3,930	109.2	0.146	9.3	25.8	
431		952	284	538	412	36.1	0.4	3,920	109.2	0.148	8.48	23.5	
432		951	284	555	419	36.4	0.5	4,860	134.5	0.150	9.29	25.7	
433		949	284	536	411	36.0	0.66	6,500	188.0	0.146	10.7	29.7	
434		951	284	570	426	36.7	0.32	3,080	85.6	0.153	7.6	21.1	
435		959	234	555	426	36.7	0.22	2,120	59.0	0.153	6.34	17.6	
436		940	234	540	419	36.4	0.21	2,400	56.7	0.150	5.68	16.3	
437		947	275	521	396	35.5	0.16	1,650	45.9	0.142	5.53	15.4	
438		952	260	510	388	35.1	0.14	1,410	39.2	0.138	6.42	17.8	
439		950	260	511	385	35.1	0.14	1,410	39.2	0.138	6.45	17.85	
440		957	275	528	400	35.7	0.166	1,600	44.4	0.144	5.94	16.5	
441		949	204	467	283	31.2	0.166	1,880	56.2	0.106	6.10	16.95	
442		950	204	474	286	31.3	0.166	1,880	56.2	0.106	6.24	17.3	
443		950	15	436	228	29.0	0.166	2,020	56.1	0.087	6.05	16.8	
444		950	15	440	230	29.0	0.166	2,020	56.1	0.087	5.82	16.2	
419		950	284	527	405	35.8	1.39	13,790	382	0.145	23.9	66.2	
420		950	284	518	399	35.7	1.39	13,790	384	0.143	17.43	48.5	
421		953	284	518	399	35.7	1.39	13,790	384	0.143	16.3	45.3	
422		950	284	526	403	35.8	1.2	11,980	330	0.145	14.15	39.2	
423		955	284	533	406	35.8	1.2	11,980	330	0.145	15.37	43.8	
424		954	284	526	403	35.8	1.0	9,890	274.5	0.145	13.05	36.3	
425		952	284	526	403	35.8	1.0	9,890	274.5	0.145	13.45	37.5	
426		948	284	526	403	35.8	0.8	7,900	220	0.145	10.23	28.4	
427		948	284	526	403	35.8	0.8	7,900	220	0.145	10.85	30.2	

Table 6.5

Mass transfer coefficient as function of Re in He flow with a short calming section ($\frac{x_0}{d}$) in 0.36 cm diameter channel

k_c	= Average mass transfer coefficient over the whole length of the sample	cm/s
D	= Diffusion coefficient of oxygen in helium	cm ² /s
L = x	= Distance from entrance to end of sample	23 cm
x_0	= Distance from entrance to beginning of sample	13 cm
d	= Internal diameter of sample	0.36 cm
Re	= Reynolds Number relative to d	
Sc	= Schmidt Number	$Sc = 1.704 Sc^{1/3} = 1.202$
G	= Mass flow	g/s
Re_x	= $\frac{4G}{\pi d \mu} \frac{x}{d}$	

Test No.	Initial Impurity vpm	Graphite T_s °C	Inlets $G_{in} T_o$ °C	Outlet Gas T_L °C	Gas T_m °C	$\mu_m \times 10^{-5}$ g·cm ⁻¹ ·s ⁻¹	Flow g·s ⁻¹	Re_m	Re_{xm} $\times 10^{-3}$	D_m cm ² s ⁻¹	k_c cm s ⁻¹	$\frac{k_c \cdot d}{D_m}$
505	76	955	304	518	411	36.1	1.0	9,800	593	0.147	4.18	10.20
506	68	955	304	514	409	36.0	1.0	9,830	595	0.147	4.03	9.87
507	61	952	304	508	406	35.9	1.0	9,860	597	0.146	3.98	9.75
508	75	951	304	554	429	36.7	1.2	11,580	701	0.154	6.6	15.4
509	79	951	304	557	430	36.7	1.2	11,580	701	0.154	6.17	14
510	53.5	949	304	502	403	35.8	0.8	7,900	478	0.145	3.92	9.75
511	50	949	304	500	402	35.8	0.8	7,900	478	0.145	3.14	7.8
512	51	949	304	514	409	36.0	0.65	6,390	387	0.147	3.2	7.85
513	52.5	949	304	516	410	36.0	0.65	6,390	387	0.147	3.08	7.55
514	50	951	302	545	423	36.5	0.5	4,840	294	0.151	2.94	7.04
515	52	950	302	545	423	36.5	0.5	4,840	294	0.151	3.03	7.20
516	48	952	293	578	435	37.0	0.34	3,250	197	0.156	2.66	6.14
517	51.5	953	293	576	434	37.0	0.34	3,250	197	0.156	2.82	6.5
518	59	955	296	550	423	36.5	0.41	3,980	242	0.151	3.02	7.17
519	55.5	951	304	560	432	36.8	0.229	2,200	1,335	0.154	2.52	5.9
520	50.5	951	301	556	428	36.7	0.20	1,930	1,172	0.153	2.38	5.58
521	49	951	292	542	417	36.3	0.17	1,660	101	0.149	2.06	4.97
522	51.5	952	276	528	402	35.7	0.14	1,390	84	0.144	2.145	5.37
523	46	951	255	506	380	35.0	0.113	1,142	69	0.136	2.28	5.98
524	46	951	15	416	215	28.4	0.209	2,620	159.5	0.083	1.617	7
525	46.5	953	15	435	225	28.8	0.166	2,040	124.5	0.086	1.42	5.94
526	46	951	15	437	226	28.8	0.115	1,412	85.5	0.086	1.44	6.04
527	81	952	304	580	442	37.2	1.2	11,410	692	0.158	6.34	14.45
528	61	950	304	537	420	36.4	1.0	9,720	589	0.151	4.16	9.9
529	55.5	950	304	504	402	35.7	0.82	8,130	492	0.144	3.10	7.77
530	55.5	950	304	528	416	36.3	0.58	5,750	348	0.149	2.96	7.13
531	53	951	297	561	429	36.7	0.41	3,960	240	0.153	2.84	6.7

Table 6.6

Mass transfer coefficient function of $\frac{x}{d}$ in non established laminar helium flow (Re 1382) with a sharp edge entrance in 0.36 cm diameter channel

k_c	Average mass transfer coefficient over the whole length of the sample	cm/s	Properties evaluated at $T_m = \frac{T_o + T_L}{2}$																	
$k_{c\bar{x}}$	Average mass transfer coefficient between x_o and x	cm/s																		
D	Diffusion coefficient of oxygen in helium	cm ² /s																		
x	Distance from entrance to end of active sample	cm	Constant = $\frac{2.03 \cdot 11}{0.2114 \cdot 1.5}$	Mean $k_c = 2.03$																
d	Internal diameter of sample	0.36 cm																		
Re	Reynolds Number relative to d		$k_{c\bar{x}} = \text{constant} \cdot \frac{\text{cps}}{n}$																	
Sc	Schmidt Number = Sc = 1.704	$\frac{1}{Sc^3} = 1.202$																		
G	Mass flow	g/s	$k_{c\bar{x}} = 0.664 \cdot D \cdot Sc^{\frac{1}{3}} \cdot \sqrt{\frac{u_s}{\nu \cdot x}}$	or $\frac{k_{c\bar{x}} \cdot d}{D} = 0.664 \cdot Sc^{\frac{1}{3}} \cdot Re^{\frac{1}{2}} \cdot \left(\frac{d}{x}\right)^{\frac{1}{2}}$																
Valid for $x < \frac{Re \cdot d}{43} = 11,6 \text{ cm}$																				
Test No.	Initial Impurity vpm	Graphite T_s °C	Gas Inlet T_o °C	Gas Outlet T_L °C	Gas T_m °C	$\mu_m \times 10^{-5}$ g cm ⁻¹ s ⁻¹	Flow g · s ⁻¹	Re _m	x	D _m cm ² s ⁻¹	$\frac{\text{cps}}{[CO_2] + [CO]}$	k_c cm s ⁻¹	Mean $\frac{\text{cps}}{[CO_2] + [CO]}$	Mean k_c cm s ⁻¹	$\sum_{o}^x \frac{\text{cps}}{n}$	$\frac{x}{n}$ cps	$k_{c\bar{x}}$	$\frac{k_{c\bar{x}} \cdot d}{D}$	$\frac{x}{d}$	$\frac{k_{c\bar{x}}}{D}$
399	48.3	950			399															
400	87.0	950	246	552	402	35.8	0.14	1,382	1.8	0.144	0.118	1.84	0.0905	1.85	0.0905	0.0905	6.38	15.95	5	44.3
401	77.0	949		557	408				1.8		0.160	1.79								
402	70.2	950		570	408				1.8		0.093	1.81								
403	75.0	950		570	408				1.8		0.089	1.86								
404	81.0	949		570	403				1.8		0.894	1.87								
405	82.0	948		559	407				3.3		0.0358	1.87	0.0366	2.07	0.1271	0.0635	4.47	11.18	9.16	31
406	81.8	948		567	407				3.3		0.0341	1.997								
407	120.0	948		568	407				3.3		0.04	2.36								
408	107.0	948		543	399				4.8		0.0274	1.96	0.030	1.935	0.1571	0.0524	3.69	9.23	13.7	25.6
409	109.0	948		552	404				4.8		0.036	1.915								
410	113.0	949		561	406				4.8		0.0266	1.94								
411	109.0	951		566	412				6.3		0.0192	1.85	0.0201	1.915	0.1772	0.0443	3.42	7.8	17.5	21.6
412	100.0	952		578	418				6.3		0.0210	1.98								
413	114.0	949		590	406				6.3		0.020	1.91								
414	158.0	950		566	404				7.8		0.0185	1.925	0.0194	2.2	0.1966	0.0393	2.77	6.93	21.7	19.3
415	170.0	948		561	404				7.8		0.0174	2.32								
416	160.0	951		557	401				7.8		0.0223	2.36								
417	160.0	949		569	408				9.3		0.0134	2.10	0.0148	2.2	0.2114	0.0353	2.48	6.2	25.8	17.2
418	153.0	952		573	410				9.3		0.0144	2.24								

Table 6.7

Average mass transfer coefficient as function of $\frac{x}{d}$ in non established turbulent helium flow with a sharp edge entrance in a 0.36 cm diameter channel

Test No.	Graphite T_s °C	Gas inlet T_o °C	Gas Outlet T_L °C	Gas T_m °C	$\mu \times 10^{-5}$ g · cm ⁻¹ · s ⁻¹	Flow G g · s ⁻¹	Re_m	x cm	D cm	$\frac{cps}{CO_2 + CO}$	Mean $\frac{cps}{CO_2 + CO}$	\sum_a^x cps	\sum_o^x $\frac{cps}{n}$	k_{cx}	$\frac{x}{d}$	$\frac{k_{cx} \cdot d}{D}$								
447	950	280	531	406	35.7	1.0	9,900	1.8	0.144	0.0849	0.0842	0.0842	0.842	8.86	5	22.18								
448	950	280	531	406				1.8		0.0765														
452	944	280	522	401				1.8		0.0913														
456	947	280	516	398				3.3		0.0631														
459	950	280	524	402				3.3		0.0603														
460	950	280	526	403				3.3		0.0685														
462	949	280	522	401				4.8		0.0467														
465	946	280	523	402				6.3		0.0366														
466	950	280	516	398				6.3		0.0367														
467	950	280	520	400				6.3		0.0380														
468	950	280	528	404	7.8	0.0296																		
469	951	280	524	402	7.8	0.0279																		
470	950	280	528	404	9.3	0.0241																		
474	955	280	518	399	9.3	0.0164																		
451	949	280	512	396	0.8	7,920	1.8	0.144	0.1025	0.1025	0.1025	0.1025	8.30	5	20.75									
455	951	280	528	404			3.3		0.0764															
461	949	280	514	397			4.8		0.0493															
476	952	280	540	410			6.3		0.0439															
479	948	280	518	399			7.8		0.0272															
473	952	280	522	401			9.3		0.0205															
449	952	280	531	406			1.2		11,900							1.8	0.144	0.0601	0.0685	0.0685	0.0685	8.64	5	21.60
453	952	280	529	405												1.8		0.0770						
457	952	280	532	391	3.3	0.0705																		
463	951	280	509	395	4.8	0.0510																		
475	951	280	532	406	6.3	0.0396																		
478	952	280	514	397	7.8	0.0224																		
471	952	280	526	403	9.3	0.0230																		
450	950	280	536	408	1.5	14,850	1.8	0.144	0.0853	0.0899	0.0899	0.0899	12.55	5	31.4									
454	948	280	499	390			1.8		0.0946															
458	952	280	500	390			3.3		0.070															
463	949	280	497	389			4.8		0.0529															
477	952	280	514	397			6.3		0.0368															
480	951	280	496	388			7.8		0.0259															
472	953	280	500	395			9.3		0.0192															

Properties evaluated at $T_m = \frac{T_o + T_L}{2}$

Flow	Mean k_c	Constant
0.8	3.52	80.08
1.0	4.125	105
1.2	4.73	226
1.5	5.61	138.7

For $\frac{x}{d} < 0.625$ $Re^{0.25} \frac{k_{cx} \cdot d}{D} = 1.11 \times (0.0384 \cdot Re^{0.75} \cdot Sc) \cdot \left[Re^{-\frac{1}{5}} \left(\frac{x}{d} \right)^{4/5} \right]^{-0.275}$
 For $\frac{x}{d} > 0.625$ $Re^{0.25} \frac{k_{cx} \cdot d}{D} = (0.0384 \cdot Re^{0.75} \cdot Sc) \cdot (1 + 0.144 Re^{0.25} \cdot \frac{d}{x})$

Table 6.9

Average mass transfer coefficient as function of $\frac{x}{d}$ in established turbulent nitrogen flow with a sharp edge entrance 0.36 cm diameter channel

Test No.	Initial Impurity vpm	Graphite T_s °C	Gas T_o °C	Gas T_L °C	Gas T_m °C	$\mu_m \cdot 10^{-5}$ $\frac{g}{cm \cdot s}$	Flow G $g \cdot s^{-1}$	$Re \cdot 10^3$	x	D cm	$\frac{cps}{CO_2 + CO}$	Mean $\frac{cps}{CO_2 + CO}$	Mean k_c $cm \cdot s^{-1}$	$\sum_0^x cps$	$\sum_0^x \frac{cps}{n}$	$k_{c\bar{x}}$	$\frac{k_{c\bar{x}} \cdot d}{D}$	$\frac{x}{d}$
620	38.5	951	374	594	484	33.7	12.55	132	1.8	0.072			5.06					5
621	42	953							1.8									
622	37	951							1.8		0.471							
623	38	952							1.8		0.686	0.686		0.686	0.686	8.03	40.15	
625	40	949							3.3		0.584	0.584		0.270	0.635	7.43	37.2	9.17
627	41	952							4.8		0.511	0.511		1.781	0.594	6.94	34.7	13.3
629	42	950							6.3		0.521	0.521		2.302	0.575	6.72	33.6	17.5
631	41	951							7.8		0.460	0.460		2.762	0.552	6.56	32.8	21.65
633	36	950							9.3		0.306	0.276		3.038	0.506	5.23	29.7	25.8
634	45	950							9.3		0.246							
636	49	951							10.8		0.129	0.129		3.167	0.452	5.28	26.4	30.3
624	38	953	390	598	494	34.0	7.9	82.1	1.8	0.074	0.633		4.07	0.633	0.633	5.96	29	5
626	38	952							3.3		0.675			1.308	0.654	6.16	29.98	9.17
628	42	953							4.8		0.560			1.868	0.623	5.87	28.57	13.3
630	37	952							6.3		0.567			2.435	0.609	5.74	27.9	17.5
632	38.5	950							7.8		0.335			2.770	0.554	5.21	25.35	21.65
635	38	952							9.3		0.222			2.992	0.498	4.69	22.8	25.8
637	50	949							10.8		0.174			3.166	0.452	4.37	21.2	30.3

$k_{c\bar{x}}$ Average mass transfer coefficient over the whole length of the sample cm/s
 k_{cx} Average mass transfer coefficient from inlet up to a distance x cm/s
 D Diffusion coefficient of oxygen in nitrogen at 20 atm cm^2/s
 L Length of sample 10 cm
 d Internal diameter of sample 0.36 cm
 Re Reynolds Number relative to d
 Sc Schmidt Number $Sc = 0.528$
 G Mass flow g/s

Flow 12.55 g/s Constant = $\frac{5.06 \cdot 11}{3.167 \cdot 1.5}$

$k_{c\bar{x}} = \text{constant} \times \sum_0^x \frac{cps}{n}$

Flow 7.9 g/s = Constant = $\frac{4.07 \cdot 11}{3.166 \cdot 1.5}$

Properties evaluated at bulk temperature $T_m = \frac{T_o + T_L}{2}$

Table 6.10

Cases under which mass transfer has been measured

Case	Table and Fig.	Regime Type of entrance Geometry							Carrier Variables			
		Lam	Tur	Long calm.	sharp edge	short calm.	sharp edge C ¹⁴	bellmoth C ¹⁴	Gas		G	$\frac{x}{d}$
									He	N ₂		
I	6.1	x		x					x		x	
II	6.2		x	x					x		x	
III	6.3		x	x						x	x	
IV	6.4	x			x				x		x	
V	6.5	x	x			x			x		x	
VI	6.6	x					x		x			x
VII	6.7		x				x		x			x
VIII	6.8		x					x	x			x
IX	6.9		x				x			x		x

E R R A T A

page	line	read	instead of
9	17	(Re = 1382)	(Re = 138)
10	5	formulae	formula
14	3	eddy kinetic viscosity	eddy kinetic
	6	$\frac{\bar{v}^2}{\rho v_{\infty}^2}$	$\frac{v}{\rho v_{\infty}^2 s}$
	11	cm / s ²	cm ² / s
15	5	k _{cx}	k _{ex}
	6	k _{c\bar{x}}	k _{ex}
16	5	cm ³ / s	cm ³ /
17	5	cup-mixing	cu -mixing
18	4,5	fraction	function
		$v^* = \frac{\sum_{i=1}^n C_i \cdot v_i}{\sum_{i=1}^n C_i}$	$v^* = \frac{\sum_{i=1}^n C_i \cdot v_i}{\sum_{i=n}^n C_i}$
37	11		
40	21	$\frac{(r_A + r_B)}{2}$	$(r_A + r_B) / 2$
43	15	.. a thin film <u>boundary layer</u> a thin <u>boundary layer</u> ..
	27	formulae	formula
44	16	$\rho \left(\frac{\partial u}{\partial x} + \frac{\partial v}{\partial y} + \frac{\partial w}{\partial z} \right) + (u \frac{\partial \rho}{\partial x} + v \frac{\partial \rho}{\partial y} + w \frac{\partial \rho}{\partial z}) + \frac{\partial \rho}{\partial t} = 0$	$\frac{\partial \rho}{\partial t} + \frac{\partial u}{\partial x} + \frac{\partial v}{\partial y} + \frac{\partial w}{\partial z} = 0$
45	3	disregarded	disregarded
	14	.. Definition of the Laminar Boundary Layer Definition of the Boundary Layer ..
46	4,7,11,24	laminar boundary layer equations	boundary layer equations
47	1,8,24,28	.. integral momentum equations	.. momentum equations

page	line	read	instead of
47	9, 19	-the flow of momentum or -the rate of change of momentum	-the change of momentum
49	13, 15, 16, 17	lumps	edcies
	13	randomly	ranomly
52	1, 2, 6, 12	film boundary layer	boundary layer
	14	$= \frac{\tau_s}{\rho \cdot u_\infty^2 (1 + a (Sc - 1))}$	$= \frac{\tau_s}{\rho \cdot u^2 (1 + a (Sc - 1))}$
53	10	in the laminar sub-layer	in the suplaminar layer
	12	.. zone $5 < y^+ < 30$.. zone $5 < y < 30$
	23	$= \frac{E_{M_0}}{E_D}$	$= \frac{E_D}{E_{M_0}}$
54	20	Dimensional Analysis Method	Methods of Similarity
55	21	"	"
57	5	.. the integral momentum equation	.. the momentum equation
	21	$\frac{u}{u_\infty} = \frac{3}{2} \cdot \frac{y}{\delta} - 1/2 \left(\frac{y}{\delta}\right)^3$	$\frac{u}{u_\infty} = \frac{3}{2} \cdot \frac{y}{\delta} - 1/2 \left(\frac{y}{\delta}\right)^2$
58	2	$\frac{39}{280} \rho u_\infty^2 \cdot \frac{d\delta}{dx} = \frac{3}{2} \mu \cdot \frac{u_\infty}{\delta}$	$\frac{39}{280} \rho \cdot u_\infty^2 \frac{d\delta}{dx} = \frac{3}{2} \cdot \frac{\mu u_\infty}{\delta}$
	12	$\frac{\tau_s}{\rho \cdot u_\infty^2} = f$	$\frac{\tau_s}{\rho u^2} = f$
	16	$f_x = \frac{0.646}{\sqrt{Re_x}}$	$\frac{f_x}{x} = \frac{0.646}{Re_x}$
59	22	$\tau_s = -\mu \cdot \frac{\partial u}{\partial y} = \mu \cdot \frac{u}{y}$	$\tau_s = \mu \cdot \frac{\partial u}{\partial y} = \mu \cdot \frac{u}{y}$
	24	$u = 0.0228 \cdot \rho \cdot u_\infty^2 \frac{1}{\mu} \left(\frac{y}{u_\infty \delta}\right)^{1/2} \cdot y$	$u = 0.0228 \cdot \rho \cdot \frac{u_\infty^2}{\mu} \left(\frac{y}{u_\infty \delta}\right)^{1/4} \cdot y$
	7	$= 0.376 \cdot x^{0.8} \cdot \left(\frac{y}{u_\infty}\right)^{0.2} + \text{Const.}$	$= 0.376 \cdot x^{0.8} \cdot \left(\frac{y}{u_\infty}\right)^{0.25} + \text{Const.}$
69	11	$\dot{M} = \pi R^2 \cdot u_m \cdot C_\infty (1 - 0.820 e^{-m_o x} + \dots)$	$\dot{M} = \pi \cdot r^2 \cdot u_m \cdot C_\infty (1 - 0.820 e^{-m_o x} + \dots)$
	12	$m_n = \frac{\beta^2}{2^n} \cdot \frac{D}{R^2 \cdot u_m}$	$m_n = \frac{\beta^2}{2^n} \cdot \frac{D}{r^2 \cdot u_m}$

page	line	read	instead of
71	15	$C_{ma} = \frac{1}{\pi r^2} \int_{r=0}^R \dots$	$C_{ma} = \frac{1}{\pi d^2} \int_{r=0}^r \dots$
	17	$C_m = \frac{\dot{M}}{Q} = \frac{1}{Q} \int_{r=0}^R \dots$	$C_m = \frac{\dot{M}}{Q} = \frac{1}{Q} \int_{r=0}^r \dots$
73	21	$Sr = 0.664 \cdot Re^{1/2} \cdot Sc^{1/3} \cdot (d/x)^{1/2}$	$Sr = 0.0664 \cdot Re^{1/2} \cdot Sc^{1/3} \cdot d^{1/2} \cdot (d/x)^{1/2}$
75	17	.. the gas near the wall and the bulk the gas near and the bulk ..
82	27	$\frac{dZ}{dt} = \left(\frac{k \exp^s}{V_o} \cdot \frac{P_m}{\theta_m} + \frac{qo}{V_o} \right) \cdot Z$	$\frac{dZ}{dt} = - \left(\frac{k \exp^s}{V_o} \cdot \frac{P_m}{\theta_m} + \frac{qo}{V_o} \cdot dt \right) \cdot Z$

Fig. No.	read	instead of
2.6	• 1 and • 4 on the ordinate scale	1 and 4
3.3	°C in abscissa	
3.6	$k_c = 1.25 \text{ cm/s}$	$k_c = 1.25 \text{ cm}$
3.7	extend the logarithmic scale in ordinate - Temp. test 950°C	
3.8	abscissa (x/d)	

Answer to the questions and remarks raised by the commission of professors of the Brussels university during the private defence of the thesis

Page 21 - 24: A new list of references is prepared.

Page 28: The difference between $k_{c\bar{x}}$ and k_c as defined in page 28 is:

$k_{c\bar{x}}$ is used to indicate the average mass transfer coefficient from the inlet of the sample up to a point distant of x from the inlet,

k_c is used instead of k_{cL} and indicates the average mass transfer coefficient over the whole length of the sample.

Page 33: Definition of $Deff$: the effective diffusion coefficient in the pores. The diffusion of a substance in a porous material may proceed following different mechanisms:

bulk diffusion in the large pores,

molecular diffusion (Knudsen flow) where the diameter is smaller than the mean free path of the gaseous molecules,

laminar flow of the "Poiseuille" type, if a pressure gradient is added to the concentration gradient.

Moreover in some cases physisorption of the diffusing substances on the porous material may also interfere with the diffusion process. The $Deff$ to be used in equation (2.4) is a diffusion coefficient which takes into account all those effects. In practice the $Deff$ must be experimentally determined for each case.

Pages 43, 45, 46, 48, 52:

The use of the term "boundary layer" instead of "film boundary layer" or "laminar sub-layer" as it is sometime done for the flow in pipes may lead to some confusion. The appropriate precision has been indicated in the ERRATA!

Page 47:

The momentum equation (2.42) is the integral equation of von Karman. It is recommended to use the terminology "Integral momentum equation" instead of "Momentum equation" although this terminology is used in the literature [1] [2]. Moreover the term "change of momentum" used in the text should in fact be read "rate of change of momentum".

Page 49:

It is recommended to use the term "lumps" instead of the term "eddies". This terminology was taken from reference [3].

Page 52:

It was questioned why in equation (2.55)

$$\frac{Sr}{Re \cdot Sc} = \frac{k}{u_{\infty}} = \frac{\tau}{\rho \cdot u_{\infty}^2} \frac{s}{[1 + a(Sc - 1)]}$$

only the ratio $a = \frac{\tau}{\rho \cdot u_{\infty}^2} s$ was introduced and not the ratio $b = \frac{\epsilon}{\rho \cdot u_{\infty}^3}$

The presence of the term Sc takes into account the proportionality between velocity boundary layer properties and the concentration boundary layer properties.

Pages 54, 55:

The term "Methods of similarity" used to express various methods including the "Dimensional analysis" although used by Jakob [4] may be misleading. The appropriate modification to the text is being given in the ERRATA.

Page 55 last paragraph should for more precision read as follows:

In the "Dimensional analysis method" (Raleigh's method), it is assumed that the relation between the different physical quantities can be expressed in the form of sums of power functions. Generally one term is used. For instance

$$Q_r = C \cdot Q_1^{\alpha} \cdot Q_2^{\beta} \cdot Q_3^{\gamma} \dots$$

where C is a dimensionless constant, Q_1, Q_2, Q_3 are quantities upon which Q_r is supposed to depend and α, β, γ are constant exponents. The method consists of converting this equation in an equation of dimensionless groups $G_A, G_B, G_C \dots$ of the form

$$G_R = A \cdot G_A^a \cdot G_B^b \cdot G_C^c$$

If the constants A, a, b, c are found by experiments for one set of groups $G_A, G_B, G_C \dots$ they are supposed to be valid for any other sets with arbitrary values $G'_A, G'_B, G'_C \dots$

The selection of the dimensional grouping is dictated by the physical criteria and tradition. For the determination of the local mass transfer coefficient the following dimensionless grouping is generally used

$$Sr = A \cdot Re^a \cdot Sc^b \cdot \left(\frac{\mu_m}{\mu_s}\right)^c \cdot f\left(\frac{x}{d}\right) \cdot f Gr$$

Page 57:

"The relation $(\frac{\partial^2 u}{\partial y^2}) = 0$ (2.37) derived from the boundary layer equation for $y=0$ " is correct. The conclusion that $(\frac{\partial u}{\partial y})_{y=0} = \text{cst}$ is wrong and this sentence should be deleted.

Pages 66,71:

For the establishment of equation (2.116) which deals with an established velocity profile Latzko started from Prandtl's and von Karman's equations on shearing stress, velocity distribution in turbulent flow, and turbulent conductivity E_H which includes the effect of turbulent mixing movements. For the establishment of equation 2.111 and 2.133 which deal with non established velocity and concentration profile Latzko derived expressions for the velocity and temperature distribution in the stabilisation length of the tube, based on the boundary-layer concept.

Consequently from the flow model point of view the hypothesis used by Latzko are correct. The main remark which could be made is that in its hypothesis implied that $Pr=1$. or $Sc=1$ in our case; which fact explains the non agreement of equation (2.116) with measured values in He where $Sc=1.7$.

Page 69:

The expression for the integrated mass transfer up to a distance x of the entrance as well as the terms $m_n = \frac{\beta_n^2}{2} \cdot \frac{D}{R \cdot u_m}$ should be written for $r=R$. Because in the solution of differential equation (2.114) the terms β_n are determined by using the boundary conditions for $r=R$, and moreover the value of \dot{M} is determined by using the cup-mixing concentration across the whole section.

Pages 73,75:

The last paragraph of page 75 is a repetition of the last paragraph of page 73. The last paragraph of page 75 should be reduced to -" $(\frac{\mu}{\mu_s} m -)^c$ is introduced to take into account the large temperature gradient which exists between the wall and the gas".

Page 106:

Four Zones have been distinguished for the analysis of the results, based on the following criteria:

- calculated thickness of velocity boundary layer in the stabilisation length
- Re_x which should indicate if the flow had become turbulent or not in the stabilisation length.

Two equations which should theoretically be applicable in the zone A and zone C so defined are presented.

In the Fig. 6.5 the theoretical lines drawn from these theoretical equations are compared to the experimental results. The fit of these lines to these experimental points is far from being perfect. However these equations give lines which are nearer to the experimental points than any other theoretical or semi-empirical expression available for the Re ranges

$$Re < 1.500$$

$$2.730 < Re < 9.200$$

The printed text on page 107 should be corrected and the sentence

"... but it should be observed that the four zones predicted theoretically can be seen and ..."

should be deleted.

The questions related to Fig. 3.7, Fig. 3.1 and the tables 6 are answered in the answer to the written questions of Mr. le Professeur Decroly, here attached.

Réponse aux questions écrites de Mr. le professeur Decroly

relatives aux Fig. 3.7, Fig. 3.1, et tableaux 6

Question no. 1: relative à la Fig. 3.7

1a: Fig. 3.7 L'échelle des ordonnées de la fig. 3.7 est une échelle logarithmique dont le dessinateur n'a malheureusement reproduit que la première décade
- La température de l'essai no. 247 représenté à fig. 3.7 était de 950°C .

1b: Mécanisme de formation de l'oxyde de carbone

Pour répondre à cette question j'aimerais reproduire textuellement un extrait de l'exposé général de Mr. le professeur Duval (Faculté des Sciences de Nancy) à la 10^{me} réunion de la Société de Chimie Physique "Juin 1960". [5]
"Alors qu'au-dessus de 1000°C (et sous basse pression tout au moins) le produit de la réaction est seulement du CO, il apparaît du CO_2 en quantités de plus en plus grandes au fur et à mesure que l'on abaisse la température au-dessous de 1000°C . On a discuté depuis longtemps pour savoir si le CO_2 obtenu dans ces conditions provenait d'une oxydation secondaire du CO, mais il est généralement admis actuellement que les deux gaz sont des produits primaires de la réaction. D'ailleurs la décomposition sous vide des oxydes de surface donne des rapports CO/CO_2 comparables à ceux obtenus dans la combustion.

Le rapport CO/CO_2 présente avec l'élévation de température une augmentation régulière dont ROSSBERG et BONNETAIN [6] ont déterminé des coefficients thermiques compris entre 10 et 18 Kcal environ, variables avec les graphites. La valeur du rapport CO/CO_2 et ses variations sont d'un intérêt fondamental dans les tentatives d'élucidation du mécanisme de la réaction. Les recherches les plus détaillées dans cette direction ont été effectuées par BONNETAIN, mais ses observations sont malheureusement trop complexes pour être rapportées et discutées ici. Elles montrent qu'on ne doit pas considérer les vaporisations de CO et de CO_2 comme des actes élémentaires indépendants. Les probabilités pour un atome de carbone superficiel d'être vaporisé soit à l'état de CO, soit de CO_2 , doivent dépendre du degré d'oxydation d'un ensemble d'atomes de carbone et d'oxygène chimisorbé. Les interactions peuvent être rendues

possibles soit simplement par suite d'une migration superficielle de l'oxygène chimisorbé, soit indirectement par l'intermédiaire d'influence électroniques à travers le réseau."

Le phénomène général décrit par Mr. DUVAL a été observé dans nos expériences c.a.d; pour une graphite de qualité déterminée le rapport des produits de réaction CO/CO_2 croît à température croissante. D'autre part il semble que ce rapport dépende, à une température donnée, du type de graphite utilisé. Nous pouvons en outre signaler les références suivantes [7] [8].

Il faut d'autre part faire remarquer que nos équations (3.1), (3.2), (3.6) pour le calcul du transfert d' O_2 à la surface de réaction, sont rendues indépendantes du mécanisme de production de CO et de CO_2 par l'utilisation de Y fraction molaire de produits de réaction sous la forme $\text{CO} + 2 \text{CO}_2$.

1c: Maximum de la réaction O_2 graphite

Indépendamment du mécanisme de formation de CO et de CO_2 nos expériences effectuées jus-qu'à 1000°C à la pression atmosphérique (grand coefficient de diffusion) et sous vide par DUVAL et STRICKLAND-CONSTABLE ont montré que la réaction chimique ($\text{O}_2 - \text{C}$) croît jus-qu'à des températures supérieures à 1700°C .

Question no.2: relative à la figure 3.1

2a: La qualité du graphite 1 a été imprégné à l'alcool furfurilyque qui est ensuite carbonisé dans les pores par un traitement thermique à haute température. L'objectif de l'imprégnation était d'obtenir un graphite imperméable aux produits de fission.

Le graphite de qualité 3 contient les mêmes matériaux de base que le graphite de qualité 1, mais la graphitisation s'effectue dans un four dont l'atmosphère contient du fluor pour le purifier de ces impuretés métalliques. Le tableau (1) ci-joint donne une idée de l'efficacité de la purification. Le fait de ne présenter que des échantillons du type 1 imprégnés, et du type 3 non imprégnés,

peut faire croire que la différence de réactivité résulte du fait de l'impregnation. Mais d'autres essais qui ne sont pas mentionnés dans la thèse indiquent que la différence de réactivité est essentiellement due à la catalyse induite par les impuretés. Ces résultats peuvent d'ailleurs être comparés à des résultats similaires obtenus par le professeur WALKER. [9] Reference peut également être faite aux figures ci-jointes. Fig. 1 and Fig. 2

2b:

Possibilité d'influence le calcul des taux de réaction par la réaction parasite
 $\text{CO}_2 + \text{C} \longrightarrow 2\text{CO}$

- les fig. 3.6 et 3.9 montrent qu'à 950°C le taux de réaction du CO_2 avec le graphite est au moins un ordre de grandeur plus petit que le plus petit taux de transfert de masse de O_2 mesuré et compte tenu de la faible teneur en CO_2 du gas, nous avons considéré que ces réactions parasites sont négligeables: fait qui a été confirmé par des essais de précalibration.

- D'autre part les calculs ne tiennent compte que du nombre de molécules O_2 qui ont réagi avec le graphite qu'elles soient sous forme de CO ou de CO_2 n'influence guère l'exactitude des calculs de transfert de masse de O_2 .

Question no. 3

relative aux tableaux 6 .

3a:

Les teneurs initiales des impuretés indiquées dans les tableaux 6 est uniquement de l'oxygène.

3b:

Les impuretés sont présentées en "volume par million" dans les tableaux car cette valeur était directement lue aux instruments. Les équations qui furent utilisées pour le calcul des taux de réaction convertissent ces fractions molaires en concentration absolues en tenant compte de la pression P_m et température T_m existant au point de réaction. Voir équations (3.1), (3.2), (3.6).

- [1] ECKERT, E. & DRAKE, R.,
Heat and mass transfer; Mac Graw-Hill Book Comp. Inc. New York (1959) p. 131
- [2] COULSON, J. & RICHARDSON, J.,
Chemical Engineering Vol. 1; 1964 p. 346 - Pergamon Press Oxford -
- [3] COULSON, J. & RICHARDSON, J.,
Chemical Engineering Vol. 1; 1964 p. 331 - Pergamon Press Oxford -
- [4] JAKOB, M.,
Heat transfer; p. 428 (1958) Vo. 1; John Wiley & Sons - New York -
- [5] DUVAL, X.,
Journal de chimie physique; 58 - No. 1 p. 3 (1961)
- [6] BONNETAIN, L.,
Journal de chimie physique; 58 - No. 1 p. 34 (1961)
- [7] LANG, F. et al.,
Journal de chimie physique; 58 - No. 1 p. 53 (1961)
- [8] GUERING, H.,
Journal de chimie physique; 58 - No. 1 p. 77 (1961)
- [9] WALKER, P.L. et al.,
Gas reactions of carbon advance in catalysis, XI, 133-221, (1959) -Academic Press
Inc., New York -

Table (1)

Typical Impurities present in the
Graphite Investigated

	Grade-0	Grade-1	Grade-3
Ash	200-320	200-280	250-370
B	0.17-02	1.0-2.3	2-12.2
Cd	0.04	-	-
Cl	2	-	2
Cu	0.7-0.9	1.5-4.2	0.9-1.0
Fe	5-7	70-150	6-15
Al	2-4	7-30	0.5-0.7
Ba	3-4	0.8-2.0	2-4
Be	0.05	0.05	0.04
Bi	0.25	0.25	0.2
Ca	60-80	40-80	50-70
Cr	0.1-0.5	0.3-0.8	0.7-1.0
Co	0.05	0.1	0.04
In	0.15	0.15	0.15
Pb	0.15-0.30	0.1-0.3	0.07-0.15
Li	0.15-0.20	0.15	-
Mg	0.1-0.7	0.3-1.0	0.25-1.0
Mn	0.3	0.25-1.0	0.04
Mo	0.25	0.05-0.15	0.3
Ni	0.7-2.0	1.0-1.5	5-10
Si	50-70	5-50	30-50
Na	0.5-2.5	2.0-6.0	1.5-2.0
Sr	1.0-2.0	0.5	0.4-2.0
Sn	0.15	0.05-0.50	0.06
Ti	1.5-4.0	2.5-7.0	20-30
W	0.4	0.4	0.3
V	20-40	15-20	40-50
Zn	0.4	0.5	0.3

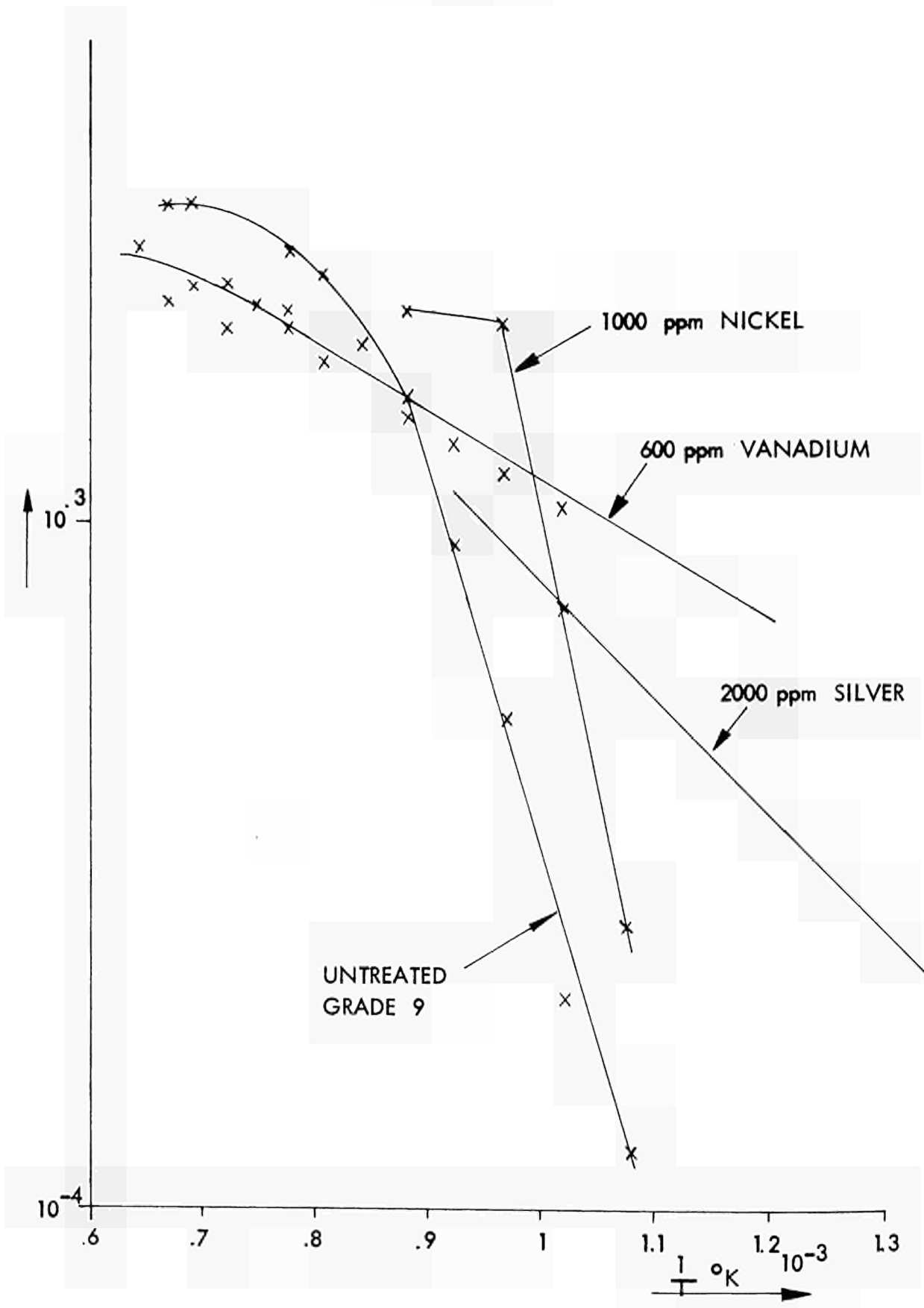


FIG. 1

EFFECT OF DIFFERENT METAL CATALYSTS ON
OXIDATION OF GRADE 9 GRAPHITE

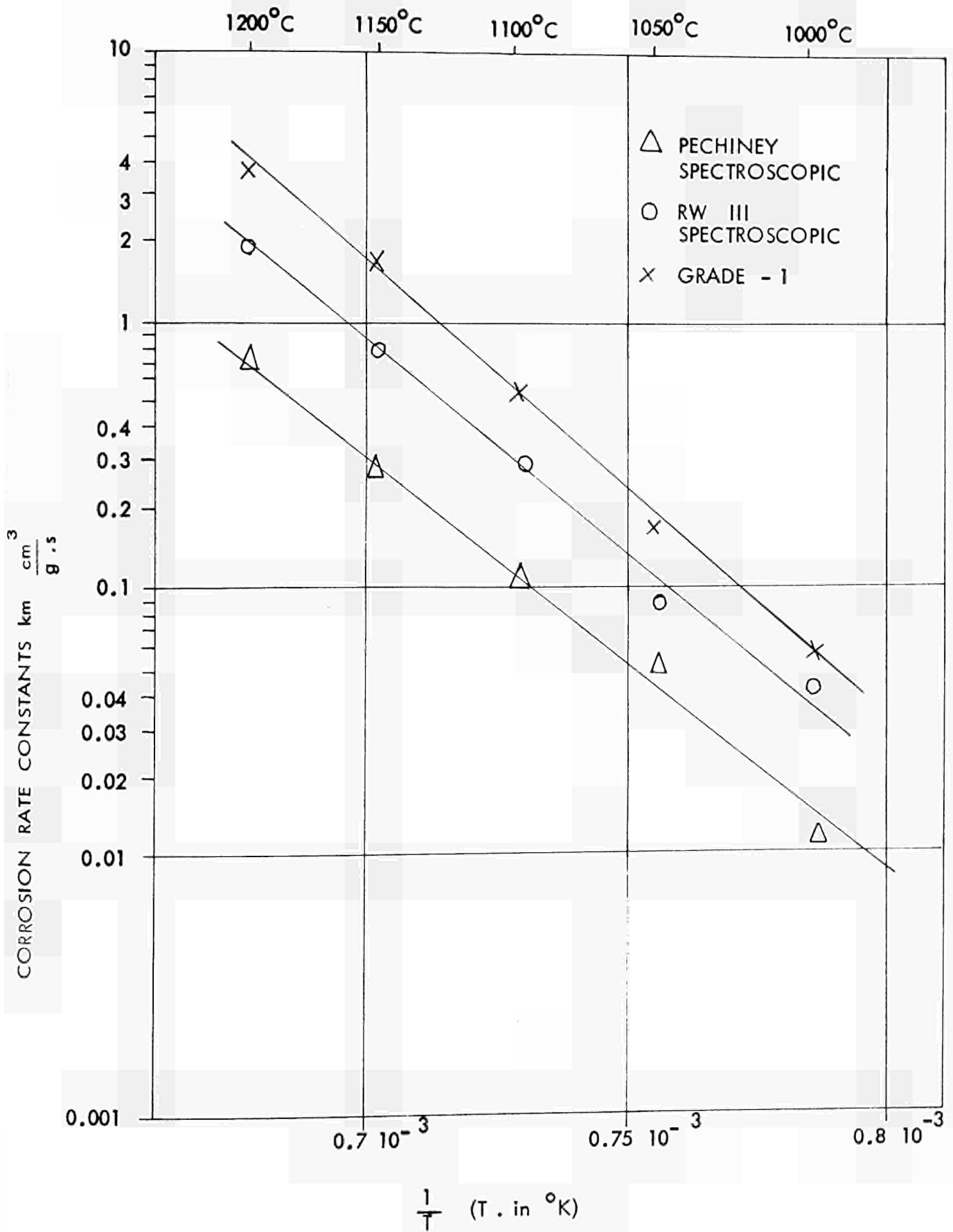


FIG. 2

GRAPHITE CORROSION - ARRHENIUS PLOT

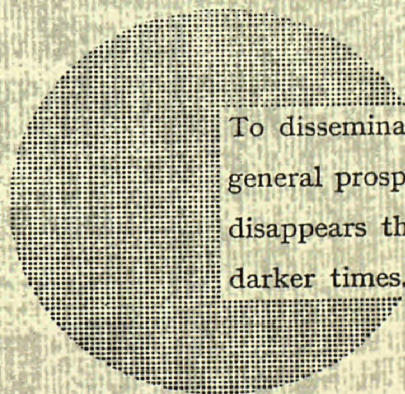
NOTICE TO THE READER

All Euratom reports are announced, as and when they are issued, in the monthly periodical **EURATOM INFORMATION**, edited by the Centre for Information and Documentation (CID). For subscription (1 year : US\$ 15, £ 5.7) or free specimen copies please write to :

Handelsblatt GmbH
"Euratom Information"
Postfach 1102
D-4 Düsseldorf (Germany)

or

Office de vente des publications
des Communautés européennes
2, Place de Metz
Luxembourg



To disseminate knowledge is to disseminate prosperity — I mean general prosperity and not individual riches — and with prosperity disappears the greater part of the evil which is our heritage from darker times.

Alfred Nobel

SALES OFFICES

All Euratom reports are on sale at the offices listed below, at the prices given on the back of the front cover (when ordering, specify clearly the EUR number and the title of the report, which are shown on the front cover).

OFFICE CENTRAL DE VENTE DES PUBLICATIONS DES COMMUNAUTES EUROPEENNES

2, place de Metz, Luxembourg (Compte chèque postal N° 191-90)

BELGIQUE — BELGIË

MONITEUR BELGE
40-42, rue de Louvain - Bruxelles
BELGISCH STAATSBAD
Leuvenseweg 40-42, - Brussel

DEUTSCHLAND

BUNDESANZEIGER
Postfach - Köln 1

FRANCE

SERVICE DE VENTE EN FRANCE
DES PUBLICATIONS DES
COMMUNAUTES EUROPEENNES
26, rue Desaix - Paris 15^e

ITALIA

LIBRERIA DELLO STATO
Piazza G. Verdi, 10 - Roma

LUXEMBOURG

OFFICE CENTRAL DE VENTE
DES PUBLICATIONS DES
COMMUNAUTES EUROPEENNES
9, rue Goethe - Luxembourg

NEDERLAND

STAATSDRUKKERIJ
Christoffel Plantijnstraat - Den Haag

UNITED KINGDOM

H. M. STATIONERY OFFICE
P. O. Box 569 - London S.E.1

EURATOM — C.I.D.
51-53, rue Belliard
Bruxelles (Belgique)